Maria de Fátima Gomes Pina

AN INVESTIGATION INTO THE SOLID STATE PROPERTIES OF OLANZAPINE AND PAROXETINE HCI AND THEIR SOLID DISPERSION SYSTEMS

· U   C ·

UNIVERSIDADE DE COIMBRA

An Investigation into the Solid State Properties of Olanzapine and Paroxetine HCl and their Solid Dispersion Systems

Maria de Fátima Gomes Pina

Tese apresentada à Universidade de Coimbra para apreciação nas provas de Doutoramento em Farmácia, especialidade de Tecnologia Farmacêutica

Faculdade de Farmácia
Universidade de Coimbra
2014

To my Loving Parents and Sister

Acknowledgments

FCT Fundação para a Ciência e a Tecnologia
MINISTÉRIO DA EDUCAÇÃO E CIÊNCIA

Nothing in life is to be feared, it is only to be understood.

Now is the time to understand more, so that we may fear less.

Marie Curie

Abstract

Physical characterisation of pharmaceutical solids is an integral aspect of the drug development process and has attracted increased attention over the past decades. Each active pharmaceutical ingredient (API), may exist in different crystalline forms (polymorphs), incorporate water in their structure (pseudopolymorphs) or be converted, intentionally or not, to an amorphous state. As consequence of all this variety of forms, a full toolbox of characterisation techniques is nowadays available, combining high resolution thermoanalytical techniques with highly precise diffraction methods and advanced computational resources.

The work presented in this thesis aimed to provide an in-depth understanding of the physicochemical properties of single drug molecules (olanzapine and paroxetine HCl) and final formulated systems in varying physical states including different crystalline entities and amorphous systems. In this work, a combination of thermal (standard differential scanning calorimetry (DSC), modulated temperature DSC (MTDSC), thermogravimetric analysis (TGA) and hot stage microscopy (HSM)), diffraction (X-ray powder diffraction (XRPD) combined, in some studies, with variable humidity (VH) or temperature (VT)) and spectroscopic techniques (attenuated total reflectance–Fourier transform infrared (ATR-FTIR)) were extensively used. Dynamic vapour sorption (DVS), Karl Fischer titration (KFT) and scanning electron microscopy (SEM) were as well of great importance. Dissolution performance and physical stability studies were also evaluated.

At first, a thorough investigation into the solid state of paroxetine HCl was performed. Aspects such as the interaction with water and the interconversion between the two crystalline forms, Form I and II, were fully explored. This enabled to successfully clarifying the nature, location and bonding strength of the water molecules in the crystalline structure of paroxetine HCl Form II (Chapter 3). These findings allowed proper recognition of Form II as a non-stoichiometric hydrate with unusual behaviour, and challenges the previous designation as an anhydrous form with a hygroscopic nature. On the other hand, the specific conditions that led to the dehydration of Form I were fully investigated (Chapter 4). The dehydration of Form I was found to require both ultra-dry

environment and high temperatures. As a consequence of this process a new anhydrous form of paroxetine HCl has been identified.

After this structural characterisation, studies were conducted on the conversion of paroxetine HCl to an amorphous state, either alone (Chapter 5) or molecularly dispersed in polyvinylpyrrolidone vinyl-acetate (PVPVA, Chapter 6). Chapter 5 provided a detailed thermal characterisation using thermodynamic and kinetic parameters of amorphous paroxetine HCl prepared via melt quenching method. The results obtained were then correlated with the stability of this form over storage. In Chapter 6, parameters such as the initial hydration state of the drug (paroxetine Forms I and II) and the methodology used (spray drying (SD) and hot melt extrusion (HME)) were found not only to influence the dissolution rate of the prepared systems but also its physical stability. Finally, the acquired knowledge in the preparation of solid dispersion systems was applied to a Biopharmaceutical Classification System (BCS) Class 2 drug (olanzapine, OLZ) using HME as the selected technology and considering the influence of different polymeric carriers (Chapter 7). This study showed an interesting interplay between the extrusion temperature, drug loading, drug physical state and polymer chemistry that can be further applied to other poorly soluble APIs.

To conclude, the research carried out and detailed within this thesis aims to contribute to a better understanding of the complex solid state characterisation of pharmaceutical drugs and formulated systems prepared via solid dispersion methods. To the end, this work has identified several issues and possible areas for future research in the pharmaceutical field.

Keywords: amorphous, anhydrous, hydrate, olanzapine, paroxetine HCl, polymorphism, pseudopolymorphism, solid dispersion, solid state, structural analysis, thermal analysis

Resumo

A caracterização física de fármacos e excipientes é um aspecto integrante do processo de desenvolvimento de medicamentos e tem atraído crescente atenção ao longo das últimas décadas. Cada fármaco (*active pharmaceutical ingredient* (API)) ou mesmo excipiente, pode existir em diferentes formas cristalinas (polimorfos), incorporar água na sua estrutura (pseudopolimorfos) ou ser convertido, de forma intencional ou não, num estado amorfo. Em consequência desta variedade possível de formas, um conjunto de técnicas de caracterização encontra-se hoje em dia disponível, combinando técnicas termoanalíticas de alta resolução com métodos de difração de alta precisão e recursos computacionais avançados.

O trabalho apresentado nesta tese teve como objetivo proporcionar uma compreensão profunda das propriedades físico-químicas de fármacos (olanzapina e cloridrato de paroxetina) e produtos finais em vários estados físicos, incluindo diferentes entidades cristalinas e sistemas amorfos. Neste trabalho, uma combinação de técnicas térmicas (calorimetria de varrimento diferencial (DSC), com ou sem modelação de temperatura (MTDSC)), análise termogravimétrica (TGA) e microscopia de platina aquecida (HSM)), difração (difração de raios X de pó (XRPD) combinada, em alguns estudos, com variação de humidade (VH) ou temperatura (VT)) e técnicas espectroscópicas (espectroscopia de infravermelho (ATR-FTIR)) foram amplamente utilizadas. *Dynamic vapour sorption* (DVS), Karl Fischer (KFT) e microscopia eletrónica de varrimento (SEM) foram também de grande importância. Finalmente, ensaios de dissolução e estudos de estabilidade física foram ainda conduzidos em casos específicos.

Numa primeira fase, foi desenvolvido um estudo pormenorizado sobre o estado sólido do cloridrato de paroxetina. Aspectos tais como a interação com a água e a interconversão entre as duas formas cristalinas do cloridrato de paroxetina, Formas I e II, foram cuidadosamente exploradas. Este estudo permitiu clarificar a natureza, localização e força de ligação das moléculas de água na estrutura cristalina da Forma II do cloridrato de paroxetina (Capítulo 3). Estes resultados permitiram assim identificar a Forma II como um hidrato não estequiométrico com um comportamento peculiar e excluir a sua prévia designação enquanto forma anidra com uma natureza higroscópica. Por outro lado, as

condições específicas capazes de promover a desidratação da Forma I foram também estudadas (Capítulo 4). Verificou-se que a desidratação desta forma exige um ambiente extremamente seco e altas temperaturas. Em consequência deste processo uma nova forma anidra do cloridrato de paroxetina foi identificada.

Após a caracterização estrutural das duas formas cristalinas do cloridrato de paroxetina, foram ainda realizados estudos sobre a conversão deste fármaco num estado amorfo, quer individualmente (Capítulo 5) ou disperso a nível molecular em polivinilpirrolidona vinil-acetato (PVPVA, Capítulo 6). O Capítulo 5 apresenta uma caracterização detalhada, com recurso a parâmetros termodinâmicos e cinéticos, da forma amorfa do cloridrato de paroxetina preparada por fusão e rápido arrefecimento. Os resultados obtidos foram em seguida correlacionados com a estabilidade física observada experimentalmente. Em continuação, o trabalho apresentado no Capítulo 6 concluiu que parâmetros, tais como o estado inicial de hidratação das duas formas da paroxetina e a metodologia usada para preparar as dispersões sólidas (*spray drying* (SD) e extrusão a quente (HME)), influenciam não só a velocidade de dissolução dos sistemas preparados, mas também a sua estabilidade e tendência para recristalização. Finalmente, o conhecimento adquirido na preparação de sistemas de dispersão sólida foi aplicado a um fármaco (olanzapina, OLZ) pertencente à Classe 2 do Sistema de Classificação Biofarmacêutico (BCS) usando HME como tecnologia selecionada e considerando a influência de diferentes polímeros (Capítulo 7). Este estudo revelou uma interessante relação entre a temperatura de extrusão, dosagem e estado físico do fármaco e ainda estrutura química do polímero. Os resultados obtidos neste estudo visam contribuir para um melhor entendimento das estratégias possíveis usadas no melhoramento da velocidade de dissolução de outros fármacos pouco solúveis.

A título de conclusão, o estudo conduzido e apresentado detalhadamente nesta tese pretende contribuir para uma melhor compreensão da caracterização complexa do estado sólido de fármacos e sistemas farmacêuticos preparados através de métodos de dispersão sólida. Finalmente, este trabalho identificou vários problemas e possíveis áreas de investigação futura no domínio farmacêutico.

Palavras-chave: amorfo, análise estrutural, análise térmica, anidro, cloridrato de paroxetina, dispersão sólida, estado sólido, hidrato, olanzapina, polimorfismo, pseudopolimorfismo

Table of Contents

List of Figures

Chapter III

Chapter VI

List of Tables

Chapter VII

List of Abbreviations & Symbols

API	Active pharmaceutical ingredient
ATR-FTIR	Attenuated total reflectance-Fourier transform infrared
BCS	Biopharmaceutical classification system
C_p	Heat capacity
DSC	Differential scanning calorimetry
E_a	Activation energy
FH	Flory-Huggins
GT	Gordon-Taylor
HCl	Hydrochloride acid
HME	Hot melt extrusion
HR	Heating rate
HSM	Hot stage microscopy
LTA	Local thermal analysis
MTDSC	Modulated temperature DSC
MW	Molecular weight
OLZ	Olanzapine
PM	Physical mixture
PVP	Polyvinylpyrrolidone
PVPVA	Polyvinylpyrrolidone vinyl-acetate
RH	Relative humidity
rpm	Rotation per minute
SD	Spray drying
SEM	Scanning electron microscope
SLP	Soluplus®
STDEV	Standard deviation
T_g	Glass transition temperature
TGA	Thermogravimetric analysis
T_m	Melting temperature

UV	Ultraviolet
VH	Variable humidity
VT	Variable temperature
XRPD	X-ray powder diffraction
χ	Flory-Huggins interaction parameter
δ	Solubility parameter
ρ	Density

SCOPE AND OVERVIEW

Motivation and Contextual Objectives

Solid state characterisation represents, nowadays, a well-established program in the pharmaceutical industry since an incomplete characterisation of a drug substance can jeopardize the development and commercialisation of a final product.

In the present work, a range of analytical techniques were used to obtain a more accurate and thorough understanding of the solid state of two well-known drugs: paroxetine HCl and olanzapine. These drugs were selected due to their complex nature and not yet fully understood solid state properties. Moreover, the preparation of solid dispersion systems of these two drugs using different technologies was evaluated as a way to explore the parameters that can influence the dissolution behaviour and physical stability of such systems.

Organisation of the Thesis and Main Objectives

This thesis is divided into 8 chapters. The contents and objectives of each chapter are briefly summarised as follows,

Chapter 1 provides a broad overview on the topics explored in the subsequent chapters.

Chapter 2 presents the chemical structure and main physicochemical properties of all APIs and polymers used throughout this dissertation. A brief theoretical background to the techniques used to prepare solid dispersions and all the analytical methods is also presented. Moreover, a paragraph describing the instruments characteristics is added at the end of each technique.

Chapter 3 provides a thorough investigation of paroxetine HCl Form II. Differentiation between surface water and hydrate formation was critically accessed as a function of relative humidity and temperature.

Chapter 4 explores the conditions that could lead to the dehydration of paroxetine HCl Form I. The possibility of any structural relationship between the dehydrated From II and Form I was investigated.

Chapter 5 provides the calculation of several thermodynamic and kinetic parameters as possible predicting tools of the physical stability of amorphous paroxetine HCl. Correlation between those predictions and the experimental stability over storage was evaluated.

Chapter 6 provides an evaluation of the theoretical predictions used to describe miscibility between drug and polymer and the effect of different preparation methods on the processing of the pseudopolymorphs of paroxetine HCl, dissolution rates and stability over storage.

Chapter 7 presents an investigation on the effect of drug loading and physical state, extrusion temperature and physicochemical properties of the selected polymers on the dissolution enhancement and stability of solid dispersions of a poorly soluble drug (olanzapine) prepared via hot melt extrusion.

Chapter 8 presents the main conclusions and future work.

It is worth mentioning that the author of this thesis was not directly involved in the molecular modeling simulations (Chapter 3), Pawley refinement, unit cell parameters determinations and high performance liquid chromatography (HPLC) analysis (Chapter 4).

Scientific Publications and Conferences

International Peer-Reviewed Publications:

- ❖ M. F. Pina et al. 2012. Identification and Characterisation of Stoichiometric and Non-Stoichiometric Hydrate Forms of Paroxetine HCl: Reversible Changes in Crystal Dimensions as a Function of Water Absorption. *Molecular Pharmaceutics*, 9, 3515-3525.

- ❖ M. F. Pina et al. 2014. The Influence of Drug Physical State on the Dissolution Enhancement of Solid Dispersions Prepared via Hot Melt Extrusion: A Case Study using Olanzapine. *Journal of Pharmaceutical Sciences* (Accepted for Publication).

- ❖ M. F. Pina et al. An Investigation into the Dehydration Behaviour of Paroxetine HCl Form I using a Combination of Thermal and Diffraction Methods: The Identification and Characterisation of a New Anhydrous Form (Submitted to *Crystal Growth and Design*).

Oral Communications:

- ❖ An Investigation into the Dehydration Behaviour of Paroxetine HCl Form I using a Combination of Thermal and Structural Analysis – Pharmaceutical Solid State Research Cluster, Lille, 4th July 2013

- ❖ Identification and Characterisation of a Non-Stoichiometric Hydrate Form of Paroxetine HCl: Reversible Changes in Crystal Dimensions as a Function of Water Absorption – Pharmaceutical Solis State Research Cluster, Lisbon, 27th August 2012

❖ Theoretical and Practical Approaches in Drug-Polymer Miscibility/Solubility and the Influence of Preparation Methods – 8th World Meeting on Pharmaceutics, Biopharmaceutics and Pharmaceutical Technology, Istanbul, 21st March 2012

1   INTRODUCTION

. . . a major deficiency in our current knowledge and understanding concerns the relationship among the members of a polymorph cluster—what is their relative mutual stability, how do they transform, one into another, what are the thermodynamic factors governing their mutual stability, what are the kinetics of the transitions. Answers to the last of these questions are very important to users of, and sufferers from, polymorphism.

Herbstein

1.1   General Introduction

Interest in the solid state properties of pharmaceutical compounds has grown greatly in recent decades. Firstly, an insufficient understanding of solid state properties can lead to serious complications in the development of a final pharmaceutical product, including their physical and chemical stability. Secondly, a thorough characterisation of any new, or even existent, molecule can create new opportunities and uncover important properties that can enhance its bioavailability. This is extremely important from the patient perspective. In addition, from a commercial point of view, companies can see their patents extended with economic benefits.

This section provides a background on the concepts and principles related to the solid state of pharmaceutical compounds. Additionally, some relevant topics on formulation strategies, new preparation techniques and principal obstacles frequently encountered during the manufacturing process are also explored.

1.2   States of Matter

Matter is broadly classified as being either a solid, liquid or a gas. At normal room temperature and pressure the majority of active pharmaceutical ingredients (APIs) and excipients exist as solids. In the solid state, molecules are held in close proximity to each other by intermolecular forces such as hydrogen bonding and van der Waals interactions. In the liquid state, there are still molecular interactions but the molecules are more mobile and lack long-range order. Finally, in the gas phase the molecules only interact weakly with each other and travel large distances without colliding.

The solid phase can be classified into two major types of sub-phases based upon the order of molecular packing. The most common type of state is the crystalline state where the structural units, called unit cells, are regularly repeated in a three dimension (3D) lattice, presenting both short and long-ranges order. In this context, 'short-range order' refers to

the way (molecular coordination) that molecules arrange next to each other, while 'long-range order' refers to the regularity or periodicity that hundreds and thousands of molecules aggregate, first through 'neighbouring' (short-range) and then propagate to an 'appreciable' distance, to form a phase crystalline (Ossi, 2010). On the contrary, amorphous solids have a regularity of structure limited to the immediate neighbours of any particular molecule within the solid, which means that they only have short-range order and therefore greater mobility when compared to crystalline solids (Florence and Attwood, 2006).

Crystalline solids can also exist in multiple sub-phases, such as polymorphs, solvates, co-crystals and salts (Figure 1.1).
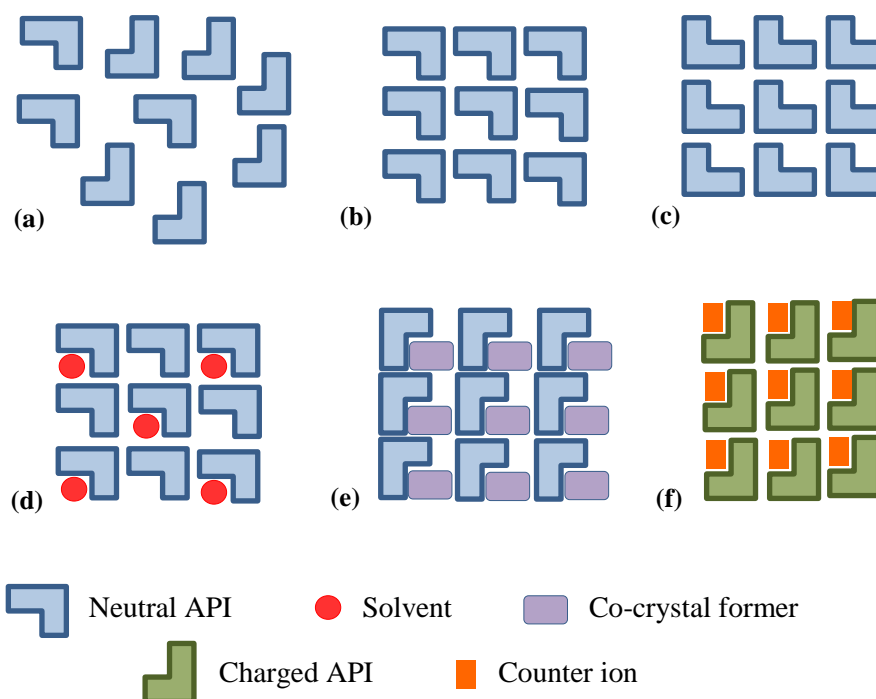
Figure 1.1: Schematic depiction of the various types of solids: amorphous (a) and crystalline (b-f). Crystalline solids can be further classified as polymorphs (b and c), solvates/hydrates (d), pharmaceutical co-crystals (e) and salts (f).

Polymorphs are compounds with same chemical composition but different crystal arrangements. On the other hand, solvates and co-crystals are multicomponent crystals. A solvate is defined as a solid in which molecules of solvent are incorporated into the crystal

lattice (Hosokawa et al., 2004). The incorporated solvent is often termed the *guest* and the major component is termed the *host* (Herbstein, 2004). When the solvent is water, the solvate is called hydrate. The terminology of hydrates is related to the amount of molecular water compared to one molecule of host and is denoted by terms such as 'hemihydrate', 'monohydrate', 'dihydrate', etc. 'Anhydrate' is actually a redundant term but is used to emphasise that water (or solvent) is not incorporated in the crystal structure. The suggested nomenclature of this particular group as pseudopolymorphs generated a polemic discussion and it was recently replaced by solvatomorphs (Seddon, 2004; Desiraju, 2004; Nangia, 2005).

Several APIs are commercialised in a hydrate phase (Lee et al., 2011), such as alendronate sodium trihydrate (Fosamax®), amoxicillin trihydrate (Amoxil®) and atorvastatin calcium trihydrate (Lipitor®). Solvates other than hydrates are usually not selected for development owing to risk of desolvation and toxicity concerns with organic solvents that are not Class III. Class III solvents are considered to be less toxic and with lower risk to Human health. This is the outcome of acute and short-term safety studies, although there are no long-term toxicity or carcinogenicity studies for many of the solvents belonging to this class. Nonetheless, there are some drug products marketed in the solvate form such as darunavir ethanolate (Prezista®), indinavir sulfate ethanolate (Crixivan®) and warfarin sodium isopropanol solvate (Coumadin®) (Lee et al., 2011).

Co-crystals are multiple component crystals in which all components are solid under ambient conditions when in their pure form (Shan and Zaworotko, 2008). Co-crystallisation has gained more and more interest in pharmaceutical research, since the complexation of an API with another molecule can produce a solid form with different physical properties (Trask et al., 2006; McNamara et al., 2006).

Salts represent a considerable enlargement of the portfolio of solid forms of pharmaceutical molecules. Salts are stable and highly soluble in water. A necessary prerequisite for the formation of salts is the presence of ionisable groups in the molecule. Salts may also form hydrates such as atorvastatin calcium trihydrate and paroxetine hydrochloride hemihydrate.

1.2.1 Structural Aspects of Crystalline Solids

As mentioned above, crystals consist in a regular array of atoms and molecules organised in a basic structural motif repeated in a three-dimensional arrangement. Each motif in crystallography is called unit cell which has a geometry defined by the lengths of the three axes (*a*, *b*, *c*) and the angles between them (*α*, *β*, *γ*) (Gilmore, 2011). The convention is that *α* defines the angle between *b* and *c*, *β* defines the angle between *a* and *c*, and *γ* defines the angle between *a* and *b*. The regular and periodic arrangement of unit cells is called crystal lattice, which is organised in a way that each lattice point has an identical environment with respect to the basic motif and other lattice points (Brittain, 2009). There are seven fundamental types of primitive unit cells, as shown in Figure 1.2.
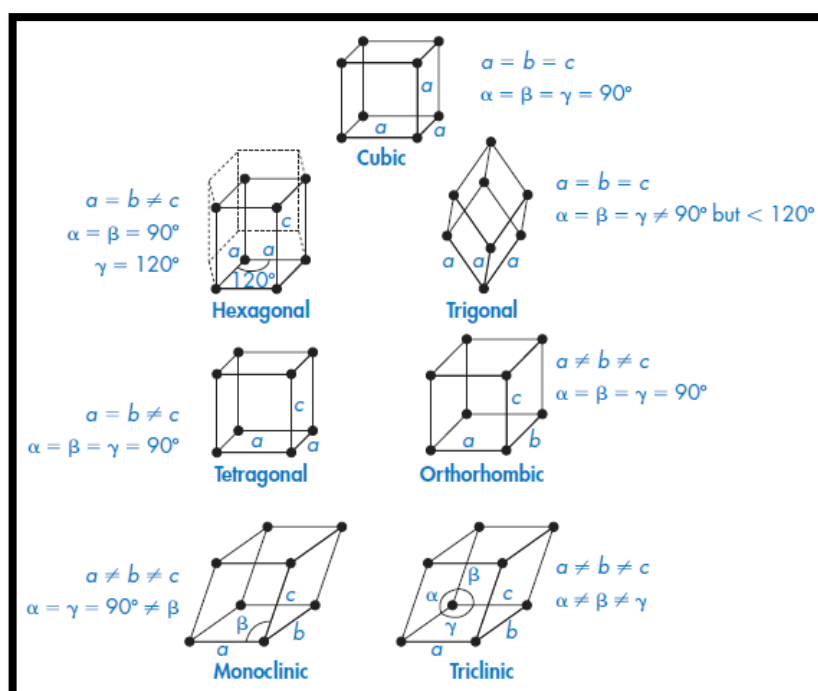
Figure 1.2: The seven crystal systems, their unit cells and the constraints on the unit cell dimensions (Florence and Attwood, 2006).

However, there are other arrangements of points which fulfil the requirements of a point lattice, namely, that each point has identical surroundings which leads to the existence of

fourteen possible point lattices and no more. This work was carried out by the French crystallographer Bravais in 1848 and therefore they are called the 14 Bravais lattices (Cullity, 1956).

1.2.2 Cambridge Structural Database

The Cambridge Structural Database (CSD) is the world's repository for the results obtained from the X-ray crystal structure analysis of small organic molecules and organometallic compounds. It contains the results of over half-a-million X-ray and neutron diffraction analyses. The CSD is compiled and distributed by the Cambridge Crystallographic Data Centre (CCDC), a fully independent institution based in Cambridge (England) since 1987.

Each entry in the CSD contains 1D, 2D and 3D information. The 1D data contains bibliographical and chemical information (name and empirical formula). The 2D information is used to generate the structural formula and chemical connectivity, which obviously is the same for polymorphs. And finally, the 3D information contains all the results obtained from X-ray structure determination, namely cell constants, space group, atomic coordinates and atomic attributes needed to generate the three-dimensional molecular and crystal structures (Bernstein, 2002).

This unique database of accurate 3D structures has become an essential resource to scientists around the world providing high quality information, software and services.

1.3 Polymorphism

Polymorphism, is a term originally derived from Greek (*poly* = many; *morph* = form) and according to McCrone's definition (Haleblian and McCrone, 1969): "*Polymorphism is the ability of any element or compound to crystallize as more than one distinct crystal*

species". This author also states that "*every compound has different polymorphic forms and that, in general, the number of forms known for a given compound is proportional to the time and money spent in research on that compound*". Earlier in 1788, Klaproth found that calcium carbonate crystallises both as calcite and aragonite, giving the first insight on polymorphism. A few years later, Humphrey Davy in 1809 presented that diamond and graphite are both carbon, but they differ on the way carbon atoms are arranged in the solid state. This became the classical and most famous example of polymorphism.

Different polymorphs exhibit different properties, favourable or not in a particular context, which became the subject of considerable practical, and hence financial, importance, especially in the pharmaceutical arena (Herbstein, 2004). Polymorphs of a drug substance can have different chemical and physical properties, including melting point, chemical reactivity, apparent solubility, dissolution rate, optical and mechanical properties, vapour pressure, and density. These properties can have a direct effect on the ability to process and/or manufacture the drug substance and the drug product, as well as, on drug product stability, dissolution, and bioavailability. Thus, polymorphism can affect the quality, safety, and efficacy of the drug product.

From an industrial perspective, the drug development program is a highly interdisciplinary field connecting chemistry, technology, pharmacology and toxicology, at the last instance. At first it involves solid state knowledge covering crystal chemistry and materials properties with a goal to select the appropriate crystal form with the desired physical and chemical properties. The following step then embraces formulation development and process design. The general program of a drug product development is illustrated in Figure 1.3.
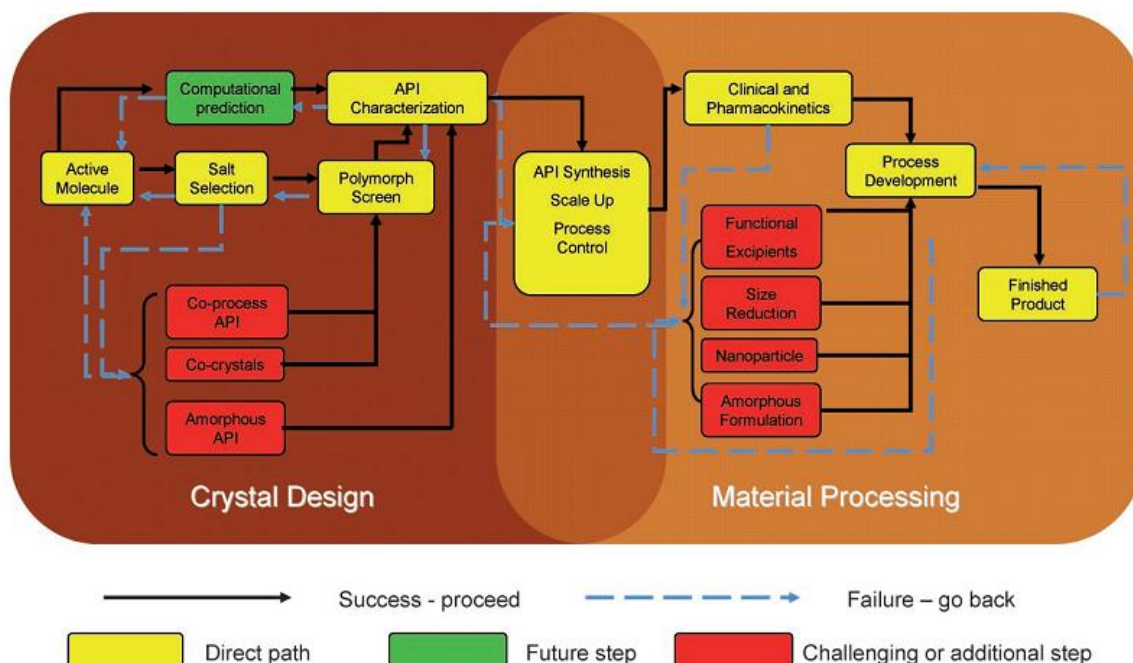
Figure 1.3: Relationship between the selection/optimisation of a drug candidate and the development stages (Chow et al., 2008).

In the case of a new drug substance, it is crucial to perform a thorough polymorphic screening prior to the initiation of pivotal clinical studies and primary stability batches. The importance and difficulties related to polymorphism in the pharmaceutical industry can be exemplified by examining the history of a number of well-known drug products as shown in Figure 1.4.

In most of the cases, the products are recalled owing to ambiguous product performance and quality as a result of unpredicted changes in the polymorphic form which resulted in problematic quality release and stability testing (i.e. dissolution) of the finished dosage form. As a consequence, companies have experienced market shortages due to manufacturing troubleshooting, batch rework, and delays in project or clinical trials timelines.

1998 – Withdrawal of Norvir® (ritonavir) due to the conversion to a more thermodynamic stable and less soluble polymorph.

2008 – Batch recall of Neupro® (rotigotine) patches due to crystallisation of a new polymorph.

1988 – Clinical failure of Tegretol® (carbamazepine) due to the conversion of the anhydrate form to the dihydrate.

1999– Examination of the raw material of Velmox® (mebendazole) confirmed a mixture of Forms A and B, found to be inactive/less effective than the intended Form C.

2010 – Recall of Coumadin® (warfarin sodium 2-propanol) as a result of variability in the content of 2-propanol.

Figure 1.4: A timeline of events concerning solid state issues with polymorphism/pseudopolymorphism of pharmaceutical drugs (adapted from (Lee et al., 2011)).

1.3.1 Structural Aspects of Polymorphism

1.3.1.1   Packing and Conformational Polymorphism

Polymorphism in molecular crystals can be divided into two categories: packing and conformational polymorphism. In the former, molecules exhibit as rigid grouping of atoms that may be stacked in different motifs to occupy the points of different lattices. On the other hand, conformationally flexible molecules adopt more than one conformation in the solid state (Bernstein, 2002; Yu et al., 2000). The differentiation between packing polymorphism and conformational polymorphism is not always obvious. Several examples of drugs that exhibit conformational polymorphism can be scattered from literature such as the antidepressant venlafaxine hydrochloride (Kavitha et al., 2005), the antipsychotic olanzapine (Reutzel-Edens et al., 2003a) and the non-steroidal anti-inflammatory drug nimesulide (Sanphui et al., 2011).

Conformers have very similar conformational energies which makes possible the existence of different molecular conformations in a single crystal structure. This energy is enough to provoke changes in molecular torsional parameters about single bonds, but it is generally

not sufficient to significantly perturb bond lengths and bond angles. Differences in the torsion angles are usually the first focus to identify conformational polymorphism, though this is not a rigid and straight rule (Bernstein, 2002).

1.3.1.2   Monotropism and Enantiotropism

Thermodynamically, polymorphs can be classified as monotropics or enantiotropics, depending upon whether one can reversibly transform to another or not. In an enantiotropic system, there is a transition temperature (T_{trans}) before melting (T_m), at which the stability order between two polymorphic forms is reversed. On the contrary, in a monotropic system, one form is more stable than the other at any temperature before melting (Vippagunta et al., 2001). Figure 1.5 shows phase diagrams representing each system.

In an enantiotropic system, Form I has a lower free energy over the lower temperature range, while Form II is shown to have a lower free energy over a higher temperature range. At the T_{trans}, the free energy curves cross and the forms are isoenergetic. For a monotropic system, one polymorph has the lowest free energy at any given temperature and therefore is the most thermodynamically stable form. The free energy curves do not cross, so no reversible transition can be observed below the melting point (Brittain, 2009).
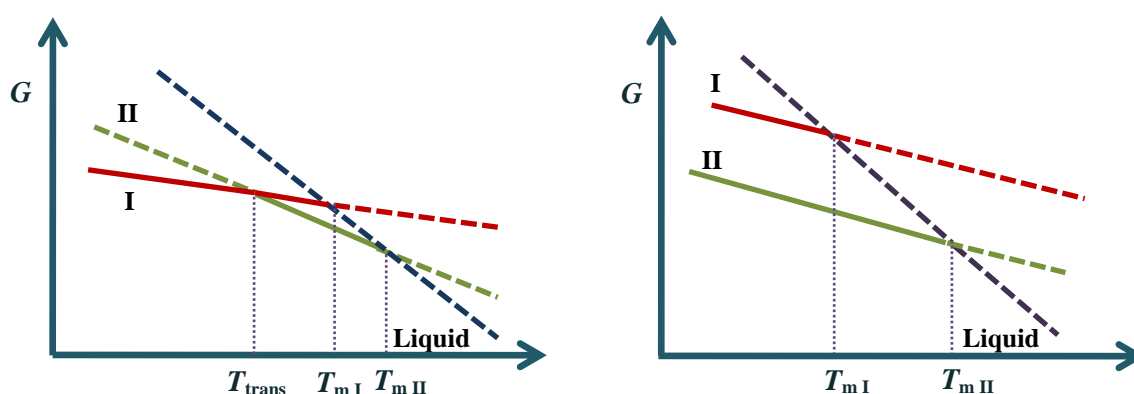
Figure 1.5: Free energy (G) as a function of temperature for enantiotropic (left) and monotropic (right) systems (adapted from (Craig and Reading, 2007)).

To understand if a polymorphic system is monotropic or enantiotropic is of considerable relevance from the stability perspective. Such knowledge can help to determine whether a compound will be stable at a certain temperature during manufacture and storage conditions. There are a series of rules that have been developed to help differentiating and characterising these two systems, as presented next.

1.3.2   Thermodynamics of Polymorphic Systems

In a polymorphic system, the relative stability of polymorphs depends on their free energies, with the most stable form having the lowest free energy under determined experimental conditions. In those circumstances, the other forms are thermodynamically unstable and therefore considered metastable with a rate of conversion to the most stable form that can vary from seconds to years.

An example is the well reported case of ritonavir. Ritonavir is a protease inhibitor for Human Immunodeficiency Virus (HIV), discovered in late 1992 and introduced to the market in 1996 as a semisolid capsule formulation and as a liquid formulation. The final product, Norvir®, was withdrawn two years later because some lots of capsules failed the dissolution tests specification. It was found that a large portion of the drug substance was precipitating out of the final (semisolid) formulated product. Further investigation into this matter revealed that a new, previously unknown, thermodynamically more stable and much less soluble crystalline form had emerged (Chemburkar et al., 2000).

The main approaches used to assess thermodynamic stability relationships of polymorphs are based on the Burger and Ramberger rules established in 1979 (Burger and Ramberger, 1979a;b). Three particularly important rules proposed by these authors are the heat of transition, the heat of fusion, and the density rule, described below.

Heat of Transition Rule

This rule states that if, at some temperature, an endothermic transition between two crystal forms is observed, then there is a transition point below this temperature and the two polymorphs are enantiotropically related. On the contrary, if an exothermic transition is

observed at some temperature, there is no thermodynamic transition point below this temperature. As a result, this could be an indication of a monotropic system, but also of an enantiotropic system with the thermodynamic transition temperature happening at a higher temperature (Hilfiker, 2006).

Heat of Fusion Rule

The heat of fusion rule states that the polymorph with higher melting point has the lower heat of fusion thus the two polymorphs are enantiotropic, otherwise they are monotropic. Frequently, the rate of polymorphic transition is too slow to allow for an accurate measurement of the heat of transition, in which case the heat of fusion rule may be applied (Hilfiker, 2006).

Density Rule

True density is a physical property of both fundamental and practical importance to the study of pharmaceutical powders. The density rule states that for a system at absolute zero, the most stable polymorph will have the highest density, as a result of the closer packing of the molecules. This is the case of nabumetone, for example, with the stable Form I having a density of 1.26 g/cm^3 while the metastable Form II possesses a density of 1.21 g/cm^3 (Price et al., 2002). However, if crystal packing is dominated by energetically more favourable directional or electrostatic interactions, such as hydrogen bonding, crystals with a closer packing may not always exhibit a lower lattice energy and free energy even at 0 K (Sun, 2007). An example of this situation, is the case of oxybuprocaine hydrochloride, a local anaesthetic drug, with the metastable Form III having a higher density (1.21 g/cm^3) than the stable Form II (1.20 g/cm^3) (Griesser et al., 2008).

The thermodynamic stability between polymorphs represents one of the most important points of concern in the pharmaceutical industry. It is crucial to ensure that the final product contains the desired polymorph, which was previously selected due to its physical properties combined with a suitable stability. The well-known expression of *disappearing polymorphs* perfectly exposes the numerous cases of crystals being observed over a period of time but not thereafter. Over the past decades, the combination of new crystallisation techniques and more accurate and precise screening approaches have significantly reduced the tendency for this phenomenon to happen.

1.4 Hydrates in the Pharmaceutical Industry

Hydrates are the most common type of solvates and the ones with highest importance from a pharmaceutical perspective. Hydrates can be formed as a result of processing (wet granulation, crystallisation, freeze drying or spray drying) or during storage, when exposed to an atmosphere containing water vapour.

The incorporation of water molecules into the crystal lattice produces a new unit cell different from that of the anhydrate. As a result, the intermolecular interactions within the solid change, which contribute to alter the enthalpy and entropy of the solid. This fact will result in changes in the free energy which consequently affects the thermodynamic activity of hydrates (Khankari and Grant, 1995).

Figure 1.6 below presents the effect on the physical properties of a drug as a consequence of hydration.

In this dissertation, a considerable attention was paid to the study of hydrates, Chapters 3 and 4. Although each of those chapters has its own introduction and related theoretical concepts, a general overview in the study of pharmaceutical hydrates is presented as below.

Water Molecules in the Crystal Lattice

Interactions between the molecules within the solid

Internal energy

Disorder due to thermal motions and spatial locations

Changes in the Free Energy

Thermodynamic activity

Solubility

Stability

Dissolution rate

Bioavailability and Product Performance
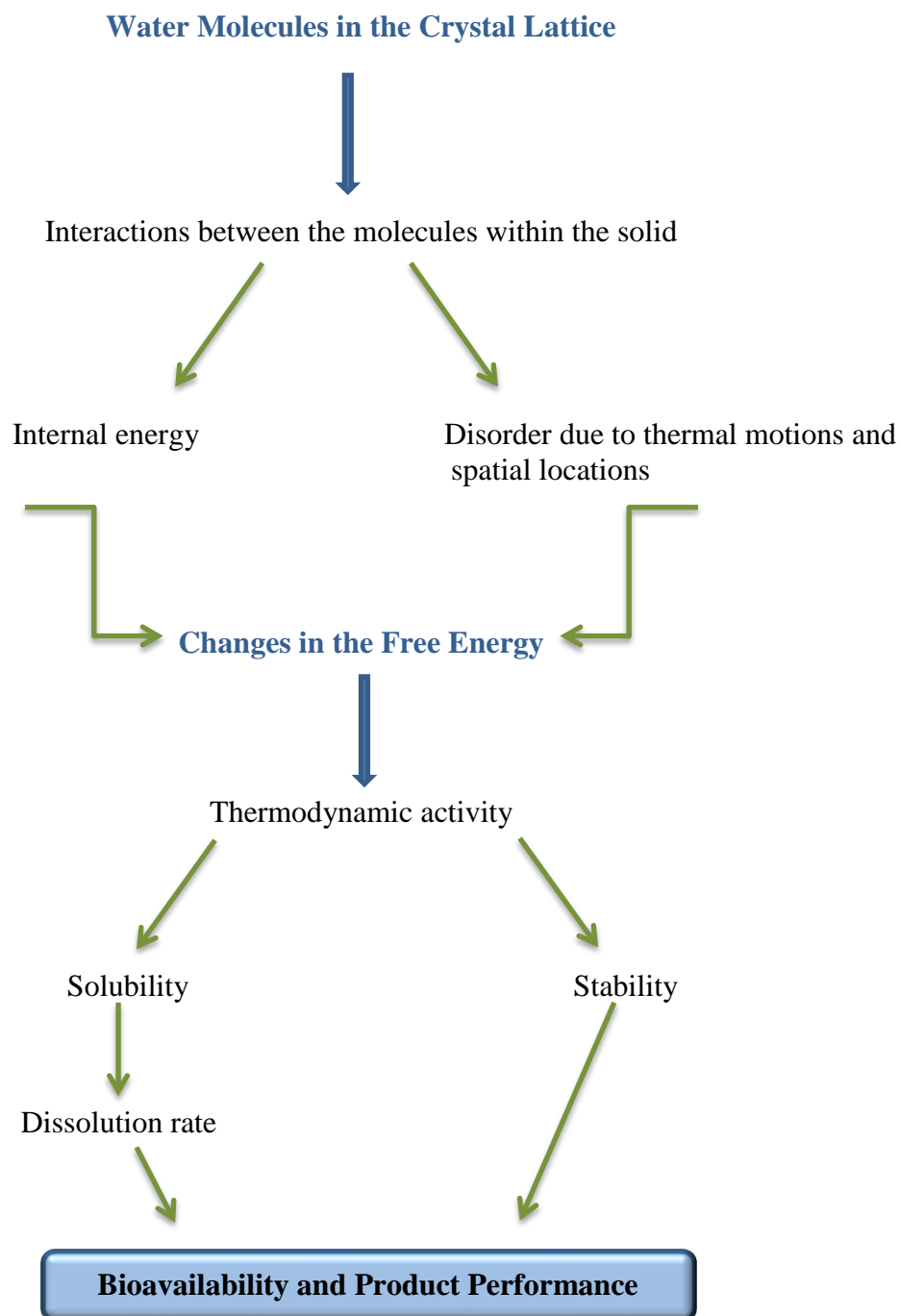
Figure 1.6: Effect of hydration on the physical properties of a pharmaceutical API (Khankari and Grant, 1995).

1.4.1 Classification of Hydrates

As referred earlier, hydrates incorporate water molecules in their crystal lattice, which can happen in a stoichiometric or non-stoichiometric manner.

Stoichiometric hydrates have a fixed, although not strictly integral, ratio of water to the compound (Hilfiker, 2006; Vippagunta et al., 2001). Generally, in this type of hydrates, water plays a structural role in the whole crystalline network and its dehydration frequently can lead to a disordered or amorphous state.

Non-stoichiometric hydrates have their water content dependent on the surrounding water vapour pressure and temperature. The water acts as a space filler of structural voids or channels and it is usually present in uncommon, yet well-defined, solvent/compound ratios (Rodríguez-Spong et al., 2004). Though, it is common practice in the pharmaceutical literature to wrongly round odd numbered water ratios to integer values. For example, caffeine 0.8 hydrate (Griesser and Burger, 1995) is still quoted as monohydrate. Non-stoichiometric hydrates can lose their water without changing the main structural characteristics and therefore, in this case, are called isomorphic dehydrates (Pfeiffer et al., 1970; Stephenson et al., 1998).

Hydrates in general and, non-stoichiometric hydrates in particular, represent a challenge for development due to its instability. The characterisation of hydrates doubtlessly needs more effort and time when compared to the characterisation of polymorphs and can be a real challenge. In the next section, specific points are presented to be considered in the characterisation of hydrated systems.

1.4.2   Insights on the Characterisation of Hydrates

Thermal Analysis

Dynamic scanning calorimetry (DSC) in combination with thermogravimetric analysis (TGA) and hot stage microscopy (HSM) are the most common techniques used in the study of hydrates. The use of DSC alone may not be very elucidative as endothermic transitions due to dehydration can be easily seen as melting, or the other way around. Furthermore, the distinction between true hydrates and sorbed water is not always straightforward (Craig and Reading, 2007). Different scenarios can be observed when carrying on a study of a hydrate compound in DSC (Giron, 1995). The dehydration and melting of the anhydrous phase can be observed in separate and therefore two endotherms are observed. On the contrary, if these two phenomena cannot be isolated and dehydration happens at the melting temperature, an exotherm might be seen as the new anhydrous phase recrystallises from the melt. The picture can become even more complex when a change in the hydration level is observed (see Chapter 3). The pan configuration, closed or open, can also influence the outcome of a DSC experiment, as well as the heating rate, crystal size and sample mass.

TGA measurements give information about the thermal stability of the hydrate form depending on the onset of the water loss. Less stable forms will show dehydration starting from low temperatures. More stable hydrated forms, usually the case of stoichiometric hydrates, show a water loss signal at well-defined temperatures. TGA has recently been used in combination with infrared spectroscopy to understand the thermal behaviour of other solvates and at the same time to confirm the nature of the vapour (Rastogi et al., 1999).

Moreover, TGA experiments performed under isothermal and/or non-isothermal conditions can be used to quantify the kinetic parameters of dehydration, such as activation energy (E_a) (Vyazovkin et al., 2011). Both methods have advantages/disadvantages and the hard decision is to know which one can give results with more accuracy. The biggest disadvantage of isothermal methods is the unavoidable non-isothermal heat-up time in the beginning of the experiment. As a result, if lower temperatures cannot allow the complete

dehydration in a reasonable time, higher temperatures can lead to a significant extent of conversion during that heating-up period. With regard to non-isothermal experiments, the biggest disadvantage is the difficulty in differentiating between the different kinetic models (Vyazovkin et al., 2011).

HSM is also a very helpful technique in the characterisation of hydrates. A widely used procedure when studying hydrates under HSM is by dispersing the sample in silicone oil in order to aid the visualisation of the thermally induced release of any included solvent. As dehydration occurs it is supposed to observe the formation of bubbles in the oil (Zhu and Grant, 2001; Zhu, 2006). Thus, attention must be paid during the data interpretation since this observation could be potentially complicated by the release of entrapped air from the solids or by the simple presence of air bubbles in the dispersion medium (Brittain, 2009).

The use of HSM often provides unique insights not afforded by other techniques and the combination with the results obtained from DSC and TGA, constitute an optimal routine approach.

Dynamic Vapour Sorption

Dynamic vapour sorption (DVS) experiments give information on the equilibrium water content as a function of relative humidity (RH) at a constant temperature. In the case of stoichiometric hydrates the water content at equilibrium may experience stepwise jumps whereas for non-stoichiometric a continuous increase in the water content until complete saturation of the structure might be observed (Hilfiker, 2006). Commonly, non-stoichiometric hydrates show identical profiles during sorption and desorption and hysteresis is not observed.

Attention should be paid to the kinetic stability observed during moisture sorption isotherm experiments. One would expect that at higher RH, a hydrated crystal form is more stable than the anhydrous form, however this cannot be readily transported when solubility experiments are performed. In fact, cases are reported of the opposite stability relationship, such as the example of LY334370 HCl used for the treatment of acute migraine, where the

anhydrous form is more stable in water than the dihydrate crystal (Reutzel-Edens et al., 2003b). Mannitol is an example of a metastable hydrate that converts to the anhydrous form when exposed to moisture (Yu et al., 1999).

Another important piece of information that can be derived when performing DVS experiments is related to the hygroscopic behaviour of the dehydrated phase. The definition of hygroscopicity combines thermodynamic driving forces and kinetic rates and can be broadly described by the amount and the rate of moisture uptake at a certain RH. Among all the classification systems that can be found in the literature, the one commonly followed was proposed by Callahan and it is based on data obtained from sorption isotherm experiments (Callahan et al., 1982), as presented in Table 1.1.

Table 1.1: Hygroscopicity classification scheme according to Callahan.

Class	Classification	Features
I	Non-hygroscopic	Essentially there is no moisture uptake at RHs below 90%. Furthermore, the increase in moisture content after storage for one week above 90% RH is less than 20%.
II	Slightly hygroscopic	There is no significant moisture uptake at RHs below 80%. The increase in moisture content after storage for one week above 80% RH is less than 40%.
III	Moderately hygroscopic	The moisture content does not increase more than 5% after storage at RHs below 60%. The increase in moisture content after storage for one week above 80% RH is less than 50%.
IV	Very hygroscopic	The increase in the moisture content may increase at RHs as low as 40 to 50%. The increase in moisture content after storage for one week above 90% RH may exceed 30%.

Adapted from (Callahan et al., 1982).

Crystallographic Studies

X-ray crystallography is a powerful technique for characterising water-solid interactions in crystalline hydrates, providing information about their structural behaviour and stability. The dehydration of non-stoichiometric hydrates lead to the formation of isomorphic dehydrates that tend to retain the three-dimensional structures of the parent compound. Dehydration resulted in shifts in the X-ray peak positions, as a function of lattice expansion or contraction. This is the behaviour of paroxetine HCl Form II described in Chapter 3 of this thesis. The use of variable temperature (VT) and variable humidity (VH) X-ray powder diffraction (XRPD) is sometimes imperative to monitor dehydration *in situ* or to investigate potentially complex solid state transformations (Rastogi et al., 2001).

Recently, significant developments in crystallographic computing systems have allowed to solve the structure of compounds by powder diffraction methods that have not been possible to be solved by single crystal methods (David et al., 1998; Stephenson, 2000). This represents a great achievement as many crystalline substances are complex or beyond the capability of single crystal techniques.

Nuclear Magnetic Resonance

In the past decade, nuclear magnetic resonance (NMR) relaxometry has been widely used to study water-solid interactions. Water absorption generally has a strong influence on molecular dynamics in solids and therefore ^{1}H and ^{13}C spin lattice relaxation is affected. Hydrogen bonding interactions between thiamine HCl and water were studied using NMR and the results showed a reduced molecular mobility for the hydrate phase in comparison with the isomorphic dehydrate (Te et al., 2003). In addition, the non-stoichiometric behaviour of LY297802 tartrate, a muscarinic agonist, was studied using solid state NMR in combination with X-ray crystallography (Reutzel, 1998).

1.4.3   Stability and Performance of Hydrates

When dealing with hydrates, their physical and chemical stabilities are important parameters to consider. Hydrates might dehydrate or change their hydration level during processing or storage, especially if they are in a metastable thermodynamic state. It is therefore crucial to understand their dehydration behaviour from both kinetic and thermodynamic standpoints before including a hydrated API in a final drug product formulation.

The physical stability of hydrates depends on the temperature and water vapour pressure in the surroundings of the solid. Dehydration can be described in a simplistic manner by the reaction below,

$$A(H_2O)n\ (s) \leftrightarrow A\ (s) + nH_2O\ (g)$$
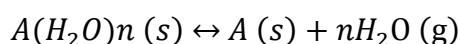
Please note the above reaction can be, from a thermodynamic point of view, reversible or irreversible.

Dehydration of crystalline solids represents an important group of heterogeneous reactions. Galwey proposed a classification for solid state dehydrations entitled '*Water Evolution Type*' (WET) based on a structural, observational and kinetic criteria (Galwey, 2000). This complex classification system was developed with the primary objective to reconcile the differences and inconsistencies related to the dehydration reactions.

In this classification, the author divided dehydration reactions into six main groups as briefly described below:

> **WET 1:** Crystal structure is maintained. This class includes hydrates that lose their intracrystalline water without significant modification of the host (original) structure.

> **WET 2:** Diffusion across an adherent and coherent barrier layer of product. In this group, the rate of dehydration is controlled by the diffusion of the water across the crystalline barrier formed by the dehydrated layer.

WET 3: <u>Interface advance, nucleation, growth and contracting envelope.</u> In general, the nucleation step determines the subsequent geometric development and starts at the crystal imperfections.

WET 4: <u>Homogeneous dehydration reactions in crystals.</u> The chemical change occurs with equal probability throughout the crystalline reactant.

WET 5: <u>Melting and the formation of poorly permeable outer layers.</u> Melting can be complete or partial, leading to difficulties in interpretation and development of kinetic equations to describe the process.

WET 6: <u>Comprehensive melting.</u> When the water is liberated during the complete melting of the solid.

Parameters such as particle size, morphology and the existence of crystal defects can strongly affect the dehydration behaviour of hydrates. Generally, the smaller the particle size, the faster is the dehydration process. Also, the presence of crystal defects, usually as a result of high-energy particle size reduction processes, can enable dehydration to start at that imperfection points and thus accelerating the whole process. The impact on the crystal morphology is normally more subtle (Brittain, 2009).

Apart from the physical stability, it is also important to consider the chemical stability of hydrates, namely pharmaceutical hydrates. An intriguing example of chemical stability is the case of cefixime trihydrate (Kitamura et al., 1990). When partially dehydrated, cefixime trihydrate was found to be unstable due to a highly disordered crystal structure caused by loss of its water of crystallisation, which enables a hydrolytic reaction. Although the anhydrous form is chemically stable it cannot be used because it readily picks up water and rehydrates on storage. Therefore a careful control of temperature and humidity conditions is needed upon storage in order to maintain the hydration state of this drug.

In terms of bioavailability and performance, anhydrous forms are, in general, more soluble in aqueous media than the corresponding hydrate forms (Pudipeddi and Serajuddin, 2005). This could be explained by the lower release of free energy when the hydrated form interacts with water in comparison with the anhydrate form. Nevertheless, some examples can be scattered from the literature showing hydrates to be more soluble than the

anhydrous form. An example is the case of norfloxacin, a broad spectrum fluoroquinolone antibacterial agent, where its hydrates are more soluble than the anhydrate form (Roy et al., 2008).

These differences in the hydration level of an API will be translated into distinct aqueous solubility/dissolution rates and, as a consequence, bioavailability. An example is the study carried out with ampicillin administrated to humans as anhydrous and trihydrate forms (Poole et al., 1968). This study showed higher blood serum concentrations for the formulations containing anhydrous ampicillin when compared to the concentrations produced by the trihydrate. Another aspect to be carefully considered as well is the phase transitions occurring during storage or dissolution experiments, as observed with nitrofurantoin (Wafik Gouda et al., 1984) and theophylline (Herman et al., 1989), respectively.

The determination of the aqueous solubility of metastable forms can in some cases be a challenge. This is the case of carbamazepine that can crystallise as an anhydrate and as a dihydrate form. The anhydrous form is reported to be practically insoluble in water, however this observation is difficult to be confirmed due to the transformation to the dihydrate, once it makes contact with water (Young and Suryanarayanan, 1991).

Above all, solid state hydrates represent a great slice in the pharmaceutical industry and their erratic behaviour hitherto still provides significant manufacturing and processing challenges. Nowadays, and taking advantage of characterisation methods, such as, dynamic vapour sorption, thermoanalytical, spectroscopic and X-ray diffraction techniques can be implemented to evaluate the kinetics, solid state properties and the nature of both tightly bound and disordered hydration water.

1.5   Polymorphism and Patents

Finally, a brief overview on the patent systems and legal aspects related to polymorphism is presented. Since crystal modifications of a compound represent different crystal entities with potentially different physical properties, pharmaceutical companies have all the

interest to claim the new discovery to be potentially recognised in the awarding of a patent. This will confer the inventor exclusive rights regarding the preparation, sale and use of the patented subject matter, which can be used to restrain competition and set prices higher than those that would have existed if competitive products were available (Hilfiker, 2006).

Several disputes in Court have been recorded over the past decades involving drugs with a strong position in the market. It is the case of ranitidine HCl, cefradoxil and paroxetine HCl. For the relevance to this study, the latter case will be presented in more detail.

Paroxetine HCl is a selective inhibitor of serotonin and it was firstly prepared as a maleate salt by Ferrosan, a Danish company in the 1970s. In 1980, Beecham (now Glaxo SmithKline – GSK) started scaling up the preparation of the hydrochloride salt of paroxetine and a hemihydrate crystal (Form I) was found (Barnes et al., 1988). GSK was able to start marketing paroxetine HCl hemihydrate since 1993 as Paxil$^{®}$.

Two years later, a Canadian generic company Apotex submitted an Abbreviated New Drug Application (ANDA) to the US FDA to market a formulation based on the anhydrate form of paroxetine HCl (Form II), and filed a certification that its proposed product would not infringe GSK's patent for the paroxetine HCl hemihydrate product. However, GSK claimed that Apotex's Form II naturally converts into the Form I, making it likely that there would be some Form I in Apotex's product, therefore infringing GSK's patent. Although the district court interpreted the claim as requiring the presence of commercially significant amounts of the hemihydrate for infringement to take place and found no reason to limit the scope in such a way.

The above case demonstrates the value of fully understanding the relationship between all the physical forms of an API. That information can therefore be used to develop the most effective and stable product in order to maintain the intellectual property protection for the innovator.

1.6   Amorphous Systems

Amorphous materials, also known as glasses, can be defined by the lack of long-range order between the molecules when compared to the crystalline structure, as described earlier. However, they do possess short-range order and each molecule can establish interactions with the neighbour molecules through hydrogen bonding, van der Waals or electrostatic interactions (Brittain, 2009).

In considering the importance of the amorphous state in pharmaceutical systems, they can be a result of three main circumstances. Firstly, a material may exist intrinsically in a fully or partially amorphous state, examples of which include mainly polymers such as polyvinylpyrrolidone (PVP), polyethylene glycol (PEG) and microcrystalline cellulose. Secondly, glassy drugs can be prepared intentionally to enhance aqueous solubility and dissolution behaviour. Common routes that can be used to prepare amorphous solids include quench cooling, solvent precipitation, mechanical activation, freeze drying and spray drying. Thirdly, crystalline materials can be inadvertently converted to amorphous during processing, some examples are milling, granulation and compression (Craig et al., 1999; Bruno and George, 1997).

1.6.1   Amorphous Solids: Formation and Properties

Familiar routes used to prepare amorphous solids include quench cooling, solvent precipitation, mechanical activation, freeze drying and spray drying. However, the most common technique to generate glasses is by the rapid cooling from the melt. The latter two technologies (freeze drying and spray drying) will be explained in more detail in further sections.

1.6.1.1   Generation of Amorphous Materials by Cooling from the Melt

Crystals have lower potential energies than glasses and therefore their formation should be more thermodynamically favourable. However, glasses are formed due to kinetic reasons. More specifically, crystallisation of supercooled liquids often 'needs some time' and may fail if 'insufficient' time is given. If this happens, a supercooled liquid may form a glass upon cooling.

When a liquid is rapidly cooled below its melting point (T_m) no discontinuity in enthalpy or volume is observed and the system forms a supercooled liquid, as shown in Figure 1.7. As the material is cooled further, there is a stage where the rate of cooling exceeds the rate of molecular rearrangement. At this point, the thermodynamic properties deviate from those of the supercooled liquid and a glass is formed (Taylor and Shamblin, 1999; Bruno and George, 1997). At this temperature, all the translational and rotational motions of the 'frozen' system are dramatically reduced and a change in heat capacity, C_p (which is the derivative of enthalpy with respect to temperature, $\partial H/\partial T$) is detected. This is known as the glass transition temperature (T_g).

When the thermodynamic properties (enthalpy, entropy and volume) of a supercooled liquid are extrapolated to temperatures below T_g, they converge with those of the crystalline materials, shown by the dashed line in Figure 1.7. This hypothetical point is known as the Kauzmann temperature (T_K) (Kauzmann, 1948). The T_K is considered to mark the lower limit of the experimental T_g and to be the point at which the configurational entropy of the system reaches zero (see Chapter 5). As a result, T_K can be a valuable indicator for the long-term storage stability of amorphous solids (Bruno and George, 1997).
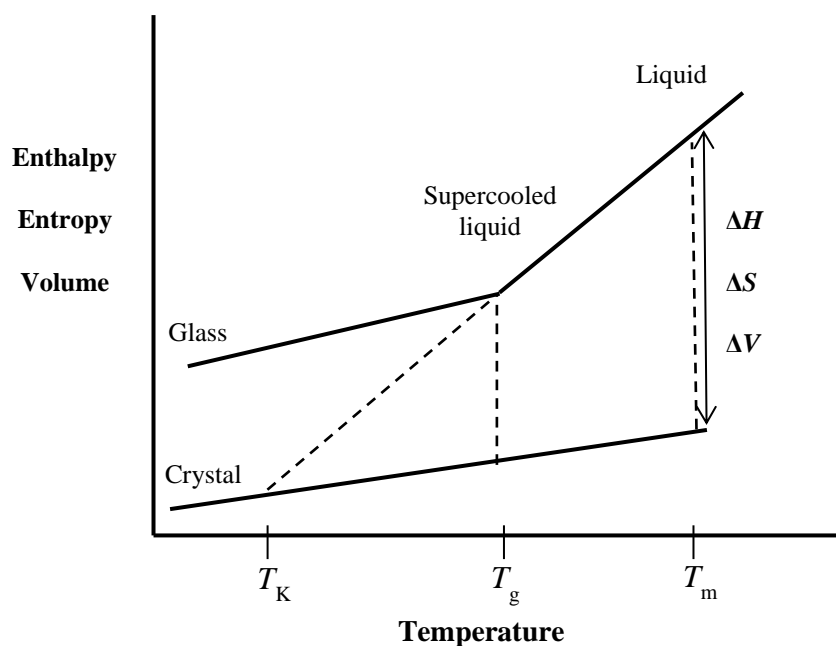
Figure 1.7: Schematic illustration of how the enthalpy, entropy and volume of a system changes as a function of temperature. Upper line denotes the pathway of an amorphous material while the lower line denotes the behaviour of a crystalline material (Bruno and George, 1997).

1.6.1.2   The Glass Transition Temperature

As outlined above, the glass transition temperature, T_g, is by definition, the temperature at which changes in the physical state of a material take place from a rubbery viscous liquid to a glassy mechanical material. Amorphous systems are mainly characterised by their thermodynamic instability where the excess in enthalpy and entropy trapped in the glassy material tends to be released over time and at temperatures near T_g. Therefore, T_g is a parameter often used to determine the physical and chemical stability of an amorphous material (Craig et al., 1999).

To carry out a measurement of T_g value for a pharmaceutical system, thermal approaches are commonly employed, such as differential scanning calorimetry (DSC), thermomechanical analysis (TMA), dynamic mechanical analysis (DMA) and dieletric analysis (DEA). DSC represents the most used method to characterise an amorphous system. TMA has been employed in the study of polymeric systems or cast films (Hancock et al., 1995), whereby the dimensional changes of an amorphous sample are measured as a

function of temperature. By using DMA, the changes in the viscoelastic properties of an amorphous material with temperature can be measured (Craig and Johnson, 1995). In the case of DEA, a sinusoidal oscillatory electric field is applied to the sample and the dielectric permittivity is measured as a function of temperature, showing an abrupt change through the T_g (Stickel et al., 1995).

1.6.1.3   Molecular Mobility and Enthalpy Relaxation

Molecular mobility of amorphous systems can be defined as the molecular motions associated with glass transition and represents one of the most important aspects for a comprehensive approach of the amorphous state (Bhattacharya and Suryanarayanan, 2009).

Since the molecular volume within an amorphous solid is larger than that in the corresponding crystalline phase, the enhanced molecular mobility in disordered solids affects their chemical and physical reactivity. Molecular motions are temperature dependent and, as a result minimal in the glassy state (in the sense of a system being below T_g) and greater above the glass transition. Another point of concern is the fact that amorphous materials are not static solids, but rather dynamic systems. As a consequence, their stability is determined by kinetic aspects which governs their transformation towards a more stable form (Byrn et al., 1994). For instance, recently numerous studies have been devoted to the characterisation of molecular mobility of pharmaceutical amorphous systems in order to predict their physical stability. These studies rely largely on the measurement of bulk properties, such as relaxation enthalpy or heat capacity (Shamblin et al., 2000).

One means of measuring mobility is to introduce a perturbation to the system (heat) and to see how the system returns to the initial state, a process known as relaxation. As the initial state is of higher enthalpy, heat is given off during the relaxation process, and this process is also known as enthalpy relaxation (Liu et al., 2002). Relaxation can be divided into α and β relaxation. The β-relaxation also called Johari-Goldstein relaxation is normally correlated to the motion of some constitutional parts of the molecules (i.e., groups of atoms), which is not coupled with the motion of the entire molecule. On the other hand,

α-relaxation or commonly known as structural relaxation reflects the motion of the whole molecule, i.e., changes in atomic/molecular arrangements that happen during the spontaneous conversion from the amorphous to crystalline state, in a scale of time and temperature influence (Kawakami and Pikal, 2005; Hilden and Morris, 2004).

The Kohlraush-William-Watts (KWW) equation is generally used to determine relaxation constants, which can be used to describe structural relaxation and correlate molecular mobility between different systems. First of all, it is necessary to estimate the maximum enthalpy recovery at that particular storage temperature, $\Delta H_{\text{max},T}$ (also called enthalpy relaxation at time infinity $\Delta H_{\infty,T}$), according to Equation 1.1 (Hancock et al., 1995; Hancock and Shamblin, 2001),

$$\Delta H_{max,T} = \Delta C_p^{Tg}(T_g - T)$$

Equation 1.1

where, ΔC_p^{Tg} is the heat capacity change between the glass and the liquid at T_g and T is the temperature at which isothermal relaxation is carried out.

From the maximum enthalpy recovery, it is possible to calculate the relaxation function (φ) at a given time (t) and under a defined temperature T, according to Equation 1.2,

$$\varphi_t = 1 - \frac{\Delta H_t}{\Delta H_{max,T}}$$

Equation 1.2

where, ΔH_t is the measured enthalpy recovery under those defined conditions.

This expression can then be used to calculate the molecular relaxation time (τ) as a meaningful and direct approach for quantifying molecular mobility as shown by Equation 1.3 known as the KWW equation,

$$\varphi_t = \exp(-\frac{t}{\tau})^{\beta}$$

Equation 1.3

where, β is the relaxation time distribution parameter, with a value between 0 and 1.

β is an indication of the homogeneity of the relaxation process. Values near to the unit correspond to an exponential function and are an indication of a narrow distribution of

states; values close to zero represent a broad distribution of states, and therefore, wide distribution of relaxation times. During the ageing experiments, τ increases with time and β decreases with time, therefore some authors recommend to use τ^{β} as a stability indicator, since it remains more or less invariant and it is less sensitive to experimental error (Kawakami and Pikal, 2005; Liu et al., 2002).

1.6.1.4   Physical and Chemical Stability

Amorphous solids are characterised by their intrinsic thermodynamic instability and irreversible tendency towards a most stable state. This phenomenon is known as recrystallisation and implies the release of the excess of energy stored by the amorphous material. The recrystallisation mechanism involves nucleation followed by crystal growth and is influenced by the storage conditions such as temperature and relative humidity. Molecular aggregation results in the formation of nuclei, followed by a nucleation phase that initiates growth, leading consequently to an actual growth phase (Bruno and George, 1997).

The molecular mobility in amorphous systems is low at temperatures below the glass transition but increases rapidly above it. It has been suggested that in order to reduce molecular mobility and therefore extent the physical stability, amorphous materials should be stored at a temperature at least 50 $^{\mathrm{o}}$C below its T_{g} (Hancock et al., 1995). However, this fact cannot be taken as a guarantee of stability; firstly, molecular mobility exists even below the glass transition temperature; secondly, it is not always possible to keep the amorphous samples 50 $^{\mathrm{o}}$C below the T_{g} value; thirdly, the stability of amorphous materials is system dependent. An example is the study carried out with glassy indomethacin and phenobarbital, both of which have similar T_{g} values and were stored below their T_{g} (Fukuoka et al., 1989). Phenobarbital was found to recrystallise within one week whereas indomethacin was stable for several years. Dissimilarities in their structure and the hydrogen bonding might be behind the differences observed. The relationship between T_{g} and the physical stability is therefore complex and certainly not straightforward.

Another aspect to consider on the stability of amorphous materials is the presence of residual amounts of water. Water has a very low T_{g} value around -135 $^{\mathrm{o}}$C (Hallbrucker et

al., 1989) and can act as plasticiser of amorphous solids by increasing the free volume of these materials, hence increasing its molecular mobility and leading to a decrease in T_g (Ahlneck and Zografi, 1990). On the contrary, some excipients can act as stabilisers in amorphous pharmaceutical formulations and consequently have an antiplasticising effect increasing the overall glass transition of the mixed system (Bruno and George, 1997).

In terms of chemical reactivity, amorphous solids show, in general, greater chemical reactivity when compared to crystals. This is due to the enhanced degree of molecular mobility and therefore higher potential for intramolecular and intermolecular chemical reactions (Brittain, 2009). A well-documented example is the case of cefoxitin sodium (Oberholtzer and Brenner, 1979). Amorphous cefoxitin sodium showed a considerably higher rate of thermal degradation and colour change compared to its corresponding crystalline form.

One plausible reason for the increased reactivity of amorphous compounds could be related to their tendency in absorbing high amounts of water. According to Shalaev and Zografi, water can promote chemical reactivity in amorphous systems acting in four different possible ways: a reactant, a product, plasticiser or as a reaction medium (Shalaev and Zografi, 1996). The versatility of water alone makes it a critical participant in many types of reactions. In addition, the ubiquitous nature of water, in combination with its plasticising effect, makes water a culprit in the chemical degradation of many amorphous drugs.

1.7   Solid Dispersion Technology

The use of solid dispersions was firstly introduced in the pharmaceutical field in the early 1960s by Sekiguchi and Obi (Sekiguchi and Obi, 1961). The authors found that the formation of eutectic mixtures of drugs with water soluble carriers by the melting of their physical mixtures resulted in a significant bioavailability enhancement. An eutectic mixture simply consists of two compounds which are completely miscible in the liquid state but only to a very limited extent in the solid state (Goldberg et al., 1965). As a result,

the faster dissolution rate and thereby improved bioavailability is a consequence of the reduced particle size and better wettability of the API in the polymer matrix.

Currently, the definition of solid dispersion refers to the dispersion of the drug in a biologically inert matrix at a solid state prepared by fusion or solvent methods (Chiou and Riegelman, 1971). This formulation strategy has been explored for decades in order to improve bioavailability of poorly soluble compounds. Figure 1.8 is a schematic timeline representation of the different carriers used to prepare solid dispersions. In the early beginning crystalline carriers were used such as urea (Goldberg et al., 1966) and sugars (Kanig, 1964). These systems have the disadvantage of forming crystalline solid dispersions, which did not release the drug as quickly as the amorphous ones, though they were thermodynamically more stable.

Therefore, a second generation of solid dispersions emerged, containing amorphous carriers instead of crystalline. Commonly, the amorphous carrier is a synthetic polymer such as polyvinylpyrrolidone based polymers (PVP) (Simonelli et al., 1969; Weuts et al., 2005), polyethyleneglycols (PEG) (Urbanetz, 2006; Bley et al., 2010) or polymethacrylates (Huang et al., 2006); natural product based polymers can also be used to prepare solid dispersions and are mainly composed by cellulose derivatives, such as hydroxypropylmethylcellulose (HPMC) (Konno and Taylor, 2006), ethylcellulose (Desai et al., 2006), hydroxypropylcellulose (Repka et al., 1999) or starch derivate, like cyclodextrins (Mura et al., 1999b).

Recently, the third generation of solid dispersions appeared taking advantage of the surface activity or self-emulsifying properties of certain carriers or specific materials. These systems are designed to achieve the highest degree of bioavailability for poorly soluble drugs and to maximise the stability of the prepared solid dispersion system. Examples of surfactants selected for this purpose are inulin (Van Drooge et al., 2006), Gelucire 44/14^{TM} (Yüksel et al., 2003) and poloxamer 407 (Majerik et al., 2007). The association of amorphous polymers and surfactants is also a common approach (Ghebremeskel et al., 2007). The inclusion of surfactants in the formulation containing a polymeric carrier may help to prevent precipitation and agglomeration of fine crystalline particles. On the other hand, lipid-based formulations have been shown to enhance oral absorption of lipophilic drugs, although the exact mechanism is complex and not yet fully understood (Pouton,

2000). Finally, the combination of polymers with different physicochemical properties can represent a good strategy in increasing the physical stability of solid dispersions when compared with single polymer based systems (Yang et al., 2013; Sakurai et al., 2012).
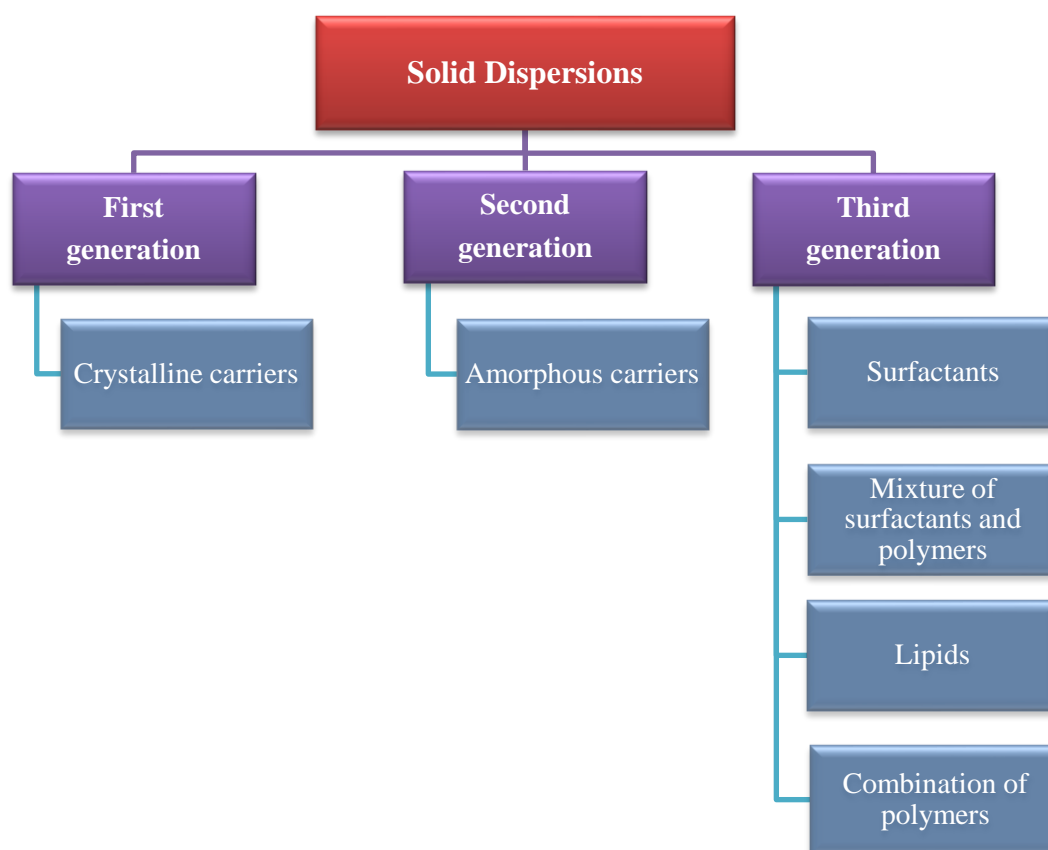
Figure 1.8: Classification of solid dispersions according to the nature of the carrier selected (adapted from (Vasconcelos et al., 2007)).

1.7.1 Preparation Methods for Solid Dispersions

1.7.1.1   Melting Methods

1.7.1.1.1. Traditional Melting Methods

The melting method is the oldest and the easiest way to prepare solid dispersions, provided the drug and the carrier are miscible in the molten state. This method consists of melting the drug within the carrier followed by cooling and pulverisation of the obtained product (Lloyd et al., 1997). The time allowed for the formation of the glass in the supercooled melt is considered a critical parameter for the stability of the resulting amorphous material. The cooling rate of the melt should be chosen depending on the spontaneous tendency of each compound to recrystallise, and can be slow at room temperature or fast in an ice bath or by immersion in nitrogen liquid. Generally, faster cooling rates lead to the preparation of more stable amorphous systems, as the time scale available for molecular reorganisation is lower.

Limitations of this method include the thermal stability of both drug and polymer at the melting temperature and the existence of miscibility gaps in the phase diagram that can lead to the formation of a product not homogeneously dispersed. Moreover, this method is not suitable to a scale-up preparation of solid dispersions.

1.7.1.1.2   Hot Melt Extrusion

Hot melt extrusion (HME) method consists of the extrusion of the drug and carrier, previously mixed, at an elevated temperature for a short period of time. The resulting product is then collected after cooling at room temperature (Shah et al., 2012). Since this technique was used in this work to prepare solid dispersions it will be described in more detail in Chapter 2.

1.7.1.2   Solvent Methods

1.7.1.2.1   Solvent Evaporation Methods

Solvent evaporation methods were firstly introduced in the 1960s and since then many workers have taken up this method for the preparation of solid dispersions (Tachibana and Nakamura, 1965). The solvent evaporation method consists of the dissolution of the drug and carrier in a volatile solvent that is later evaporated. In this method, the thermal decomposition of drugs or carriers can be prevented, since the evaporation of the organic solvent occurs at low temperatures. However, it is a prerequisite that both the drug and polymer are soluble in the solvent, usually ethanol, chloroform or dichloromethane.

1.7.1.2.2   Freeze Drying

The basic freeze drying process consists in three main steps: freezing, primary drying (by sublimation) and secondary drying (by desorption). The drug and carrier are dissolved in a common solvent (usually water), which can be immersed in liquid nitrogen until it becomes completely frozen (Tang and Pikal, 2004).

In this first step, two phases are formed: one is the frozen solvent and the other is the highly concentrated solute termed as 'freeze concentrate'. The next step is the primary drying which involves the sublimation of the frozen solvent under vacuum and with relatively low temperature in order to enhance the sublimation of the solvent. After this step, the product still contains a certain amount of water, ranging from 5 to 20%, depending on the nature of the formulation. Therefore, in the secondary drying the shelf temperature is raised at much higher temperature than in the primary drying step so that desorption of the residual solvent occurs at a high rate (Tang and Pikal, 2004; Craig et al., 1999).

Besides of its use to prepare rapidly dissolving oral dosage forms, freeze drying has also gained considerable application in the processing of pharmaceutical products of biological origin including vaccines, peptides and liposomes (Craig et al., 1999).

1.7.1.2.3   Spray Drying

Spray drying is a well-established method for processing solutions, emulsions and suspensions into powders, efficiently controlling the size, density and morphology of the particles. Spray drying is one of the most commonly used solvent evaporation techniques in the preparation of solid dispersions. It consists of dissolving or suspending the drug and carrier, then spraying it into a stream of heated air flow to remove the solvent.

Similarly to HME, spray drying will be discussed in more detail in Chapter 2 of this dissertation.

1.7.1.2.4   Electrospinning

Electrospinning has gained particular interest in the last five years due to its simple and versatile ability to produce nanofibers suitable for the delivery of poorly water soluble drugs. During the electrospinning process a solution containing the polymer and API is pumped through a thin nozzle with an inner diameter on the order of 100 mm. The nozzle simultaneously serves as an electrode, to which a high electric field of 100–500 kVm is applied. This results in charge being induced within the solution, which causes the initiation of a jet. As this jet travels the solvent's evaporation is accelerated and the electrospun fibers can be collected (Greiner and Wendorff, 2007). This process is schematically represented in Figure 1.9. As the solvent evaporates, the drug molecules are dispersed in the polymer fibers matrix, producing electrospun fibers that can enhance drug solubility (Bikiaris, 2011; Ignatious et al., 2010).
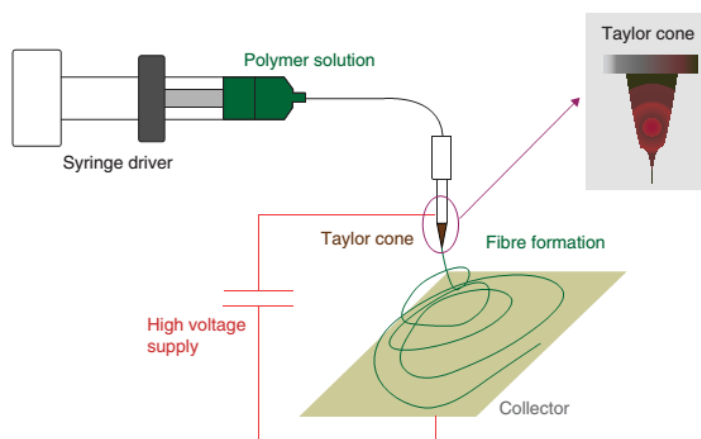
Figure 1.9: Illustration of the electrospinning procedure (Bikiaris, 2011).

Electrospinning technology has several advantages when compared with other solvent based techniques used to prepare solid dispersions: firstly, it is a one-step manufacturing process of amorphous solid dispersions that can be easily scalable; secondly, the prepared electrospun fibers have a very large area-to-volume ratio organised in a three-dimensional continuous web structure, which gives higher available surface area; thirdly, a small solvent content was found to remain in the final products (Yu et al., 2010).

1.7.2   Advantages, Disadvantages and Concerns of Solid Dispersions

In recent years, there has been an increased interest in the use of amorphous APIs in various formulations, especially when their crystalline forms are shown to exhibit poor aqueous solubility. This often compromises dissolution within the gastrointestinal tract and may be the rate limiting step to absorption, ending with inadequate oral bioavailability (Brouwers et al., 2009). Amorphous forms tend to exhibit high levels of supersaturation in aqueous media relative to the crystal, and thus higher apparent solubility. This increase arises from the lack of a highly ordered crystal with lattice energies that must be overcome to attain adequate solubility of the crystal.

As compared to single component amorphous APIs, the presence of a hydrophilic carrier in amorphous solid dispersions can contribute to increase the wettability of the drug and at the same time act as crystallisation inhibitor improving their physical stability.

However, despite the advantages of solid dispersion formulations they are not broadly used in commercial products, mainly because there is the possibility that during processing (mechanical stress) or storage (temperature and humidity stress) the amorphous state may undergo crystallisation. Moreover, phase separation between the drug and the polymer can also promote crystal growth. This may result in decreased solubility and dissolution rate (Pokharkar et al., 2006; Vasconcelos et al., 2007). Therefore, exploitation of the full potential of amorphous solids implies a suitable stabilisation in solid state, as well as during *in vivo* performance.

The first concern when intending to prepare solid dispersions with an API and a polymer is to evaluate their degree of miscibility. Approaches such as melting point depression (MPD) and solubility parameter (δ) are often used to infer on the miscibility of a system; these two methods will be discussed in Chapters 6 and 7. It is also well-recognised that the addition of polymers with a high T_g can increase the T_g of the miscible mixture, thereby reducing the molecular mobility at regular storage temperatures (Weuts et al., 2005). Additionally, drug-polymer specific interactions between functional groups, in general through hydrogen bonds, tend to increase the energy barrier against recrystallisation (Matsumoto and Zografi, 1999). Finally, specific properties of the polymer such as the degree of hygroscopicity can represent a considerable advantage in the stabilisation of these systems. The influence of the polymer type in the preparation of amorphous solid dispersions of olanzapine, a poorly water soluble antipsychotic drug, will be explored in Chapter 7 of this thesis.

1.8   Phase Transformations during Processing

After the identification and thorough characterisation of the most appropriate physical form of an API, it is important to ensure that the selected crystal form is retained in the

final pharmaceutical product. Stresses induced during production and interactions with formulation components can lead to phase transformations. Understanding the effect of each processing step on the API physical form is therefore very important in ensuring the phase purity of the drug substance used throughout the product development stream (Brittain, 2009).

Generally, the transformations of the materials can be simply classified as solid-solid (phase transition, deformation), solid-liquid (melting, crystallisation) or solid-gas (sublimation, condensation) (Morris et al., 2001). More specifically in the pharmaceutical field, scenarios of amorphisation, crystallisation, polymorphic transitions and incorporation or removal of solvents from the crystal lattice are the most relevant physical solid state transitions (Figure 1.10). As a result, properties such as stability, solubility, dissolution, bioavailability, density, hardness, etc., might be influenced by phase transformations. A brief description of the impact of pharmaceutical processes on solid phase transformations is presented.
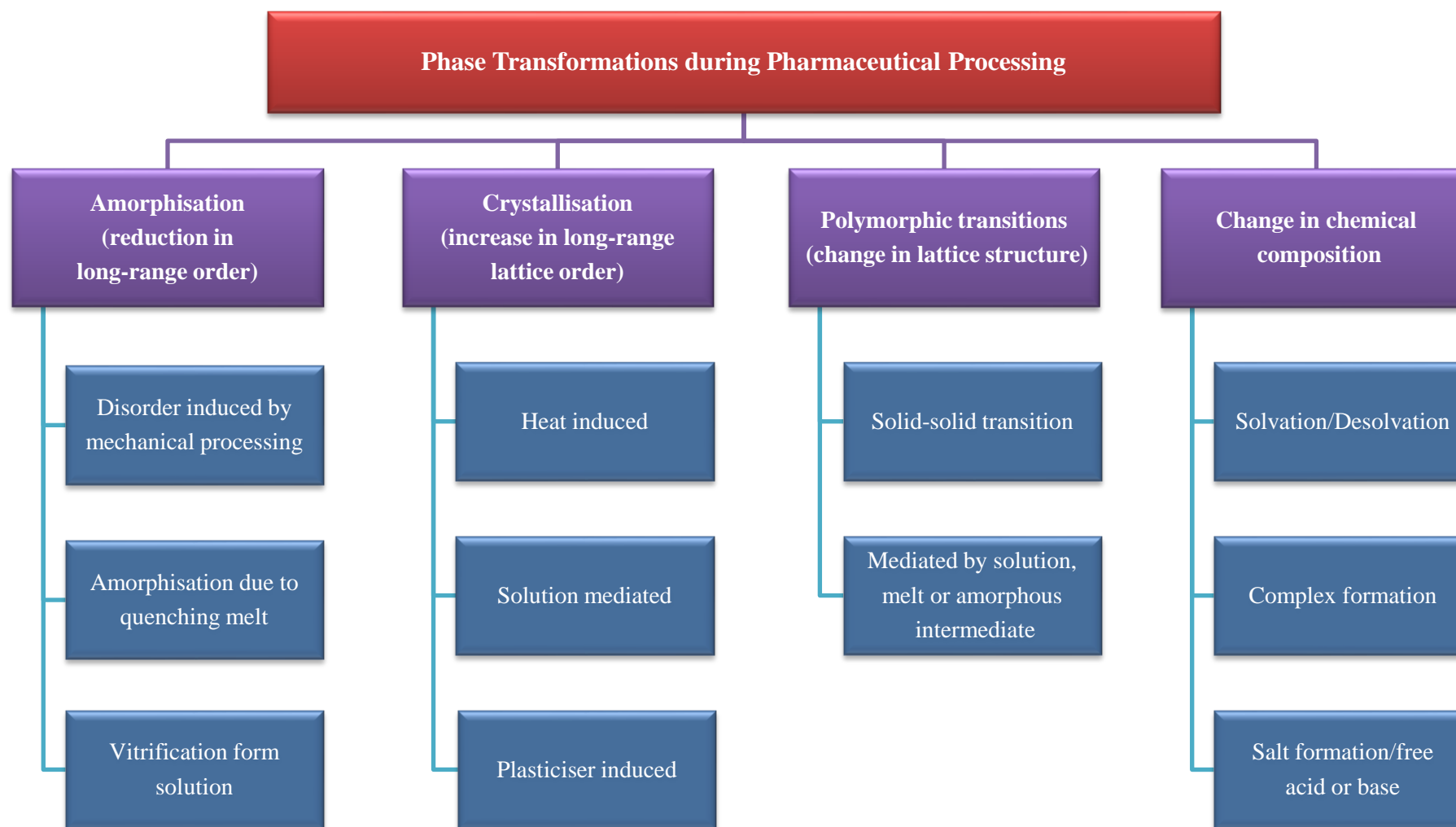
Figure 1.10: Schematic representation of possible phase transformations induced during processing (adapted from reference (Hilfiker, 2006)).

1.8.1 Milling

Milling is one of the first steps during solid product processing that leads to particle's fracture and size reduction. This might facilitate subsequent processing and enhance product performance. Nevertheless, it is important to account that milling normally imparts mechanical stress and generates heat and vibrational energy that can induce phase transitions such as polymorphic transitions and vitrification via solid state (amorphisation) (Zhang et al., 2004).

Several cases can be found in the literature reporting solid phase transformations during milling. One example is the case of ranitidine HCl (Chieng et al., 2006). The authors studied the effect of the milling conditions on the polymorphic stability of ranitidine HCl Form I. Ranitidine HCl Form I was found to convert to Form II or an amorphous form depending on the temperature at which the milling process was carried out. Additionally, it is important to bear in mind that crystalline materials can also be converted to amorphous solids by continuous grinding via dehydration/desolvation. Carbamazepine dihydrate was milled at different environmental humidity conditions and it converted to an amorphous phase after the removal of the first mol of water. The amorphous form then transformed into the anhydrate after dehydration of the second mol of water (Otsuka et al., 1999). A direct polymorphic transition was observed with caffeine metastable Form I that rapidly converted to the stable Form II after 3 min of milling time (Pirttimaki et al., 1993).

1.8.2 Wet Granulation

In general, a granulation step may be required in order to improve the flow and consolidation properties of a blend as it proceeds into tableting. Commonly, two methods are used to prepare suitable granules: (1) wet granulation, that involves an aqueous or hydro-alcoholic binder solution (alone or with a polymer) is added to a dynamic powder bed and a drying step is followed; (2) dry granulation on the other hand is typically used

when the formulation ingredients are sensitive to moisture or elevated drying temperatures (Zhang et al., 2004). As a result, wet granulation is more likely to induce phase transitions, especially with compounds that tend to form stable hydrates at ambient conditions. Therefore, depending on the exposure time to the granulation liquid and drying conditions, the final product can be a mixture of an anhydrous, a metastable or even partially or total amorphous forms.

Anhydrous forms of theophylline and carbamazepine were found to be transformed into their respective hydrates during aqueous wet granulation (Otsuka et al., 1997; Debnath and Suryanarayanan, 2004). Another example is the case of thiamine HCl, a relatively water soluble nutritional factor (vitamin B_1) that was found to dissolve in the granulation fluid (Wostheinrich and Schmidt, 2001). As a consequence, multiple phase changes were detected during processing, with conversion into the most stable hemihydrate form during storage.

1.8.3   Compression

As with milling, the compression of powders to prepare tablets involves the application of significant force, which may cause solid phase transformations in either the API or the excipients. Compression can induce dissolution of crystals in adsorbed water or conversion to stable/unstable or even amorphous forms. Polymorphic transformations of caffeine, sulfabenzamide and maprotiline HCl were studied as function of powder particle size and compression forces (Chan and Doelker, 1985).

1.8.4   Freeze Drying

Another process that can result in phase transitions is freeze drying. Lyophilised products are often unstable and may also undergo phase conversions during processing. A complex

example is mannitol that has a tendency to freeze dry as a combination of crystalline and amorphous solids. Therefore, slight variations in the lyophilisation process can result in the generation of different solids (Haikala et al., 1997).

Overall, APIs and excipients are exposed to different kinds of stresses during manufacture which can result in phase transformations. The most commonly observed transitions are amorphous ↔ crystalline, anhydrate ↔ hydrate and polymorphic conversions. The characterisation and identification of such transitions is not always straightforward due to the presence of multiple components in the formulation. Therefore it is important to perform a thorough physical characterisation of the API throughout the manufacturing line as a way to detect and control possible phase transformations during processing.

1.9   Research Objectives

In this thesis, structural characterisation from basic structure of two APIs (olanzapine and paroxetine HCl) was carried out and extended through the formulation into solid dispersion systems. Furthermore, the structure-property relationship was linked to the experimental performance and physical stability. The main objectives of each individual chapter are presented in more detail in the preceding Scope and Overview section.

2   MATERIALS AND METHODS

2.1 Materials

2.1.1 Paroxetine Hydrochloride

Paroxetine hydrochloride (HCl) is functionally classified as a selective serotonin re-uptake inhibitor (SSRI) that enhances serotonergic transmission by blocking the pre-synaptic active membrane transport mechanism and therefore increases the serotonergic activity at the post-synaptic receptor, as illustrated in Figure 2.1. Paroxetine HCl has been used for the treatment of depression, obsessive-compulsive disorder, panic disorder and social phobia (Bourin et al., 2001; Johnson, 1992).

Paroxetine HCl can exist in two different crystal forms, Form I and II. Form I is a hemihydrate and the most stable form of paroxetine HCl. Paroxetine HCl Form II had been previously classified up to this study as a very hygroscopic anhydrous form (Buxton et al., 1988). This form was thoroughly studied in this work and results are presented in Chapter 3 of this dissertation.
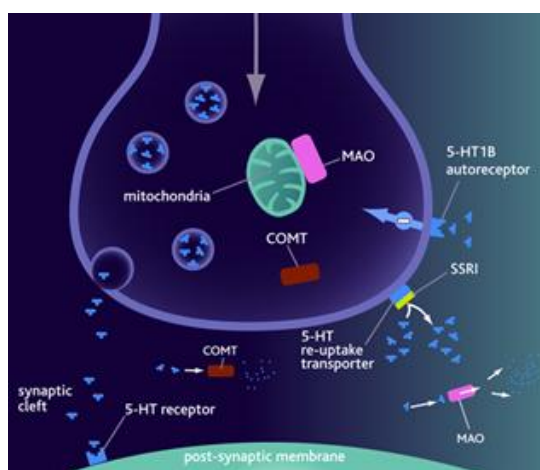
Figure 2.1: Mechanism of action of specific serotonin (5-HT) reuptake inhibitors (SSRI) (www.cnsforum.com).

Figure 2.2 presents the chemical structure of paroxetine HCl.
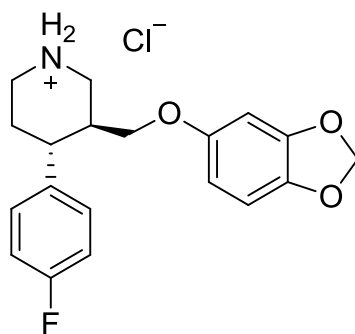
Figure 2.2: Chemical structure of paroxetine HCl.

Table 2.1 presents a list of general physicochemical properties of the two forms of paroxetine HCl, Forms I and II, which will be studied further in the following chapters.

Table 2.1: General physicochemical properties of paroxetine HCl Forms I and II.

Properties	Form I	Reference	Form II	Reference
IUPAC Name	(3S,4R)-3-[(1,3-Benzodioxol-5-yloxy)methyl]-4-(4-fluorophenyl)piperidine		(3S,4R)-3-[(1,3-Benzodioxol-5-yloxy)methyl]-4-(4-fluorophenyl)piperidine	
Chemical Formula	$C_{19}H_{20}FNO_3.HCl.^1/_2H_2O$		$C_{19}H_{20}FNO_3.HCl$	
General Designation	Stoichiometric hydrate (Hemihydrate)	(Barnes et al., 1988)	Non-stoichiometric hydrate*	Chapter 3
Molecular weight (MW)	374.83 g/mol		365.83 g/mol	
Density (ρ)	1.35 g/cm^3	(Yokota et al., 1999)	1.36 g/cm^3	(Howard et al., 2003)
Entries in the CSD**	GODVAW GODVAW01		EHOXEE	

*Note that this is a finding of the current work and the evidence for this assertion is outlined in Chapter 3
**Cambridge Structural Database

2.1.2 Olanzapine

Olanzapine, a thienobenzodiazepine derivative, is a second generation (atypical) antipsychotic agent used in the treatment of schizophrenia, depressive episodes associated with bipolar disorder and acute maniac episodes (Bhana and Perry, 2001; Bhana et al., 2001). It has shown *in vitro*, binding affinity for a broad range of neurotransmitter receptors (serotonin 5-HT$_{2A-C}$, adrenergic, histamine H$_1$ receptors, dopamine D$_1$ and all five types of the muscarinic receptors).

Olanzapine has been suggested to crystallise in more than 25 crystal forms, including several anhydrates, hydrates and solvates. Recently, a paper published by Bhardwaj et al. determined the crystalline structure of 24 new solvate forms (Bhardwaj et al., 2013). The same group calculated the crystal energy landscape of different forms of olanzapine and concluded that olanzapine molecules have a packing efficiency no more than 70%, which explained the prolific tendency to form solvates.

In this work olanzapine Form I was used to prepare solid dispersions with different polymers via hot melt extrusion (Chapter 7). Form I is an anhydrous form and the most stable crystalline form of olanzapine. Its chemical structure and main physicochemical properties are presented below in Figure 2.3 and Table 2.2, respectively.
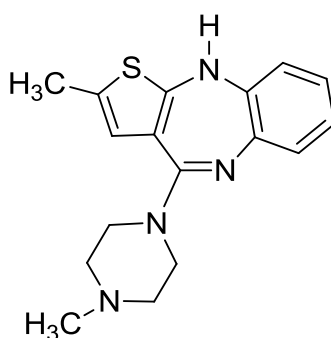
Figure 2.3: Chemical structure of olanzapine.

Table 2.2: Physicochemical properties of olanzapine Form I.

Properties	Olanzapine Form I	Reference
IUPAC Name	2-methyl-4-(4-methylpiperazin-1-yl)-5H-thieno [3,2-c][1,5]benzodiazepine	
Chemical Formula	$C_{17}H_{20}N_4S$	
General Designation	Anhydrate Form I	(Reutzel-Edens et al., 2003)
Molecular weight (MW)	312.43 g/mol	
Density (ρ)	1.30 g/cm^3	(Reutzel-Edens et al., 2003)
Entries in the CSD	UNOGIN UNOGIN01	(Reutzel-Edens et al., 2003, (Wawrzycka-Gorczyca et al., 2004a)
Recrystallisation from solvents	Can be recrystallised from anhydrous solvents such as ethyl acetate, toluene, propyl acetate, isopropyl acetate, butyl acetate, tetrahydrofuran and acetone. As well as from desolvation of several low alcohol solvates viz., methanol, ethanol and propanol and from dihydrates B, D and E	(Bunnell et al., 1996, 1998; Wawrzycka-Gorczyca et al., 2004a; Bunnell et al., 2001; Reutzel-Edens et al., 2003a)
Entries in the CSD	UNOGIN UNOGIN01	(Reutzel-Edens et al., 2003, (Wawrzycka-Gorczyca et al., 2004a)
Others	Adopts mirror-related conformation (conformer A and B)	(Reutzel-Edens et al., 2003)

Table 2.3 below presents a resume of several polymorphic and pseudopolymorphic forms of olanzapine described in the literature, their properties and preparation methods.

Table 2.3: Principal characteristics and properties of other forms of olanzapine.

Solid State Classification	Designation	Principal Features
Anhydrates	Form II	❖ Considered to be metastable and not well suited for commercial use in pharmaceutical formulations; ❖ Prepared from desolvation of methanol solvate and crystallised from acetonitrile and dichloromethane (Reutzel-Edens et al., 2003a; Bunnell et al., 1997); ❖ Single crystals of this form were isolated in a recent work (Bhardwaj et al., 2013), which allowed to finally obtain its crystal structure;
	Form III	❖ Prepared by dissolving Form I or II in aqueous acid solution (HCl, H_2SO_4, CH_3COOH) followed by a precipitation of olanzapine from the resultant salt using a methanolic solution (Hamied et al., 2002); ❖ Reutzel-Edens et al. (2003) stated in their work that the attempts to prepare pure Form III were not successful. However the desolvation in mild conditions of CH_2Cl_2 and $CHCl_3$ solvates result in Form III free of Form II, but still not yield to a pure Form III;
Hydrates	Dihydrates B, D and E	❖ The structure of three dihydrates (B, D and E) and its relative stability has been reported by Reutzel-Edens et al. (2003). In their work, the dihydrates B and E showed a lower dehydration temperature ($\approx 25\ ^{o}$C) in comparison to the dihydrate D ($\approx 50\ ^{o}$C); ❖ The hydrates B and E are considered to be channel hydrates; ❖ Dihydrate D is considered to be the most stable, having a more organised crystal packing and therefore a higher dehydration temperature; ❖ Refcodes of the dihydrates of olanzapine deposited in the CSD: AQOMAU (dihydrate D), AQOMAU01 (dihydrate B) and AQOMAU02 (dihydrate E);

89

	Higher hydrate	❖ Crystallise from EtOAc-toluene-water mixtures at temperatures lower than 55 $^{\circ}$C and dichloromethane-water mixtures; ❖ It is a metastable form containing 2-2.5 mol of water; ❖ It converts to the dihydrate E within few minutes after being isolated from the crystallisation solution; ❖ Two hydrate forms are reported in the CSD: AQOMEY (Reutzel-Edens et al. 2003) and AQOMEY01; the last entry, is described to be submitted into CSD by (Wawrzycka-Gorczyca et al. 2007), however no information is available in the published paper;
Two components (solvent-olanzapine) solvates	Ethanol and 1-propanol solvate	❖ Its desolvation leads to Form I (Bunnell et al. 1997);
	Methanol solvate	❖ The desolvation of this solvate lead to Form I (Bunnell et al., 1997); ❖ Its structure has been reported (Wawrzycka-Gorczyca et al., 2004b) and deposit into the CSD (UNOGOT); ❖ Accordingly to the solved structure, the methanol molecules are localised in channels;
	Dichloromethane solvate	❖ It has been firstly prepared (Larsen, 1997) by dissolving olanzapine in CH_2Cl_2 at 30 $^{\circ}$C and keeping the mixture isothermal for 30 min, followed by a rapid cooling in an ice-bath; ❖ The structure of this form solved later in 2007 and submitted to the CSD with the refcode WEXQAS (Wawrzycka-Gorczyca et al., 2007); ❖ It is described to crystallise in a ratio of 1:2 solvent-drug molecules; ❖ The intermolecular hydrogen bonds N-H···N found in Form I, were also reported for this structure; ❖ It is an unstable form and its desolvation results in olanzapine Form I;

Three components (water-solvent-olanzapine) solvates	Methanol solvate monohydrate	❖ The structure of this solvate was solved (Capuano et al., 2003) and submitted to the CSD (refcode: ELEVOG); ❖ The piperazine ring adopts a chair conformation with the methyl group in a equatorial position;
	Dimethylsulfoxide solvate monohydrate	❖ The solved structure (Polla et al., 2005) showed a water:DMSO proportion of 1:0.40 and to be isostructural to others solvates, viz., methanol solvate and methanol solvate monohydrate; ❖ Refcode in CSD: CAYTUS; ❖ It completely desolvates upon heating (weight loss = 13%) and melts as olanzapine Form I;
	Methanol solvate dihydrate	❖ Its structure has been solved (Wawrzycka-Gorczyca et al., 2007); ❖ It is described to crystallise in a ratio of 2:1:2 olanzapine:ethanol:water, respectively; ❖ As previously mentioned, olanzapine molecules are arranged into dimers which are hydrogen bonded to water and ethanol molecules; ❖ Refcode in the CSD: WEXQEW;
	Butan-2-ol solvate monohydrate	❖ The crystalline structure showed that the olanzapine dimers are linked through bridges established by the water molecules (Wawrzycka-Gorczyca et al., 2007); ❖ The stoichiometry of this three component solvate is 1:1:1 (olanzapine:butan-2-ol:water) and its refecode in CSD is WEXPUL;
	Isopropanol solvate dihydrate	❖ It is described to crystallise with a stoichiometry 2:1:2, olanzapine:isopropanol:water, respectively (Kotar-Jordan et al., 2011); ❖ It can be converted into to a methylene chloride solvate and then to olanzapine Form I;

2.1.3 Polyvinylpyrrolidone

Soluble polyvinylpyrrolidone (PVP), also known as Povidone, is obtained by free-radical polymerisation of vinylpyrrolidone in water or 2-propanol (Bühler, 2005), yielding the chain structure shown in Figure 2.4.
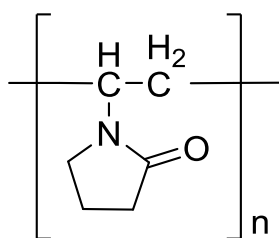
Figure 2.4: Chemical structure of PVP.

PVP is classified as an extremely hygroscopic substance, which is attributed to the electronegative groups of the carbonyl group in the pyrrolidone structure able to establish hydrogen bonding with water (Callahan et al., 1982).

Differentiation between the different grades of PVP homopolymers is made based on their molecular weights and relative viscosity in water. Therefore, it is possible to calculate a K-value for each grade according to the Ph. Eur. and USP monographs. Within the PVP homopolymers family, higher K-values are related to higher molecular weight and therefore higher viscosity (Bühler, 2005).

In terms of pharmaceutical applications, PVP is commonly used as adhesive and binder, particularly important in tableting and also incorporated in the film-coating of tablets, in transdermal systems and in medicinal sprays (Bühler, 2005). PVP has been extensively reported in the literature to have good stabilising effects on amorphous APIs (Khougaz and Clas, 2000; Tantishaiyakul et al., 1999, 1996). Therefore, in this work, PVP K30 was used as a carrier in solid dispersion formulations, as a means of stabilising amorphous olanzapine prepared via hot melt extrusion. The physicochemical and general properties of PVP K30 are described in Table 2.4.

Table 2.4: Physicochemical properties of PVP K30.

Properties	PVP K30	Reference
IUPAC Name	Polyvinylpyrrolidone	
Chemical Formula	$(C_6H_9NO)_n$	
General Designation	Povidone	
Molecular weight (MW)	31 700 – 51 400 g/mol	(Bühler, 2005)
Glass transition temperature (T_g)	$\approx 160\ ^{\circ}C$	(Bühler, 2005)
Density (ρ)	1.16 g/cm^3	(Chokshi et al., 2005)

2.1.4 Polyvinylpyrrolidone Vinyl-Acetate

Polyvinylpyrrolidone vinyl-acetate (PVPVA), also known as Copovidone, is manufactured by free-radical polymerisation of 6 parts of vinylpyrrolidone and 4 parts of vinyl-acetate in 2-propanol. Figure 2.5 below shows the chemical structure of the repeating units of PVPVA 6:4.
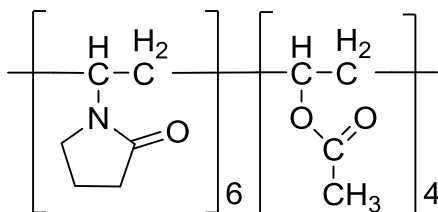
Figure 2.5: Chemical structure of PVPVA 6:4.

Table 2.5 lists the main physicochemical properties of PVPVA 6:4.

Table 2.5: Physicochemical properties of PVPVA 6:4.

Properties	PVPVA 6:4	Reference
IUPAC Name	Polyvinylpyrrolidone vinyl-acetate	
Chemical Formula	$(C_6H_9NO)_6(C_4H_6O_2)_4$	
General Designation	Copovidone	
Molecular weight (MW)	45 000 – 70 000 g/mol	(Bühler, 2005)
Glass transition temperature (T_g)	$\approx 105\ ^oC$	(Bühler, 2005)
Density (ρ)	1.17 g/cm^3	(Chokshi et al., 2005)

The applications of PVPVA, in line with PVP, rely mainly on its good binding and film-forming properties, its affinity to hydrophilic and hydrophobic surfaces. Because of these properties, it is commonly used as a processing aid in the production of granules and tablets, as a binder in direct compression, in film coatings on tablets, as a protective layer and sub-coat for tablet cores and as a film-forming agent in sprays. In addition, the 40% replacement with the lipophilic vinyl-acetate functional groups makes this co-polymer to be relatively less hygroscopic which has resolved some processing and handling issues of the homopolymer system (Bühler, 2005).

2.1.5 Soluplus[®]

Soluplus[®] (SLP) is a polymeric solubiliser with an amphiphilic chemical structure. Due to its dual character, SLP shows excellent solubilising properties for poorly soluble APIs and therefore it was particularly developed for the formulation of solid dispersions (Shamma and Basha, 2013). For use in hot melt extrusion approaches, the T_g of this polymer was adjusted to approximately 70 $^{\circ}$C in order to enable extrudability at lower temperatures compared to the already known polymers (Reintjes, 2011).

SLP has a polyethylene glycol (PEG) 6000 backbone with one or two side chains consisting of vinyl-acetate randomly copolymerised with vinyl-caprolactam (13% PEG 6000/57% vinyl-caprolactam/30% vinyl-acetate) as shown in Figure 2.6.
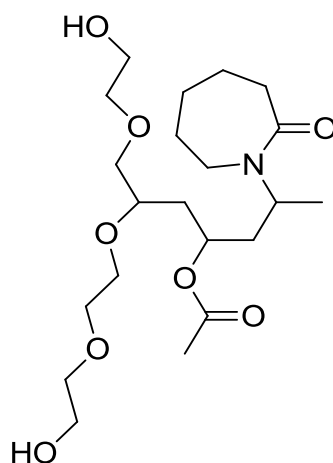
Figure 2.6: Chemical structure of Soluplus[®].

Table 2.6 displays the main physicochemical properties of Soluplus[®].

Table 2.6: Physicochemical properties of Soluplus®.

Properties	Soluplus®	Reference
IUPAC Name	Polyethylene glycol/vinyl-caprolactam/vinyl-acetate	
Chemical Formula	$(C_{21}H_{39}NO_8)_m$	
Molecular weight (MW)	118 000 g/mol	(Reintjes, 2011)
Glass transition temperature (T_g)	≈ 70 ^{o}C	(Reintjes, 2011)
Density (ρ)	1.20 g/cm^3	(Djuris et al., 2013)

2.1.6 Raw Materials Sourcing

As a resume, Table 2.7 lists the suppliers of all APIs, polymer carriers and other chemicals used in this study.

Table 2.7: Sources of chemicals used in this study.

Category	Substance	Supplier
APIs and Polymers	Paroxetine HCl Form I	Afine (China)
	Paroxetine HCl Form II	Huahai Pharmaceuticals (China)
	Olanzapine Form I	Myjoy Ltd. (India)
	PVP K30	BASF (Germany)
	PVPVA 6:4	BASF (Germany)
	Soluplus®	BASF (Germany)
DSC Standards	n-Octedacane	Sigma Aldrich (UK)
	Benzoic acid	Sigma Aldrich (UK)
	Indium	Sigma Aldrich (UK)
	Tin	Sigma Aldrich (UK)
	Sapphire disc	TA Instruments (US)
DVS Standard	Sodium Bromide	Sigma Aldrich (UK)
Salts used for Stability Test	Sodium Chloride	Fischer Scientific (UK)
	Magnesium Nitrate Hexahydrate	Fluka (Germany)
	Calcium Chloride	BDH Laboratory (UK)
	Potassium Acetate	Alfar Aesar (UK)
	Phosphorus Pentoxide	Alfar Aesar (UK)
Solvents	Methanol	Sigma Aldrich (UK)
Karl Fischer Reagents	Hydranal® Solvent	Fluka Analytical (US)
	Hydranal® Titrant	Fluka Analytical (US)
	Hydranal® Standard	Fluka Analytical (US)
Materials used to Prepare Dissolution Media	Hydrochloride Acid	Sigma Aldrich (UK)
	Potassium Dihydrogen Orthophosphate	Fischer Scientific (UK)
	Sodium Phosphate Dibasic	Sigma Aldrich (UK)

2.2 Preparation of Solid Dispersions

2.2.1 Spray Drying

Spray drying (SD) is a technique used to dry aqueous or organic solutions, suspensions or pastes into a dry particle form. The use of drying of products from an atomised liquid stream was firstly reported by Percy in 1872 (Percy, 1872). Since that time, and due to significant equipment development, SD became a versatile technique with application in several different areas, ranging from food, ceramics and fertilisers to the pharmaceutical industry.

In the pharmaceutical industry, SD has been used from simple drying operations to the process of peptides and vitamins and has particular importance for the production of particles with optimal properties for inhalation therapy (Vidgren et al., 1987). In this work, SD was selected to prepare amorphous solid dispersions due to the main advantage of the very fast solvent evaporation that leads to rapid viscosity increase and permits kinetic trapping of the API in the carrier matrix (Paudel et al., 2012).

A typical spray drying process consists of four basic steps (Bu☐chi, 2003):

1. Atomisation of the liquid feed
2. Mixing of the liquid with the drying gas
3. Evaporation of the liquid
4. Separation of the dried particles from the gas

Atomisation transforms the liquid stream into fine droplets by applying a force. The more energy supplied during this step, the smaller the droplets and consequently the smaller the spray dried particles produced.

The liquid spray is subsequently mixed with the drying gas. Normally, compressed air is the medium of choice; however, if organic solvents are being used then an inert gas such as nitrogen should be used to minimise the risk of explosion. The drying gas needs to have

the right temperature and humidity, which must be adjusted accordingly to the nature of the sample. For instance, if the solvent is water, higher temperatures would be required compared to organic solvents.

The contact between the droplet and the heated gas resulted in the evaporation of the solvent from the saturated vapour film at the droplet surface. The design of the drying chamber and the gas flow allows the droplets to reside in the chamber until the desired moisture content is achieved and then the product is immediately discharged from the chamber. The last step in the SD process is the collection of the particles, which requires the separation of the dried droplets from the drying gas stream, most commonly via a cyclone.

Reviews have been published in recent years concerning the fundamentals of spray drying (Cal and Sollohub, 2010; Sollohub and Cal, 2010; Vehring et al., 2007) and exploring the influence of process and formulation parameters on the quality of the resulting spray dried products (Corrigan, 1995; Paudel et al., 2012).

The main steps involved in the spray drying process and referred above are identified in Figure 2.7. In this study a Bu☐chi Mini Spray Dryer B-290 (Bu☐chi, Switzerland) was used.
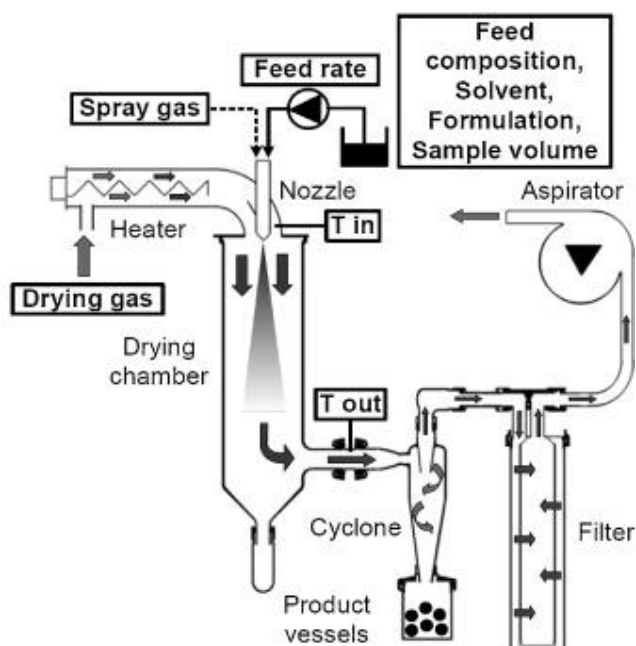
Figure 2.7: Büchi Mini Spray Dryer B-290, a laboratory-size model (Büchi brochure).

2.2.2   Hot Melt Extrusion

Hot melt extrusion (HME) is a processing technique widely applied in the plastic, rubber and food industry. In the past few years, an extensive number of studies have shown the potential of this technology in the pharmaceutical field for manufacturing a variety of dosage forms and formulations such as granules, pellets, tablets, implants, transdermal systems and ophthalmic inserts (Breitenbach, 2002). HME is a continuous manufacturing process in which a blend of API, thermoplastic polymeric carrier and other processing aids, including plasticisers and antioxidants, is heated and softened inside the extruder barrel and then pressurised through a die into granules, cylinders or films (Crowley et al., 2007; Repka et al., 2007).

The extrusion process can be categorised as either ram extrusion or screw extrusion. Screw extrusion consists of one or two rotating screws inside a heated barrel, while ram extrusion operates with a positive displacement ram capable of generating high pressures to push materials through the die. Ram extrusion has limited melting capacity that causes poor temperature uniformity in the extrudate compared to screw extrusion and for that reason is not used for HME (Crowley et al., 2007). Screw extruders used for pharmaceutical applications typically consist of two screws (twin screw) and can be categorised, depending on the direction of rotation of the screw, as co-rotating or counter-rotating.

Figure 2.8 displays a schematic representation of a typical lab scale extruder. An extruder can be divided into three main zones: the feeding, the melting or compression and the metering zone. The different zones of the barrel are pre-set to specific temperatures prior the extrusion process. The API and polymer are premixed and fed into the extruder via a hopper. The feedstock is further transported along the length of the barrel, where it is melted, plasticised, mixed and compressed. The material transfer should be efficient in order to maintain an increase in pressure in the compression zone and the metering zone. The primary function of the metering zone is to ensure thickness, consistent flow and steady delivery rate through the die (Breitenbach, 2002).
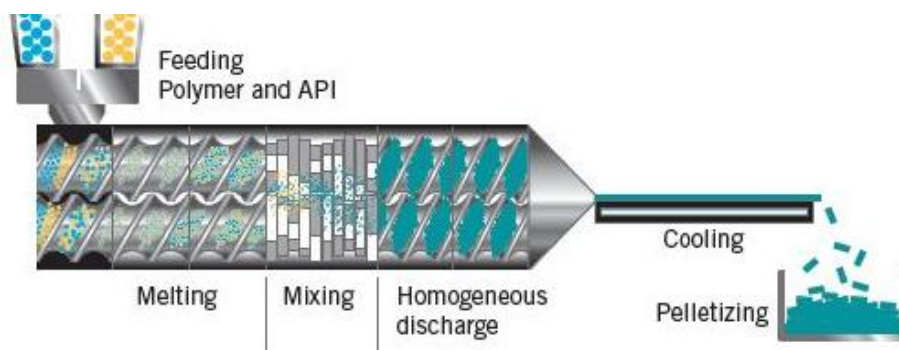
Figure 2.8: Illustration of a typical HME equipment (www.particlesciences.com).

Overall, HME offers the possibility of continuous process and thus efficient scale up. Moreover, it is a solvent free processing technique and therefore it is environment friendly and cost effective. However, it also has some drawbacks, such as the limitation to process heat or mechanical sensitive drugs.

Based on these characteristics, HME has been successfully applied on the design and manufacture of delivery systems for poorly soluble drugs (Tho et al., 2010; Lakshman et al., 2008; Feng et al., 2012). Basically, the solubility enhancement occurs through dispersion of the poorly soluble API in a polymeric (or lipid) carrier matrix essentially forming a solid dispersion. Several aspects must be considered in order to obtain an adequate solubilisation in melt extrusion, which depends on the materials (drug and carrier properties), process (processing temperature, screws rotation speed, residence time) and equipment (design and operating conditions).

In this work, a Thermo Scientific HAAKE MiniLab II (Thermo Scientific, UK) equipped with co-rotating twin screws, was used. A die of round shape with a diameter of 2 mm was attached to the extruder.

2.3   Characterisation Techniques

2.3.1   Differential Scanning Calorimetry

2.3.1.1   Principles of Operation

Differential scanning calorimetry (DSC) is a well-established method of thermal analysis within the pharmaceutical sciences. DSC technique consists in applying a heat signal to a sample and consequently measuring the response in terms of the energy and temperature associated with the relative events, such as melting, crystallisation, glass transition and decomposition reactions of the materials. The temperature profile may be a heating, cooling or an isothermal program (Craig and Reading, 2007).

There are two different types of DSC instruments according to the operating principles: heat flux and power compensation. The two types differ on the design of the DSC cell and the algorithms used to convert the measured temperature difference into differential power (heat flow). Power compensation DSC involves two separated furnaces, one for the sample and a second for the reference. The temperature difference between the two furnaces is kept similar by supplying an electric power to the sample furnace. In heat flux DSC, the sample and the reference are placed symmetrically inside the furnace and share a common heat source. As a result, the heat flow signal is derived from the temperature difference between the sample and the reference and is measured by the thermocouples which are connected in a back-to-back arrangement.

The DSC used in the experiments carried out in this thesis (TA Instruments, US) operates by heat flux and the above descriptions are schematically represented in Figure 2.9.
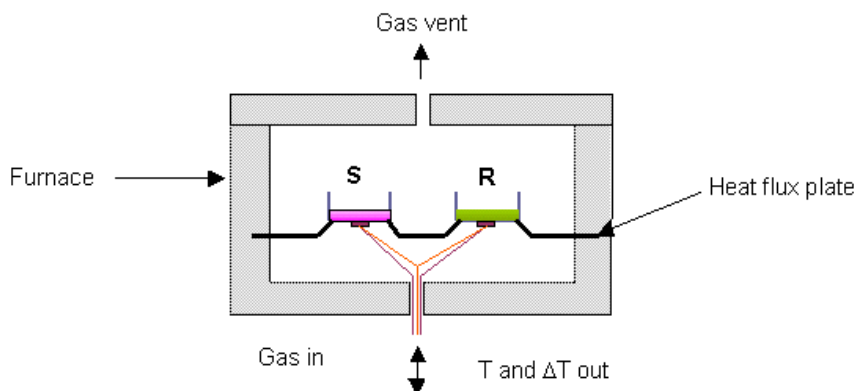
Figure 2.9: Schematic representation of a heat flux DSC showing the sample (S) and the reference (R) pan location within the same furnace (www.anasys.co.uk).

The differential heat flow measured during DSC experiments can be expressed by,

$$\frac{dQ}{dt} = \frac{\Delta T}{R}$$

Equation 2.1

where, dQ/dt represents the heat flow (where Q is heat and t is time), ΔT is the temperature difference between the furnace and the sample and R is the thermal resistance of the heat path between the furnace and the crucible.

When a material is heated, the heat flow signal is determined by the heat capacity (C_p) of the material. Heat capacity is defined as the amount of energy required to raise the temperature of the sample by 1K and can be expressed by,

$$\frac{dQ}{dt} = C_p \times \frac{dT}{dt}$$

Equation 2.2

where dT/dt is the heating rate.

2.3.1.2   Experimental Variables

An inert atmosphere is essential in all DSC experiments which can be achieved by purging an inert gas into the cell. The selected gas is usually nitrogen however, helium can also be

used. A constant purge gas, in general with a flow rate of 50 mL/min, enhances the heat transfer between the cell and the sample pan. Moreover, ensures that any volatile compounds, including water vapour, are removed from the contact with the measuring sensor and, at the same time, minimise long term damage of the DSC cell.

To ensure an accurate performance of the instrument, routine calibrations processes must be carried out each time any experimental parameter changes (heating rate, pan type). The cell constant calibration (enthalpy calibration) is conducted by heating indium through its melting transition (T_m = 156.6 ^{o}C) and the temperature calibration is performed by using high purity materials, such as n-octadecane (T_m = 28.2 ^{o}C), benzoic acid (T_m = 122.4 ^{o}C) and tin (T_m = 231.9 ^{o}C).

Another important factor to consider is the sample size. As the sample mass increases there is an increase in the thermal gradient across the sample. With conventional DSC, large sample masses are recommended if precise heat capacity data is required as this increases the ΔT and heat flow signals. However, a sample size between 3-5 mg is generally recommended.

Finally, the type of pan selected is of great importance and should be carefully chosen depending on the properties of the sample and on the type of data extrapolated from the DSC run. For example, when analysing solid dispersions the presence of water influences the measured T_g and therefore as a way to dry the sample upon heating, pans with a hole in the lid (pinhole pans) are often used. Open pans (pans without lids) can also be used for this purpose, though the linearity of the baseline might be compromised. In contrast, when dealing with suspensions, liquid formulations or samples that must be kept in their hydrated state, hermetically sealed pans must be used. In the present Thesis, these three different types of pans (pinhole, open and hermetic) were used depending on the desired experimental measurements in each case.

2.3.1.3   Modulated Temperature Differential Scanning Calorimetry

2.3.1.3.1   Principles of Operation

Modulated temperature differential scanning calorimetry (MTDSC) is an extension of the conventional DSC technique in which a sinusoidal modulation is superimposed on the linear temperature ramp combined with a mathematical procedure designed to separate different types of sample behaviour (deconvolution) (Coleman and Craig, 1996; Craig and Reading, 2007; Gill et al., 1993). This allows the direct measurement of heat flow and changes in heat capacity simultaneously, as expressed by Equation 2.3,

$$\frac{dQ}{dt} = C_p \frac{dT}{dt} + f(t,T)$$

Equation 2.3

where, $f(t,T)$ is a function of time and temperature and it is used to express the response associated with the physical or chemical transformation.

The first term on the right hand side of the Equation 2.3 describes the heat flow associated with the heat capacity of the sample and represents reversing processes. On the other hand, the second term is related to the enthalpy of the reaction and it is often identified as an irreversible event. As a result, events such as glass transition are accurately measured in the reversing heat flow signal whereas irreversible processes which are kinetically hindered, for example relaxation and crystallisation, are observed in the non-reversing heat flow signal.

Overall, MTDSC technique gives three signals in a single heating run, allowing the heat capacity, kinetic and total heat flow components to be delineated. This technique has been of undoubted use for the study of amorphous systems.

2.3.1.3.2   Experimental Variables

MTDSC experiments depend on three parameters: the underlying heating rate, the temperature modulation amplitude and the reciprocal period. In general, MTDSC implies

the use of much slower heating rates, typically varying from 1-5 ^{o}C/min, compared with the 10-20 ^{o}C/min heating rates employed in conventional DSC. The combination of low underlying heating rates with large modulation amplitudes, generally selected from the range $\pm$ 0.1 to $\pm$ 1 ^{o}C, enables an increase in sensitivity without any compromise of resolution. The modulation period is normally selected within 30-80 sec. However, an important requirement is to have at least six modulation cycles throughout the duration of each thermal event in order to enable the complete separation of cycle and underlying processes (Coleman and Craig, 1996).

The baseline and temperature calibration of the MTDSC cell does not differ from that of the conventional DSC although an additional step for the calibration of the heat capacity is needed. This will allow a correct measurement of the sample heat capacities and an adequate separation of the total, reversing and non-reversing heat flow signals. The heat capacity calibration is performed by scanning a material with known heat capacity, such as sapphire.

DSC and MTDSC studies were carried out on a DSC Q1000 and Q2000 series TA Instruments (US) with an integrated cooling system (RCS) attached. The purge gas used was nitrogen with a flow rate of 50 mL/min.

2.3.2 Hot Stage Microscopy

Hot stage microscopy (HSM) consists in an optical microscope fitted with a hot stage accessory, and therefore combines the best properties of microscopy and thermal analysis. This analytical technique enables the characterisation of the physical properties of materials as a function of temperature such as melting, solid state transformations, recrystallisations, etc.

High resolution colour cameras and image manipulation software are nowadays powerful accessories of HSM, which enable to record thermal events happening during the heating/cooling cycle of the sample (Vitez et al., 1998).

In this thesis, HSM studies were performed using a microscope Leica DM L52 (Germany) with a 20x lens connected to a hot stage plate Mettler Toledo FP82HT (UK) and a FP90 central processor.

2.3.3   Thermogravimetric Analysis

Thermogravimetric analysis (TGA) is a technique where the change in weight of the sample is measured as a function of temperature (non-isothermal experiments) or time (isothermal experiments).

Water content and chemical decomposition of solid drugs and pharmaceutical excipients are the two main applications of this technique in the pharmaceutical arena. Moreover, it can be used to determine the stoichiometry of solvates (calculated from the weight loss per known amount of original sample) and at the same time give an indication on the strengths of the water binding on the basis of the temperature at which the solvent is lost. Finally and in the same field of the study of solvates, vital information can be obtained when combining DSC and TGA techniques with a view to differentiating between solvent loss and melting.

TGA instruments are generally equipped with high precision balances that allow accurate measurements of the sample weight during heating. A purge gas with an optimised flow is also required to establish a stable environment around the sample and the furnace.

In this work, experiments were carried out using a Hi-Res TGA 2950 TA Instruments (US) equipment. Nitrogen gas was used at a flow rate 60 mL/min and 40 mL/min through the furnace and TGA head, respectively. A more modern equipment Q5000 series also from TA Instruments equipped with an autosampler device was also used in some of the experiments. In this case, the furnace was also blanketed with dry nitrogen but with a flow rate of 10 mL/min and 25 mL/min to the balance and furnace/sample areas, respectively.

2.3.4   Dynamic Vapour Sorption

Dynamic vapour sorption (DVS) analysis is a technique in which a sample is subjected to varying conditions of humidity and temperature, and the response of the sample is measured gravimetrically.

Measurements of the equilibrium water content of a solid as a function of RH (constant or variable) at a certain temperature are commonly used to assess the hygroscopicity of pharmaceutical solids. More specifically, DVS experiments are also helpful in differentiating different types of hydrates. Therefore, compounds that have the tendency to form stoichiometric hydrates show stepwise jumps in their weight whereas non-stoichiometric hydrates present a gradual increase in weight as the water is continuously incorporated into the structure, as it is presented in Chapter 3. Apart from this, the DVS technique has also been used to study and quantify amorphous systems (Buckton and Darcy, 1995; Mackin et al., 2002). Overall, from a pharmaceutical perspective, a thorough understanding of the effects of water (bonded or adsorbed onto the surface) on the structure of APIs and excipients is essential for its formulation and development.

DVS instruments operate in a closed system at a controlled temperature and either ambient or controlled pressure. The sample is placed on a sensitive microbalance inside the humidity chamber and exposed to a continuous flow of air or nitrogen.

In this work, DVS experiments were performed on a Sorption Analyzer Q5000, TA Instruments (US). All samples were tested using quartz pans and at a constant nitrogen flow of 10 mL/min. The instrument was calibrated according to the deliquescence point of sodium bromide (57.6% RH).

2.3.5   Attenuated Total Reflection–Fourier Transform Infrared

Fourier transform infrared (FTIR) is a spectroscopic non–destructive, non–invasive technique that provides information about the molecular composition, structure and

interactions within a sample based on its chemical bonds. Infrared (IR) spectroscopy is used for identification, characterisation, quantification, structure elucidation, reaction monitoring, quality control and quality assurance.

With IR spectroscopy, the sample is irradiated with a polychromatic light in the IR region (4000 to 400 cm^{-1}) and a photon of light is absorbed when the frequency (energy) of the absorbed light matches the energy required for a particular bond to vibrate within the sample. In order for a vibration to be IR active, the molecular dipole moment must change during the vibration. Any IR light that has not been absorbed is transmitted to the sample to a detector. The fraction of transmitted light allows the absorbed frequencies to be determined.

The difficulties associated with the analysis of solid samples in the conventional IR spectroscopy that involved the preparation of KBr disks was overcome by the use of attenuated total reflection (ATR) mechanism applied to the FTIR. ATR is based on the principle of the reflection of radiation when it passes from a denser to a less dense medium. During this process the beam acts as if it has penetrated a small distance into the less dense medium. Samples are generally placed on opposite sides of a transparent crystalline material of high refractive index, generally diamond. The penetration depth into the sample is usually just a few microns (0.5-5 μm) thus a good contact between the sample and the crystal surface must be ensured (O'Neil and Edwards, 2011).

The FTIR studies presented throughout this thesis were carried out using a Bruker Optics IFS 66/S (UK) spectrometer with an ATR accessory fitted to a heating system (SPECAC, UK). Spectra were collected from 4000 to 550 cm^{-1} with a total of 64 scans at a resolution of 2 cm^{-1}, unless otherwise stated.

2.3.6   X-Ray Powder Diffraction

X-ray powder diffraction (XRPD) is a gold standard technique in the characterisation of pharmaceutical materials in the solid state. It is mainly used for fingerprinting and quantification analysis due to its high sensitivity to small chemical changes.

Basically, X-rays are generated by heating a filament (the cathode) which works as a source of electrons. These electrons are then accelerated and strike a target (the anode) that is usually Cu, Mo, Cr or Ag and produces a characteristic X-ray spectrum (Gilmore, 2011). When X-rays pass through the sample they interact with the electron cloud of atoms in the molecules and the intensity and position of the emergent X-rays are recorded by a detector. Additional equipment can be fitted to the conventional XRPD in order to proportionate analyses under the effect of temperature or humidity. This is of great importance when studying polymorphic and pseudopolymorphic transitions.

Variable humidity XRPD (VH-XRPD) is commonly used to investigate the structure of variable hydrates. The amount of water present in a variable hydrate is typically a function of the RH environment of the sample. Since the XRPD peak positions are directly related to the dimensions of the unit cell, subtle changes in the size of the unit cell due to the presence of water may be evaluated by comparison of XRPD patterns collected for the species under different RH environments.

Variable temperature XRPD (VT-XRPD) on the other hand permits the direct identification of a crystalline phase as a function of temperature, especially important in the study of thermal stability of pharmaceutical hydrates.

In this thesis, general XRPD analysis of solid dispersion systems and polymers were performed using a Thermo ARL Xtra (Thermo Scientific, UK) model equipped with a copper X-ray Tube (1.540563 Å). The samples were exposed to an X-ray beam with a voltage of 45 kV and a current of 40 mA. All XRPD experiments were performed at 2θ and step scan of 0.01^o. The scanning range was based on the characteristics peaks of each sample.

The changes in the crystal structure of paroxetine HCl Form II as a function of humidity (Chapter 3) were evaluated using a XRPD, Philips XPERT Pro (Netherlands) equipped with a relative humidity generator (RH-200, L&C, Germany) and a temperature control unit (TUC 50, Anton Paar, Austria). Patterns were collected from scans in the range of 2θ from 5.0^o to 50.0^o with a step size of $0.0010°$, at different RHs.

The dehydration study of paroxetine HCl Form I (Chapter 4) was studied *in situ* using a VT-XRPD Bruker D8 Advance (Bruker, UK) fitted with a TTK450 (Anton Paar, Austria) chamber. The temperature was controlled by a Temperature Control Unit TCU 100

(Anton Paar, Austria) and the applied heating rate was set by default to 0.167 K/s. Spectra were collected from 4.0° to 30.0° at 2θ under nitrogen purge with a flow rate of approximately 50 mL/min.

2.3.7   Scanning Electron Microscopy

Scanning electron microscopy (SEM) enables specimens to be examined at much higher magnification and resolution than it is possible using a light microscope. In SEM, a beam of electrons is produced at the top of the microscope by an electron gun. The electron beam follows a vertical path through the microscope, which is held within a vacuum. The beam travels through electromagnetic fields and lenses, which focus the beam down toward the sample. Once the beam hits the sample, electrons are ejected from the sample. Detectors collect these backscattered electrons and secondary electrons and convert them into a signal that is sent to a screen similar to a television screen. This produces the final image.

SEM photographs were taken using a JSM 4900LV SEM (JOEL, Japan) mounted with a tungsten filament with an acceleration voltage of 5-20 kV. To improve conductivity prior to examination, samples were coated with gold using a Polaron SC7640 sputter gold coater (Quorum Technologies, UK).

2.3.8   Karl Fischer Titration

Karl Fischer titration (KFT) is a classic titration method that determines the water content in a sample.

KFT is based on a quantitative reaction of water with iodine (I_2) and sulfur dioxide (SO_2) in the presence of a lower alcohol (ROH) such as methanol and an organic base (RN) such as pyridine, as shown in the following reactions:

$$ROH + SO_2 + RN \rightarrow (RNH)SO_3R$$

$$(RNH)SO_3 + I_2 + 2RN + H_2O \rightarrow (RNH)SO_4 + 2(RNH)I$$
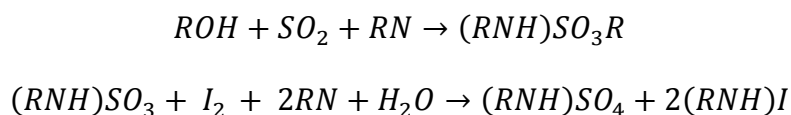
There are two types of Karl Fischer titrators: volumetric and coulometric. The main difference between the two is that with the volumetric method, the titrant is added directly to the sample by a burette. Conversely, with the coulometric method, the titrant is generated electrochemically in the titration cell.

When performing KFT several aspects must be taken into consideration to prevent misleading results. First of all, the choice of the reagents is of great importance especially when dealing with aldehydes and ketones. These compounds can react with the standard methanol reagents and form water. Therefore, methanol-free reagents must be used in these particular cases. Another aspect is regarding the time and the speed of stirring the sample inside the titration vessel. Too low a stirring speed can lead to irregular titration and over titration may occur whereas a speed too high can generate bubbles in the solution and falsify the measured values. Moreover, the influence of atmospheric moisture in the titration process must also be accounted. Moisture can enter not only the titration vessel but also the titrant bottle leading to a decrease in the titrant concentration.

KFT was performed using a DL38 (Mettler Toledo, UK) volumetric titrator with Hydranal® solvent and Titrant® 5. The titrant concentration was determined daily by using di-sodium tartrate dihydrate, which has a water content of 15.66%.

2.3.9 Dissolution Studies

Dissolution testing of pharmaceutical solids is one of the most important tests in drug product development and manufacturing as well as in regulatory assessment of the drug product quality. It provides information on the rate and extent of drug absorption and at the same time assesses the effect of drug substance properties and formulation principles on the release profile of the drug substance (Lee et al., 2008).

The dissolution process of solids consists of two main steps. At first, the molecules at the solid-liquid interface are wetted and solvated and detached from the solid surface. Secondly, the solvated molecules diffuse away from the interface to the bulk solution. It is described that it is the diffusion rate of the molecules in the media and/or the wetting and solvation of the surface molecules that defines the dissolution profile of a certain compound (Hörter and Dressman, 2001).

The dissolution rate ($\delta M/\delta t$) of a solid in a liquid can be described by the well-known Noyes-Whitney equation as presented below.

$$\frac{\delta M}{\delta t} = A \times \frac{D}{h} (C_s - C_b)$$

Equation 2.4

where M is the mass, t is the time, A is the surface are of the undissolved solid in contact with the solvent, D is the diffusion coefficient (m^2/s), h is the thickness of diffusion layer, C_s is the solubility, C_b is the concentration in the bulk solution and C_s-C_b is the concentration gradient. The above Equation 2.4 assumes that the surface area and thickness of the hydrodynamic diffusion layer remain constant.

Dissolution experiments were carried out using a BP Apparatus I, Copley CIS 8000 dissolution bath (Copley Scientific, UK) paddle method. Each vessel was filled with 900 mL of dissolution medium, the temperature was set at 37.0 °C and a rotation speed of 50 rpm was used. The concentration of each API through the dissolution tests was assessed spectrophotometrically at the respective wavelength of maximum absorbance, λ_{max}, using a Perkin-Elmer Lambda XLS (Perkin Elmer, US) spectrophotometer. Calibration curves were constructed for each API in the respective dissolution media.

3   Identification and Characterisation of Stoichiometric and Non-Stoichiometric Hydrate Forms of Paroxetine HCl: Reversible Changes in Crystal Dimensions as a Function of Water Absorption

Abstract

Paroxetine hydrochloride (HCl) is an anti-depressant drug, reported to exist in the anhydrous form (Form II) and as a stable hemihydrate (Form I). In this study, the hydration behaviour of paroxetine HCl Form II was investigated with a view to understanding both the nature of the interaction with water and the interchange between the Forms II and I as a function of both temperature and water content. In particular, new evidence is presented for both the structure and the interconversion process to be more complex than previously recognised.

A combination of characterisation techniques was used, including thermal (differential scanning calorimetry (DSC) and thermogravimetric analysis (TGA)), spectroscopic (attenuated total reflectance-Fourier transform infrared (ATR-FTIR)), dynamic vapour sorption (DVS) and X-ray powder diffraction (XRPD) with variable humidity, along with computational molecular modeling of the crystal structures.

The total amount of water present in Form II was surprisingly high (3.8% w/w, 0.8 mol of water/mol of drug), with conversion to the hemihydrate noted on heating in hermetically sealed DSC pans. XRPD, supported by ATR-FTIR and DVS, indicated changes in the unit cell dimensions as a function of water content, with clear evidence for reversible expansion and contraction as a function of relative humidity (RH). This data suggested that paroxetine HCl Form II is not an anhydrate but rather a non-stoichiometric hydrate. However, no continuous channels are present and, according to molecular modeling simulation, the water is moderately bonded to the crystal, which is in itself an uncommon feature when referring to non-stoichiometric hydrates. Overall, therefore, it is suggested that the anhydrous form of paroxetine HCl is not only a non-stoichiometric hydrate, but also one that shows highly unusual characteristics in terms of gradual unit cell expansion and contraction despite the absence of continuous channels. These structural features in turn influence the tendency of this drug to convert to the more stable hemihydrate. The study has implications for the recognition and understanding of the behaviour of pharmaceutical non-stoichiometric hydrates.

3.1 Introduction

Polymorphism and pseudopolymorphism are well studied phenomena within the pharmaceutical arena, with the most widely studied manifestation of the latter being hydrate formation. Indeed, the possible interaction with water during certain processing steps (freeze drying, spray drying or wet granulation) as well as contact with atmospheric humidity upon storage renders hydrate formation extremely common (Koradia et al., 2011; Giron et al., 2002). Typically, such materials are considered to be stoichiometric, with a precise and defined molecular ratio between the water and host in the crystal lattice, although undefined incorporation is also possible, these being known as non-stoichiometric or variable hydrates (Griesser, 2006; Khankari and Grant, 1995). For stoichiometric hydrates, the water may play a crucial role in the stabilisation of the molecular network and therefore dehydration may result in a disordered or amorphous state (Kobayashi et al., 2009; Vogt et al., 2006; Guguta et al., 2006). In contrast, non-stoichiometric hydrates may reversibly gain or lose water while retaining the same crystalline structure (isomorphic dehydrates), with the water molecules entering and leaving the crystal lattice in a manner determined by the environmental relative humidity (RH) (Stephenson et al., 1998). This therefore presents issues for the formulator in that differentiation from simple surface adsorption may be challenging, with the well-known indicators of hydrate formation (e.g. powder X-ray diffraction and thermogravimetric analysis) not yielding the same unequivocal identification of lattice alteration as is usual for stoichiometric hydrates. On this basis the possible existence of non-stoichiometric hydrates is not fully appreciated within the pharmaceutical field, with an accompanying lack of the development of characterisation tools for their identification and structural elucidation.

Hydrates can also be classified based on their crystal structures (Vippagunta et al., 2001). In Class I, or isolated site hydrates, water has a well-defined isolated location and therefore hydrates of this class are often stoichiometric. In Class II, channel or planar hydrates, water is packed inside the crystalline structure so as to form continuous channels or planes. Class III refers to ion coordinated hydrates, in which water molecules are coordinated to metal ions. Class II hydrates are, in general, non-stoichiometric, while Class III hydrates can be either stoichiometric or non-stoichiometric.

Differentiation between hydrate formation and non-specific hygroscopicity may be challenging. Water can interact with crystalline materials in several ways (adsorption, absorption, deliquescence and hydrate formation), all of which may have a large impact on the solid state properties, processing and handling of drugs (Ahlneck and Zografi, 1990). This difficulty is exemplified by the study of Reutzel (Reutzel, 1998) on the muscarinic agonist, LY297802 tartrate. The considerable hygroscopicity for this material was found to be, in fact, due to non-stoichiometric hydrate formation whereby, rather than simple surface sorption, water migrates between hydrogen-bonding sites located in crystal lattice channels.

In this work, the hydration behaviour of paroxetine HCl was investigated. Paroxetine HCl is a potent and selective inhibitor of the neuronal re-uptake of serotonin (5-hydroxytryptamine, 5-HT) and is currently clinically approved for the treatment of depression, social phobia, obsessive-compulsive, post-traumatic stress and general anxiety (Bourin et al., 2001). This molecule is of particular interest due to the confusion associated with its physical forms with three nomenclature systems being used to describe them. Initially, Barnes et al. (Barnes et al., 1988) described in their patent the preparation of paroxetine HCl hemihydrate and, in Example 8 of the same document, the preparation of paroxetine HCl anhydrate. Less than one year later, Buxton et al. (Buxton et al., 1988) further investigated the above forms and named the hemihydrate as Form I and the anhydrate as Form II. Form I is described as a non-hygroscopic hemihydrate with a melting point (m.p.) of 143 °C, which represents the most stable form and is currently included in commercially available pharmaceutical formulations, while Form II is described as a hygroscopic anhydrate with a m.p. of 118 °C and a moisture content controlled by environmental humidity. More recently, Ward and Jacewicz (Ward and Jacewicz, 2000) described the preparation of three new anhydrate forms of paroxetine HCl, named as A, B and C. They suggest that paroxetine HCl Form A (m.p. 123-125 °C) can be distinguished from the anhydrate Form II by the crystal shape, as reported by Buxton et al. (Buxton et al., 1988). However, the data available (infrared and thermal analysis) suggests that in terms of internal structure these two forms (A and II) are probably, but not definitely, equivalent. The reported characteristics of the other two forms, B (m.p. at 137 °C) and C (m.p. at 161 °C) do not comply with those of the form investigated here and

no such transitions were seen in the present study, hence these forms do not impinge on the present study.

This therefore leads to an immediate issue of nomenclature, as three classifications are currently in use (anhydrate/hemihydrate, I and II, A, B and C). In this work, the nomenclature Form I (hemihydrate) and II (anhydrate) was chosen for the sake of simplicity. However, as it will be demonstrated, the notion of Form II as being a true anhydrate is challenged in this work, hence it is avoided the use of this term other than to point out its nominal description so as to avoid confusion.

In this investigation a combination of thermal analysis, variable humidity powder XRD with associated modeling, attenuated reflection FTIR and dynamic water sorption studies was used to examine the interplay between the Form II and hydrated forms, with a view to clarifying the physical structures and transformation processes associated with exposure of Form II to water.

3.2   Materials and Methods

3.2.1   Materials

Paroxetine HCl Form II was purchased from Huahai Pharmaceuticals (China) and was used as received as well as, pre-dried over phosphorus pentoxide (P_2O_5), Alfa Aesar (UK), as stated. The correspondence to the nominally anhydrous form was confirmed using thermal and spectroscopic analysis, as outlined below.

3.2.2   Methods

3.2.2.1   Thermal Analysis

Standard differential scanning calorimetry (DSC, Q1000 TA Instruments) was performed at heating rates of 5, 10, 20 and 50 $^{\circ}$C/min. Modulated temperature DSC (MTDSC, Q1000

DSC TA Instruments) analysis was performed using a heating rate of 2 ^{o}C/min, amplitude $\pm$ 0.318 ^{o}C and a period of 60 seconds. Scans were carried out within the temperature range 0 °C to160 °C except for the collection of the Form I prepared *in situ* DSC whereby the runs were stopped at 125 ^{o}C. Pinhole, hermetically sealed and open pans (pinhole pans without lid) were used as stated.

Thermogravimetric analysis (TGA, Hi-Res 2950 TA Instruments) was performed in open aluminium pans with a heating rate of 10 ^{o}C/min, from 30 ^{o}C to 300 ^{o}C.

3.2.2.2   Karl Fischer Titration (KFT)

KFT (Mettler Toledo DL38) were carried out by accurately weighing between 40 to 41 mg of bulk and pre-dried samples. The bulk sample was kept under ambient conditions and the dried sample was stored at P_2O_5 for 7 days prior to testing. The reagents used were Titrant$^{®}$ 5 and Hydranal$^{®}$ solvent. Each determination was repeated five times (n = 5).

3.2.2.3   Attenuated Total Reflection-Fourier Transform Infrared (ATR-FTIR)

The infrared spectra of the samples were collected using a Bruker Optics IFS 66/S spectrometer, with 64 scans being acquired for each sample from 4000 cm^{-1} to 550 cm^{-1} with a resolution of 2 cm^{-1}. Variable temperature ATR-FTIR experiments were carried out by connecting a temperature controller to the diamond ATR top-plate. A constant heating rate of 2 ^{o}C/min was employed.

3.2.2.4   Dynamic Vapour Sorption (DVS)

DVS (SA Q5000 TA Instruments) experiments were performed at a constant temperature set at 30 ^{o}C. The sample previously stored over P_2O_5 for 7 days was equilibrated at 0% RH for 2h inside the DVS chamber before starting the sorption/desorption experiments. The starting relative humidity was 10% RH, which was firstly increased to 30% RH, and then at 10% RH/step to 90% RH. Desorption was studied by reducing the relative humidity from 90% to 25% RH, then to 15%, 5% and 1% RH. At each target RH, the isothermal

sorption procedure was performed for 40 minutes (min). Note that for RHs higher than 10%, no mass change was detected after 40 min in any of the steps.

3.2.2.5   X-Ray Power Diffraction (XRPD) and Variable Humidity XRPD (VH-XRPD)

Spectra of raw and prepared Form I *in situ* DSC were collected using XRPD (Thermo-ARL Xtra, Thermo Scientific) from 5.0^o to 40.0^o at 2θ.

VH-XRPD (Philips XPERT Pro) patterns were collected from scans in the range of 2θ from 5.0^o to 40.0^o with a step size of $0.0010°$, at different RH using a relative humidity generator (RH200). The temperature was controlled by using temperature control unit (TUC 50, Anton Paar). The RH steps and equilibration time were the same as in the DVS experiment. Unit cell parameters were determined by Pawley refinement of the collected patterns using the program TOPAS-Academic (Coelho, 2007). A specimen displacement parameter was included in the refinement to account for the macroscopic expansion or displacement of the sample in response to environmental changes. The value of the displacement parameter varied between 0.63 and 0.67 mm, which would, in itself, cause very little change in the powder pattern ($\approx 0.02^o$ shift of peak positions around $2\theta = 20^o$).

3.2.2.6   Computational Modeling of Crystal Structures

Lattice energy minimisations were performed using the rational function optimisation method implemented in the GULP package (Gale, 2005). The force field used comprised of the Dreiding parameter set (Mayo et al., 1990) and AM1-BCC charges (Jakalian et al., 2002). The initial ($P2_1$) symmetry of the crystal structure was maintained during the minimisations. The starting configurations were generated from the experimental structure by assuming either full or zero occupancy for the water molecule.

3.3   Results and Discussion

3.3.1   Differential Scanning Calorimetry (DSC)

Initially, the thermal behaviour of paroxetine HCl Form II was explored using standard and modulated DSC. Three types of pans, pinhole, hermetic and open, were used to examine the influence of water on the thermal behaviour while modulated measurements were used in order to aid identification of any non-obvious thermal events that may arise such as glass transitions. Figure 3.1 presents data for paroxetine HCl Form II at 10 °C/min in pinhole and open pans. A single endotherm melting point was detected in both cases with an onset temperature of 117.1 ± 0.7 °C in pinhole and 121.8 ± 0.3 °C in open pans. This is in good agreement with the reported values from Buxton *et al.* (Buxton et al., 1988) (118.3 °C) for Form II and also from Ward and Jacewicz (Ward and Jacewicz, 2000) (123-125 °C) for Form A. The 'bowing' endotherm seen for the open pan systems is associated with water loss which will be expected to occur over a relatively narrow temperature range, and hence be thermally visible, due to the unrestricted nature of the water evaporation on heating for an anhydrous form; this notion will be revisited later.
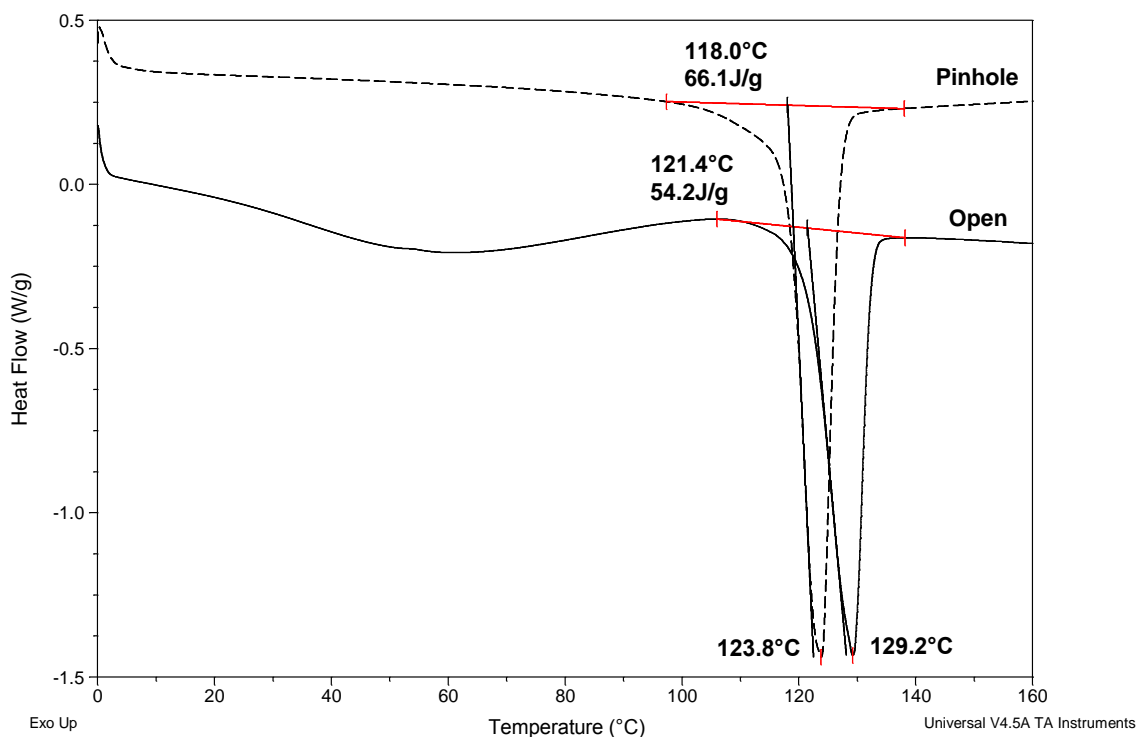
**Figure 3.1: Standard DSC analysis (10 °C/min) of paroxetine HCl Form II
in pinhole pans and open pans.**

It is apparent that the melting event of paroxetine HCl Form II is influenced by the experimental conditions, with a difference of almost 5 °C in the onset melting temperature seen using different pan types. This indicates the inherent difficulties in establishing the 'correct' value for the melting point of this form; again an explanation for this difference will be shown later.

When using hermetically sealed pans, a distinct thermal profile was obtained (Figure 3.2). The melting response was detected at 111.8 ± 0.6 ^{o}C, followed by an exotherm (possibly associated with recrystallisation, T_{rec}) at 118.1 ± 0.6 °C and finally an endotherm at 139.8 ± 0.5 °C corresponding to the reported melting of the Form I, as per previous studies (Barnes et al., 1988). It is therefore reasonable to conclude that the Form II is forming the hydrate form on heating, using the associated water to form the stoichiometric hydrate. This is a highly unusual behaviour pattern and, up to this study, there are no previous reports to this effect.
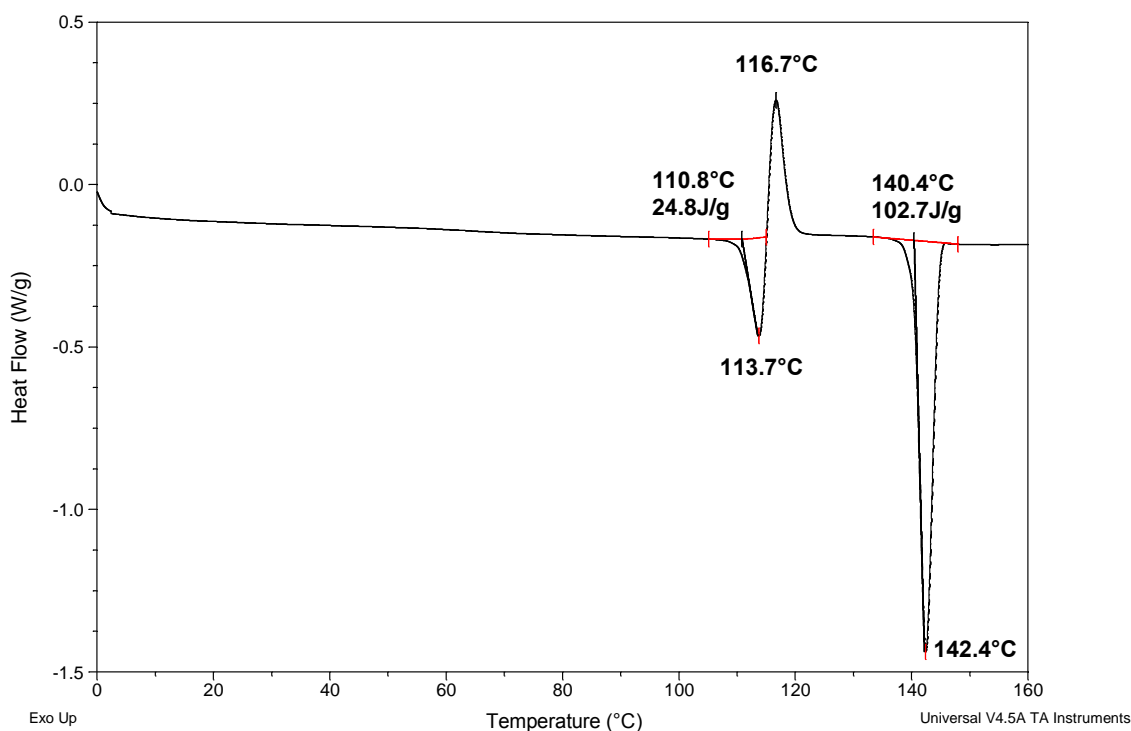
Figure 3.2: MTDSC analysis (total heat flow, 2 $^{\circ}$C/min) of paroxetine HCl Form II in hermetically sealed pans.

This observation was confirmed by using XRPD and the results are shown in Figure 3.3. The diffractogram of paroxetine HCl Form I is presented for comparison with the recrystallised product obtained after heating paroxetine HCl Form II in the DSC furnace in hermetically sealed pans. The DSC runs were stopped at 125 °C (after the recrystallisation step) and samples were collected for the XRPD experiments. The data obtained confirmed that the form obtained after recrystallisation is, in fact, the stoichiometric hemihydrate, paroxetine HCl Form I.
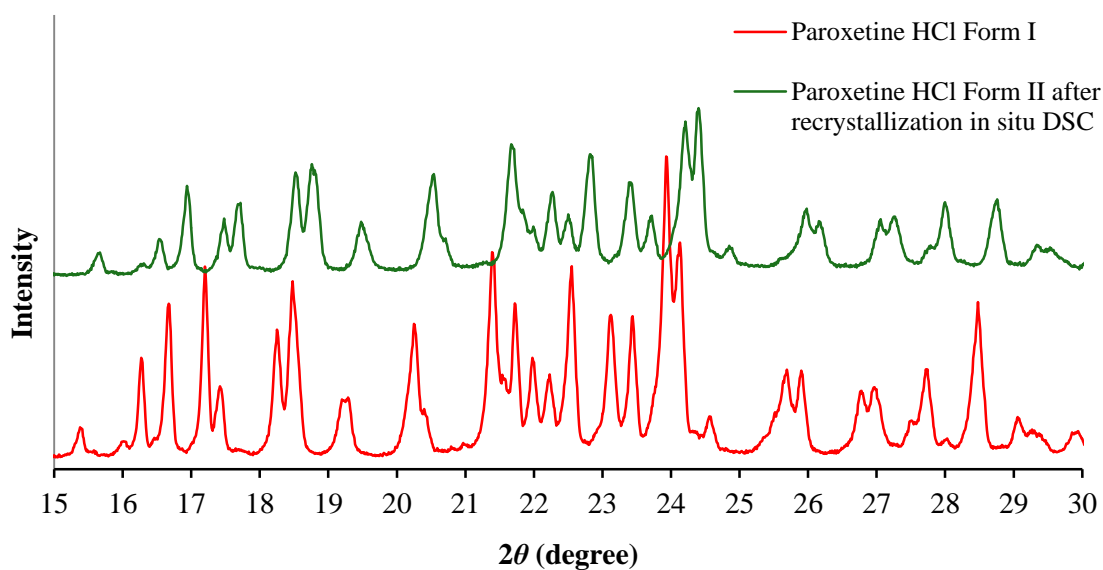
Figure 3.3: XRPD data comparing the form obtained after the recrystallisation of paroxetine HCl Form II when heated in hermetic sealed pans in the DSC furnace (top) and paroxetine HCl Form I (bottom).

Furthermore, when using higher heating rates (HRs) the recrystallisation signal disappeared and, at 50 ^{o}C/min, no melting of the Form I was detected (Figure 3.4).

The melting peak of Form II showed a broader appearance, as is usual when increasing heating rate due to thermal lag effects. However it is also suggested that the recrystallisation to Form I is kinetically hindered and hence does not take place at higher heating rates. Moreover, samples run in hermetically sealed pans at 2 ^{o}C/min but pre-dried over P_2O_5 also showed no evidence of transformation to the Form I (data not shown), further supporting the hypothesis that the conversion involved sorbed water becoming stoichiometrically bound on heating.
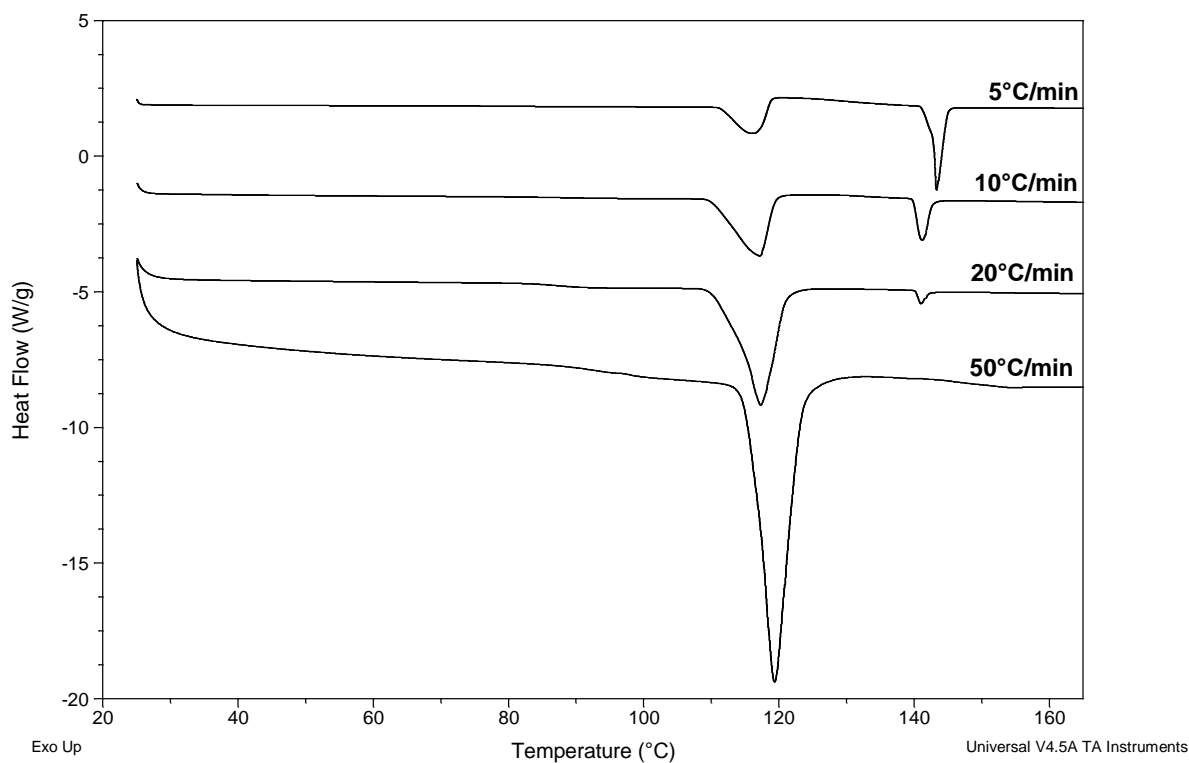
Figure 3.4: Influence of the heating rate on the transformation between Form II and Form I of paroxetine HCl. Standard DSC runs at 5, 10, 20 and 50 °C/min (downwards) were performed in hermetically sealed pans.

3.3.2   Thermogravimetric Analysis (TGA)

Given the role of sorbed water (using the term loosely) that has been identified above, it was clearly essential to have some measurements of both the quantity and binding characteristics of the water present. The TGA signal (Figure 3.5) showed a water weight loss process completed by approximately 140 °C. A continuous weight loss was observed from the starting temperature until approximately 90 °C and after that an evident sharper drop in the weight was noticed, between 100 °C and 130 °C, which corresponds, in total, to a weight loss of $4.45 \pm 0.26\%$. The last and higher drop in the weight around 260 °C is due to the decomposition of the sample. These processes are shown in the derivative signal for clarity.
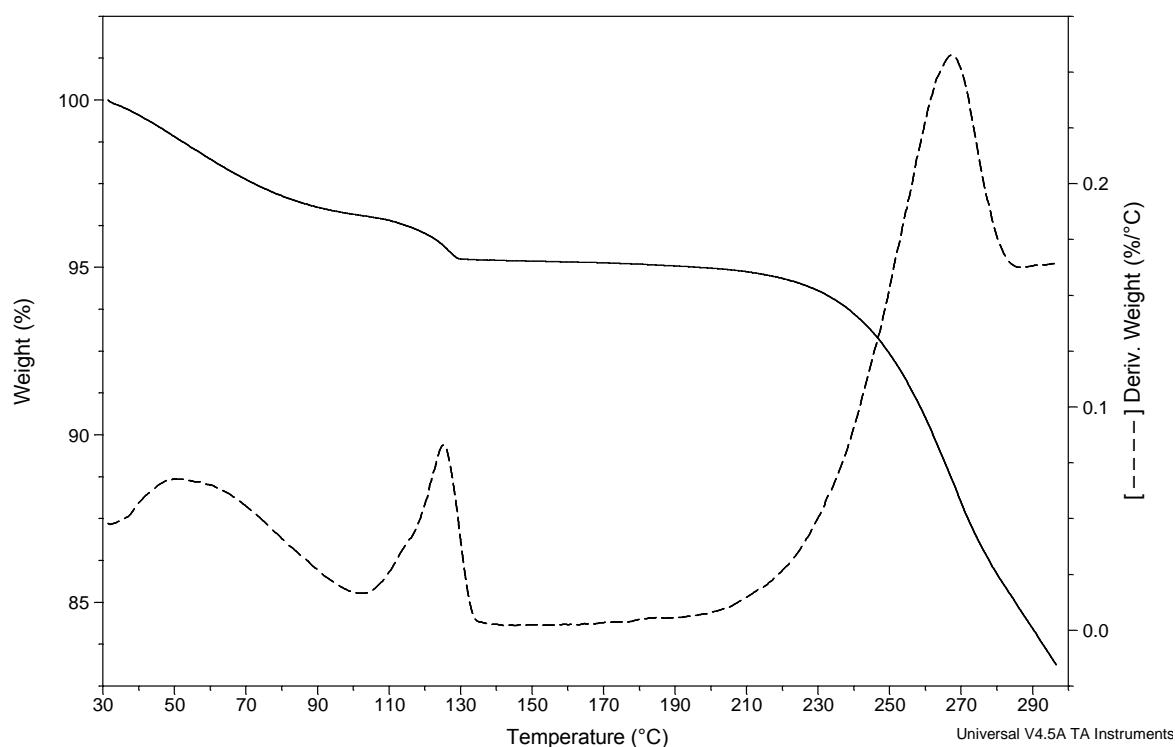
Figure 3.5: TGA curve of paroxetine HCl Form II, showing the weight loss and associated derivative loss curve.

In general, when a stoichiometric hydrate is present, the water molecules are incorporated in the crystal lattice and the water loss signal shows a sharp discontinuity, typically between 80 and 140 $^{\circ}$C. Alternatively, when the water molecules are simply present on the crystal surfaces (adsorbed water), the water loss signal tends to be broader and appears over a wider and lower temperature range, frequently between 60 to 90 $^{\circ}$C (Craig and Reading, 2007). The behaviour shown here appears to demonstrate a steady water loss, typically associated with sorbed water, followed by a sharper loss corresponding to the melting of Form II, indicating release of any remaining water on breakdown of the crystal structure.

On the other hand, the TGA trace of Form I at the same heating rate (data not shown) did not show a continuous weight loss, but rather a sharp drop in weight in a narrow temperature range between 100 and 130 $^{\circ}$C. This is in good agreement with the typical dehydration behaviour of stoichiometric hydrates. The weight loss at this temperature corresponds to $2.60 \pm 0.15\%$ (0.55 ± 0.02 mol of water per mol of drug), which matches well the designation of Form I as a hemihydrate.

3.3.3 Karl Fischer Titration (KFT)

The water content of untreated and dried samples was determined by Karl Fischer titration under ambient humidity (53% RH) and temperature (25.5 ^{o}C). The untreated sample was found to have a water content of $3.83 \pm 0.05\%$ w/w, which corresponds to 0.80 ± 0.01 mol of water per mol of paroxetine HCl. The water content of the sample previously dried over P_2O_5 for 7 days was calculated as $1.65 \pm 0.17\%$ w/w, 0.33 ± 0.03 mol of water per mol of paroxetine HCl.

These results are surprising in that they are high for such a relatively non-polar low molecular weight material; indeed, the amount of water in the dry sample is quite high for a material stored for 7 days at 0% RH. However, as the measurements were performed under atmospheric conditions, the time between weighing and measurement may have been sufficient for some moisture sorption. Even so, this implies quite considerable hygroscopicity. This may be a result of high surface adsorption or, alternatively, molecular internalisation of water, i.e. non-stoichiometric hydrate formation. On this basis a series of spectroscopic and water sorption studies were performed in order to investigate the possibility of such hydrate formation.

3.3.4 Attenuated Total Reflection-Fourier Transformer Infrared (ATR-FTIR)

Infrared spectroscopy is a potentially useful tool to distinguish between the two forms of paroxetine HCl (Form II and Form I) by analysing the spectrum between 3700-3200 cm^{-1} corresponding to the OH stretching region. This area is also useful to monitor temperature-dependent transitions between those forms. The spectrum of Form II, as shown in Figure 3.6, has two main bands at 3633 cm^{-1} and 3395 cm^{-1}, which can be assigned to stretching vibrations involving weakly and strongly H-bonded water H atoms, respectively. If paroxetine HCl Form II was a true anhydrate, it should not show any OH vibration at high wavenumbers, as no water would be present in the crystal lattice. In contrast, Form I

shows a double band at 3401 cm^{-1} and 3339 cm^{-1}, which correspond to two strong H-bonds in different chemical environments.

Some misinterpretations can be easily made in this region due to the presence of a secondary amine, as it was shown in Figure 2.2. The NH stretching in secondary amines usually appears as a single band in the range between 3380-3205 cm^{-1}. However the HCl salt formation can cause a considerable attenuation of the normal NH stretching band and displace it towards lower frequencies (2760 and 2690 cm^{-1}) (Nakamoto et al., 1955; Heacock and Marion, 1956). Owing to the complexity of the spectra in this region, especially due to the overlapping of the aromatic ring vibrations, a clear and precise assignment of the NH band is hard to make.
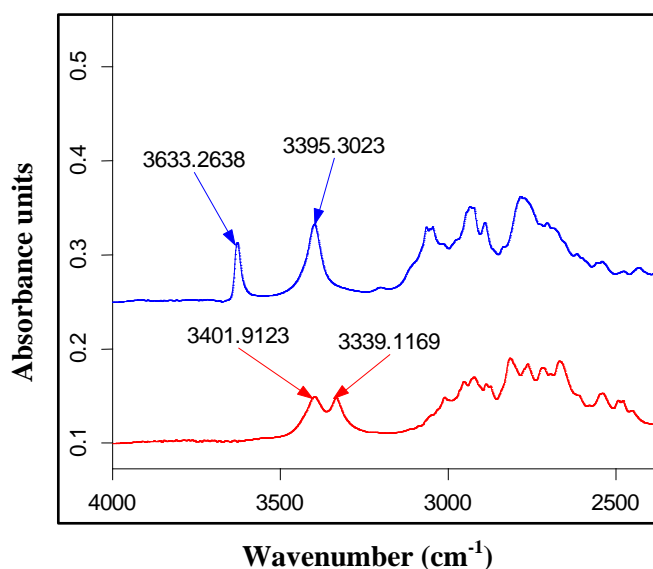
Figure 3.6: ATR-FTIR spectra of paroxetine HCl Form II (top) and Form I (bottom).

The assignment of the OH stretching bands presented in this section for paroxetine HCl Forms I and II is consistent with their respective structural models and H-bonding. Since these will be described in more detail in the molecular modeling section, only a brief discussion, relevant to differences in the ATR-FTIR spectra, will be presented here. The water molecules in Form II can establish two different types of hydrogen bonding: a very weak one to an oxygen from the dioxole ring, which appears as a free OH band with a sharp appearance at a high wavenumber (3633 cm^{-1}); and a strong one to a chloride ion,

which appears as a broad band at a lower wavenumber (3395 cm^{-1}), an indication of stronger hydrogen bond formation (Tang et al., 2002). In Form I the water molecules can establish three strong hydrogen bonds. In two of them the water molecules donate their hydrogen atoms to chloride ions, giving the double band observed at 3401 and 3339 cm^{-1}. The third hydrogen bond is formed with the protonated ammonium nitrogen as the donor and water as the acceptor.

By using variable temperature ATR-FTIR spectroscopy with a constant heating rate of 2 ^{o}C/min, it was possible to observe the pseudopolymorphic transformation between the Form II and the Form I (Figure 3.7). It should be noted that the sample holder is such that, while the sample is not sealed hermetically, water movement is nevertheless partially restricted rendering these results only partially comparable to the DSC data. Nevertheless, the data set provides a useful corroborative perspective by which the transformation may be further studied.
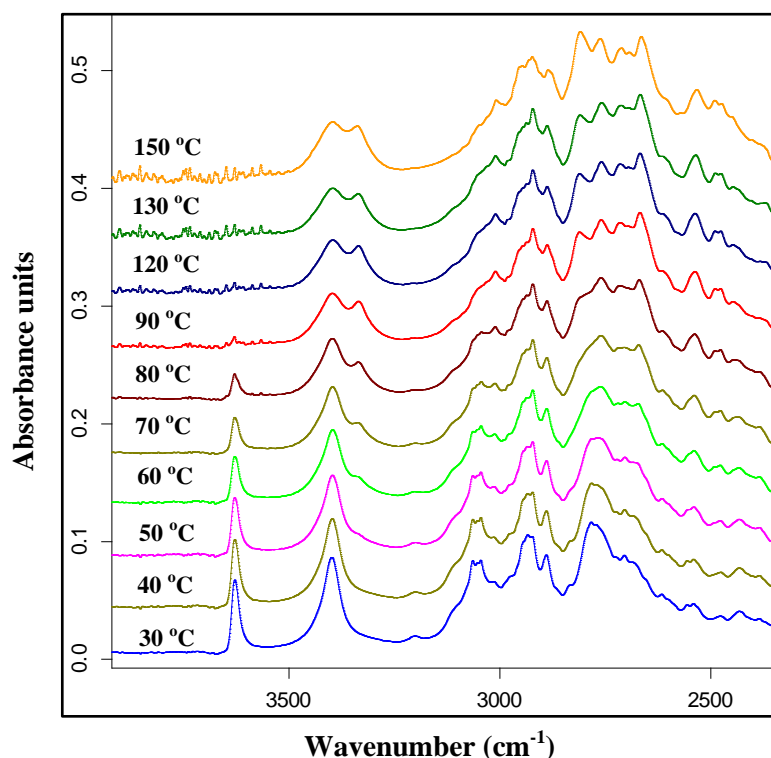
Figure 3.7: Variable temperature ATR-FTIR spectra of paroxetine HCl Form II, measured using a constant heating rate of 2 ^{o}C/min.

Initially, the spectra show the response associated with the Form II (from top to bottom). However, when the temperature reached 50 $^{\circ}$C, a small shoulder started to appear in the region of the hydrogen-bonded OH (3339 cm^{-1}) and the intensity of the free OH stretching band started to decrease. These observations, together with the initial description of those bands, suggest that a new intermolecular hydrogen bond between the OH group from the water molecules and the chloride ion starts to become established, which results in a split of this band characteristic of the Form I. Changes in the spectrum can also be observed in the region at 2500-3000 cm^{-1}.

Overall, not only does Figure 3.7 clearly show transformation between the Form II and the Form I but also indicates that, at temperatures as low as 50 $^{\circ}$C, the interaction between the drug and water is specific and intrinsic to the crystalline lattice structure, rather than being a simple surface adsorption process. While the highest temperatures clearly indicate Form I formation, the intermediate temperatures indicate a mixture between Form II and the Form I, which again is supportive of the suggestion of non-stoichiometric hydrate formation.

3.3.5   Dynamic Vapour Sorption (DVS)

The hydration behaviour of paroxetine HCl Form II under defined humidity and temperature conditions was investigated. Pre-treatment of the sample included drying over P_2O_5 for 7 days, plus an additional drying step of 2 h at 30 $^{\circ}$C and 0% RH inside the DVS chamber to ensure that any residual water was dried off prior to starting, as confirmed by the achievement of a constant weight. Figure 3.8 shows the DVS data for paroxetine HCl Form II. During the sorption cycle a weight gain of 3.53% was observed from 10 to 90% RH, which corresponds to 0.73 mol of water per mol of drug, with 81% of the total water uptake taking place between 10 and 30% RH. From 40 to 90% RH the change in weight is significantly smaller.

The high absolute amounts of water gained, together with the reversibility of the uptake and desorption, again supporting the existence of a non-stoichiometric hydrate. More specifically, the reversibility of the sorption process and the relatively rapid time scales

over which the process takes place is, in general, a property of channel hydrates. Several non-stoichiometric hydrates have been identified to have such water channels at a molecular level (Stephenson and Diseroad, 2000; Ahlqvist and Taylor, 2002; Kumar and Bansal, 2011), which enables the water molecules to move easily both within the structure and between the solid and its environment without causing any structural disruption. On this basis it was considered essential to examine the X-ray powder diffraction profile as a function of both temperature and humidity in order to elucidate whether paroxetine HCl Form II shows similar structural characteristics.
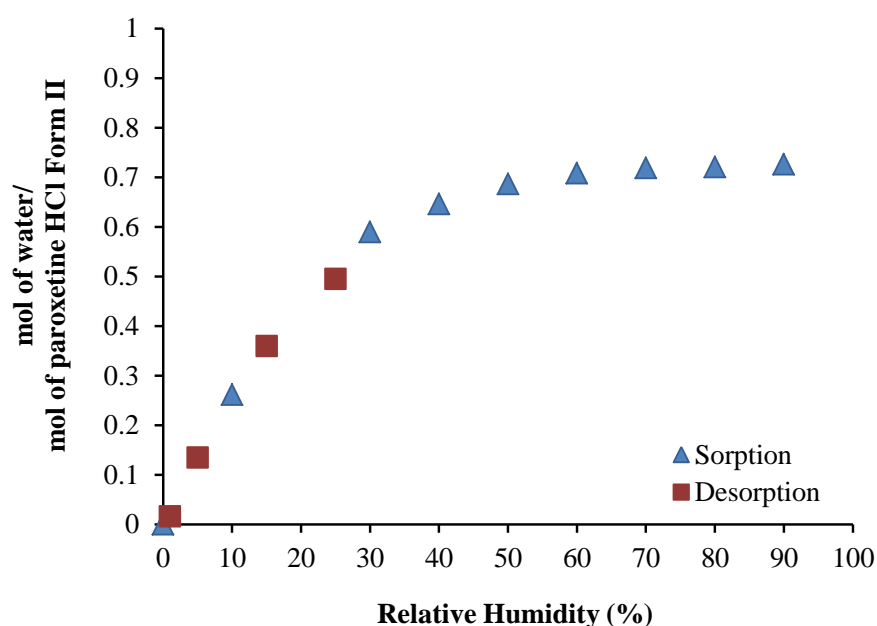
Figure 3.8: Dynamic vapour sorption data for paroxetine HCl Form II.
Sorption and desorption cycles are superimposable.

3.3.6   Variable Humidity X-Ray Powder Diffraction (VH-XRPD)

The crystal structures of two paroxetine HCl hydrate forms have been determined previously: the Form I (Yokota et al., 1999) and a form with the composition paroxetine HCl · 0.8 H_2O (Howard et al., 2003). The latter structure has been submitted to the Cambridge Structural Database (Allen, 2002) as a private communication (reference code EHOXEE), so no detailed information about the origin or preparation of the sample is

available. However, the powder diffraction pattern calculated for paroxetine HCl · 0.8 H_2O matched the experimental diffraction pattern measured for the Form II, confirming that they represent the same crystal structure. While the drug : water ratio of 1 : 0.8 suggests a non-stoichiometric hydrate, the water molecules of this Form II are located in isolated voids (Figure 3.9) an observation which is usually associated with stable stoichiometric hydrates. It also noted that this ratio of water to drug is very similar to the saturation value found from the DVS studies hence it is possible to conclude that the structure given in (Howard et al., 2003) represents the equivalent of a hydrated form of paroxetine HCl but, if this hypothesis is correct, that form is in fact a non-stoichiometric hydrate.
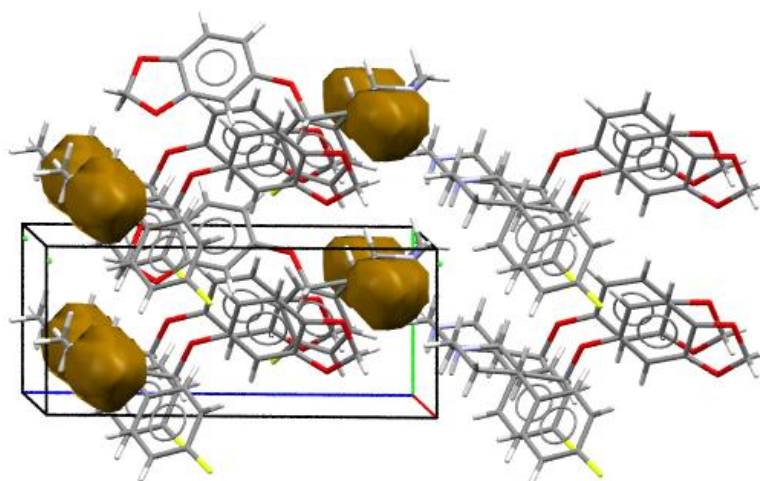
Figure 3.9: Crystal structure of Form II with the water-containing voids highlighted in brown. Generated from data presented in (Howard et al., 2003).

To establish the nature of Form II, variable humidity powder X-ray experiments (VH-XRPD) were performed. If Form II is a variable hydrate then the crystal structure should change continuously with changing RH. If Form II is not a variable hydrate and the gradual change of mass seen in the DVS experiments is caused by the adsorption of water on the surface, hence the powder diffraction pattern should remain the same.

The results showed that the peak positions shifted in response to changes in RH (Figure 3.10 and Figure 3.11). In accordance with the DVS results, most of the change occurs at low RH (below 30%), after which the peak shifts are very small. No appearance/disappearance of peaks was observed in the 1-90% RH range suggesting that humidity alone is insufficient to induce the transformation between Form II and the

Form I; however changes in humidity are capable of causing changes in the lattice spacings, indicating that the lattice is expanding to allow entry of the water.
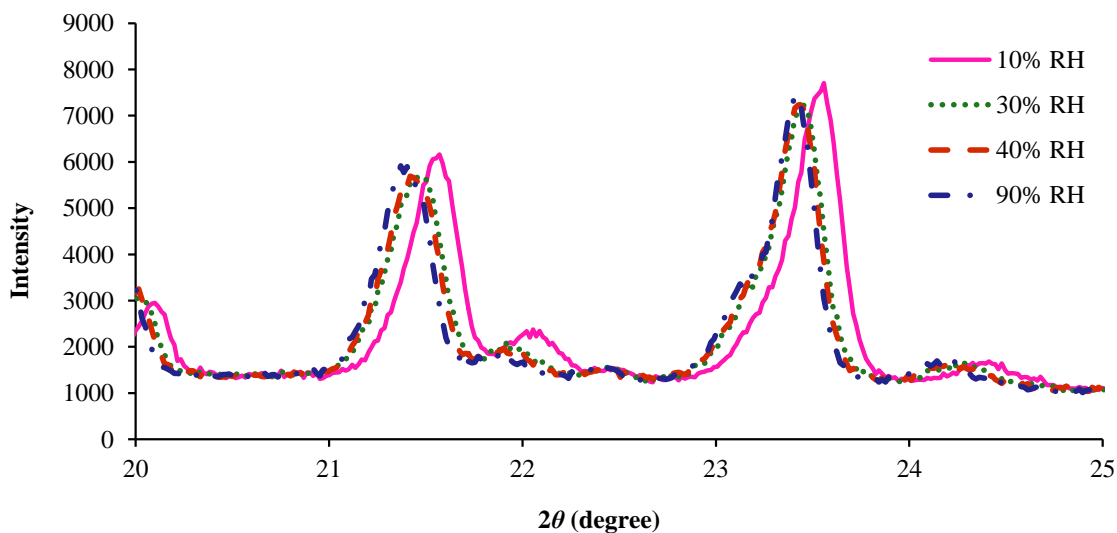
Figure 3.10: Shifts in the diffractogram peaks upon increasing RH.
Only a part of the full XRPD diffractogram (5.0 to 40.0°) is shown to make the peak shifts visible.
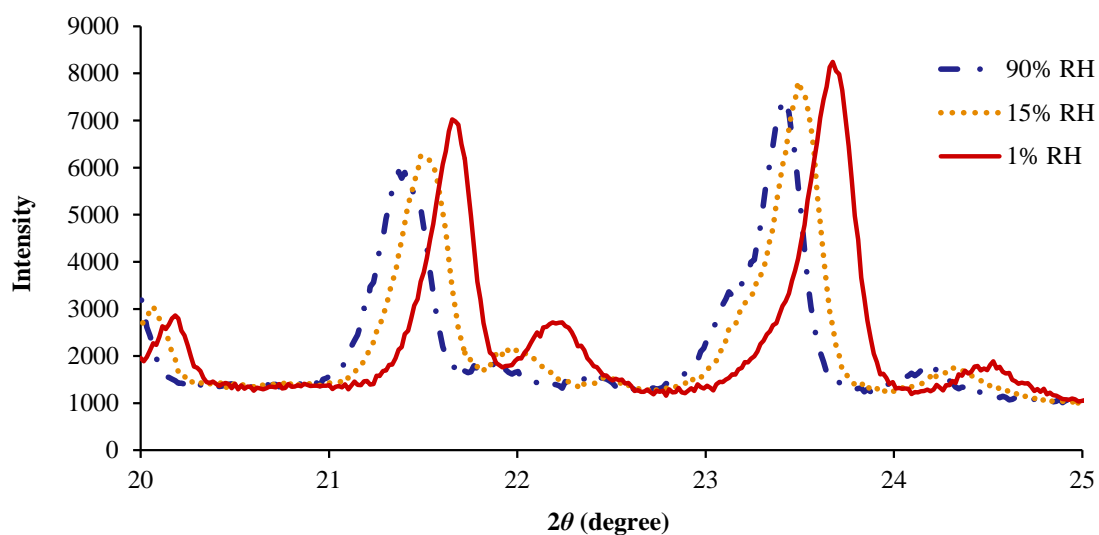
Figure 3.11: XRPD patterns of paroxetine HCl Form II during desorption of water.

The peak shifts indicate changes in the dimensions of the unit cell, namely expansion upon sorption and contraction during desorption (Figure 3.12). The cell volumes determined

during sorption and desorption fall on the same trend line, demonstrating that the transformation is reversible with no apparent hysteresis. The remarkable similarities between the unit cell volume vs RH (Figure 3.12) and the mass vs RH (Figure 3.8) curves confirm that vapour sorption occurs predominantly by incorporating water molecules into the crystal structure, *i.e.*, that the 'anhydrate' Form II is in fact a variable hydrate.
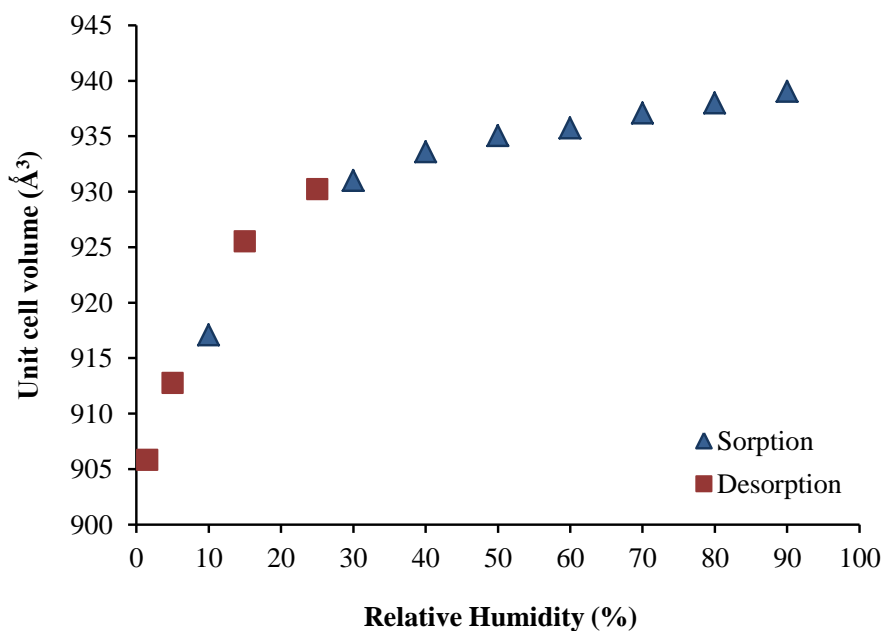
Figure 3.12: Changes in the unit cell volume of paroxetine HCl Form II according to variation in relative humidity (RH).

The gradual peak shifts in the XRPD pattern are again characteristic of non-stoichiometric channel hydrates *e.g.*, risedronate (Redman-Furey et al., 2005), cefazolin and cromolyn sodium (Stephenson and Diseroad, 2000), where water molecules can move in (sorption) and out (desorption) of the crystal while its basic structure remains the same. As a typical example, the crystal structure of cromolyn sodium (Cox et al., 1971; Chen et al., 1999) contains wide channels, which readily explains why water can move within the lattice without disrupting it.

However, in paroxetine HCl Form II the water molecules are located in small voids/pockets instead of channels, so dehydration without disruption is unexpected. The only other example of a variable hydrate with no continuous solvent channels and with an isomorphic desolvate known up to this study is the `monohydrate' form of vitamin B_1

(Te et al., 2003). It has been suggested that dehydration/hydration of this material occurs through a cooperative deformation mechanism, which allows retention of structural information (Chakravarty et al., 2009a;b). A unique feature of paroxetine HCl Form II is that it reaches equilibrium at each RH within minutes. Such a fast equilibration is more characteristic of surface water than of hydrates, which explains why this material is currently believed to be a hygroscopic anhydrate form.

3.3.7 Crystal Structure Models

The experimental crystal structure of the Form II is incomplete, because the H atom positions of the water molecule have not been determined. The O atom from water appears to be involved in an extremely short CH···O bond ($d_{H··O}$ = 2.26 Å), which is probably an experimental error arising from the high uncertainty with which the water O coordinates could be determined from powder diffraction data. To obtain a more detailed description of the structure, models of both a monohydrate and an isostructural dehydrate were generated computationally from the experimental structure. In the initial configuration of the monohydrate model, one of the missing H atoms was placed to point towards a nearby chloride ion, which is well within H-bonding distance of the water molecule ($d_{O··Cl}$ = 3.14 Å in the experimental structure). The other water H atom was pointing in an arbitrary direction enclosing a bond angle of 109.5^o with the first one. The initial configuration for the anhydrate was generated by simply removing the water O atom from the experimental structure. The final computational models were then obtained by geometry optimisation starting from these initial configurations.

The unit cell volumes for the fully hydrated and the anhydrate models are 948 Å^3 and 915 Å^3, which are in good agreement with the highest and lowest unit cell volumes found in the VH-XRPD experiments, 939 Å^3 and 905 Å^3, respectively (see Appendix A, Table A1).

As expected, the two structures remain highly similar both to each other and to the experimental structure (Figure 3.13). In contrast to most channel hydrates, the dehydrate form does not contain residual voids, *i.e.* it is non-porous. The fact that such a simple

computational protocol gave a non-porous model highlights the possibility of a smooth and continuous transition between the hydrated and dehydrated states of Form II, and it is consistent with the experimentally observed retention of the same overall structure even when the RH is reduced to 1%.
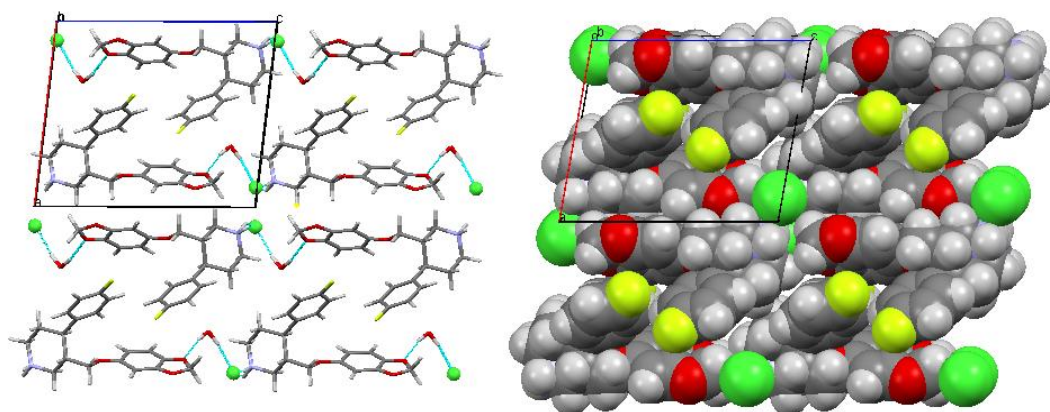
Figure 3.13: Comparison of the hydrate (left) and anhydrate (right) models of Form II. The anhydrate model is presented as a space-filling model to show the lack of unoccupied space in the structure.

In general, the water molecules of non-stoichiometric hydrates are weakly bound and can be removed without significant changes in the rest of the structure. The model of paroxetine HCl Form II shows (Figure 3.14) that each water molecule hydrogen bonds to a chloride ion (strong acceptor) and to an oxygen atom in the dioxole ring of the drug molecule (weak acceptor).
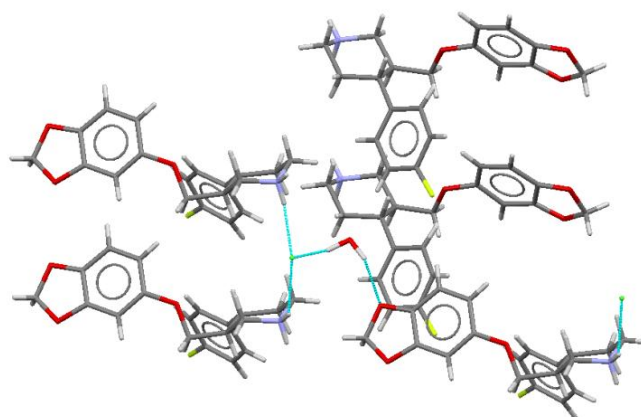
Figure 3.14: Hydrogen-bonding environment of the water molecule in paroxetine HCl Form II.

Consequently, removal of a water molecule from Form II requires breaking of at least one strong hydrogen bond in addition to some structural rearrangement to allow movement of the water molecule between adjacent cavities. These requirements make the quick hydration/dehydration of Form II rather surprising. Note, however, that the water molecules of the Form I are involved in three strong hydrogen bonds, formed with two chloride ions and with a protonated ammonium nitrogen, respectively, so the higher stability of the Form I is readily explained (Figure 3.15).
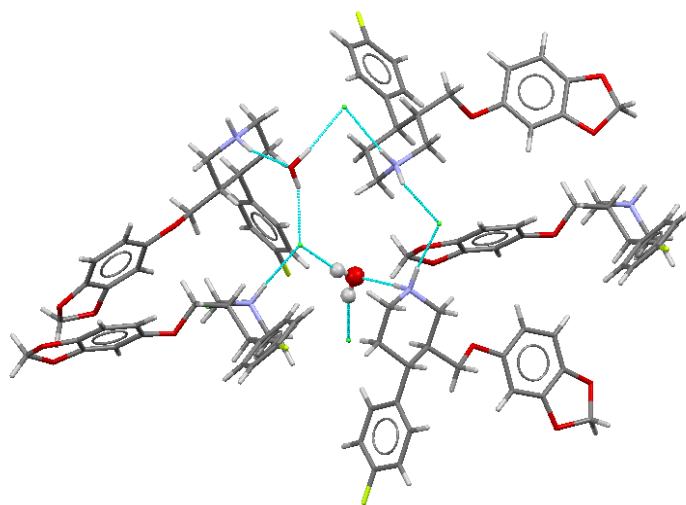
Figure 3.15: Hydrogen-bonding environment of the water molecule in Form I.

3.4   Conclusions

The distinction between strong hygroscopic behaviour and hydrate formation is sometimes very opaque and can lead to misinterpretations. In this study, it was shown that the hygroscopic nature of paroxetine HCl has led to incorrect classification of this material as an anhydrate. The evidence for this is as follows. First, the large amount of water content determined by using TGA, KF titration and DVS raise doubts regarding the anhydrate classification of this drug. In general, the water adsorbed on the surface of an API is around 1%, but paroxetine HCl Form II has a water uptake more than three times higher than this. The rapid and extensive water uptake into the structure at low RH ($\approx 30\%$) in itself indicates that paroxetine HCl Form II is likely to be a non-stoichiometric hydrate. This is also supported by the thermal analysis (DSC) data that indicated that the sorbed water associated with this form, on heating slowly under hermetic conditions, become incorporated into the crystal structure of the drug to form the Form I. This is in itself very unusual behaviour, but is consistent with the notion of the water being incorporated into the structure rather than simply sorbed onto the surface.

Secondly, to support the non-stoichiometric hydrate hypothesis, variable humidity XRPD studies were performed. It was observed that on increasing the RH, shifts in the peak positions of the XRPD diffractogram were evident until 30% RH, which is in accordance with the observations in DVS. During desorption, the shifts in the peaks followed the decrease in the RH. In both cases there were no changes to the crystalline pattern, showing that the water sorption process led to changes in lattice spacing but no fundamental change to the lattice arrangement.

In most recorded cases, this water sorption behaviour is characteristic of a specific subgroup of non-stoichiometric hydrates, the channel hydrates, where the existence of connecting pathways allows the smooth departure of the water without any structural deformation. However, the analysis of the structure of Form II indicates that the water in not located in channels but in small voids and also is not weakly bonded to the crystalline structure, as expected, which makes the hydration/dehydration of this material an uncommon feature. The location of the water within the structure together with the energy supply, explains the pseudopolymorphic transformation observed either in the MTDSC,

when hermetic sealed pans were used, as well as, in variable temperature ATR-FTIR experiments.

As a conclusion, this work suggested that the classification of paroxetine HCl Form II should be reviewed, since the designation as an anhydrate form is no longer reliable. Also the non-standard behaviour for this non-stoichiometric hydrate in that the water is not present in channels but in pores, rendering the absence of hysteresis on sorption and desorption, along with the change in lattice dimensions, it was found extremely unusual. However, the broader implications of the study lie with the notion that differentiation between a hygroscopic anhydrate and a non-stoichiometric hydrate may be extremely difficult and hence the question naturally arises as to whether such non-stoichiometric systems are more common than is generally appreciated. Such knowledge is of considerable relevance to pharmaceutical performance, both in terms of quality control of a system which changes its crystal structure reversibly in different humidity environments but also in terms of physical and possibly chemical stability.

4 An Investigation into the Dehydration Behaviour of Paroxetine HCl Form I using a Combination of Thermal and Diffraction Methods: The Identification and Characterisation of a New Anhydrous Form

Abstract

As already described in Chapter 3, paroxetine HCl can exist as a non-stoichiometric hydrate (Form II) or as a stoichiometric hemihydrate (Form I); the latter is considered to be the stable form and its structure is well-known. However, little work has been performed to investigate its dehydration behaviour, hence the generation of the anhydrous form via dehydration of paroxetine HCl Form I was investigated. A combination of thermal (standard differential scanning calorimetry (DSC) and modulated temperature DSC (MTDSC), thermogravimetric analysis (TGA) and hot stage microscopy (HSM)) and diffraction (variable temperature X-ray diffraction, VT-XRPD) techniques were used. Karl Fischer titration (KFT) and scanning electronic microscopy (SEM) were used to determine the water content and collect microphotographs of the crystals, respectively. Dehydrated Form I was prepared using ultra-dry conditions and the resulting product compared to dehydrated Form II. DSC indicated that the two dehydrated forms of Form I and II had distinct melting points. TGA experiments allowed the calculation of the activation energy for the dehydration of Form I, which varies between 86–114 kJ/mol. Pawley refinement of the VT-XRPD data suggested that Form I dehydrates to an isostructural anhydrate, since the unit cell parameters of this new form were very similar to those of Form I with only a smaller volume as consequence of dehydration. Comparison with dehydrated Form II indicated that these two forms represent different crystal entities, hence a new anhydrous form of paroxetine HCl has been identified.

4.1 Introduction

Hydrates are often the most physically stable form of an active pharmaceutical ingredient (API) under conditions of relative humidity (RH) typically found on storage, hence their use remains extremely widespread. Nevertheless, their dehydration and rehydration behaviour is often complex, with multiple forms possible which render thorough investigation of such interchanges necessary for both practical and regulatory reasons. The dehydration process occurs when the water activity of the surrounding environment is lower than the water activity in the solid compound (Cui and Yao, 2008). Once the water is removed from the crystal structure packing, different structural consequences may occur (Petit and Coquerel, 1996):

(a) breakage of the crystal lattice, followed by a rearrangement into a new anhydrous form (Leung et al., 1998);

(b) the crystal structure remains the same after dehydration forming an isomorphic/isostructural dehydrate (Hirayama et al., 2000; Suzuki et al., 2012; Te et al., 2003; Stephenson et al., 1998);

(c) partially or totally disordered state followed by a collapse into an amorphous phase (Chen et al., 1999; Vogt et al., 2006).

Isostructural dehydrates (b) are associated with high free energy, which may be reduced by re-incorporation of solvent molecules into the lattice, rendering this type of compounds highly hygroscopic (Hilfiker, 2006). Dehydration is not always a straightforward process and a mix of phases can be obtained with a combination of more than one of the aforementioned mechanisms taking place. An example is the case of eprosartan mesylate dihydrate (Sheng et al., 1999) whereby after losing the first water molecule, the monohydrate dehydrates and collapses into an amorphous state, followed by recrystallisation into an anhydrate form of eprosartan mesylate. Another case is the dehydration of trehalose dihydrate whereby the product obtained is highly dependent on the dehydration conditions employed (Willart et al., 2002). More specifically, fast dehydration produces an amorphous phase, whereas a slow dehydration produces a crystalline phase (α-polymorph) of anhydrous trehalose.

Thermal analysis techniques such as differential scanning calorimetry (DSC) and thermogravimetric analysis (TGA) are widely used to evaluate the dehydration behaviour and the solid state stability of pharmaceutical hydrates. Two main approaches can be used to evaluate solid state kinetics (Khawam and Flanagan, 2006a): the sample is held at a constant temperature for a specified period of time (isothermal methods), or heated at a constant heating rate (non-isothermal methods). For both methods, it is possible to calculate the conversion fraction (α) where isothermal methods produce α-time data (Equation 4.1) and non-isothermal methods produce α-temperature data (Equation 4.2),

$$\alpha = \frac{m_0 - m_t}{m_0 - m_\infty}$$

Equation 4.1

where, m_0 is the initial sample weight, m_t is the sample weight at the time, t, and m_∞ is the final sample weight.

$$\alpha = \frac{m_0 - m_T}{m_0 - m_\infty}$$

Equation 4.2

where, m_T is the sample weight at temperature, *T*. The extent of conversion, α, increases from 0 to 1 as the process progresses and kinetic analysis (isothermal or non-isothermal) can be performed either by model-fitting or model-free methods (Khawam and Flanagan, 2006a).

Model-fitting approaches involve expressions (Appendix B, Table B3) to which the experimental data (isothermal or non-isothermal) is fitted. The model that gives the best fitting (R^2 closer to 1) is selected to calculate the kinetic triplet which involves: the activation energy, E_a (kJ/mol), as the energy barrier to overcome dehydration (for the present study), the pre-exponential factor, *A* (min^{-1}) and the kinetic model (Khawam and Flanagan, 2006a). Model-fitting methods assume a single value of E_a for the overall reaction process, thereby implying a single reaction mechanism and do not provide an adequate interpretation of complex kinetic reactions (Vyazovkin et al., 2011). Another approach used to calculate the kinetic parameters of a dehydration reaction is by using model-free methods. As the designation implies, model-free methods are applied without any modelistic assumptions and therefore irrespectively of the underlying reaction model.

As a result, they are capable to quantify the dependence of the E_a at each conversion fraction, *α*, and thus are also known as isoconversional methods. Model-free methods enable to highlight the complexity of the kinetic reactions, which allows a more accurate determination of the Arrhenius parameters (Khawam and Flanagan, 2006a).

Paroxetine HCl Form I is a stoichiometric hydrate with half mol of water per mol of drug, as shown by its chemical structure in Figure 4.1.
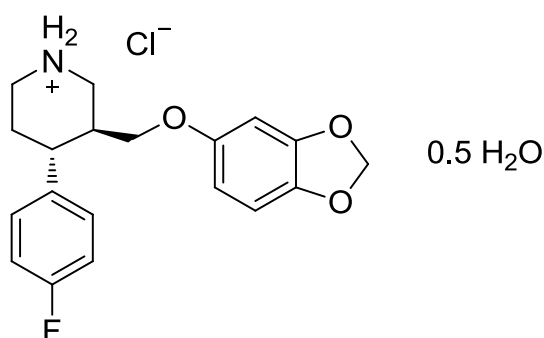
Figure 4.1: Chemical structure of paroxetine HCl Form I.

Barnes et al. (Barnes et al., 1988) reported the preparation of paroxetine HCl Form I and described this form as being extremely stable, with the removal of the water from the crystalline structure being possible under extreme desiccant conditions, with a quick rehydration to the hemihydrate form. A decade later, Ibers (Ibers, 1999) published the crystal structure of paroxetine HCl Form I, which indicated that the water molecules are linked to a N-H··O via a hydrogen bond 2.772(6) Å in length. The author suggested that this was the bond associated with dehydration and should be easily cleaved, hence theoretically dehydration should occur readily. It is now believed that the water molecules of the Form I are involved in three strong hydrogen bonds, formed with two chloride ions and with a protonated ammonium nitrogen, respectively, explaining the observed stability of Form I (shown in Chapter 3). Though the crystal structure of paroxetine HCl Form I is now well-known, an important gap in the understanding of this form is related to its dehydration behaviour (Farjas et al., 2010).

Paroxetine HCl can also exist in Form II, as shown in Chapter 3, identified as being a non-stoichiometric hydrate. Form II retains the same crystal structure when dehydrated

forming an isostructural dehydrate with only expansion and contraction on the crystal lattice volume, respectively.

In an effort to better understand the interplay between hydrated and anhydrous forms, a thorough investigation into the dehydration behaviour of paroxetine HCl Form I was carried out using a combination of thermoanalytical techniques (standard differential scanning calorimetry (DSC) and modulated temperature DSC (MTDSC), thermogravimetric analysis (TGA) and hot stage microscopy (HSM)) and high resolution variable temperature X-ray powder diffraction (VT-XRPD). The water content of the sample was determined by Karl Fischer titration (KFT) and the morphology of crystals was observed under scanning electron microscopy (SEM). The purity of the sample obtained after the dehydration of Form I was determined using high performance liquid chromatography (HPLC). Additionally, the activation energy, E_a, needed to dehydrate Form I was calculated using non-isothermal model-free (Ozawa-Flynn-Wall) approaches; isothermal model-fitting (Standard) methods were used in order to identify the best kinetic model as a means of describing this dehydration process. The work presented in this chapter aims to examine whether dehydration from two significantly distinct hydrate forms leads to the same anhydrate for this material. This question is particularly pertinent given the unusual nature of the non-stoichiometric Form II and, as will be shown, the very unstable nature of the Form I anhydrate, hence little precedent exists to determine whether the Form I (hemihydrate) will yield the same dehydrated form.

4.2   Materials and Methods

4.2.1   Materials

Paroxetine HCl Form I was purchased from Afine (China) and was used as received or after being kept over phosphorus pentoxide (P_2O_5), Alfa Aesar (UK) or in a static oven, as stated. For HSM observations, Form I was recrystallised from methanol by solvent evaporation method.

4.2.2 Methods

4.2.2.1 Thermal Analysis

Standard differential scanning calorimetry (DSC, Q2000 TA Instruments) analysis was performed at heating rates of 2, 5, 10, 20 and 50 ^{o}C/min. Modulated temperature DSC (MTDSC, Q2000 TA Instruments) analysis was conducted using a heating rate of 2 ^{o}C/min, amplitude $\pm$ 0.318 ^{o}C and a period of 60 seconds. Scans were carried out within the temperature range 0 °C to 170 °C. Pinhole, hermetically sealed and open pans (pinhole pans without lid) were used as stated.

Thermogravimetric analysis (TGA, Q5000 TA Instruments) of paroxetine HCl Form I was performed in aluminium open pans by weighing approximately 5 mg of sample with controlled particle size between 63-106 μm. Nitrogen purge at a constant rate, 25 mL/min, was maintained during each run. Non-isothermal experiments were performed at heating rates of 1, 2, 3, 4 and 5 °C/min from 30 °C until 300 °C. Isothermal studies were carried out at 75, 80, 85, 90 and 95 °C with each sample been rapidly heated to the set temperature at a 50 °C/min and kept isothermal until a constant weight change was achieved.

Hot stage microscopy (HSM, Leica DM L52) studies were conducted by placing Form I between a slide and a cover slip inside a hot stage chamber (FP82HT, Mettler Toledo) connected to a FP90 central processor. The sample was heated up at 2 ^{o}C/min from 30 to 150 ^{o}C and the observed thermal events were digitally captured (Studio 86 Design Capture Software).

4.2.2.2 Karl Fischer Titration (KFT)

KFT (Mettler Toledo DL38) for water determination of Form I was carried out by weighing between 40 to 50 mg of the untreated bulk sample.

4.2.2.3 Scanning Electron Microscopy (SEM)

SEM (JSM5900 LV) was used to acquire microphotographs on the untreated Form I and after being kept isothermal in TGA for 1 h at 90 and 110 ^{o}C. To improve conductivity prior

examination, samples were coated with gold using a Polaron SC7640 sputter gold coater (Quorum Technologies).

4.2.2.4   High Performance Liquid Chromatography (HPLC)

HPLC (Agilent HP 1100 Series System) was carried out using a Supelco Ascentis Express C18 (Sigma). Mobile phase consisted of 0.1% TFA in water and 0.085% TFA in acetonitrile and a flow rate of 2.0 mL/min was used. The samples were analysed at 255.9 nm.

4.2.2.5   Variable Temperature X-Ray Power Diffraction (VT-XRPD)

VT-XRPD experiments (Bruker D8 Advance, Bruker) data sets were collected from 5.0° to 30.0° at 2θ under nitrogen purge with a flow rate of approximately 50 mL/min and 99.9% purity. The sample was placed in an Anton-Paar TTK450 (Anton-Paar) chamber at 25 °C. The temperature was controlled by a Temperature Control Unit TCU 100 (Anton-Paar) and the applied heating rate was set by default to 0.167 K/s. Diffractograms were recorded during heating at 25, 50, 75, 100 and 110 °C, and cooling at the same temperatures as during heating. The sample was maintained under isothermal conditions for different periods of time at each temperature, according to the knowledge provided by preliminary studies.

Unit cell parameters were determined by Pawley refinement of the collected patterns using the software TOPAS-Academic (Coelho, 2007). The initial values of the cell parameters for the refinement at 25 °C were taken from the single crystal structure of Form I. Refinements of powder patterns at higher temperatures were initiated from cell parameters refined in the previous heating or cooling step. The pattern recorded at 100 °C during cooling was indexed in TOPAS-Academic and the refinement was based on the cell parameters from indexing.

4.3   Results and Discussion

4.3.1   Thermoanalytical Investigation of the Dehydration Process

The thermal behaviour of paroxetine HCl Form I was investigated by DSC using three types of pans: pinhole, hermetic and open. As presented in Figure 4.2, the type of pan used has a profound effect on the thermal response observed. As expected, it was found that the accurate melting point of Form I has to be measured in hermetic pans (in order to avoid dehydration) and has an onset temperature of 142.0 ± 0.2 °C, which matched the reported value in the literature (Barnes et al., 1988). However, when pinhole and open pans were used, the onset melting temperature of Form I was shifted to lower temperatures and appeared as a broad and poorly resolved profile.
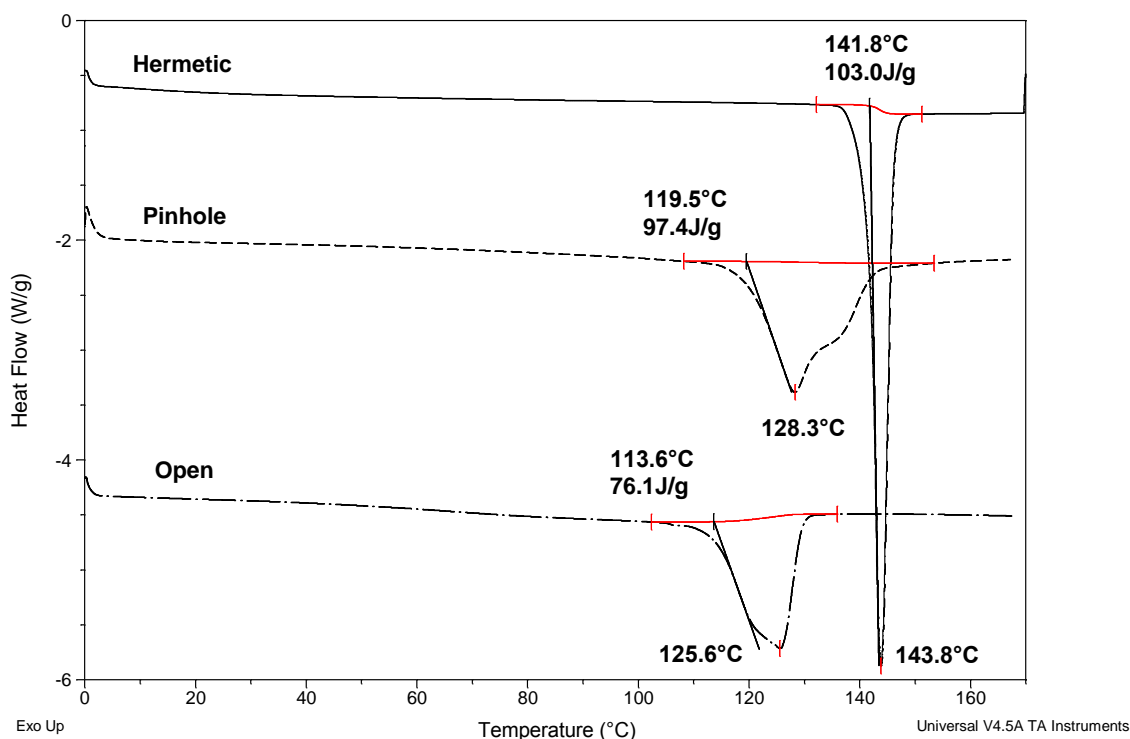
Figure 4.2: DSC traces of paroxetine HCl Form I at 10 °C/min in hermetic, pinhole and open pans.

The effect of the heating rate (HR) (2, 5, 10, 20 and 50 ^{o}C/min) was tested using the three types of pans (data not shown). In pinhole pans, as the heating rate increased, the peaks became broader and at 50 °C/min the melting event was shifted closer to the melting of the hydrate Form I. The results obtained at different HRs with hermetic pans were the same at all the heating programs used. With open pans, a significant dependence on heating rate was observed, with slower rates indicating a distinct endotherm which we associate with a dehydration process (supported by TGA studies as discussed later).

Figure 4.3 shows the DSC responses of paroxetine HCl Form I and II in open pans (2 ^{o}C/min) so as to highlight the differences in behaviour between the two forms studied under identical conditions. First of all, the water loss was detected at different temperature ranges for the two forms. In the case of Form II, the water loss started from the beginning of the run, while for Form I the loss occurred roughly between 50 and 100 ºC. The onset melting temperature was detected at 111.9 ± 0.4 ºC for Form I and at 117.5 ± 0.4 ºC for the Form II, resulting in a difference of almost 6 ºC between the onset melting points of these two forms, while the peak melting temperatures differed by almost 3 ^{o}C. At this early stage of the investigation these results, while not conclusive, indicated that there may be differences in the anhydrate forms generated from the dehydration of the two hydrate forms.
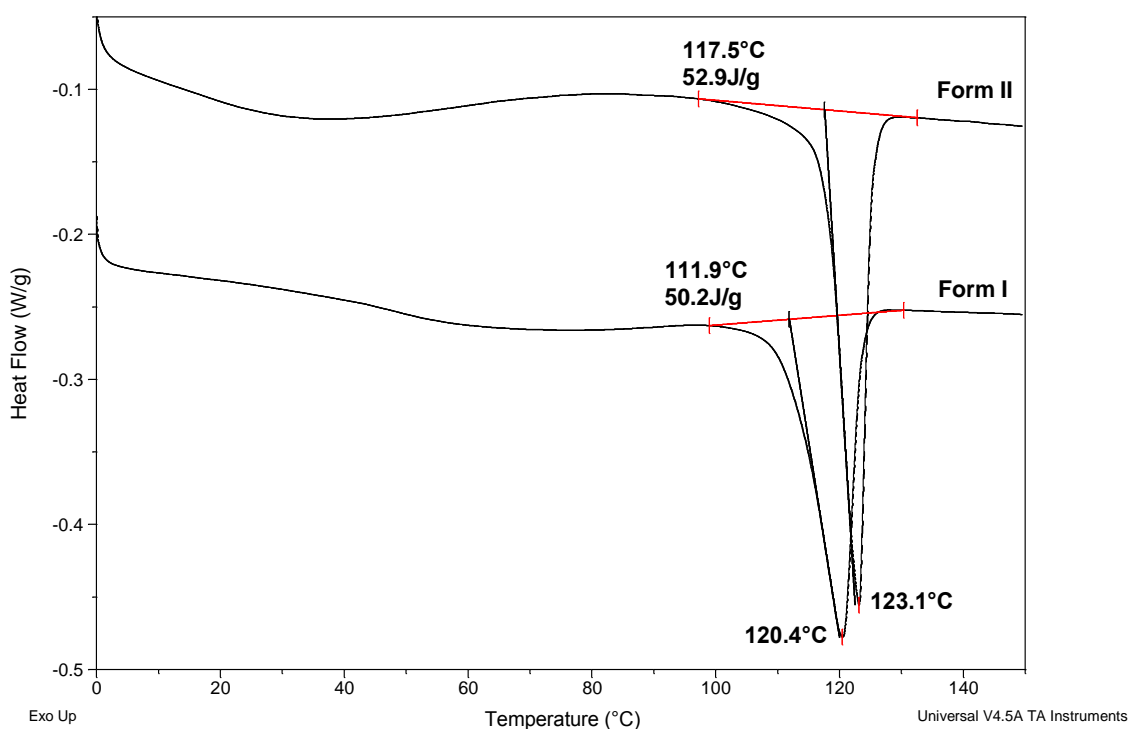
Figure 4.3: Standard DSC traces of paroxetine HCl Form I and II when heated in open pans at 2 °C/min.

After this, the conditions required to dehydrate Form I were investigated, working on the assumption that the anhydrate could be identified by a melting point onset of circa 112 °C. Surprisingly, the only means of producing this form was within the DSC, with storage over P_2O_5 or oven drying both resulting in only partial dehydration (Table 4.1). Preliminary studies indicated that a functioning water filter on the nitrogen supply was also essential (data not shown), further reinforcing the hypothesis that the environment must be extremely dry to allow dehydration of Form I to occur. This also led to the consideration that physical isolation of the anhydrate was extremely difficult, as any exposure to humidity resulted in reconversion. Consequently, all the subsequent studies involve the assessment of the structure within the instrument used to generate the anhydrate.

In contrast, Form II was completely dehydrated inside the DSC, when held isothermally in the oven or stored over P_2O_5. Complete dehydration of Form II was confirmed by the detection of a single endotherm event corresponding to the melting of the dehydrated Form II ($\approx$ 117 °C). Overall, this set of comparative experiments suggested that the

dehydration of Form II is a much simpler process than the dehydration of Form I, able to happen over a wider range of conditions with a more stable product being generated.

Table 4.1: Dehydration studies of paroxetine HCl Form I and Form II performed at different drying conditions.

Sample	Experimental drying procedure	$T_{\text{m onset}}$ (°C)	$\Delta H_{\text{melting}}$ (J/g)	$T_{\text{m peak}}$ (°C)
Form I	DSC open pans	111.9 ± 0.4	50.4 ± 1.4	120.4 ± 0.1
	*Oven 100 ºC/24 h	136.7 ± 0.8	85.2 ± 0.2	140.9 ± 0.1
	*P$_2$O$_5$/48 h	138.9 ± 0.9	91.5 ± 2.4	141.1 ± 1.5
Form II	DSC open pans	117.5 ± 0.4	53.1 ± 1.0	123.1 ± 0.1
	*Oven 100 ºC/1 h	116.6 ± 0.2	56.2 ± 2.0	120.1 ± 0.3
	*P$_2$O$_5$/48 h	117.2 ± 0.9	53.2 ± 0.2	120.5 ± 1.7

*Measurements were made in hermetic pans. All the experiments were performed at 2 ºC/min.

Another important aspect in this study was to ensure that the complete dehydration of paroxetine HCl Form I was not associated with any amorphisation of the sample. Therefore, a heat-cool-heat procedure was set up at 2 ºC/min using open pans; MTDSC was used to identify particular transitions such as T_g in case the sample becomes amorphous after dehydration. As presented in Figure 4.4 it is possible to observe a typical water loss signal for Form I in the 1$^{\text{st}}$ heating cycle. On cooling, no thermal events were detected either in total or reversing heat flow. Surprisingly however, on the 2$^{\text{nd}}$ heating cycle a broad endothermic transition between 40 and 60 ºC was noticed. The first assumption made was that this transition could be a glass transition event as consequence of amorphisation after dehydration. However, the transition was not observed on the reversing heat flow signal, which then excluded this hypothesis. The possibility of this transition being an artefact was eliminated, with the same results being obtained either

using pans from different batches or the same procedure carried out using different DSC instruments.
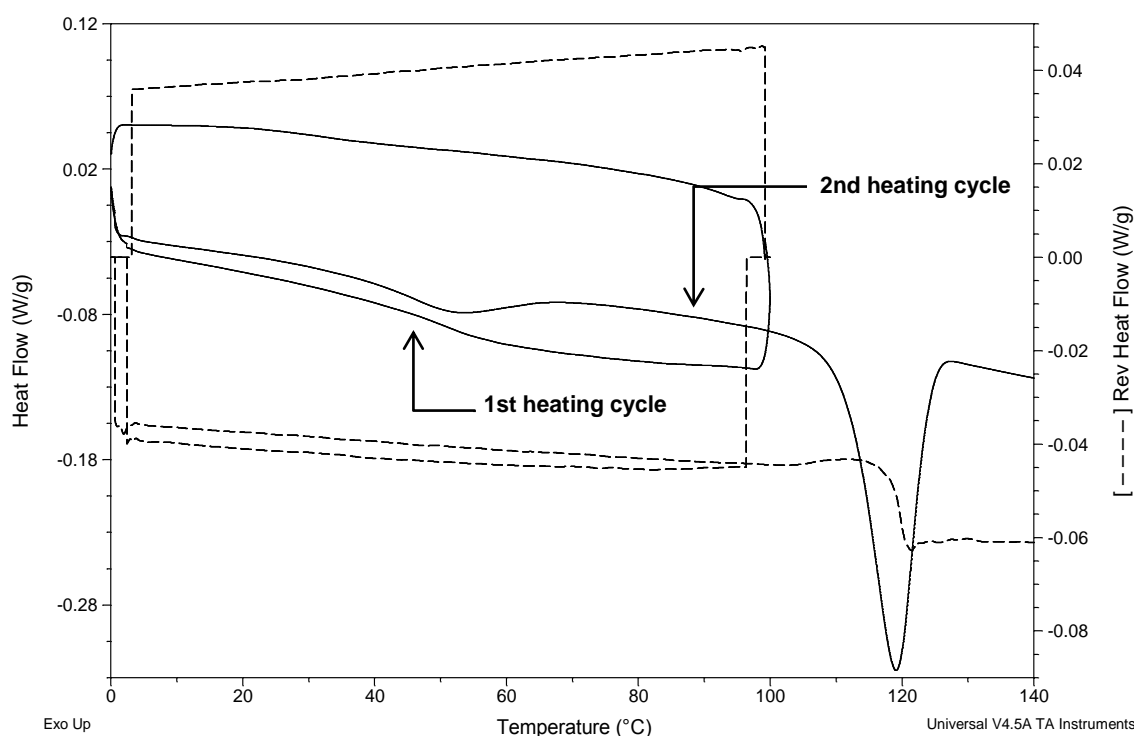
Figure 4.4: Dehydration of paroxetine HCl Form I inside DSC through heat-cool-heat cycling procedure in open pans. MTDSC was used with a HR of 2 $^{\circ}$C/min, modulation amplitude of 0.318 $^{\circ}$C and a period of 60 sec.

At this point, the most likely explanation for the transition was water evaporation. However, as the DSC cell is a closed system, the only possible source of moisture would be the nitrogen purge gas. To confirm this possibility the same cycling procedure was carried out in pinhole pans, which would partially restrict the exposure of the sample to the nitrogen gas. Under these conditions, the endothermic transition was not observed in the 2nd heating cycle (data not shown). These observations suggest that even with a water filter, the system is sufficiently hygroscopic to pick up water, probably via surface sorption as there was no evidence of regeneration of the hydrate form. This further demonstrates the experimental difficulties associated with handling such a hygroscopic sample.

The thermal behaviour of paroxetine HCl Form I under heating was confirmed by using hot stage microscopy (HSM). However, the crystals of paroxetine HCl Form I as received

were not big enough for a clear observation under HSM, therefore paroxetine HCl Form I was recrystallised in methanol (solvent evaporation method) and crystals with a greater size were obtained. The DSC traces and the water content measured by TGA confirmed the recrystallised form to be Form I.

From the microphotographs collected at different temperatures, as shown in Figure 4.5, paroxetine HCl Form I dehydrated upon heating and at around 120 ^{o}C some surface melting of the crystal can be observed. The overall melting process happened over a broad range of temperature ($\approx$ 13 ^{o}C) with the offset melting temperature being detected at around 133 ^{o}C. It should be noted that the environment inside the hot stage furnace is obviously different from the DSC cell and as a result, the complete dehydration of the sample was not achieved. These facts are fairly understood, firstly due to the non-hermetically conditions provided by the HSM furnace and secondly the inexistence of nitrogen purge which makes the dehydration of this form harder to happen. In a broader view, however, these results support the DSC data and the idea of the dehydration of Form I followed by the melting of the anhydrous form.
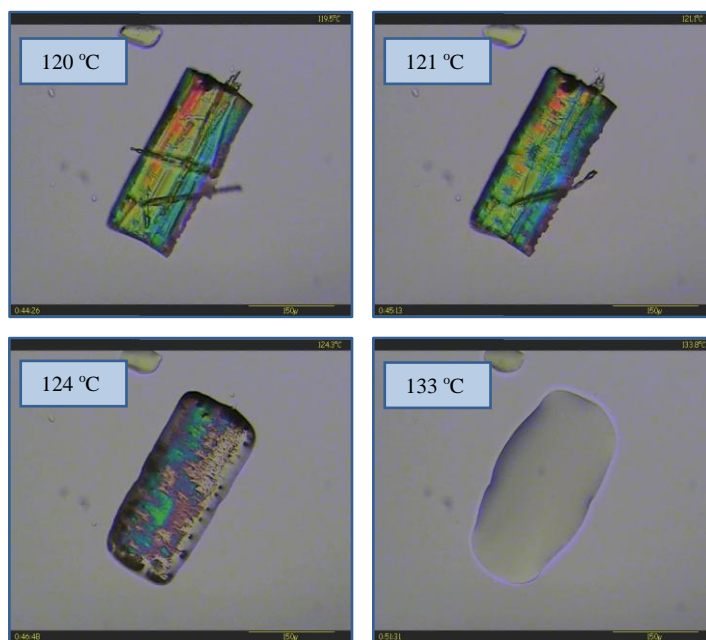
Figure 4.5: Microphotographs of paroxetine HCl Form I heated at 2 ^{o}C/min. Scale bar represents 150 μm.

Given the above results, it was considered important to evaluate the strength of the interactions between the water and the drug within the hydrate, which may be achieved using TGA. In Figure 4.6, the DSC and TGA thermograms of paroxetine HCl Form I have been overlaid. For a particular slow HR of 2 ^{o}C/min, the water loss commenced at around 50 ^{o}C and occurred continuously until approximately 115 ^{o}C; the loss can be divided in two main temperature regions. The first one between 50-95 ^{o}C covered the majority of the water loss and the second one near the endothermic melting event, as observed from the DSC curve.
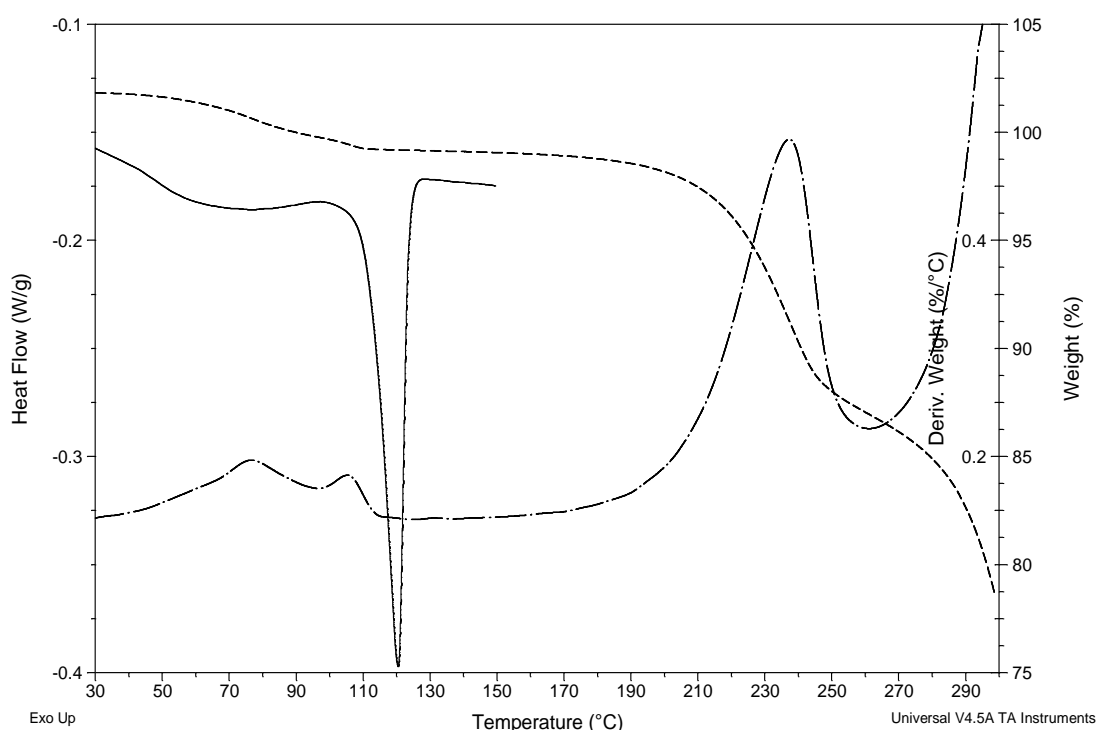
Figure 4.6: DSC (——) and TGA (- - -) thermographs for paroxetine HCl Form I in open pans at 2 ^{o}C/min. The derivative weight curve (-·-·-) is presented for clarity.

The water content of the raw Form I was determined by KFT to be 2.71 ± 0.25% w/w. This value was in a good agreement with the designation of this form as hemihydrate, 0.56 ± 0.05 mol of water per mol of drug and matched the total weight lost measured by TGA. In addition, HPLC was used to confirm that dehydration and subsequent melting process did not yield to any degradation of the sample. Analyses were performed on the

untreated paroxetine HCl Form I and on the sample heated in the TGA until 130 $^{\circ}$C. No sign of degradation was found on the heated sample (purity of 99.6%) when compared to the raw Form I (purity of 99.5%).

A closer inspection of the derivative curve shows that, at a HR of 2 $^{\circ}$C/min, part of the water (0.61% of the 2.59%) could only be released at high temperatures, i.e., near the melting point of the dehydrate Form I. However, this idea is not supported by the isothermal experiments, as shown in Figure 4.7. For example, when the sample was kept at 90 $^{\circ}$C, the dehydration was completed after 30 min. The TGA isothermal experiments are also important to access the dehydration conditions when performing VT-XRPD, though a direct correspondence could not be made due to the environmental differences between the two techniques. Moreover, this set of data was also fundamental to calculate the activation energy (E_a) for dehydration, as described earlier in the Introduction of this chapter.
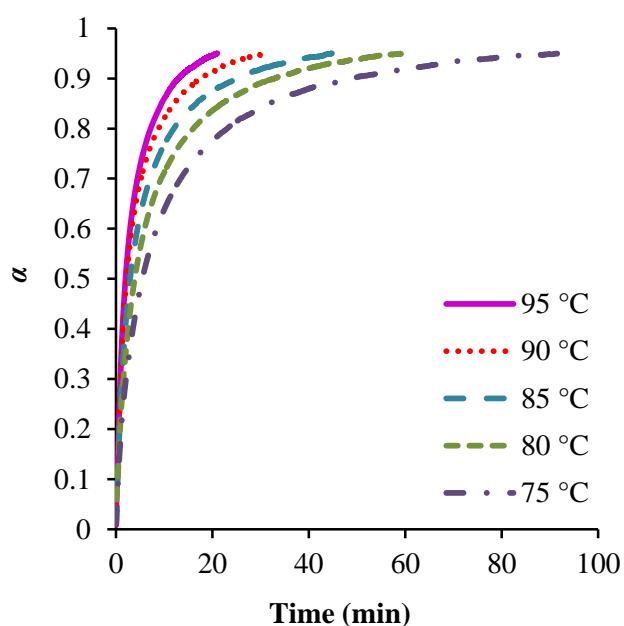
Figure 4.7: Representation of the conversion fraction (α) versus time obtained from TGA isothermal data at the different temperatures.

4.3.2   Dehydration Kinetics

The dehydration kinetics of paroxetine HCl Form I was studied using model-free and model-fitting approaches. Model-free analysis were performed using non-isothermal data, allowing the calculation of the Arrhenius parameters as a function of the conversion fraction, α. Model-fitting approaches were carried out using isothermal data that yields to the evaluation of a suitable kinetic model that better defines the overall reaction.

Based on the graphical shape of the isothermal curves, as shown previously in Figure 4.7, the dehydration rate decreases as the reaction proceeds and thereby the kinetic model for this reaction is known as decelerating. There are three other major groups of kinetic models described in the literature as accelerating, linear and sigmoidal (Vyazovkin et al., 2011). Non-isothermally, plots of α vs. temperature are not distinctive in their shapes as they are isothermally and thereby not used to preclude on the kinetic model of the solid state reaction (Khawam and Flanagan, 2006b).

Model-Free Analysis

The activation energy for the dehydration of paroxetine HCl Form I was calculated using a non-isothermal isoconversional method developed by Ozawa, Flynn-Wall (Ozawa, 1965; Flynn and Wall, 1966) and therefore commonly referred to as the OFW method, which can be expressed by the Equation 4.3

$$\log \beta = log \frac{AE_a}{g(\alpha)R} - 0.457 \frac{E_a}{RT} - 2.315$$

Equation 4.3

where, β is the heating rate, $g(\alpha)$ is the integral reaction model and R the gas constant.

Plotting $\log \beta$ versus $1000/T$ at each α yields E_a from the slope and from the intercept of the linear equation, the frequency factor, A, can be obtained. However the determination of A requires modelistic assumptions and as consequence, model-free methods usually only focus on the calculation of E_a at each value of α (Khawam and Flanagan, 2006a). An

example for the calculation of the E_a at a specific conversion fraction is presented in Appendix B (Table B2 and Figure B2).

Figure 4.8 shows the variation of the E_a as a function of α. By analysing in more detail the dependence of E_a with α through the kinetic reaction, a decrease in the E_a from 114.1 to 99.2 kJ/mol within $0.15 \leq \alpha \leq 0.40$ can be observed, followed by an approximately constant value of 85.9-96.2 kJ/mol in the range $0.45 \leq \alpha \leq 0.75$. The initial decrease of the E_a vs. α is characteristic of reversible reactions and could indicate a departure from the initial equilibrium (Vyazovkin et al., 2011). After this nearly constant period, the E_a started to increase gradually until an abrupt high value (211.8 kJ/mol) when $\alpha = 0.9$. This increase in the E_a for the final conversion fractions can be linked to the observations in TGA, showing that the removal of the final fractions of water took place at higher temperatures, therefore requiring more energy. However, one should also bear in mind that a loss of linearity and a higher error are expected at the final points of α, weakening the correlation with the TGA results. Nevertheless, this variation of E_a with α indicates that the process is kinetically complex and a single-step rate equation cannot describe the whole reaction.

Attempts to analyse isothermal data using model-free methods were unsuccessful since good correlations could just be obtained for high values of conversion ($\alpha \geq 0.40$) since the rate of the reaction is faster in the beginning (decelerating model). As a result, there is a significant extent of conversion during the heat-up time even using a heating rate of 50 ^{o}C/min to quickly reach the desired isothermal temperature.
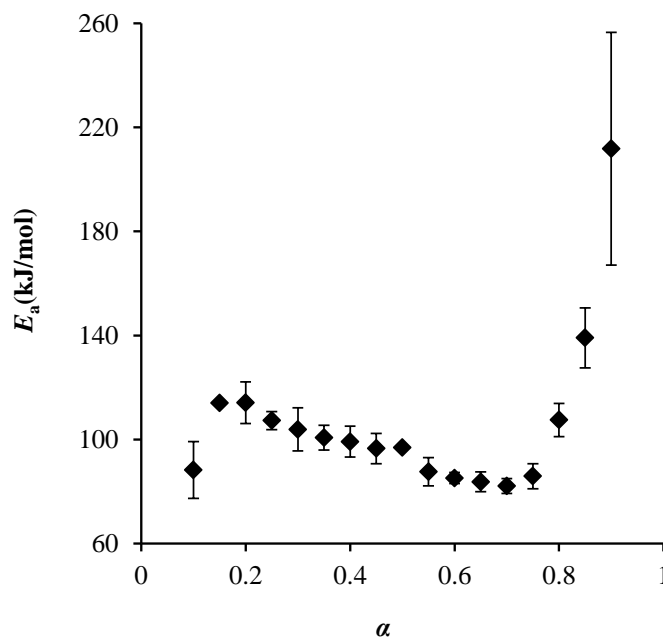
Figure 4.8: Activation energy, E_a, plotted as a function of the extent of conversion, α, for the dehydration of paroxetine HCl Form I under non-isothermal conditions.

Model-Fitting Analysis

Model-fitting methods of isothermal data were performed within the conversion region where E_a is approximately constant ($0.45 \leq \alpha \leq 0.75$), as determined previously by model-free analysis. The data was fitted to the integral form, $g(\alpha)$, of 17 models listed in Appendix B Table B3.

Two different models were found to have the best fit for the dehydration kinetics of paroxetine HCl Form I: F2 ($E_a = 71.8 \pm 2.4$ kJ/mol, $R^2 = 0.9968$) and D3 ($E_a = 74.3 \pm 2.2$ kJ/mol; $R^2 = 0.9974$). Each model affords a similar value of E_a, however from the shape of the isothermal curves, the reaction follows a deceleratory model, as mentioned above. Therefore, D3 (three dimensional diffusion model) provides a good description of the dehydration kinetics over this range of conversion.

The acquired knowledge up to this stage allowed to understand the thermal behaviour of Form I when exposed to different dehydration conditions and carefully set up the XRPD experiments, as follow, which are essential to provide information on the structure of the dehydrated form.

4.3.3 Structural Studies using VT-XRPD

VT-XRPD experiments were performed in a closed system constantly purged with dry nitrogen gas in order to mimic the conditions inside the DSC and TGA furnace. A change in the XRPD pattern started to be apparent after 1 h at 75 ^{o}C, with some of the diffraction peaks becoming broader. The changes were clearly observed as the temperature increased (Figure 4.9). After 5 h isothermal treatment at 100 ^{o}C, the existing peaks became less sharp and new peaks appeared which may be associated with the departure of the water molecules and the concomitant appearance of a new phase. This phenomenon was more evident when the temperature increased to 110 ^{o}C and the sample was kept isothermal for 12 h. After that time, and analysing the spectrum at lower angles, it is possible to distinguish the new peaks that appeared (*) and the peaks from the hydrated Form I that started to disappear ($^{\#}$). However, at higher angles the discrimination between the two phases is more difficult due to the overlap between some of the peaks. Pawley refinement (Coelho, 2007) using the unit cell parameters of Form I gave a good fit to the experimental patterns at temperatures below 75 °C, but at 100 and 110 ^{o}C the fit was very poor due to the presence of more than one form (Appendix B, Figure B1 and Table B1).
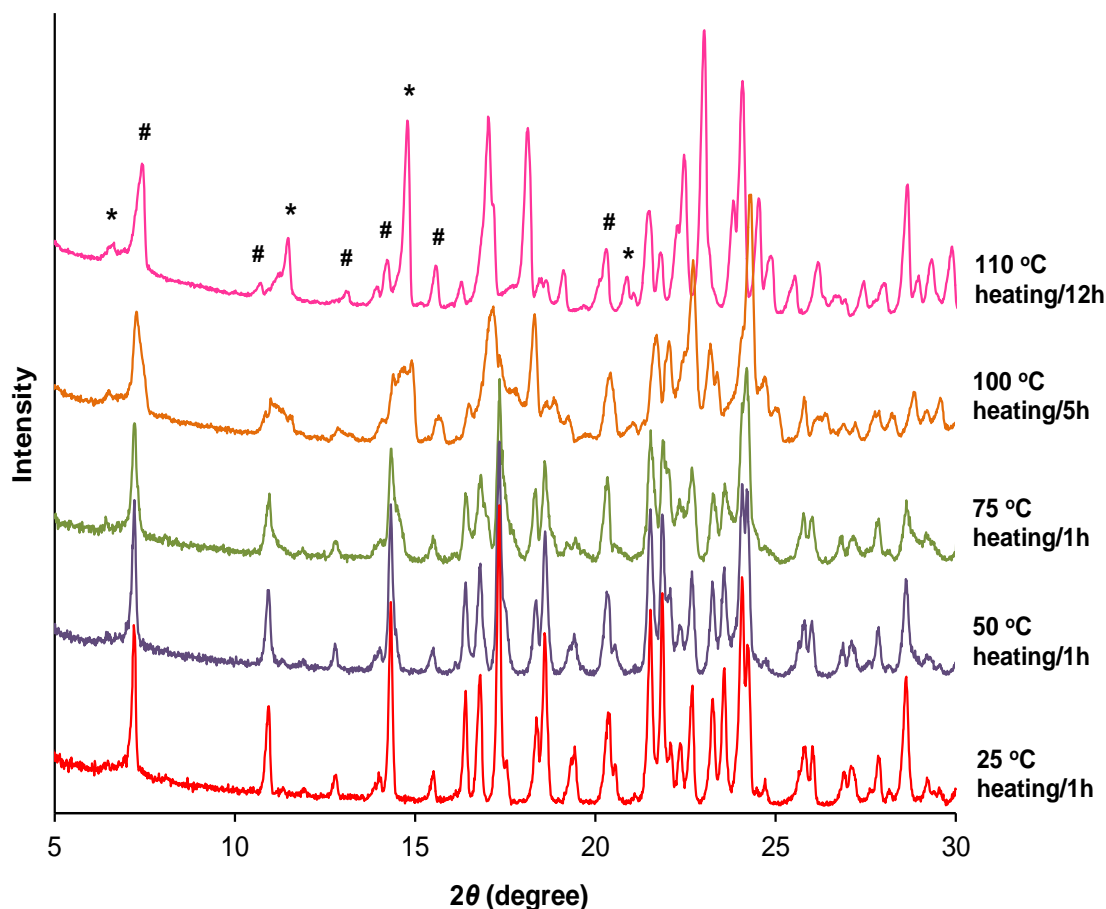
Figure 4.9: VT-XRPD diffractograms collected on paroxetine HCl Form I at 25, 50, 75, 100 and 110 °C (upwards). Peaks identified with (*) correspond to the new anhydrous form and those identified with (#) are related to the initial Form I.

On cooling, it was possible to index the pattern collected after 1 h at 100 °C. Pawley refinement with the new unit cell parameters gave a good fit to the diffraction pattern. The refined cell parameters (a = 14.400(2) Å, b = 10.5362(15) Å and c = 12.7706(13) Å) were found to be very similar to those of the hemihydrate Form I at 75 °C (a = 14.655(5) Å, b = 10.191(3) Å and c = 13.039(5) Å), but with a smaller unit cell volume. The space group of the new anhydrous form was found to be P2$_1$, the same as Form I. A similar pattern to the one collected at 100 °C was maintained on further cooling down to 50 °C (Figure 4.10). When the temperature dropped to 25 °C the pattern changed significantly, which might be ascribed to the re-entry of water molecules into the crystal structure. At this stage, the fitting using the anhydrous unit cell parameters became very poor, as the pattern started gradually to revert to the initial Form I.
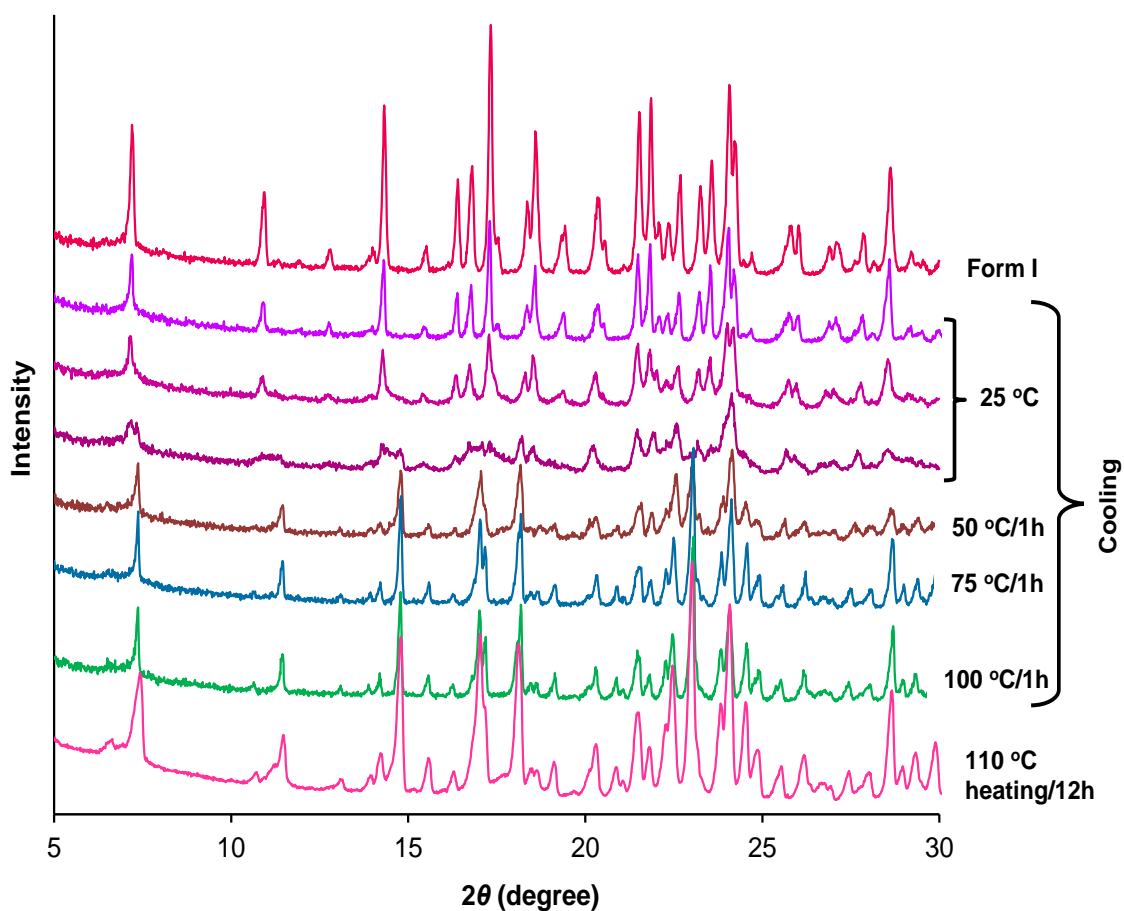
Figure 4.10: VT-XRPD patterns of paroxetine HCl Form I collected during cooling from 110 ^{o}C to 25 ^{o}C (upwards). At 25 ^{o}C, the diffractograms were collected after 1, 2 and 6 h isothermal at that temperature.

Figure 4.11 depicts the changes in the unit cell volume as a function of temperature. It is clear that during heating the unit cell volume increased slightly, as expected for thermal expansion. The unit cell volume of the new form at 50 °C was found to be 56 Å^{3} smaller than that of Form I at the same temperature, which is consistent with dehydration (Appendix B, Table B1). After 6 h at 25 ^{o}C, the unit cell volume was found to be the same as the hydrate Form I, indicating that full rehydration took place.
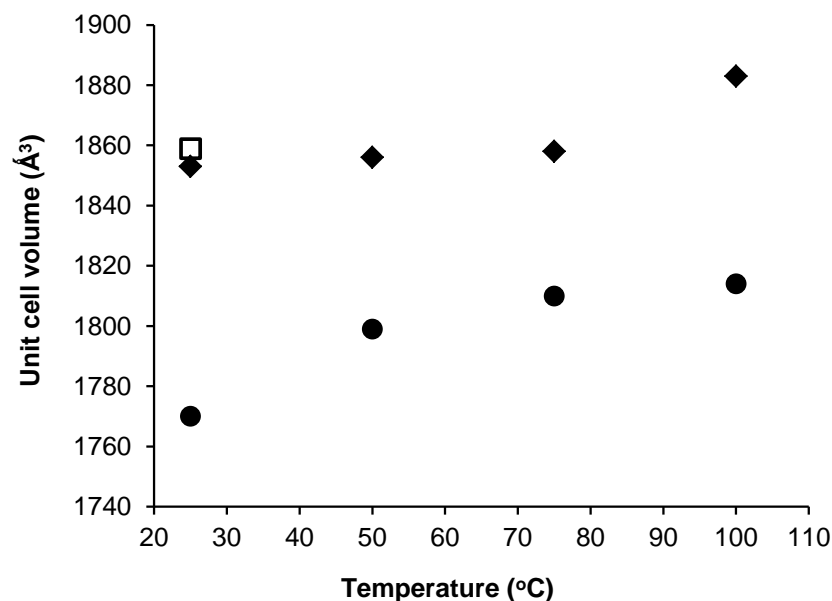
Figure 4.11: Changes in the unit cell volume of paroxetine HCl Form I during heating at 25, 50, 75 and 100 °C (♦); during cooling of the anhydrous form (●) at the same temperatures as during heating; and after cooling at 25 °C for 6 h (□). Note that the refinement at 100 °C on heating and after 1 h at 25 °C on cooling gave a poor fitting, thus these results are less reliable.

From these observations, Form I is likely to dehydrate to an isostructural anhydrous form, which explains its extremely high instability and propensity to interact with water, as no major changes in the structure were needed for the rehydration to occur.

Furthermore, SEM microphotographs (Figure 4.12) taken on the raw Form I (a) and compared with Form I (b) held isothermal for 1 h at 90 °C in TGA, did not show any differences in their crystal appearance. This fact is not surprising and can be readily explained by the higher hygroscopic behaviour of this new anhydrous form able to rehydrate using the residual moisture present in the nitrogen gas (XRPD experiments during cooling). Therefore, differences related to dehydration would be hard to observe under SEM. A sample held at 110 °C for 1 h (c) had a partially glassy appearance under SEM. This is due to surface melting of the dehydrated sample kept under these isothermal conditions and subsequent cooling. Thermogravimetric analysis is primarily designed for dynamic heating rates and the offset is not affected by heating rate but the actual temperature may be different in the isothermal experiment. As a result, these observations are expected since the onset melting point of the dehydrated Form I

is $\approx$ 112 ^{o}C, matching well with the possibility of small variations in temperature when isothermal experiments are performed in TGA.
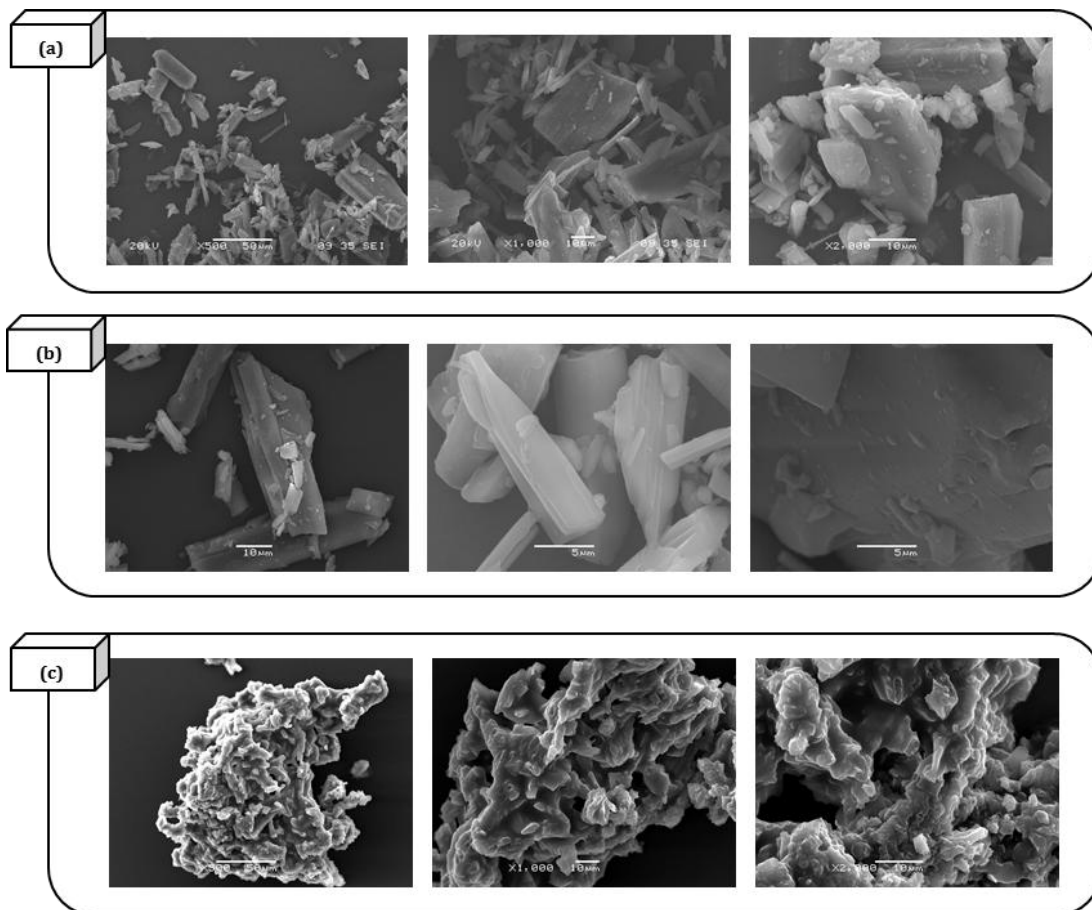
Figure 4.12: SEM pictures of raw paroxetine HCl Form I (a), isothermal for 1 h at 90 ^{o}C (b) and isothermal for 1 h at 110 ^{o}C (c) in TGA.

Finally, by comparing the pattern obtained for the dehydrated Form II at 30 ^{o}C/1% RH (data presented in Chapter 3) and the pattern collected in this study at 50 ^{o}C for the dehydrated Form I, it is possible to see that these two crystalline patterns are different (Figure 4.13). As Form II forms an isostructural anhydrate when dehydrated, only shifts on the diffraction peaks were observed without any changes in terms of appearance/disappearance of peaks. Attempts to fit the pattern of dehydrated Form I using the unit cell parameters of the dehydrated Form II were unsuccessful, reinforcing the hypothesis that these two dehydrated forms are structurally different.
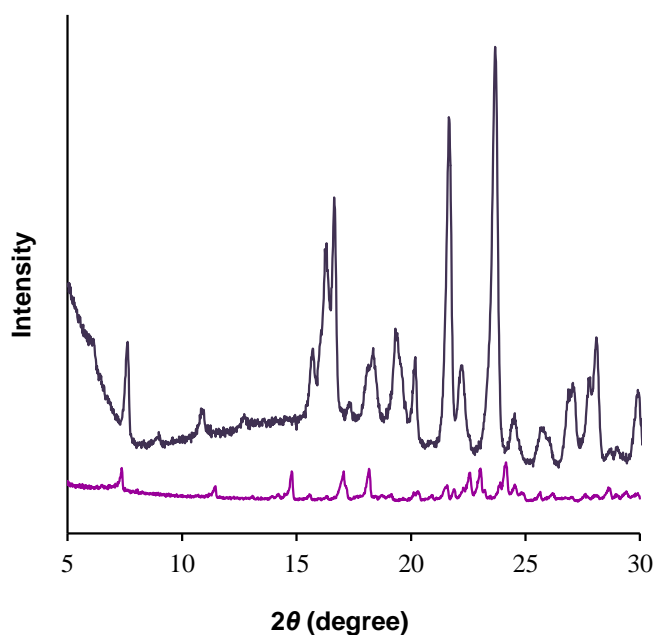
Figure 4.13: VT-XRPD pattern of the dehydrated Form I at 50 °C on cooling (bottom) and VH-XRPD pattern of the dehydrated Form II (top) collected at 30 °C/1% RH (data presented in Chapter 3).

Figure 4.14 is a schematic representation of the relationships between hydrated and dehydrated forms of paroxetine HCl. Form II dehydrated to an isostructural anhydrous form that rehydrated back at 10-30% RH (Chapter 3). The dehydration of Form I was a more complex process implying a completely dry environment and high temperatures. The dehydrated Form I was found to be very unstable with quickly reconversion to the hydrate Form I when RH ≈ 1%. The two dehydrated forms of Form I and II were structurally different and therefore a new form of paroxetine HCl has been found.
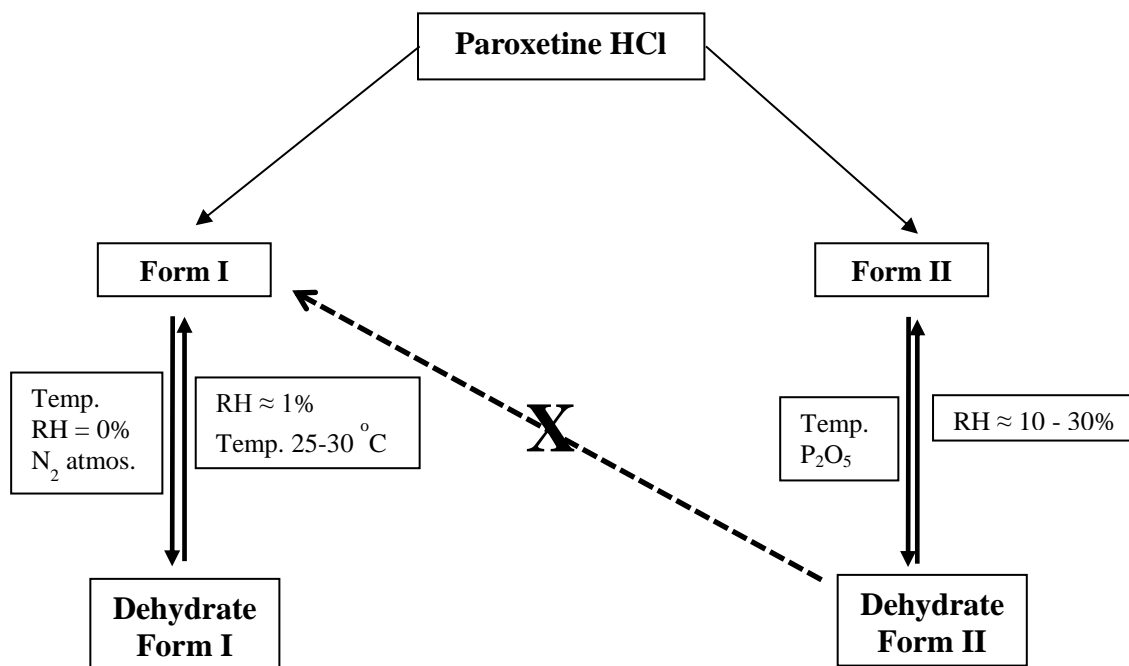
Figure 4.14: Representative scheme of the relationship between the two forms of paroxetine HCl.

4.4   Conclusions

The combination of thermal and diffraction techniques allowed investigation of the dehydration behaviour of paroxetine HCl Form I and, consequently, suggested the existence of a new anhydrous form as a result of this process. Dehydration was firstly observed when Form I was heated in pinhole or open pans in the DSC. However, the melting peak temperature observed for the dehydrated Form I (120 ºC) was fairly close to the melting of the isostructural dehydrate Form II (123 ºC), which made the differentiation between these two dehydrated forms difficult using thermal techniques.

Therefore, VT-XRPD experiments were performed in a closed system blanket with dry nitrogen gas (99.9% purity) in similar conditions as those observed in the DSC and TGA furnace. The changes in the XRPD pattern started to be observed as the temperature increased, with the appearance of new diffraction peaks after the sample being kept isothermal for 5 h at 100 $^{\circ}$C. The Pawley refinement showed that the unit cell parameters of the new anhydrous form were very similar to the hydrate Form I, the main difference being a smaller unit cell volume, as a result of dehydration. Therefore, it is possible to conclude that Form I dehydrates to an isostructural dehydrate form.

During cooling, as a result of the temperature drop, residual moisture in the N_2 source (in theory nearly 1%) and probably not completely hermetically sealed VT chamber, the pattern started gradually to revert to the initial Form I after 1 h at 25 $^{\circ}$C. Pawley refinement using the pattern collected after 6 h at 25 $^{\circ}$C showed that the unit cell had the same volume as the hydrate Form I confirming that the new anhydrous form fully rehydrated to Form I. The structural rehydration observed during cooling in the VT-XRPD experiments was supported by the results obtained when the sample was cycled inside the DSC in open pans, with the dehydrate Form I picking up moisture from the nitrogen gas.

The dehydration kinetic studies of Form I were conducted using non-isothermal TGA data with a view to estimate the E_a required to dehydrate Form I. Model-free analysis were used to calculate the E_a for dehydration of Form I, which varies between 86-114 kJ/mol. This value of E_a is much higher than the reported value (60 kJ/mol) for stable hydrates under ambient conditions, supporting again the great stability observed for the hydrate Form I (Shimanovich et al., 2012).

The significance of these findings lies not only in the identification of a new structure for an important drug molecule, but also in highlighting the complexity of dehydration and rehydration behaviour of low molecular weight molecules. The Form I anhydrate was extremely difficult to produce and isolate due to the high resistance to dehydration and extreme affinity for water. The anhydrate is extremely unstable and hence is not a viable candidate for commercial use. However, taken in the context of the unusual hydration behavior of Form II highlighted in Chapter 3, this drug also serves as a potentially highly important model for understanding the relationship between chemical structure and hydration behaviour. In particular, the current study has highlighted the extreme affinity of the Form I dehydrate for water, which is in itself of interest in understanding hydrate formation and stability.

Overall, the work presented in this chapter have shown that the dehydration of paroxetine HCl Form I is a complex and uncommon process for a stoichiometric hydrate. The prepared anhydrous form is structurally different from the dehydrated Form II, thereby a new anhydrous form of paroxetine HCl has been identified. Moreover, the structure of the new anhydrous form was found to be very similar to the hydrate Form I, which supported its high instability and tendency to quickly rehydrate. These findings are of considerable relevance on the understanding of the solid state relationships of paroxetine HCl. Furthermore, the study presents new insights into the behaviour of hydrates with high resistance to dehydration, with the possibility of new forms being identified and enhanced understanding of the driving factors determining hydrate formation and stability.

5 AMORPHOUS PAROXETINE HCL: THE RELATIONSHIP BETWEEN THERMODYNAMIC/KINETIC PARAMETERS, DRUG PERFORMANCE AND STABILITY

Abstract

Increased interest in molecular time scales below the glass transition temperature, T_g, has arisen from the need to identify the conditions at which the stability of glassy materials is maximum and unwanted changes, such as recrystallisation, are improbable. In this study, a series of well-known kinetic and thermodynamic parameters have been used to characterise amorphous paroxetine HCl and predict its physical stability. These predictions were asserted with the experimental results obtained after the amorphous sample was stored under different relative humidity (RH) environments at room temperature.

A combination of thermal (standard differential scanning calorimetry (DSC), modulated temperature DSC (MTDSC) and thermogravimetric analysis (TGA)), spectroscopic (attenuated total reflection-Fourier transform infrared (ATR-FTIR)) and diffraction (X-ray powder diffraction (XRPD)) techniques were used to characterise the freshly prepared and aged amorphous samples. Aqueous solubility and dissolution studies were also performed.

Parameters such as heat capacity, configurational thermodynamic quantities and fragility parameters classified amorphous paroxetine HCl as a moderate fragile glass with a considerable degree of molecular mobility associated. The calculated relaxation time using Adam-Gibbs-Vogel approach was found to be a reasonably good predictor of the stability of amorphous paroxetine HCl. These observations were reflected in the stability of this form. Firstly, amorphous paroxetine HCl recrystallised to the most stable Form I during the solubility experiments. Secondly, the stability studies showed that the recrystallisation of this form was greatly influenced by the presence of humidity. High RH environments (75% RH) led to a full recrystallisation within 1 to 3 days, while the same observation was detected after 30 days under 53% RH. The storage conditions were also found to affect the pathway of recrystallisation of amorphous paroxetine HCl, which happened directly to Form I at 53% RH or via metastable Form II at 75% RH, as confirmed by FTIR. This study elucidated the importance of taking advantage of the theoretical predictors in the study of amorphous systems, although the complete understanding of its physical stability and recrystallisation behaviour remains beyond these predictions.

5.1   Introduction

Thermodynamic properties such as excess of free energy, enthalpy and entropy are responsible for the advantageous uses of amorphous materials, namely the enhancement of aqueous solubility and dissolution rate of poorly soluble drugs. Amorphous compounds are highly disordered systems, thus the energy barrier to be overcome for dissolution is lower than that associated with the equivalent crystalline materials. However, due to high reactivity and instability to mechanical and thermal stresses above their glass transition, the incorporation of amorphous materials in formulated products is restricted; some examples of amorphous drugs marketed are: Kaletra[®] (ritonavir and lopinavir), Sporanox[®] (itraconazol) and Prograf[®] (tracolimus). There are many routes to transform a crystal into an amorphous phase being the most representative the mechanical activation (e.g. milling), via solution (e.g. spray drying, freeze drying, and precipitation by the addition of anti-solvents) and quench cooling after melting.

A crucial decisive factor regarding whether an active pharmaceutical ingredient (API) can be formulated as an amorphous material is its physical stability during the processing operation, dissolution testing as well as during its self-life. Therefore, several kinetic and thermodynamic parameters were used in this study to predict the stability of amorphous paroxetine HCl, as presented next.

The fundamental characterisation of an amorphous material implies the measurement of the glass transition temperature, T_g, at which the material changes on cooling from a liquid or rubbery state to a brittle or glassy state (Craig et al., 1999). This phenomenon is known as vitrification. By contrast, devitrification describes the process of conversion from the metastable amorphous state to the more stable crystalline state, as a consequence of mechanical stress and/or effect of temperature and humidity (Ambike et al., 2004). The determination of the T_g is essential to evaluate the physical and chemical stability of amorphous compounds.

Another important concept to take into consideration is known as relaxation and reflects the changes in atomic/molecular arrangements that happen during the spontaneous conversion from the amorphous to crystalline state, in a scale of time and temperature

influence (Kawakami and Pikal, 2005; Hilden and Morris, 2004). In amorphous drug studies, the structural relaxation is often referred to as enthalpy of relaxation which is a common parameter used to measure the extent of stability. Normally, in the pharmaceutical field, the bulk enthalpy relaxation is measured using calorimetric methods, such as differential scanning calorimetry (DSC) and recently MTDSC. Lately, attempts have been made in order to measure surface relaxation by using inverse gas chromatography, with a view to understanding molecular mobility at the surface (Ke et al., 2012). The enthalpy lost during a certain time and at a determined temperature below T_g is regained during the heating run in the DSC and is shown as an endothermic peak at T_g. As a result, the enthalpy relaxation is also known as enthalpy recovery. The increase in enthalpy recovery over the ageing time can be used as a direct measure of molecular mobility, which is the main aspect governing the physical stability of glassy systems (Surana et al., 2004).

Kauzmann Temperature

The Kauzmann temperature, T_K, is the temperature at which the configurational entropy of the glassy material vanishes (often called as entropy crisis); the degree of mobility at this point is reduced and can be considered to be similar to the most ordered crystalline state (Shamblin et al., 1999). T_K is considered as the theoretically lowest glass transition temperature possible, where the molecular mobility of the amorphous materials becomes negligible. T_K is an important parameter to inform the researcher regarding the likely stability of a pharmaceutical compound, since at this temperature or below, the metastable amorphous materials are expected to have the maximum stability. In practice, however, the storage at $T < T_K$ is often not possible from an industrial perspective.

The estimation of T_K can be made either using entropy, T_{KS} (Equation 5.1) or enthalpy, T_{KH} (Equation 5.2) of fusion. However, the entropy-based calculation is considered to be the most accurate approach to calculate the correct T_K value (Shamblin et al., 1999),

$$\frac{1}{T_{KS}} = \frac{1}{T_m}\left(1 + \frac{\Delta H_m}{C_{p\,conf}T_g}\right)$$

Equation 5.1

$$\frac{1}{T_{KH}} = \frac{1}{T_m}\left(\frac{\Delta H_m}{C_{p\ conf}T_g}\right)$$

<div align="right">**Equation 5.2**</div>

where, ΔH_m is the enthalpy change at melting, T_m is the melting temperature and $C_{p\ conf}$ is a the configurational heat capacity.

The $C_{p\ conf}$ is controlled by the temperature dependence of the configurational entropy, which is consequently a measure of the temperature dependence of non-vibrational molecular mobility. It can be calculated from the heat capacity of the supercooled liquid (C_p^l) and the crystal (C_p^c) by using the following expression,

$$C_{p\ conf} = C_p^l - C_p^c$$

<div align="right">**Equation 5.3**</div>

Fragile glasses are expected to have large $C_{p\ conf}$ values due to their rapid configurational entropy change with the temperature, whereas strong glass formers have small configurational heat capacities, because their configurational entropy changes slowly with temperature (Angell, 1991).

Zero Mobility Temperature

The zero mobility temperature, T_0, is defined as the temperature where extrapolated thermodynamic properties of a supercooled liquid are equal to those of the crystal and can be expressed by the Equation 5.4,

$$T_0 = T_g\left(1 - \frac{m_{min}}{m}\right)$$

<div align="right">**Equation 5.4**</div>

where, m represents the index of fragility and m_{min} the minimum value possible for that index, these parameters will be discussed in detail later.

T_0 is often reported to have the same meaning as T_K, as it represents the temperature where the configurational entropy is zero (Shamblin et al., 1999). There are however some exceptions, as reported previously for sucrose and sorbitol, where the entropy T_K was considerably higher than T_0 (Shamblin et al., 1999; Zhou et al., 2002).

Relaxation time

The relaxation time, τ, can be calculated by using the Vogel-Tamman-Fulcher (VTF) equation, in case the storage temperature, T, is higher than the T_g, following the Equation 5.5,

$$\tau = \tau_0 exp \frac{DT_0}{T - T_0}$$

<div align="right">**Equation 5.5**</div>

where, τ_0 denotes a constant taken as the time scale of atomic vibrations, 10^{-14} seconds, and D is Angells strength parameter, as further described.

On the other hand, it is also possible to describe the relaxation time of an amorphous material below its T_g by introducing a new parameter into the Equation 5.5 called the fictive temperature, T_f. The new expression is referred as Adam-Gibbs-Vogel (AGV) equation and appears as shown in Equation 5.6,

$$\tau = \tau_0 \, exp \frac{DT_0}{T(1 - T_0/T_f)}$$

<div align="right">**Equation 5.6**</div>

T_f establishes a relationship between the glass and the supercooled liquid and it is defined as the temperature at which the glassy system has the same thermodynamic properties as the equilibrium system (Shamblin et al., 1999). T_f can be calculated from the heat capacities and the T_g of the glass, (Graeser et al., 2009a; Graeser et al., 2009b), using the following Equation 5.7 and Equation 5.8,

$$\frac{1}{T_f} = \frac{\gamma_{C_p}}{T_g} + \frac{1 - \gamma_{C_p}}{T}$$

<div align="right">**Equation 5.7**</div>

$$\gamma_{C_p} = \frac{C_p^l - C_p^a}{C_p^l - C_p^c} = \frac{\Delta C_p}{C_{p \, conf}}$$

<div align="right">**Equation 5.8**</div>

γ_{Cp} is a thermodynamic parameter used to characterise fragility of pharmaceutical glass formers, with values between 0 (for fragile systems) and 1 (for strong materials) (Hodge, 1996).

Fragility

The viscosity of a supercooled liquid changes with temperature (more drastically at the T_g) and this relationship can be described by the well-known Arrhenius equation (Macedo and Litovitz, 1965),

$$\eta = A\, e^{\frac{-E_a}{RT}}$$

Equation 5.9

where, η is the viscosity, A is the pre-exponential factor, E_a the activation energy, R is the universal gas constant and T is the absolute temperature.

Fragility indicates how fast structural relaxation increases as a glass becomes closer to the glass transition region (Yu, 2001). According to Angell (Angell, 1988, 1991), fragility can be portrayed plotting the log viscosity (η) against T_g/T. From this plot, strong liquids show a linear relationship (Arrhenius behaviour), whereas fragile glasses have a behaviour that deviates from linearity (non-Arrhenius behaviour). Therefore, weak glasses having non-Arrhenius behaviour can undergo structural rearrangements as a function of temperature, showing higher mobility through the T_g. Based on this property, strong systems feature $m < 40$ and fragile systems $m > 75$.

The fragility index can be calculated using the activation energy of the structural relaxation at the glass transition (Wang et al., 2002; Crowley and Zografi, 2001), as described by Equation 5.10,

$$m = \frac{\Delta E_{T_g}}{(ln10)RT_g}$$

Equation 5.10

where, ΔE_{Tg} is the activation energy for structural relaxation at temperatures around T_g.

Significant changes in ΔE_{Tg} with temperature are characteristic of fragile systems and their viscosity deviates from the Arrhenius behaviour; on the opposite, for strong systems, the

ΔE_{Tg} changes slightly with the temperature, which follows Arrhenius behaviour (Angell, 1988).

Due to the scanning rate dependence of the T_g, it is possible to determine the ΔE_{Tg} from a plot of ln (q) against $1/T_g$, as represented by Equation 5.11,

$$\frac{d(lnq)}{d(1/T_g)} = -\frac{\Delta E_{T_g}}{R}$$

Equation 5.11

where, q represents the cooling/heating rate and (- $\Delta E_{Tg}/R$) is the slope of the plot ln (q) versus $1/T_g$.

The minimum possible fragility value, m_{min}, has been calculated to be 16 and corresponds to the relaxation of the unrestricted material at T_g, which exactly conforms to the Arrhenius behaviour (Mao et al., 2006).

Strength Parameter

The fragility of a material can be connected to the strength parameter, D, by the Equation 5.12 (Graeser et al., 2009b),

$$D = \frac{ln(10)\, m_{min}^2}{m - m_{min}}$$

Equation 5.12

For strong glass formers, D values are larger (> 30) whilst for fragile glass formers D values are quite small (< 10).

Glass Forming Ability

Some other parameters can be used to deduce on the physical stability of glassy materials. The Glass Forming Ability (GFA) is defined as the ease of vitrification of a liquid on cooling. The minimum cooling rate required to vitrify a material is known as the critical cooling rate, R_{crit}, and it is a widely used factor to measure GFA (Baird et al., 2010).

The same authors investigated the crystallisation tendency of 51 organic molecules, by using DSC, from the undercooled melt state. In the end of their study, they managed to divide them into three different groups:

Class I – crystallisation observed upon cooling from the supercooled liquid;

Class II – crystallisation detected during reheating above T_g;

Class III – no crystallisation detected either during cooling or reheating.

An additional parameter to assess the GFA is the reduced glass transition temperature T_{rg} defined in Equation 5.13,

$$T_{rg} = \frac{T_g}{T_m}$$

Equation 5.13

Presuming that the viscosity has a constant value at the T_g, materials with higher T_{rg} values would be expected to have higher viscosity between T_g and T_m and therefore be more resistant to crystallisation. The increase in viscosity enlarges the timescale for molecularly rotational and translational motions. As a result, the closer T_{rg} value to 1, the higher is the GFA of the material.

The aim of this chapter is to characterise amorphous paroxetine HCl using the aforementioned glassy parameters and establish a possible relationship with the physical stability observed experimentally for this material. Amorphous paroxetine was prepared via quench cooling from its hydrochloride (HCl) Form II. Stability studies were carried out under different relative humidities (RHs) at room temperature for 60 days and evaluated using modulated temperature DSC (MTDSC), thermogravimetric analysis (TGA), infrared spectroscopy (ATR-FTIR) and X-ray powder diffraction (XRPD).

5.2 Materials and Methods

5.2.1 Materials

Crystalline paroxetine HCl Form II was purchased from Huahai Pharmaceuticals (China) and was used as received or after being dried over P_2O_5 as stated. Form II is described to be a non-stoichiometric hydrate with a melting point of circa 120 $^{\circ}$C (as shown in Chapter 3). Storage environments with different relative humidities (RHs) were prepared using salt solutions of sodium chloride (75% RH, Fischer Scientific, UK); magnesium nitrate hexahydrate (53% RH, Fluka, Germany); calcium chloride (33% RH, BDH Laboratory, UK) and potassium acetate (22% RH, Alfar Aesar, UK). Phosphorus pentoxide (P_2O_5) was used as desiccant and was purchased from Alfar Aesar (UK).

5.2.2 Methods

5.2.2.1 Preparation of Amorphous Paroxetine HCl

Quench cooled paroxetine HCl was prepared by melting the crystalline paroxetine HCl Form II in an aluminium foil placed over a hot plate. The molten sample was kept isothermal at that temperature for 2 min to ensure a complete melting. After that, the sample was cooled down rapidly by immersion in nitrogen liquid. For the determination of C_p, the amorphous paroxetine HCl was prepared *in situ* the DSC.

5.2.2.2 Thermal Analysis

Differential scanning calorimetry (DSC, Q1000 TA Instruments) analysis was done at different heating rates (HRs): 2, 5, 10, 20 and 50 $^{\circ}$C/min in pinhole pans. Modulated temperature DSC, (MTDSC, Q1000 TA Instruments) analysis was performed with a HR of 2 $^{\circ}$C/min and a modulation of $\pm$ 0.318 $^{\circ}$C every 60 seconds. Hermetic pans were used for

the analyses of fresh and aged samples while standard crimped pans were used for the C_p measurements.

Thermogravimetric analysis, (TGA, Hi-Res 2950 TA Instruments) with a HR of 10 ^{o}C/min from room temperature to 300 ^{o}C was used to determine the water content of the samples.

5.2.2.3   X-Ray Powder Diffraction (XRPD)

XRPD (Thermo-ARL Xtra, Thermo Scientific) spectra were collected from 5.0^o to 40.0^o at 2θ.

5.2.2.4   Attenuated Total Reflection-Fourier Transform Infrared (ATR-FTIR)

The infrared spectra of the samples were collected using a Bruker IFS 66/S spectrophotometer (Bruker Optics Ltd.), with 64 scans being acquired for each sample from 4000 cm^{-1} to 550 cm^{-1} with a resolution of 2 cm^{-1}.

5.2.2.5   Solubility Measurements

Solubility measurements were performed by adding an excess of drug to distilled water and stirring for 24 and 72 h at 25 ^{o}C. After each time period, the samples were centrifuged and filtered through a 0.45 μm filter (Henwood et al., 2001; Sugano et al., 2007). The solutions were then suitably diluted with distilled water and assayed spectrophotometrically (Lambda XLS UV/VIS, Perkin-Elmer) at 293 nm.

5.2.2.6   Dissolution Studies

Dissolution studies were carried out in 900 mL of 0.1M HCl at 37.0 ± 0.5 ^{o}C on a Copley CIS 8000 dissolution bath (Copley Scientific) with a rotation speed of 50 rpm using the BP paddle method. Sixty milligrams (60 mg) of each sample were used. At predetermined intervals, 10 mL of solution was withdrawn and filtered through a 0.45 μm filter. Subsequently, the filtrate was analysed spectrophotometrically (Lambda XLS UV/VIS, Perkin-Elmer) at 293 nm. All the dissolution experiments were done under sink conditions.

5.2.2.7   Physical Stability

Stability experiments were carried out at 25 $^{\circ}$C under different RHs, 0, 22, 33, 53 and 75%. The range of humidity atmospheres were obtained by using saturated salt solutions, then stored in proper desiccators and left to equilibrate for a minimum of 24 h prior to storage of the samples.

5.3   Results and Discussion

5.3.1   Thermodynamic and Kinetic Parameters on the Classification of Paroxetine HCl as a Glass Former

In the first instance, several thermodynamic and kinetic parameters were obtained for the amorphous paroxetine HCl prepared *in situ* the DSC. The values presented in Table 5.1 were obtained directly from the MTDSC measurements or calculated using the expressions presented in the Introduction section. Standard crimped pans were used to ensure a good contact between the material and the bottom of the pans. The heat capacities of supercooled liquid, glass and crystalline paroxetine HCl Form II were obtained by deconvolution of the total heat flow curve into the non-reversing and reversing (heat capacity) signals; the T_g value was estimated at the midpoint of half-height of the stepwise change in the C_p, in the reversing signal. Each calculated parameter is to be described in more detail in later context.

Table 5.1: Thermal and kinetic parameters obtained for amorphous paroxetine HCl.

Parameter	Value
$T_g \pm$ s.d. (${}^{\circ}$C)	71.1 ± 0.6
$\Delta C_p \pm$ s.d. (J/g ${}^{\circ}$C)	0.31 ± 0.10
$C_{p\ conf}$ (J/g ${}^{\circ}$C)	0.47
T_{KS} (${}^{\circ}$C)	48.8
T_g - T_{KS}	22.2
T_0 (${}^{\circ}$C)	19.7
T_{rg}	0.6
m	107.3
D	6.5
γ_{Cp} (J/g ${}^{\circ}$C)	0.66
T_f	67.9
τ (AGV) (seconds)	3.26×10^6

Heat Capacity Change (ΔC_p) and Configurational Heat Capacity ($C_{p\ conf}$)

The changes in the heat capacity at T_g provides a way to infer information on the physical stability of glassy materials. In general, high ΔC_p is characteristic of fragile glasses and this is due to high molecular motions at T_g, while strong glasses have small ΔC_p changes at glass transition temperature. The increase in the configurational heat capacity, $C_{p\ conf}$ can also be used to classify the materials between strong and fragile liquids. Amorphous paroxetine HCl showed a ΔC_p and $C_{p\ conf}$ of 0.31 and 0.47 J/g ${}^{\circ}$C, respectively.

Figure 5.1 shows the measurement of ΔC_p and $C_{p\,conf}$ for amorphous paroxetine HCl using the reversing heat capacity against temperature. Clearly, the higher molecular mobility of the supercooled liquid is reflected in the higher heat capacities at all temperatures, whereas the crystalline heat capacities vary almost linearly with temperature.
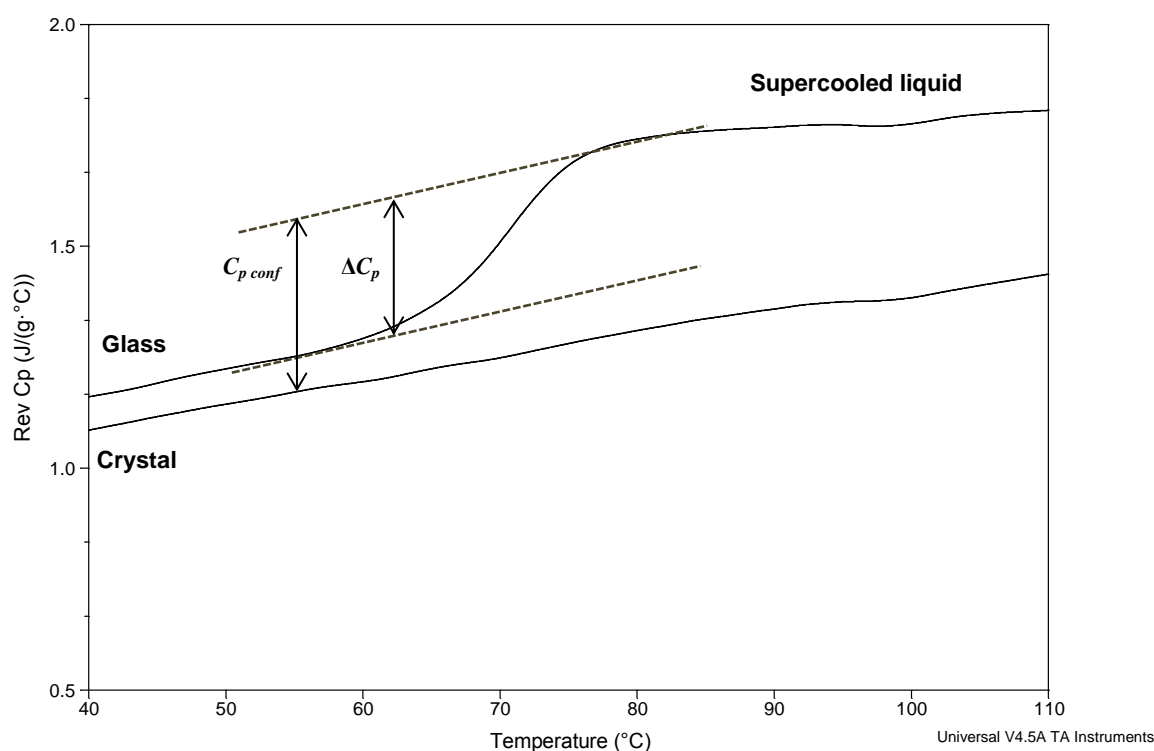
Figure 5.1: Heat capacity data as a function of temperature for crystalline Form II and amorphous paroxetine HCl.

Kauzmann Temperature (T_K), Zero Mobility Temperature (T_0) and Fictive Temperature (T_f)

The Kauzmann temperature was calculated from an entropy (T_{KS}) base instead of enthalpy (T_{KH}) base, since the Adam-Gibbs model states that is the configurational entropy that mostly influences the molecular mobility. As consequence, the T_{KS} is considered to be the closest to the entropy crisis temperature and therefore all further calculations involving T_K referrers to T_{KS} instead of T_{KH} (Andronis and Zografi, 1998). T_K for amorphous paroxetine

HCl was calculated according to Equation 5.1 and had a value of 48.8 $^{\circ}$C which was just $\approx 22\ ^{\circ}$C below its T_g.

The fact that T_K gets closer to T_g in fragile liquids leads to a relationship between these two parameters, T_K/T_g which is determinant of the deviation of glass from Arrhenius behaviour. The ratio lies between 0 (strong) and 1 (fragile). For amorphous paroxetine HCl, $T_K/T_g = 0.7$ categorising it into a moderate fragile system which is also supported by the fact that T_g - $T_{KS} < 50\ ^{\circ}$C (Kaushal and Bansal, 2008).

Another aspect is related to the equivalence between T_K and T_0. Even though both parameters refer to the temperature where the mobility of glassy materials is minimal and therefore the stability is maximum, T_0 unlike T_K has a viscosity base from the VTF equation. While a majority of organic molecules, have an identical value between T_0 and T_K, amorphous paroxetine HCl has a T_0 lower (19.7 $^{\circ}$C) than T_{KS} (48.8 $^{\circ}$C), which implies that glassy state of paroxetine HCl is greatly influenced by the effect of configurational entropy.

The fictive temperature, T_f, corresponds to the temperature when the glass and the equilibrium-supercooled liquid have the same configurational entropy, in other words, it makes possible the description of the glassy state in comparison to a reference state. T_f can be used as an alternative approach to predict molecular mobility, with a temperature dependence bounded by the two extremes of γ_{Cp}, within the range $0 < \gamma_{Cp} < 1$. In the present work, the γ_{Cp} was calculated as 0.66 J/g $^{\circ}$C and T_f is just 3.2 $^{\circ}$C below T_g, which shows the excess of entropy trapped in the glass formation below its T_g and is a characteristic of fragile glasses/non-Arrhenius behaviour. For glassy paroxetine HCl, T_f is mathematically bound to the limits $T_K < T_f < T_g$.

Reduced Glass Transition Temperature, T_{rg}

Assuming that the viscosity at T_g is constant, higher T_{rg} values reflect higher viscosity between the glass transition temperature and the melting temperature. Therefore, the closer value of T_{rg} to 1, the more resistant is the material to recrystallisation and higher the glass forming ability. Amorphous paroxetine HCl has a value of 0.6, and its behaviour during

the cycling runs in the DSC is not in agreement with the classification into three different classes made by (Baird et al., 2010). From that classification, the materials are divided into groups accordingly to the behaviour during cooling after melting and during the reheating cycle, as referred earlier in the Introduction section. Follow up this categorisation, amorphous paroxetine HCl can be included in the Class 3 (materials with high glass forming ability), since it did not show any crystallisation upon either cooling to below T_g or upon reheating up.

However, it is worth mentioning that this classification was found to have several limitations in predicting the glass forming ability of numerous compounds (Baird et al., 2010).

Fragility Index, m, and Strength Parameter, D

Fragility of amorphous paroxetine HCl was measured *in situ* DSC by heat-cool-heat cycles at different RHs (2, 5, 10, 20 and 50 ^{o}C/min). To avoid recrystallisation from paroxetine HCl Form II to paroxetine HCl Form I during the first heating cycle, the starting paroxetine HCl Form II was dried in P_2O_5 over 24-48 h prior to running in DSC and pinhole pans were used to allow any residual water to evaporate. As shown in Chapter 3, the pseudopolymorphic transformation from Form II to Form I happened when the DSC experiments were performed in hermetically sealed pans at slow heating rates.

For a better comparison, the T_g was measured in the total heat flow of the second heating for all the heating rates. Figure 5.2 shows the scanning rate dependence of the T_g, where ln (q) is plotted against the temperature.
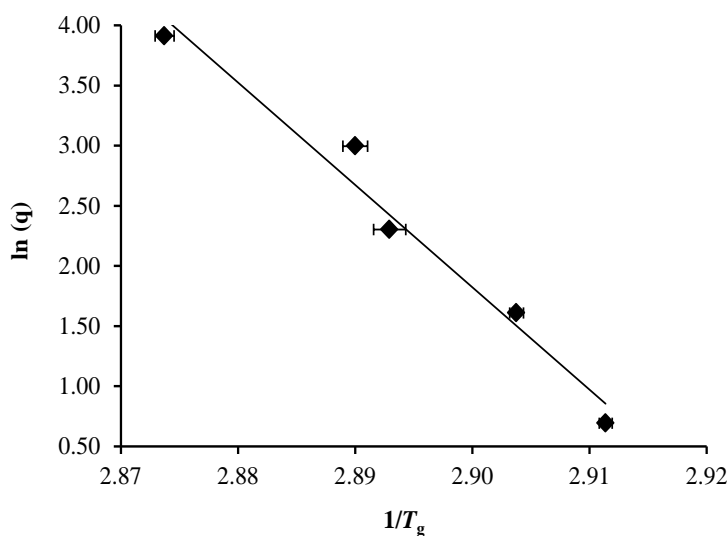
Figure 5.2: Plot of ln (*q*) (where *q* is heating/cooling rate) against the inverse glass transition (K) of amorphous paroxetine HCl.

Based on the scanning rate dependence of the T_g it is possible to obtain the activation energy of structural relaxation at T_g, ΔE_{Tg} as presented earliest by the Equation 5.11. From the slope of the plot, it is possible to calculate the value of ΔE_{Tg}/R and by using the Equation 5.10 the fragile index, *m* can be obtained.

For amorphous paroxetine HCl, *m*, was calculated as 107.3, which classifies the drug as a fragile material. The same indication was given by the strength parameter, *D*, which is related to the dependence of the relaxation time constant on the temperature, and has a value of 6.5.

Relaxation Time, τ

The relaxation time, *τ*, was estimated to be 3.26 x 10^6 seconds ($\approx$ 38 days). Since the storage temperature was below T_g, the AGV approach (Equation 5.6) was used instead of the VTF equation. The predicted value was in good agreement with the experimental physical stability results, as it will be shown later, when considering the samples stored at 53% RH as being those having an environment closer to the normal ambient humidity.

5.3.2   Characterisation of Freshly Prepared Amorphous Paroxetine HCl

5.3.2.1   Thermal Response of Amorphous Paroxetine HCl

For the solubility, dissolution and stability studies, amorphous (quench cooled, QC) paroxetine HCl was prepared by cooling from the melt in nitrogen liquid. The freshly prepared sample was analysed with MTDSC in hermetic pans. It showed a single glass transition event at 51.2 $^{\circ}$C and no signal of recrystallisation or melting was observed, the results presented in Table 5.2. The differences in the T_g and ΔC_p between the sample prepared *in situ* the DSC and the sample prepared by quench cooling method in nitrogen liquid, were probably due to the exposure to atmospheric humidity conditions which led to the adsorption of water molecules and thus lowered the T_g. The enthalpy of relaxation (ΔH_{relax}) was measured in the non-reversing signal.

Table 5.2: Thermal properties and water content of the freshly prepared amorphous paroxetine HCl.

Parameter	Value
$T_g \pm$ s.d. ($^{\circ}$C)	51.2 $\pm$ 0.6
$\Delta C_p \pm$ s.d. (J/g $^{\circ}$C)	0.28 $\pm$ 0.06
$\Delta H_{relax} \pm$ s.d. (J/g)	2.5 $\pm$ 0.7
Water content $\pm$ s.d. (%)	0.87 $\pm$ 0.13

5.3.2.2   ATR-FTIR and XRPD Characterisation of Amorphous Paroxetine HCl

Paroxetine HCl Form II has two bands in the 3700-3200 cm^{-1} range that can be assigned to O-H groups in different chemical environments (as shown in Chapter 3). In the fully

amorphous QC sample, these two bands were missed and in the rest of the spectrum some peaks appeared broadened or simply disappeared, which is characteristic of this kind of state (data not shown). These results were confirmed by the XRPD data that showed the absence of crystalline peaks from the starting paroxetine HCl Form II within the range 5° to 40°, 2θ and the appearance as halo pattern (data not shown).

5.3.3   Drug Performance Assessment

5.3.3.1   Solubility Measurements

Assessing the aqueous solubility of amorphous materials can represent a challenge and a practical problem to the formulator. The primary and most frequent obstacle is the high tendency for amorphous materials to suffer phase transformation towards a thermodynamic more stable form during the experimental measurement process (Murdande et al., 2011).

In this work, as presented in Figure 5.3, the aqueous solubility of amorphous paroxetine HCl was determined after 24 and 72 h isothermal stirring time. The measured apparent solubility of the glassy paroxetine showed, in both sampling times, a lower value than the crystalline starting material paroxetine HCl Form II, but still higher than the aqueous solubility of paroxetine HCl Form I. This low apparent solubility can be ascribed to the recrystallisation, in the media, to the more stable and less soluble crystalline hydrate form, paroxetine HCl Form I.
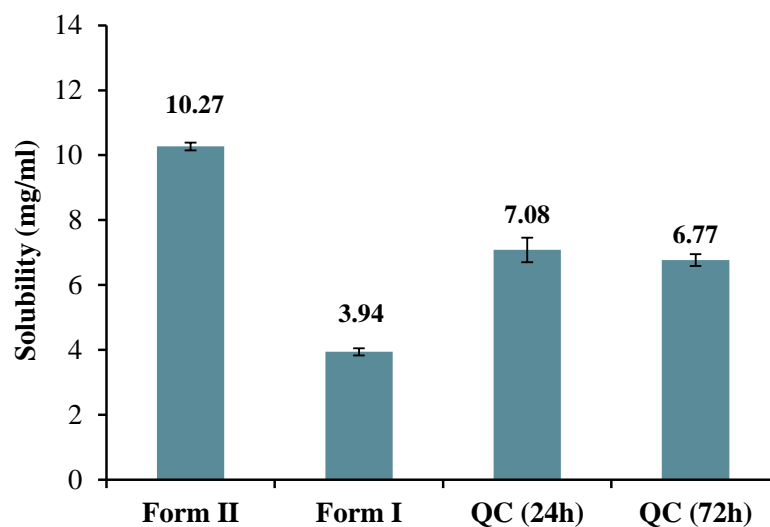
Figure 5.3: Solubility in water of two crystalline (Form I and II) and quench cooled (QC) forms of paroxetine HCl.

The residues, collected after centrifugation from the solubility experiments and after dried over night at room conditions, were analysed using XRPD and ATR-FTIR, as presented in Figure 5.4 and Figure 5.5, respectively. Accordingly, to the results obtained, both paroxetine HCl Form II and the QC amorphous form, recrystallised during the solubility experiments. However, the decrease in the solubility is higher for the QC sample than for the Form II.

In this type of dynamic solubility experiments, an initial supersaturation condition is required and therefore phase separation/recrystallisation events can occur (Grant and Brittain, 1995). This phenomenon is clearer for the glassy sample. This could probably be ascribed to the higher energy state of the amorphous material that once in contact with water led to a higher solubility of the glassy sample in the early beginning. As the experiment progressed in time, the excess of amorphous sample in solution started to precipitate out. The new form obtained (paroxetine HCl Form I) has a lower water solubility and as result the 'amorphous' solubility is nearly 2/3 when compared to the starting material.
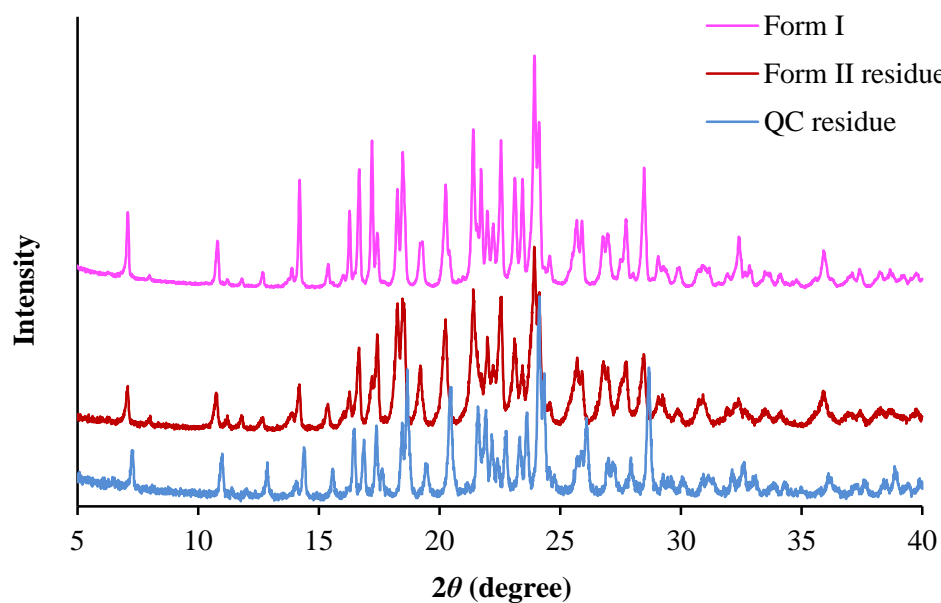
Figure 5.4: XRPD data of paroxetine HCl Form I and the solubility residues, collected after centrifugation from the solubility measurements of Form II and quench cooled (QC).
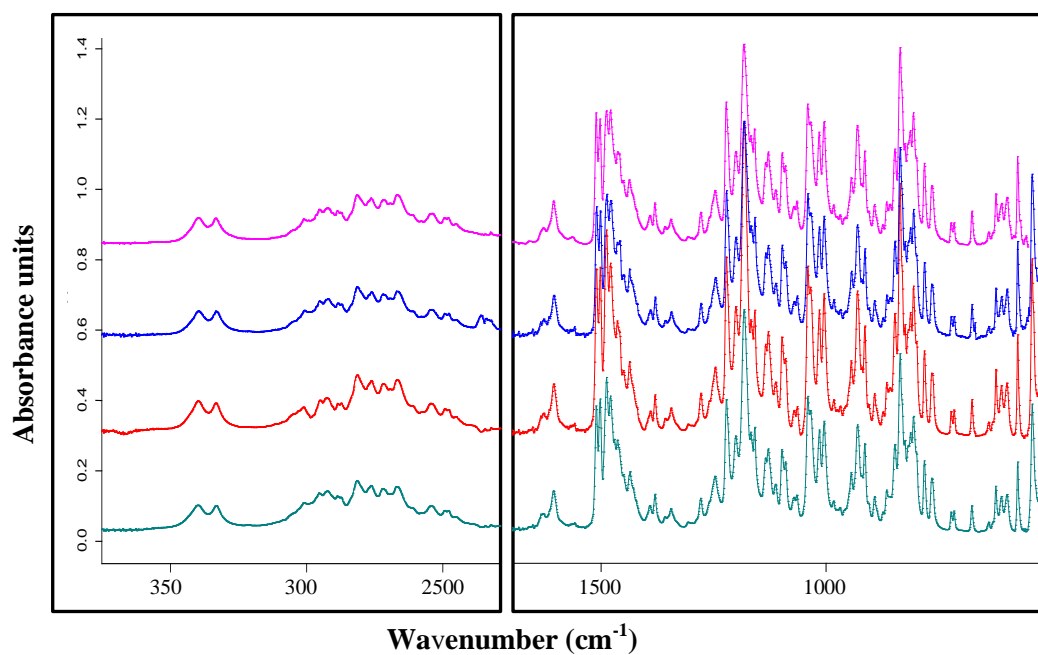
Figure 5.5: ATR-FTIR spectra of the solubility residues (amorphous QC paroxetine HCl, Form II and Form I) collected after the solubility experiments (72 h stirring at 25 °C) and paroxetine HCl Form I (upwards).

Even though the residue obtained from the paroxetine HCl Form II solubility experiments corresponded as well to the stable Form I, the solubility of this form still being higher when compared to the Form I. This can be readily explained because the recrystallisation just took place in the excess of sample added to prepare a saturated solution. Therefore, the lower solubility of paroxetine HCl Form II in comparison with the amorphous sample made the amount of Form II required to create a supersaturation solution lower than in the case of the amorphous sample.

5.3.3.2   Dissolution Studies

In contrast to the aqueous solubility results, the dissolution studies showed a clear enhancement on the extent of the dissolution rate of the drug, when the amorphous form was compared to the crystalline forms (Figure 5.6). The difference can be explained by the immediate dissolution of the amorphous form once it contacts the dissolution medium and there is no time for recrystallisation to occur.
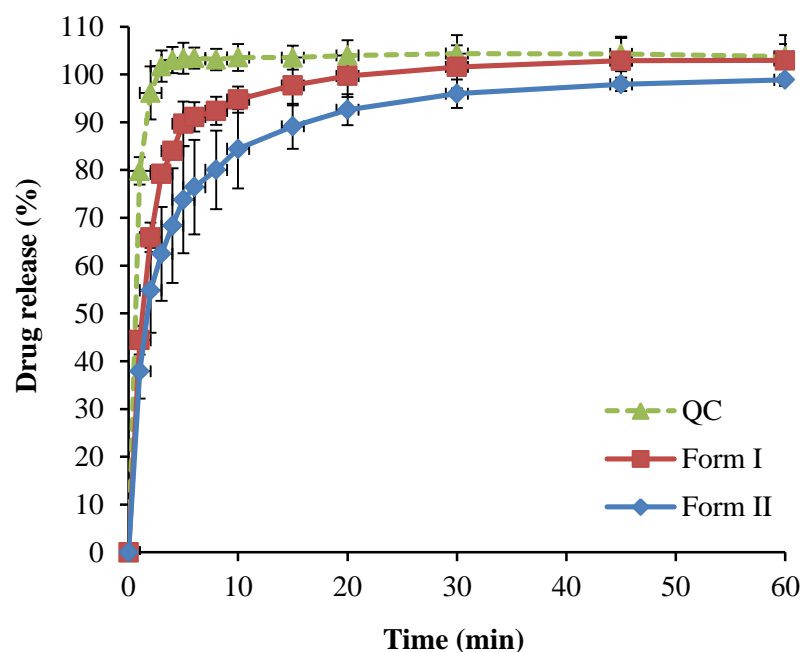
Figure 5.6: Dissolution profiles of Form I, Form II and quench cooled (QC) paroxetine HCl in 0.1M HCl.

5.3.4 Response of Amorphous Paroxetine HCl Below T_g and Under Different Humidity Conditions

Ageing experiments represent a crucial step during the development of any amorphous API, establishing a physical and chemical stability profile. Even though, below T_g, translational molecular motions are slower than above T_g, they still occur and can obviously influence the life time of these materials.

In this study, since the T_g of QC paroxetine HCl was found to be 51.2 ^{o}C, its stability behaviour was studied at room temperature ($\approx$ 25 ^{o}C), so well below T_g and under the influence of different RHs environments.

5.3.4.1 Recrystallisation Behaviour of Paroxetine HCl from the Amorphous State

The samples stored in 0% RH did not show, during all the experimental time (2 months), any signal of recrystallisation, being only possible to identify during the heating cycle in the DSC, a glass transition phenomena. On the opposite, the samples stored at 75% RH were completely recrystallised after 24 h, accordingly to DSC data, into the most stable paroxetine HCl Form I, with an onset melting temperature around 140 ^{o}C.

Apart from the samples stored under these two extreme humidity conditions (0 and 75% RH), all the others showed a glass transition event, which reduces as the relative humidity increases, followed by a recrystallisation exotherm and in the end a fusion endotherm, as can be observed below in Figure 5.7. It was also noticed that the shape of the recrystallisation peaks and the temperature at which the recrystallisation occurred, changed with the storage humidity. As the humidity increased the exotherm peak became sharper and appeared at lower temperatures, in contrast to what happened with the 22% RH samples that showed a broad appearance at much higher range of temperatures.
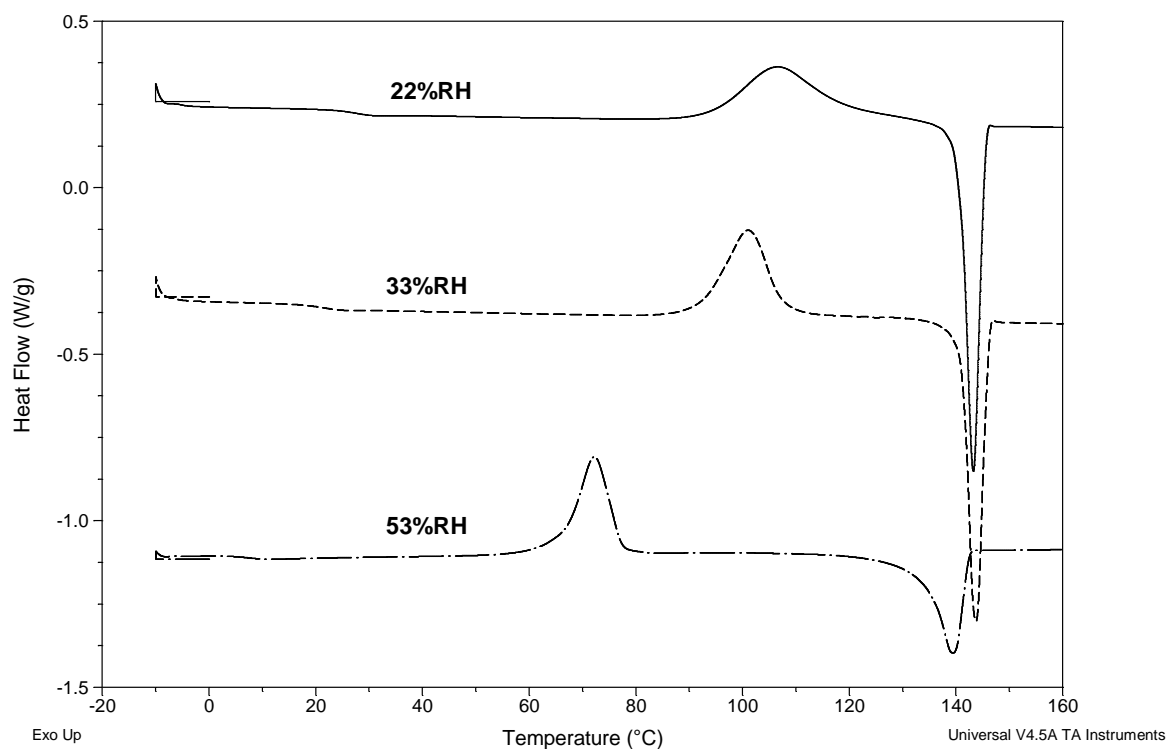
Figure 5.7: MTDSC heating cycle traces of amorphous quench cooled paroxetine HCl aged at 25 $^{\circ}$C under different RHs, as stated, for 48 h; hermetic pans were used.

5.3.4.2   Water Content

The water content was measured by TGA and the results are presented in Figure 5.8. For the samples stored under 0, 22 and 33% RH the amount of water remained nearly constant for all samples. The water content can also be used as a measure of the recrystallisation extent, as shown by the samples stored at 53% RH. These samples showed higher water content until 14 days of storage with a decrease afterwards, indicating that most of the sample was recrystallised after that period. These results are in agreement with the DSC experiments where the ΔH_{rec} decreased significantly after 30 days of storage as a meaning of isothermal recrystallisation prior the DSC test, as shown later in this study. In fact, the amorphous-crystalline transition reveals a great reduction in the water sorption capacity of the crystalline material when compared with the amorphous state.

For the samples stored at 75% RH, the amount of water remained constant since the first day of storage (2.19–2.87% w/w) due to its nearly complete recrystallisation. In addition,

the amount of water measured for this sample at 75% RH agreed with the identification of the recrystallised material as paroxetine HCl Form I (water content = 2.63% w/w).
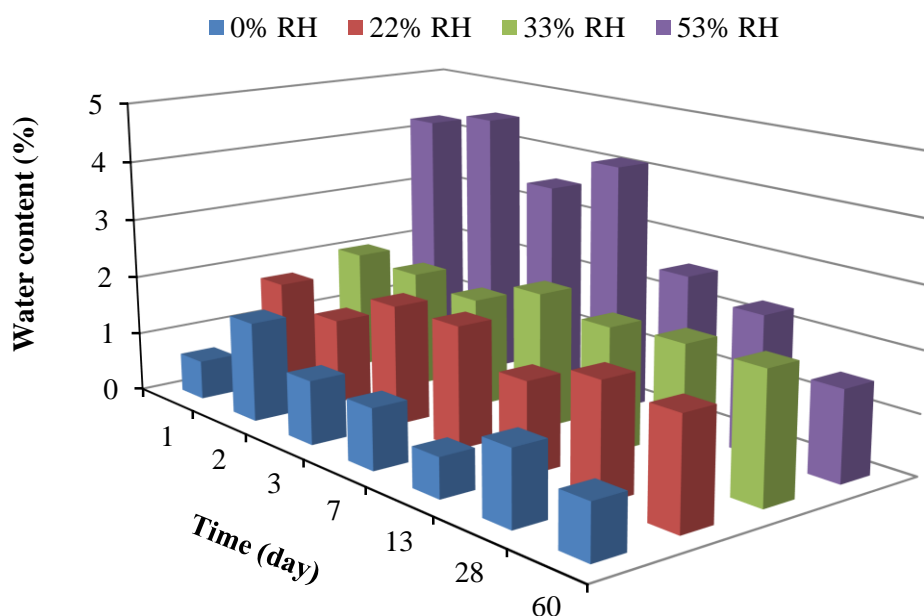
Figure 5.8: Water content of the amorphous paroxetine HCl, over time and under different storage conditions at 25 °C.

5.3.4.3   Glass Transition Temperature

The increase in the humidity storage conditions decreases the T_g values. The water molecules have the ability to plasticise amorphous materials, reduce the viscosity and at the same time enhance molecular mobility. Indeed, the presence of small amounts of absorbed water makes a high contribution in the molecular mobility of these systems, which can induce in the last instance the recrystallisation to happen. However, when glassy materials transform into the crystalline form in presence of moisture, the water sorption capacity usually decreases or slow down, as reported above.

As predicted and shown in Figure 5.9, the QC samples stored under 53% RH showed the lowest T_g for the four RHs presented. At 75% RH it was not detected any glass transition after 24 h of storage, as the sample was fully recrystallised during the DSC run. At 0% RH,

there is a slight increase in the T_g, certainly due to the dry of small quantities of water eventually present prior to storage.
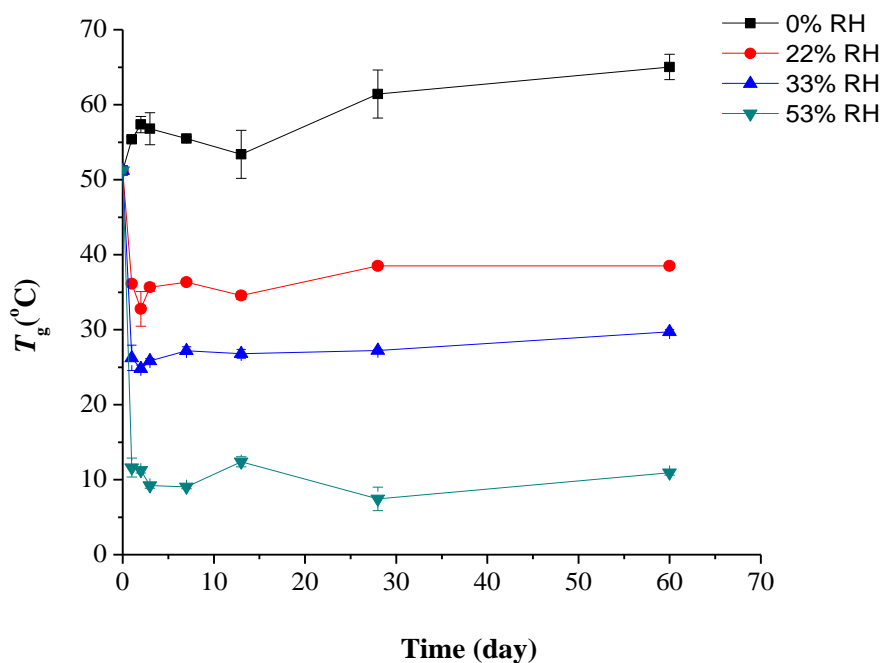
Figure 5.9: Changes in the T_g of quench cooled paroxetine HCl over time and under different RHs conditions.

5.3.4.4   Recrystallisation Temperature

The increase in the humidity, lead the amorphous materials to devitrify and promote the nucleation to happen. The transformation from glass to rubber, facilitate the crystal seeds to grow, what can be observed by the decrease in the recrystallisation temperature, T_{rec} at higher humidity. Indeed, as shown in Figure 5.10 the samples at 53% RH, showed the lowest recrystallisation temperature. This can be explained by the presence of higher nucleation seeds what facilitates the recrystallisation process and thereby lower temperature is needed for the crystal formation.
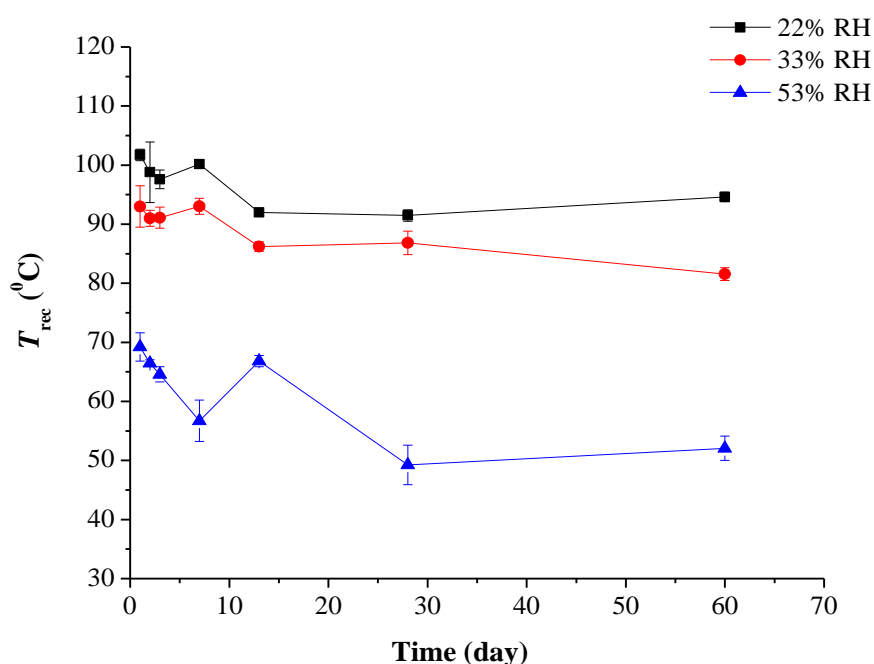
**Figure 5.10: Recrystallisation temperature (onset values) profiles
for the samples stored under 22, 33 and 53% RH for 60 days.**

5.3.4.5   Enthalpy of Recrystallisation

In Figure 5.11 is presented the variation on the enthalpy of recrystallisation, ΔH_{rec}, for the different samples stored under different humidity environments.

McGarvey et al. (McGarvey et al., 2003) studied the non-isothermal behaviour of amorphous α-trehalose with a particular emphasis on the effects of the DSC pan type used and initial water content of the samples. They observed that samples with higher water content showed lower enthalpy and recrystallisation temperatures. These results are partially in agreement with the findings in this study. In fact, the recrystallisation temperature decreased as the RH increased, although the ΔH_{rec} did not follow the same trend.

The QC samples stored at 33% RH have the higher ΔH_{rec} whereas the ones at 22% RH have the lowest. Surprisingly the 53% RH samples have an enthalpy of recrystallisation in between the other two. Considering that a lower value of ΔH_{rec} is a meaning of lower amorphous content 'ready' to recrystallise, this is true for the samples at 22% RH. The

water vapour at this humidity was not high enough to devitrify large amounts of glass and therefore low ΔH_{rec} upon heating. The explanation for what happen with the samples at 33% and 53% RH, has probably to be with different disorder stages of the glass under these conditions.
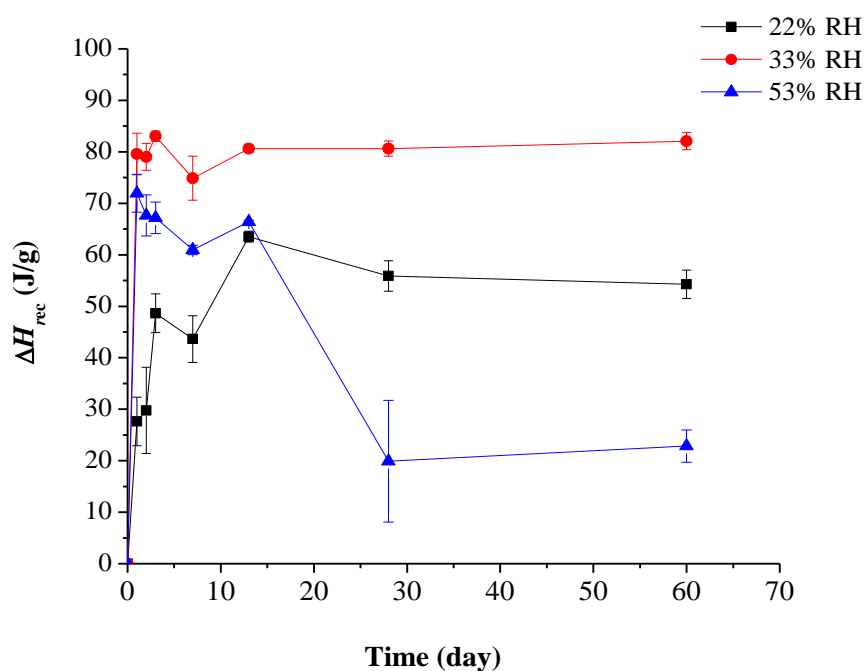
Figure 5.11: Enthalpy of recrystallisation at different storage conditions up to 60 days.

The 53% RH samples overcome through a rubbery state after a short time of storage, the molecular mobility is then reduced and the energy barrier created by the enhancement in the viscosity reduces the tendency for the crystals to growth even though the initial amount of crystal seeds is high, thus, lower value of ΔH_{rec}. This was just observed during the first 13 days of storage. After that the ΔH_{rec} of the 53% RH samples showed a big drop, even below the 22% RH ones, since most of the sample completely recrystallised.

For the samples at 33% RH, the higher ΔH_{rec} by comparison with the 53% RH samples, could possibly be explained by the higher degree of disorder together with the fact that these samples have not yet been converted into a rubbery state. This could, therefore, generate a high exothermic enthalpy upon recrystallisation. A similar interpretation was

obtained by Graeser et. al (Graeser et al., 2008), when they compared amorphous simvastatin prepared by two different techniques (cryomilling and quench cooling).

5.3.4.6 ATR-FTIR Analysis

ATR-FTIR was used to monitorise the isothermal recrystallisation of QC paroxetine HCl. The samples stored at low RH (0, 22 and 33%) remained amorphous during the total experimental time without any characteristic crystalline peak being observed. Though, an interesting observation was detected for the samples under 53 and 75% RH.

For the samples stored at 75% RH (Figure 5.12) the process of recrystallisation did not progress in one-step from the amorphous to the most stable crystalline form (Form I), being observed an intermediate state between these two forms, as explained next. At these conditions, the process of recrystallisation undergoes from the amorphous material to a mixture between paroxetine HCl Form II and Form I, which took place in the first 3 days of storage and after that, only Form I was detected. The evidences that Form II is present are related to the following peaks characteristics of that form: the single sharp peak at high wavenumber 3630 cm^{-1} and the peak at 665 cm^{-1}. Gradually, the peak at a high wavenumber disappeared and a peak at 3334 cm^{-1} started to appear until the recrystallisation to Form I was completed. The same happened with two peaks at lower wavenumber, disappearance of the peak at 665 cm^{-1} and appearance of the peak at 675 cm^{-1}, characteristic of Form I. In addition, the appearance of the peak around 1550 cm^{-1} after the 1st day and its disappearance on the 7th day of storage, assigned to the O-H bending vibration from the weakly bound water, indicates that the process of recrystallisation happened via the formation of the non-stoichiometric hydrate Form II.
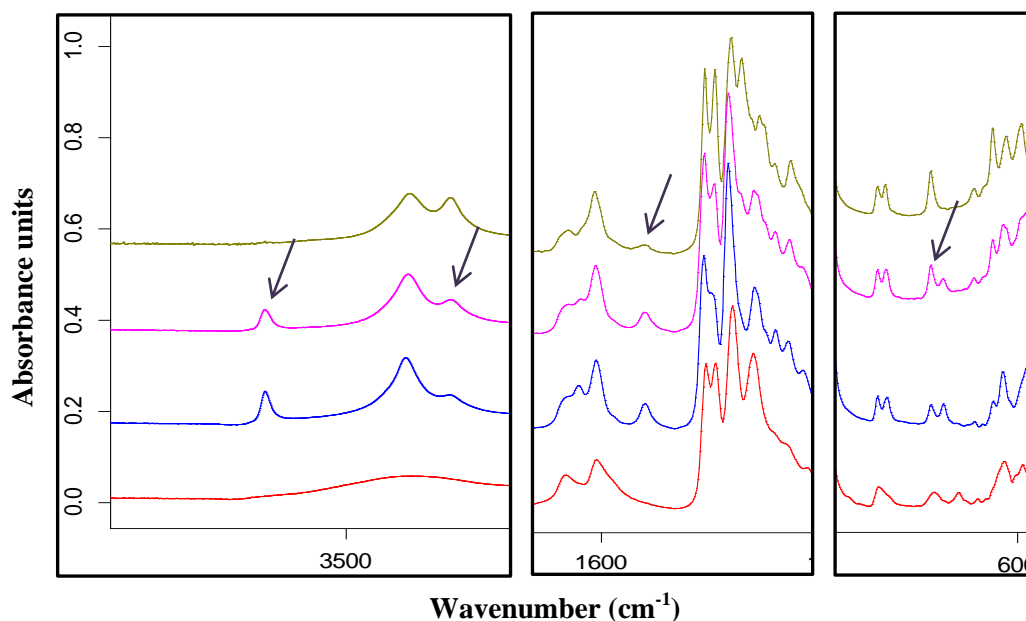
Figure 5.12: ATR-FTIR spectra of amorphous paroxetine HCl at different time points upon storage at 75% RH/25 ^{o}C: prior storage, 1, 3 and 7 days (upwards).

However, the recrystallisation behaviour mentioned for the samples at 75% RH was not observed with the samples stored at 53% RH, which recrystallised directly into Form I, as shown in Figure 5.13.

This could have been because the water vapour pressure at the 53% RH conditions allowed the sample to slowly recrystallise into the most stable form, avoiding intermediate metastable states. Another explanation could be the large sampling time interval (14 days – completely amorphous, 30 days – already Form I), with the phenomenon referred for the samples at 75% RH happening during that period.
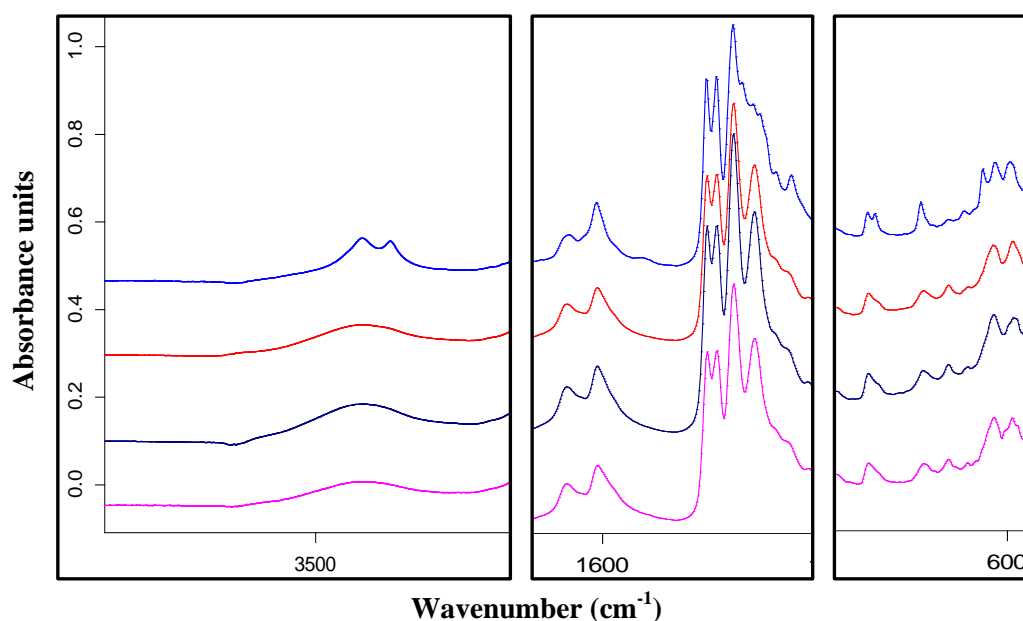
Figure 5.13: ATR-FTIR spectra of amorphous paroxetine HCl at different time points upon storage at 53% RH/25 °C: prior storage, 7, 14, and 30 days (upwards).

5.3.4.7   XRPD Analysis

The XRPD experiments were in a fair agreement with those obtained with the ATR-FTIR measurements, considering some delays in detection/differentiation between the two techniques, particularly for the samples at 75% RH. Figure 5.14 shows the XRPD diffractograms of paroxetine HCl Form I and II as received. These two forms are easily distinguished within the range between 15° and 25°.

As mentioned earlier, samples stored at 0, 22 and 33% RH remained amorphous throughout the 60 days of experiments. The samples at 53% RH showed recrystallisation peaks matching the pattern of paroxetine HCl Form I after 30 days (data not shown).
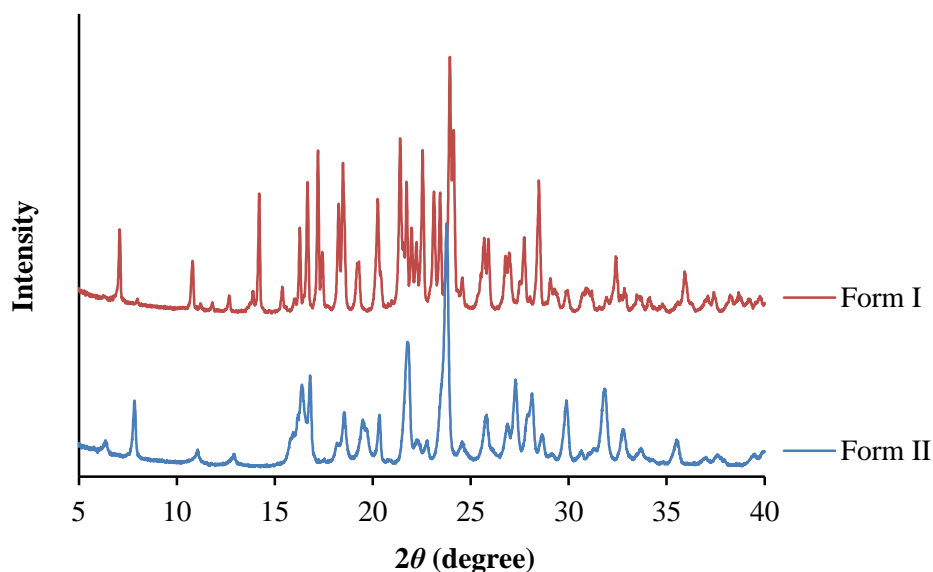
Figure 5.14: X-ray diffractograms of paroxetine HCl Form I and II, as received.

The samples under 75% RH (Figure 5.15) showed after 7 days a pattern, which revealed a mixture of Forms I and II. After 60 days, the XRPD diffractogram was to the pattern of Form I, especially considering the range between 20-25°. The poor quality of the spectra was related to the hardness of the sample and the difficulty in obtaining a complete flat surface, ideal for X-ray measurements.
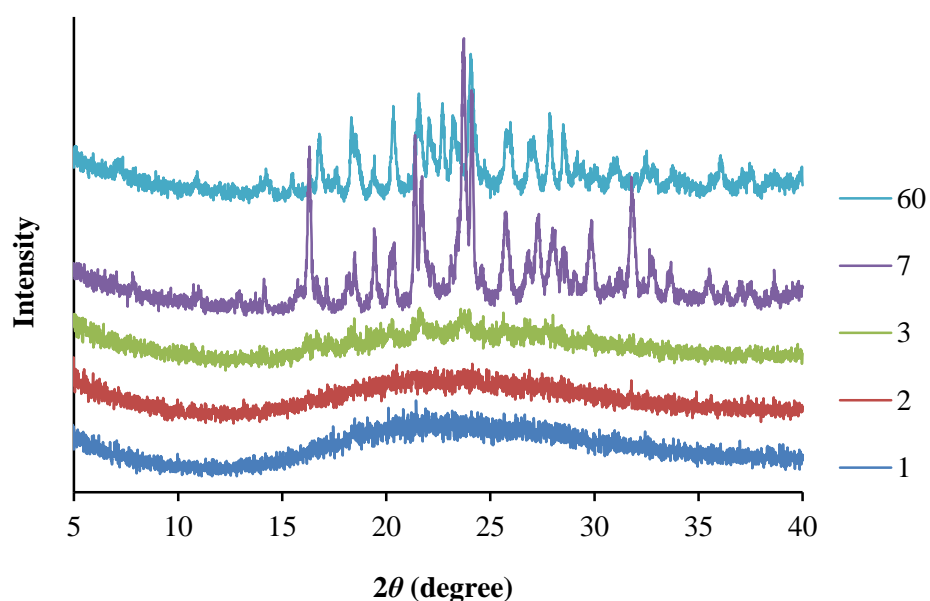
Figure 5.15: XRPD diffraction data collect at different time points (in day) for the quench cooled paroxetine HCl sample stored under 75% RH.

5.4   Conclusions

The use of thermal methods has demonstrated to be a powerful approach to predict the physical stability of amorphous compounds. In this chapter, a range of thermodynamic and kinetic parameters were used to characterise amorphous paroxetine HCl prepared via quench cooling. Overall, parameters determined by using DSC such as configurational heat capacity, fragility index and strength parameter classified amorphous paroxetine HCl as a fragile glass former. Moreover, the close value of T_K to T_g, and the non-equivalence to T_0, indicated that glassy paroxetine HCl is greatly influenced by the effect of configuration entropy. This finding was also supported by the fact that at a storage temperature of 25 ^{o}C, the T_f was only 3.2 ^{o}C below T_g indicating that under these storage conditions the glass still has a considerable degree of configurational entropy, which can be linked to a significant molecular mobility and therefore instability.

Although all the above parameters constitute a source of valuable information when dealing with amorphous materials they must be considered carefully as they do not account the influence of humidity, which has a crucial influence on the stability of this kind of compounds. In the present work, storage under different humidity environments proved not only to influence the rate, but also, the pathway of recrystallisation. The non-isothermal recrystallisation studies observed in DSC showed that the samples stored at 53% RH started to recrystallise at a lower temperature and over a narrow temperature range. Moreover, according to the ATR-FTIR results, these samples were found to recrystallise directly to the stable Form I, whereas the samples under 75% RH recrystallised via a metastable Form II.

The instability of the glassy paroxetine HCl was also noticed upon prolonged exposure to water during the solubility measurements. The measured solubility of amorphous paroxetine HCl was lower than the starting crystalline Form II, which was ascribed to the recrystallisation to the most stable Form I. This behaviour was not observed during the dissolution tests. Although it is important to bear in mind that *in vivo* the recrystallisation to the stable hydrate can occur.

6 MISCIBILITY PREDICTION AND THE INFLUENCE OF PREPARATION METHODS ON THE PROCESSING OF PSEUDOPOLYMORPHS OF PAROXETINE HCL

Abstract

This chapter presents a theoretical and practical perspective of processing two pseudopolymorphs (Form I and II) of the same drug (paroxetine HCl) using different preparation techniques, with particular attention being paid to the performance and stability of each system. A non-solvent process, hot melt extrusion (HME), and a solvent method, spray drying (SD), were used to convert the two crystalline hydrates into an amorphous solid dispersion, using polyvinylpyrrolidone vinyl-acetate (PVPVA) as a carrier. Standard differential scanning calorimetry (DSC) and modulated temperature DSC (MTDSC) were used to characterise physical mixtures (PMs), fresh and aged solid dispersions, in combination with thermogravimetric analysis (TGA), dynamic vapour sorption (DVS), X-ray powder diffraction (XRPD) and attenuated total reflection-Fourier transform infrared (ATR-FTIR) techniques. Theoretical predictions of drug-polymer miscibility were carried out using melting point depression (MPD) approach. MPD method suggested that Form I of paroxetine HCl favours a miscible system with PVPVA while Form II is inclined to generate an immiscible system with the same polymer as no depression on the onset melting point of this form was observed in the presence of the polymer. However, the corresponding experimental data showed a single T_g in DSC and a halo pattern in XRPD for both samples prepared from SD and HME, indicating the formation of a molecular dispersion. Although fully amorphous dispersions were prepared by both SD and HME methods, the Form I and Form II systems showed different dissolution and long term stability profiles. More specifically, in the case of Form I, HME formulations showed a lower release rate in the beginning of the test when compared to the SD, PMs and pure crystalline drug. In the case of Form II systems, HME showed the same release profile as the pure crystalline form, but also lower than SD and PMs. The lower release observed for the HME over the SD samples might be related to the differences in the diffusion of the dissolution media into the microparticles (63-106 μm). Regarding stability under storage, all the samples kept at 75% RH/25 $^{\circ}$C recrystallised into the sable Form I, confirmed by FTIR, though they exhibit different crystallisation rates, with spray dried samples showing a higher tendency to recrystallise. The recrystallisation profile of the HME samples was different for the Form I and Form II systems, with the former presenting a slower rate.

6.1 Introduction

Pharmaceutical formulations of a drug product should be physically and chemically stable, manufacturable, and the drug entity made bioavailable. Although, active pharmaceutical ingredients (APIs), and also excipients, exhibit polymorphism or pseudopolymorphism, the thermodynamically most stable form is, in general, selected for development. However, there are several situations in which the development of a metastable form is desirable, namely to achieve rapid absorption and efficacy, or acceptable systemic exposure for a low-solubility drug. The term polymorphism, describes the ability of a compound to crystallise in more than one form (Haleblian and McCrone, 1969). On the other hand, pseudopolymorphism is used to avoid confusion with 'true polymorphs' and describes crystalline compounds that have a heterogeneous unit cell with solvent molecules within it, such as the case of hydrates, when the solvent is water (Brittain, 2009).

Recently, particular attention has being paid to the transformation of crystalline APIs into amorphous phase by the manufacture of solid dispersions by different methods. In solid dispersion technologies, the drug is incorporated into a hydrophilic carrier, theoretically at molecular level, leading to a loss of crystal lattice energy, thereby increasing dissolution rate of the drug. Several parameters are of great importance when designing an amorphous solid dispersion formulation such as, the method of preparation used, the physicochemical properties of the selected polymer and, with less focus in the available literature, the intellectual properties of the starting material, namely water content and crystalline form. In this study, two pseudopolymorphs (Forms I and II) of the same drug, paroxetine HCl, were chosen as model drug, which allowed to evaluate the influence of the initial crystalline state on the prepared system. Paroxetine HCl Form I is a stable hemihydrate whereas Form II is a non-stoichiometric hydrate and considered metastable to Form I. The polymer selected was polyvinylpyrrolidone vinyl-acetate 6:4 (PVPVA) due to its vast use in pharmaceutical research, especially in the preparation of solid dispersions, and relatively low hygroscopic behaviour compared to the homopolymer polyvinylpyrrolidone based polymers.

Within a preliminary investigation into the preparation of solid dispersion systems, important theoretical parameters can be used to evaluate the miscibility between each form and PVPVA, which can provide a better understanding in terms of the ability of the polymer to stabilise the API. Therefore, a number of thermodynamic approaches that are available in the literature and commonly used in the pharmaceutical field were applied in this study as briefly described below.

The simpler and straight indication of the miscibility between two or more components is the detection of a single glass transition step in DSC, usually designated as the mixed phase glass transition temperature (T_{gmix}) (Gordon and Taylor, 1952). The well-known Gordon-Taylor (GT) equation is one means of predicting the T_g of amorphous solid dispersions based on the weight fractions, T_g values and coefficients of thermal expansion of their components, as presented below by Equation 6.1 for a ternary system (API-polymer-water),

$$T_{g_{mix}} = \frac{w_1 T_{g1} + K_{12} w_2 T_{g2} + K_{13} w_3 T_{g3}}{w_1 + K_{12} w_2 + K_{13} w_3}$$

<div align="right">**Equation 6.1**</div>

where, w is the weight fraction, T_g is the glass transition temperature (K) and K is a constant. The subscripts 1, 2 and 3 represent polymer, drug and water, respectively. For polymer blends of three components, the subscript 3 refers to the component of lowest T_g (Truong et al., 2002). The constants K_{12} and K_{13} can be estimated by using:

(a) Couchman-Karasz Equation (Couchman and Karasz, 1978),

$$K_{12} = \frac{\Delta C_{p2}}{\Delta C_{p1}} \qquad K_{13} = \frac{\Delta C_{p3}}{\Delta C_{p1}}$$

<div align="right">**Equation 6.2**</div>

where, ΔC_p is the heat capacity change between the supercooled-liquid and the glassy state.

(b) Simha-Boyer Rule (Simha and Boyer, 1962),

$$K_{1\,2} = \frac{\rho_1 T_{g1}}{\rho_2 T_{g2}} \qquad K_{1\,3} = \frac{\rho_1 T_{g1}}{\rho_3 T_{g3}}$$

Equation 6.3

where, ρ is the density of each component.

In theory, if a system is miscible it will exhibit a single T_{gmix}, which is intermediate to the T_g values of the individual components with a relationship to the mixture composition. It should be noted that the GT approach only works for ideal systems, i.e., systems with an ideal volume additivity and negligible tendency to interact (Schneider and Di Marzio, 1992). As a result, when an additive lowers the T_g of a substance it has a plasticising effect, such as the case of water, whereas if it raises the T_g it has an antiplasticising effect (Hancock and Zografi, 1994). In this study, the T_{gmix} was calculated using Gordon-Taylor/Couchman-Karasz Equation.

Another parameter used in the theoretical framework to correlate miscibility and thermodynamic stability of API-polymer systems, is the well-known Flory-Huggins interaction parameter, χ (Huggins, 1942; Flory, 1942). Flory-Huggins (FH) theory is based on the free enthalpy of mixing which has entropy and enthalpy components. χ is independent of composition, but it varies with concentration and temperature allowing a possible correlation between theoretical and experimental results (Kontogeorgis, 2007). Commonly, the FH interaction parameter can be obtained by using two methods: solubility parameter approach and melting point depression method (MPD). However, in this study the APIs are in their salt form, thus the solubility parameter cannot be calculated as it does not apply to compounds having specific strong intermolecular interactions, such as ionic in the case of salts (Zhao et al., 2011).

The interaction parameter has been extensively determined from melting point approach for both polymer-polymer blends (Jo and Kwon, 1991) and for polymer-solvent systems (Meaurio et al., 2005). With particular importance on the pharmaceutical area, few years ago Marsac and his collaborators developed an approach to estimate the interaction parameters between APIs and polymeric systems (Marsac et al., 2006), as shown by the relation in Equation 6.4,

$$\left(\frac{1}{T_m^{mix}} - \frac{1}{T_m^{pure}}\right) = \frac{-R}{\Delta H_{fus}} \left[ln\phi_{drug} + \left(1 - \frac{1}{m}\right)\phi_{polymer} + \chi\phi_{polymer}^2\right]$$

Equation 6.4

where, T_m^{mix} is the melting temperature of the drug in the presence of the polymer, T_m^{pure} and ΔH_{fus} are the melting temperature and the enthalpy of fusion of the pure drug, respectively; R is the gas constant, ϕ_{drug} and $\phi_{polymer}$ are the volume fractions of the drug and the polymer, respectively, and m is the ratio of the volume of the polymer to that of the lattice side (defined for this purpose here as the volume of the drug).

If a drug is miscible with a polymer, the chemical potential of the drug in the mixture must be lower when compared to the chemical potential of drug alone. Considering this fact and the enthalpy nature of the mixing being exothermic, endothermic or athermal, different reduction magnitudes in the melting point of the drug can be observed. Exothermic processes should produce a large depression on the melting point of the drug and progressive less significant for athermal and endothermic mixing processes. On the contrary, if the drug and the polymer are immiscible, no melting point depression is expected (Marsac et al., 2009). This approach is of great importance in this study as each pseudopolymorph of the model drug, showed a different melting response in the presence of the polymer.

As previously described, the Flory-Huggins lattice theory brought an important support to the understanding of the thermodynamics of polymer-solvent mixtures, which accounts for the entropy (ΔS_{mix}) and enthalpy (ΔH_{mix}) of mixing between large (polymers) and small molecules (APIs in the case of solid dispersions) (Baird and Taylor, 2012; Marsac et al., 2006). One way to better expose this relationship is by considering the free energy of mixing, ΔG_{mix}, at absolute temperature (T), as expressed by Equation 6.5,

$$\Delta G_{mix} = \Delta H_{mix} - T\Delta S_{mix}$$

Equation 6.5

Adding the Flory-Huggins interaction parameter, χ, which is related to the enthalpy of mixing, the free energy of mixing, can be described by the Equation 6.6 below,

$$\frac{\Delta G_{mix}}{RT} = n_{drug} \ln \phi_{drug} + n_{polymer} \ln \phi_{polymer} + n_{drug} \phi_{polymer} \chi$$

Equation 6.6

where, n_{drug} and $n_{polymer}$ is the number of moles of drug and polymer, respectively. The first two terms on the right hand side of the equation represent the entropy of mixing, while the third term stands for the enthalpy of mixing. The entropy contribution always favours mixing whereby the enthalpy contribution, which depends on the type and intensity of the interactions between the components, can either facilitate or prevent mixing.

After the brief exposition of some of the theoretical parameters that are commonly used to study miscibility and investigate the formation of a single phase amorphous systems, another point of concern is the processing conditions. Indeed, it is widely accepted that the properties of amorphous materials are highly dependent on their thermal history and hence, on the preparation method (Zhang et al., 2009; Janssens et al., 2010; Karmwar et al., 2011, 2012). Therefore, in this study two different preparative techniques, spray drying (SD) and hot melt extrusion (HME) were used. SD is a solvent method that involves the rapid transformation of an API-carrier solution/suspension to solid API-carrier particles due to the fast evaporation of the solvent. As referred in Chapter 2, the SD process consists of four basic stages: atomisation of the solution containing the API and carrier, mixing with the drying gas, evaporation of the liquid and finally the separation of the dried particles from the gas (Ré, 2006). HME consists in the dispersion of the API in a polymeric or lipid carrier matrix using the effect of heat. Several advantages are attributed to this technique. Firstly, it is solvent free method and therefore with great economical and safety benefits, secondly the new design of the extruders allow a good mixing and homogenising of the formulation and finally it is industrially favourable for scaling-up (Miller et al., 2007).

Later in this work, it is investigated whether the samples prepared by these two methods exhibit different structural and thermodynamic characteristics and whether these differences can be correlated to their dissolution behaviour and physical stability. Moreover, the influence of the pseudopolymorphic form on the prepared system was also evaluated, as referred to, earlier in this chapter.

Thermal analysis, such as differential scanning calorimetry (DSC) and modulated temperature DSC (MTDSC), were used to predict drug-polymer miscibility and fully

characterise the prepared solid dispersion systems as well as to investigate their physical stability under storage. Thermogravimetric analysis (TGA) and dynamic vapour sorption (DVS) were used to measure water content and water uptake, respectively. Structural techniques were carried out using X-ray powder diffraction (XRPD) and infrared analysis (FTIR).

6.2 Materials and Methods

6.2.1 Materials

Crystalline paroxetine HCl Form I is a stoichiometric hydrate with 0.5 mol of water per mol of drug (molecular weight (MW) = 374.83 g/mol, density (ρ) = 1.35 g/cm^3) and it was purchased from Afine (China). Paroxetine HCl Form II is a non-stoichiometric hydrate with 0.8 mol of water per mol of drug (MW = 365.83 g/mol, ρ = 1.36 g/cm^3) and it was obtained from Huahai Pharmaceuticals (China). Polyvinylpyrrolidone vinyl-acetate 6:4 (PVPVA, MW $\approx$ 47 000 g/mol, ρ = 1.17 g/cm^3) was kindly donated by BASF (Germany). Methanol (analytical grade) was obtained from Sigma Aldrich (UK). Storage environments with different relative humidities (RHs) were prepared using salt solutions of sodium chloride (75% RH, Fischer Scientific, UK) and magnesium nitrate hexahydrate (53% RH, Fluka, Germany). Phosphorus pentoxide (P_2O_5) was used as desiccant (Alfar Aesar, UK).

6.2.2 Methods

6.2.2.1 Preparation of the Physical Mixtures

Physical mixtures (PMs) between each API and PVPVA were prepared by gentle mixing using a mortar and pestle.

6.2.2.2   Calculation of Fragility Parameters

The glass forming ability of paroxetine HCl Form I and II was evaluated using the heating rate dependence of the T_g (Qi et al., 2008). APIs were heat-cool-heat in DSC at different heating rates, 2, 5, 10, 20 and 50 $^\circ$C/min and T_g was measured on the 2$^{\text{nd}}$ heating curve. Parameters such as fragility index (*m*) and strength parameter (*D*) are generally used to classify amorphous materials as strong or fragile and can be calculated using the following expressions:

$$m = \frac{\Delta E_{T_g}}{(\ln 10)RT_g}$$

<div align="right">**Equation 6.7**</div>

where, ΔE_{Tg} is the activation energy for structural relaxation at temperatures around T_g and *R* is the gas constant (Wang et al., 2002; Crowley and Zografi, 2001).

$$D = \frac{\ln(10)\, m_{min}^2}{m - m_{min}}$$

<div align="right">**Equation 6.8**</div>

where, m_{min} is the minimum possible fragility value and has been calculated to be 16 (Mao et al., 2006; Graeser et al., 2009b).

Finally, the zero mobility temperature, T_0, (Shamblin et al., 1999), defined as the temperature where extrapolated thermodynamic properties of a supercooled liquid are equal to those of the crystal, can be expressed by the Equation 6.9,

$$T_0 = T_g \left(1 - \frac{m_{min}}{m}\right)$$

<div align="right">**Equation 6.9**</div>

6.2.2.3   Melting Point Depression (MPD)

The APIs and the polymer were passed through a combination of sieves and the fraction between 63-106 μm was used in all melting point depression experiments. PVPVA was dried over P_2O_5 for 48 h prior usage. PMs with a drug ratio of 70, 75, 80, 85, 90 and 100% w/w were prepared at least in triplicate.

The melting temperature of paroxetine HCl Form I and II in the presence and in the absence of PVPVA was measured using DSC at a scan rate of 2 ^{o}C/min. Experiments at slower heating rates of 1 and 0.1 ^{o}C/min were also performed for the PMs of Form II with PVPVA.

6.2.2.4   Preparation of Solid Dispersions

Spray drying

Spray dried solid dispersions of paroxetine HCl Form I and II with PVPVA were prepared in a 50% (w/w) drug-polymer ratio. The API and the polymer were dissolved in 200 mL mixture of methanol-water (50:50 v/v). The solutions were spray dried using a mini spray dryer B-290 (Büchi) with an aspirator flow of 100%, solution pump rate of 5.0 mL/min and an inlet temperature of 85 ^{o}C and an outlet temperature of about 50 ^{o}C.

Hot Melt Extrusion

Hot melt extruded solid dispersions were prepared using a co-rotating twin screw extruder Thermo Scientific HAAKE MiniLab II (Thermo Scientific). Each system was prepared using a total weight of 5 g, in the same drug loading as mentioned above, at a speed of 100 rpm with a residence time inside the extruder of 10 min. The extrusion temperature was 130 and 150 ^{o}C for the Form II:PVPVA and Form I:PVPVA system, respectively.

6.2.2.5   Thermal Analysis

Differential scanning calorimetry (DSC, Q1000 TA Instruments) analysis was done at different heating rates of 2, 5, 10, 20 and 50 ^{o}C/min to calculate the heating rate dependence of the T_g of Form I. Values for Form II were calculated in Chapter 5. A heating rate (HR) of 10 ^{o}C/min was used for the stability studies, from -10 to 160 ^{o}C.

Form I was analysed in hermetic pans while Form II was analysed in pinhole pans; all the stability studies were performed using hermetically sealed pans.

Modulated temperature DSC (MTDSC, Q1000 TA Instruments) analysis was performed with a HR of 2 ^{o}C/min (modulation of ± 0.318 ^{o}C every 60 seconds) in pinhole pans for the characterisation of the freshly prepared solid dispersions.

Thermogravimetric analysis (TGA, Hi-Res 2950 TA Instruments) was used to measure the water content of the raw materials and solid dispersion formulations. Samples were kept isothermal at 110 ^{o}C for 30 min. The determination of the degradation temperatures (T_{deg}) of the raw materials was conducted at 10 ^{o}C/min from room temperature to 300 ^{o}C. Aluminium open pans were used in both measurements.

6.2.2.6 X-Ray Powder Diffraction (XRPD)

XRPD (Thermo-ARL Xtra, Thermo Scientific) spectra were collected from 5.0^o to 40.0^o at 2θ. Extrudates were scanned in powder form after gentle grinding with a mortar and pestle.

6.2.2.7 Attenuated Total Reflection-Fourier Transform Infrared (ATR-FTIR)

The infrared spectra of the samples were collected using a Bruker IFS 66/S (Bruker Optics Ltd.), spectrophotometer, with 64 scans being acquired for each sample from 4000 cm^{-1} to 550 cm^{-1} with a resolution of 2 cm^{-1}. Extrudates were pre-milled by mortar and pestle before the tests.

6.2.2.8 Dynamic Vapour Sorption (DVS)

DVS (Q5000 SA, TA Instruments) was used to study the water uptake behaviour of all solid dispersions formulations immediately after preparation and without any pre-treatment of the samples. Isothermal (25 ^{o}C) and isohumic (98% RH) conditions were used for a period of 16 h.

6.2.2.9   Dissolution Studies

The drug content of each formulation was assayed spectrophotometrically (Lambda XLS UV/VIS, Perkin-Elmer) at 293 nm. Samples were dissolved in methanol and suitable diluted with the same solvent.

Dissolution studies were performed in 900 mL of 0.1 M HCl at 37.0 ± 0.5 $^{\circ}$C, with a rotation speed of 50 rpm using the BP paddle method. Sixty milligrams (60 mg) of each sample within 63-106 μm particle size, were used. At predetermined intervals, 10 mL of solution was withdrawn and filtered through a 0.45 μm filter. Subsequently, the filtrate was analysed spectrophotometrically at 293 nm. All the dissolution experiments were done under sink conditions (see Chapter 5).

To compare the dissolution performances between the SD and HME systems a similarity factor (f_2) was used. This is an independent model that measures the similarity in percentage between two dissolution profiles (FDA, 1997). The similarity factor (f_2) is a logarithmic reciprocal square root transformation of the square error, which can be expressed by Equation 6.10,

$$f_2 = 50 \times \log\left\{\left[1 + \left(\frac{1}{n}\right) \times \sum_{t=1}^{n} (R_t - T_t)^2\right]^{-0.5} \times 100\right\}$$

Equation 6.10

where n is the number of time points, R_t is the percentage of drug release of a reference batch at the time t and T_t is the percentage of drug release of the comparison batch at time t. When f_2 is greater than 50 (i.e. 50-100), this indicates the sameness or equivalence of the both compared profiles. Conversely, when f_2 is less than 50 then it is taken as which both the profiles are different. In this study, the similarity factor was used to assess differences in the dissolution profiles of SD and HME samples acquired over the first 20 min, since the dissimilarities were more evident in the beginning of the test.

6.2.2.10   Physical Stability

The stability of the formulations was assessed over time under the effect of humidity. The samples were stored in desiccators under 53% RH and 75% RH at 25 $^{\circ}$C for 4 months. The humidity environments were obtained by using saturated salt solutions of magnesium nitrate (53% RH) and sodium chloride (75% RH). Sampling at different time points and respective characterisation was done for each system using DSC, TGA, FTIR and XRPD techniques.

6.3   Results and Discussion

6.3.1   Characterisation of Paroxetine HCl as a Glass Former

Figure 6.1 presents the scanning rate dependence of the T_g, where ln (q) (q is heating or cooling rate) is plotted against the temperature. From the slope of the curve, the glass formed from Form II showed higher activation energy of structural relaxation at T_g, ΔE_{Tg}, compared to the Form I. This fact is associated with a fragile glass nature and it is an indication that the two forms of paroxetine HCl differ in their theoretical stability/ability as glass formers (Angell, 1991). Table 6.1 presents the measured T_g (obtained from a heat-cool-heat cycle of the crystalline materials) and the calculated parameters for fragility index, m, strength parameter, D, and the temperature at which the stability is maximum, T_0. Considering the theoretical descriptions in Chapter 5, Form I is classified as a strong glass former ($m < 75$, $D > 10$ and higher value of T_0) and Form II as a fragile glass. These results can suggest greater stability of amorphous materials prepared from Form I when compared to those obtained from Form II; this was critically assessed through this study.
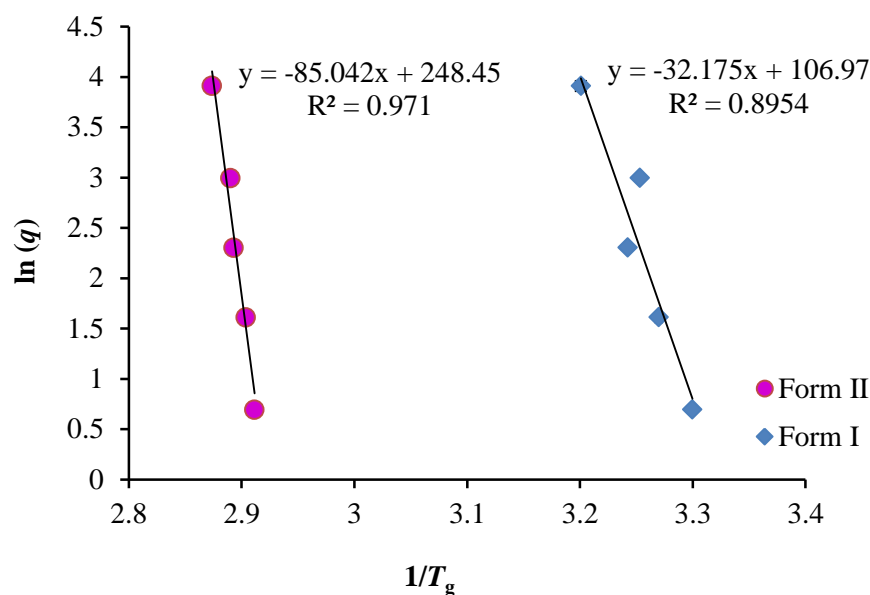
Figure 6.1: Heating rate dependence of the T_g for paroxetine Forms I and II (measurements were performed at least in triplicate).

Table 6.1: Kinetic parameters obtained from the heating rate dependence of the T_g for the two pseudopolymorphic forms of paroxetine HCl.

API/Parameter	$T_g \pm$ s.d. (^{o}C)	m	D	T_0 (^{o}C)
Form I	31.9 ± 1.8	46.1	19.6	75.3
Form II	71.1 ± 0.6	107.3	6.5	19.7

6.3.2 Estimation of Drug-Polymer Miscibility

The miscibility properties between drug-polymer systems have been claimed to be an important aspect to account when dealing with solid dispersion formulations. The term miscibility is used to refer to the formation of a single phase amorphous system through liquid-liquid mixing. As previously described, the Flory-Huggins (FH) lattice theory provides a useful tool for describing drug-polymer systems since this theory takes into account the large size discrepancy between the two components. Based on this, it is

possible to estimate the FH interaction parameter, χ, and the Gibbs free energy of mixing (ΔG_{mix}).

The FH interaction parameter was calculated using melting point depression approach (MPD) with the relationship shown by Equation 6.4. Physical mixtures between each API and PVPVA were prepared in drug rich compositions (70-90% w/w drug loading) and the onset melting temperature was measured.

Figure 6.2 presents the changes in the melting point of each API, at different drug loadings in the presence of PVPVA when compared to the melting temperature of the pure drug, ΔT_m.
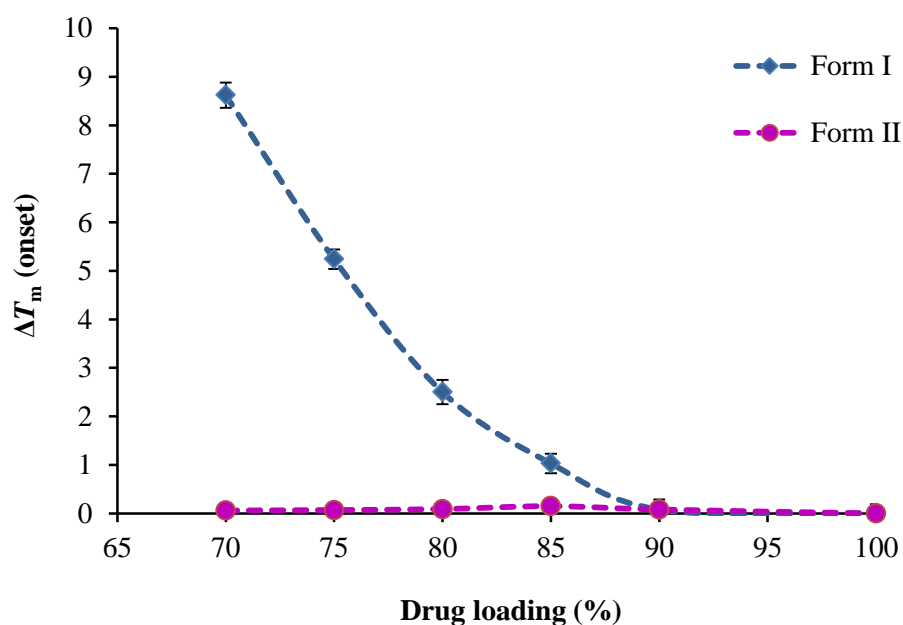
Figure 6.2: Changes in the onset melting point of paroxetine HCl Form I and Form II in the presence of PVPVA, as a function of drug loading.

Form I showed a depression of the onset melting temperature in presence of PVPVA, which indicates a degree of mixing at the melting temperature. The onset of the melting point of paroxetine HCl Form I decreased with the increase of polymer fraction, as expected. For low drug content (70 and 75% w/w) the accurate determination of the onset melting temperature can be difficult due to the broadening of the fusion peak. In contrast, the melting point of Form II remained totally unchanged in the presence of the polymer.

The first attempt to explain this observation was the small temperature interval between the T_g of PVPVA ($\approx$ 105 ^{o}C) and the melting point of Form II (117 ^{o}C). As a result, a proper drug-polymer mixing might not be achieved when a heating rate of 2 ^{o}C/min was used, since it is well-known that melting point depression is heating-rate dependent (Nishi and Wang, 1975; Marsac et al., 2006). Therefore, slower heating rates of 1 and 0.1 ^{o}C/min were used in order to induce a complete molecular mixing. The results are presented in Figure 6.3 and confirmed that even at slower heating rates (0.1 ^{o}C/min) the onset melting temperature of Form II remained unchanged. These findings allowed to conclude that according to melting point depression experiments, the system Form II:PVPVA is immiscible at temperatures close to the melting.
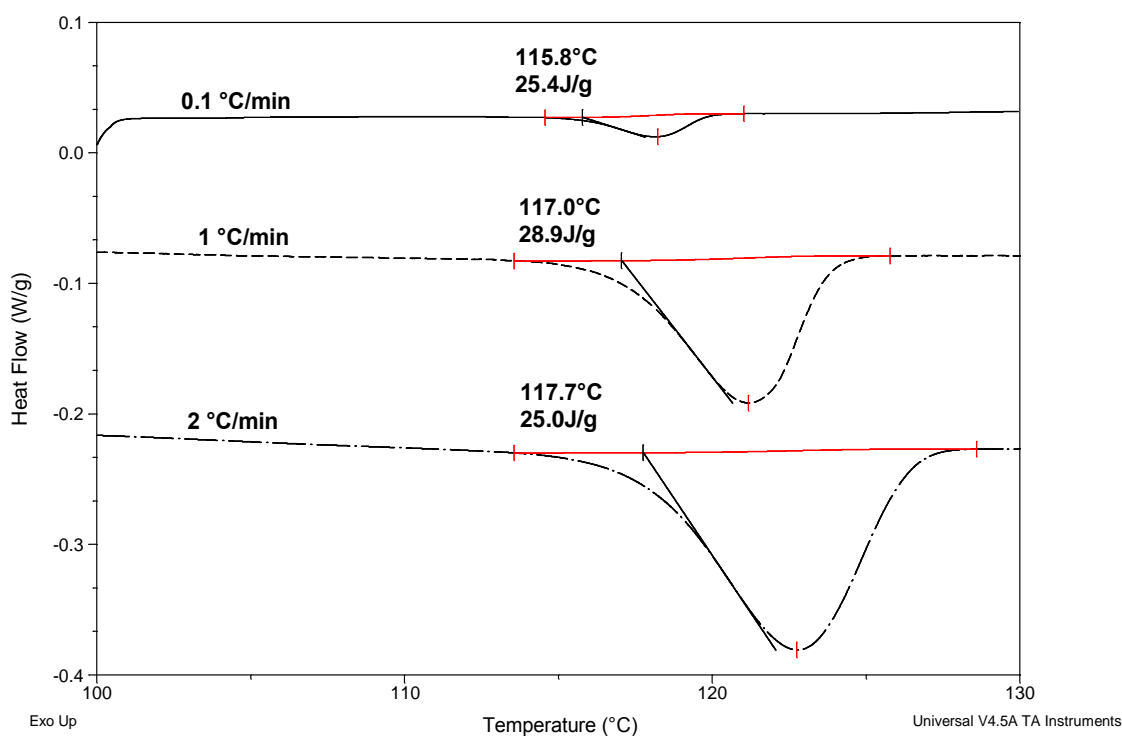
Figure 6.3: Influence of the heating rate on the onset melting point of paroxetine Form II when physically mixed with PVPVA in a 50:50 w/w ratio.

This is an interesting point to further investigate by using molecular modelling dynamics, since the difference between the two pseudopolymorphic forms is the arrangement and hydrogen bonding between the water molecules and the crystalline structure. This

approach has already revealed to be a powerful technique for predicting the miscibility of indomethacin in different carriers (Gupta et al., 2011).

Figure 6.4 shows the relationship between the melting point temperatures of each API as a function of the volume fraction of PVPVA; the FH interaction parameter can be obtained from the slope of the linear-fitted curves. The system paroxetine HCl Form I:PVPVA presents a good correlation (R^2 = 0.998) and a negative value of χ (-3.57) indicating a tendency for interaction between the drug and the polymer. On the other hand, paroxetine HCl Form II:PVPVA system shows surprisingly also a negative value of χ (-1.52) despite the fact that no melting depression was observed when this form was heated with PVPVA (Figure 6.2 and Figure 6.3) suggesting at first an immiscible system. This will need to be confronted with the subsequent experimental results.
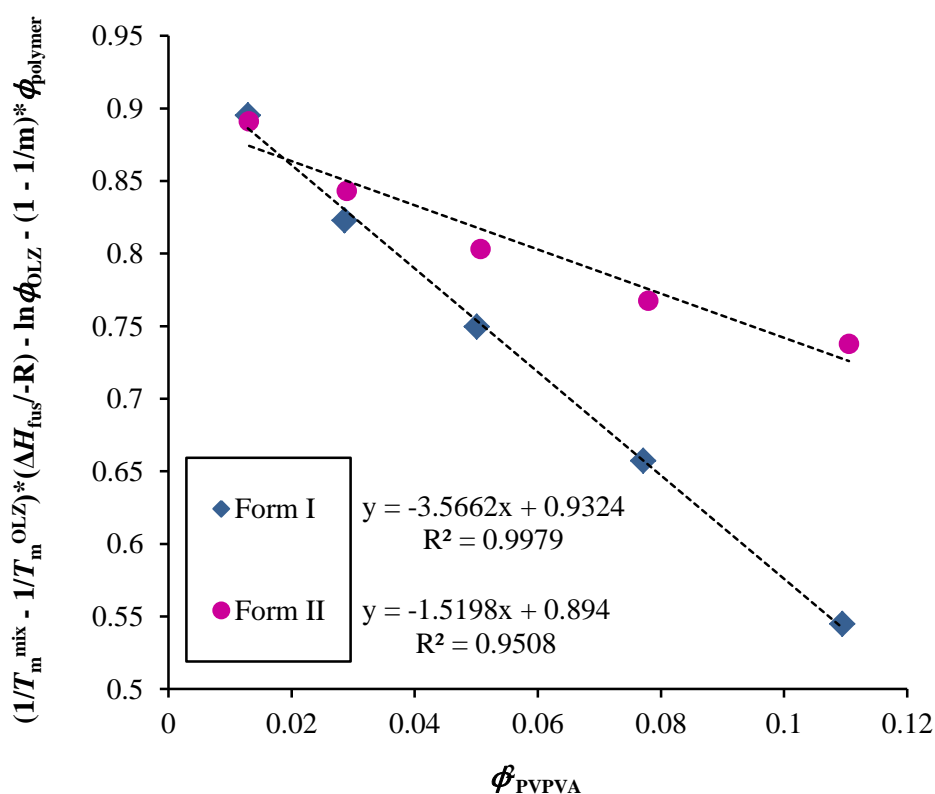
Figure 6.4: Melting point depression results for the paroxetine HCl, Forms I and II, with PVPVA. Slope of each curve included for subsequent calculation of the Flory-Huggins interaction parameter (χ).

Figure 6.5 shows the changes in the Gibbs free energy for the two systems here being studied. It is possible to observe that both systems have a ΔG_{mix} lower than zero, though lower for the Form I:PVPVA composition, as it would be predicted from the more negative value of the χ when compared to the Form II:PVPVA.

According to Equation 6.6, a favourable (exothermic) mixing between drug-polymer is obtained when the interaction parameter has a negative value and therefore $\Delta G_{mix} < 0$. As entropy always favours mixing, combined with enthalpy having an unfavourable contribution, ΔG_{mix} can still have a negative value even for athermal events ($\chi = 0$). Beyond positive values of χ, mixing is endothermic and $\Delta G_{mix} > 0$ at various compositions (Paudel et al., 2010).
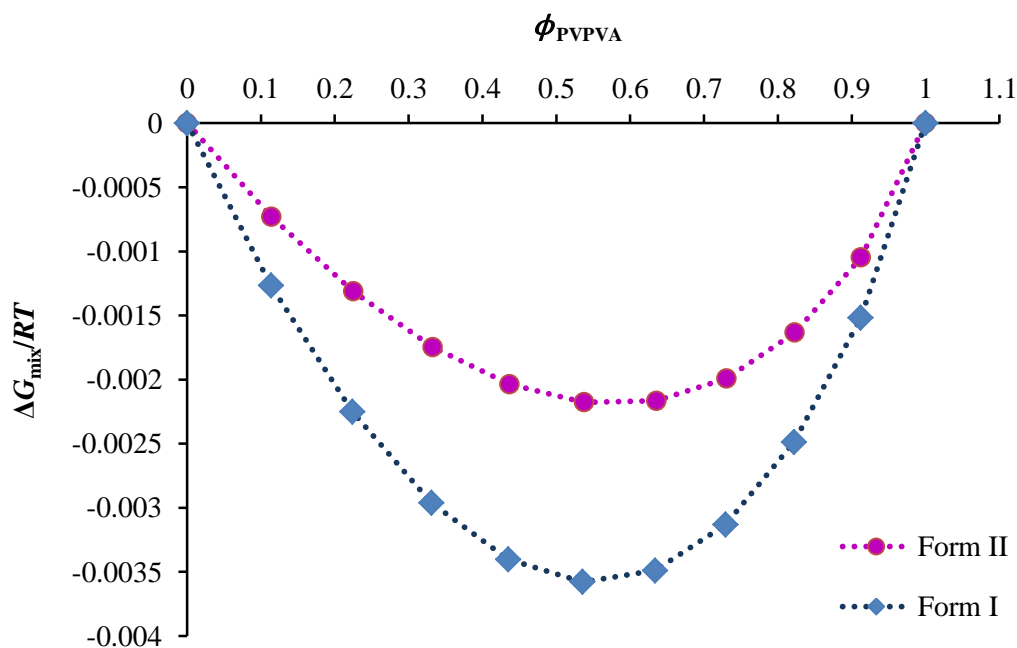
Figure 6.5: Gibbs free energy of mixing (ΔG_{mix}) versus polymer volume fraction (ϕ_{PVPVA}) for Form II:PVPVA and Form I:PVPVA.

6.3.3   Thermal Characterisation of the Raw Materials

The first aspect to take into account and requiring a careful evaluation when dealing with solid dispersion systems is related to the physical properties of the raw materials.

Therefore, properties such as melting, glass transition and degradation temperatures of each API and PVPVA were determined in the first instance and are presented in Table 6.2.

The melting temperature of the two forms of paroxetine HCl differs of about 20 ^{o}C and therefore different extrusion temperatures were used to enable a better mixing via liquid-state phase between drug and polymer prior extrusion. The degradation temperature (T_{deg}), was calculated by using TGA as the extrapolated onset temperature that denotes the temperature at which the weight loss begins. T_{deg} was found to be higher than 250 ^{o}C for all the materials, which allowed an extrusion temperature of 10 ^{o}C higher than the melting point of each API. In terms of the water content, drugs are hydrates under normal ambient conditions hence contain a relatively high level of water while PVPVA, due to its slightly hygroscopic behaviour, also showed a relatively high water content. As further presented in this work, the presence of water in these solid dispersions systems has a strong effect on their physical properties.

Table 6.2: Thermal properties of the raw materials.

Material	$T_{m\ onset} \pm$ s.d. (^{o}C)	$T_{g} \pm$ s.d. (^{o}C)	$T_{deg} \pm$ s.d. (^{o}C)	Water content $\pm$ s.d. (%)
Paroxetine HCl Form I	142.0 ± 0.2	$31.9 \pm 1.8^{*}$	264.6 ± 4.0	2.59 ± 0.04
Paroxetine HCl Form II	117.5 ± 0.4	$71.1 \pm 0.6^{*}$	269.7 ± 3.9	4.45 ± 0.26
PVPVA	n.a.	105.6 ± 1.4	283.3 ± 1.0	3.51 ± 1.20

$^{*}T_{g}$ value obtained from heat-cool-heat cycle inside the DSC at 2 ^{o}C/min.
n.a. – not applicable

The values of T_{g} (-135.0 ^{o}C) and ΔC_{p} (1.94 J/g ^{o}C) for water, needed for the calculation of T_{gmix} using Gordon-Taylor/Couchman-Karasz Equation (Equation 6.1 and Equation 6.2), were taken from literature (Hallbrucker et al., 1989).

6.3.4   Characterisation of the Freshly Prepared Solid Dispersion Systems

6.3.4.1   Thermal Characterisation

After preparation, all solid dispersion systems were immediately characterised. An important aspect to recall and correlate to the experimental results obtained is related to the previous studies on the miscibility between each API and PVPVA. From the MPD approach, Form I showed to be miscible with the polymer at a temperature near to the melting point of the drug. On the other hand, Form II showed to be completely immiscible with PVPVA, even at heating rate of 0.1 ^{o}C/min, although the calculations of the FH interaction parameter gave a negative result suggesting, somehow, a certain miscibility extent for this system. Therefore, it is important to link those predictions with the actual results and infer on the validity of the MPD approach in these systems.

Figure 6.6 shows the results for the Form II:PVPVA systems prepared by HME and SD. As it is possible to observe, both techniques were able to produce fully amorphous systems without any evidence of phase separation (two individual glass transitions), recrystallisation or melting of the drug. However, a marked difference was detected in their glass transition temperatures with the spray dried sample having a higher T_g value when compared with the melt extruded sample. In addition, an evident broad water loss signal (corresponding to a weight loss of 4.29 ± 0.32% w/w in TGA), between 20-60 ^{o}C was noticed in the total heat flow of the spray dried formulation, contrarily to the HME system, even though pinhole pans were used for both samples.
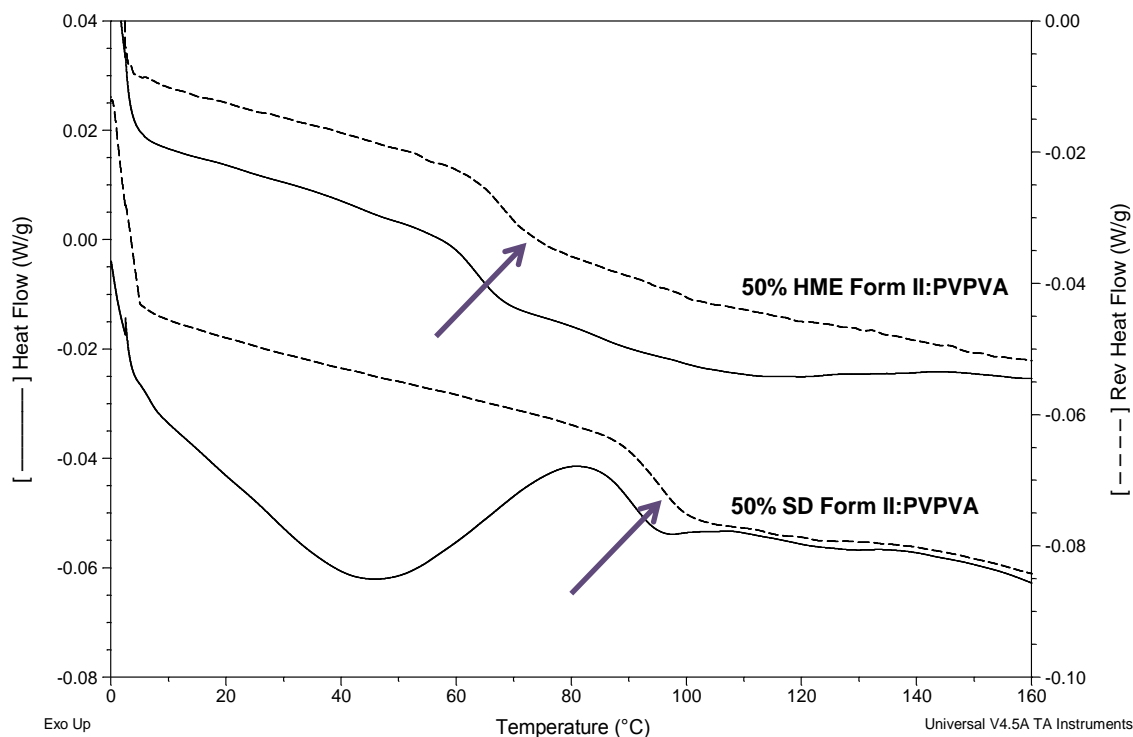
Figure 6.6: MTDSC analysis of 50% HME and SD of Form II:PVPVA in pinhole pans.
Note that the extrudates were analysed without any preliminary treatment (non-milled).

In fact, the most obvious indication of the miscibility between two components is the presence of a single glass transition temperature, already described as T_{gmix}. In this particular case, it is essential to take into account the contribution of water and include it in the calculations of the theoretical T_{gmix}. Therefore, T_{gmix} for a ternary system of Form II/PVPVA/water, based on Equation 6.1, was calculated to be about 55 ^{o}C, which is in agreement with the value obtained for the non-milled HME sample (61.0 ^{o}C). However, the T_{g} measured for the spray dried Form II:PVPVA system had a much higher value (95.9 ^{o}C). These results could, in the first instance, indicate miscibility issues between the drug and the polymer, as previously suggested by melting point depression approach for this particular system and only evident in the case of the HME sample, due to the absence of any miscibility promoter, such as a solvent. However, a simpler explanation is obtained if the effect of trapped water inside the HME samples is considered.

Considering that the HME sample was analysed as it was obtained after extrusion, compact extrudates in a cylindrical shape, which largely reduces the ability for the water to evaporate when compared with the microparticles obtained from SD, differences in their

thermal response when heated in DSC are predicted. Clearly, the T_g obtained for the spray dried sample corresponds to the 'dry' T_g whereas for the HME system, the T_g was depressed by the presence of trapped water. To further study the influence of the water in the thermal behaviour of the HME samples, the extrudates were milled (particle size between 63-106 μm) and analysed in the same conditions. This has allowed the water to freely evaporate during the heating cycle in DSC in a comparable manner to what happened with the SD sample. As expected and shown in Figure 6.7, the behaviour of the milled extrudates, in terms of both T_g value (93.3 ^{o}C) and water loss profile, are now identical to the spray dried sample.
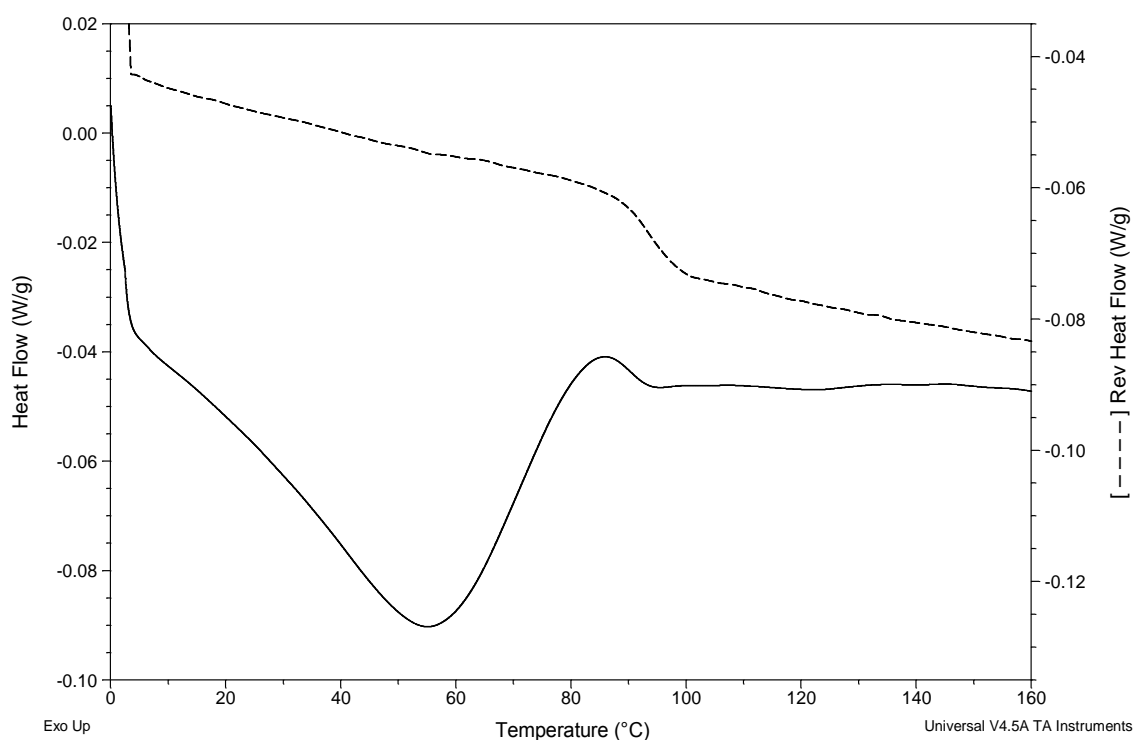
**Figure 6.7: MTDSC traces of 50% HME Form II:PVPVA after milling
and control of the particle size (63-106 µm) in pinhole pans.**

Figure 6.8 below shows the thermograms obtained for the solid dispersions of 50% Form I:PVPVA prepared via HME and SD. Molecular level mixing is recognised by the presence of one single mixed phase T_g without any other thermal event being detected. The thermal behaviour of this system was closely similar to the one observed for the

Form II:PVPVA system. More specifically, the water plasticisation effect on the non-milled HME samples was observed when compared to the milled HME (data not shown) or SD samples. However, the measured T_g for the non-milled HME sample (74.6 ^{o}C) showed a positive deviation from the predicted T_{gmix} (42.6 ^{o}C).
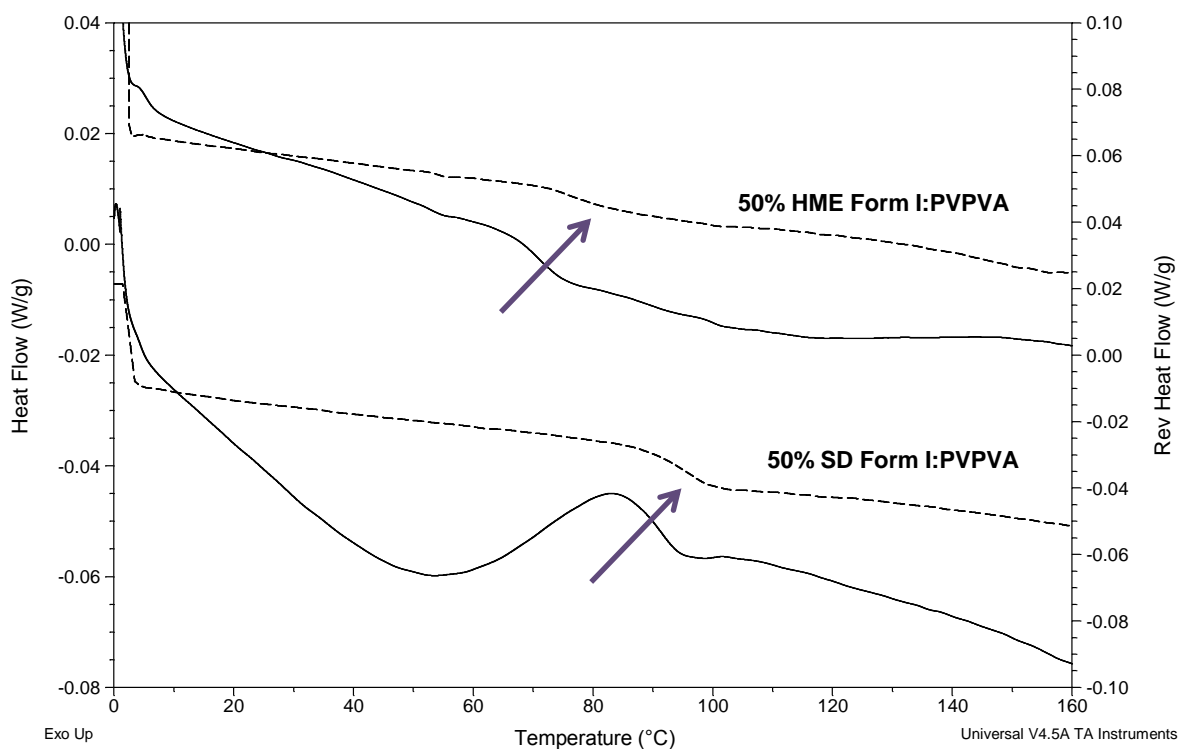
Figure 6.8: MTDSC analysis of the solid dispersions of 50% Form I:PVPVA prepared by HME (non-milled) and SD. Analyses were done in pinhole pans.

Deviations of experimental T_g values for solid dispersions from those predicted by the GT are often explained by considering the nature of the interactions between the two components (Lu and Zografi, 1998). This fact can be supported by the melting depression observed for Form I when physically mixed with PVPVA, indicating some degree of interaction.

All the T_g values were measured in the reversing heat flow signal and are presented in Table 6.3 for clarity. TGA measurements of the water content in non-milled and milled extrudates are also presented. The milled samples showed a higher water content value (nearly double) compared to the non-milled ones, as it would be expected since the water

can be released easier. This fact also supports the results observed in DSC. For the spray dried products, the water content was considerably higher for the Form II system in comparison with the Form I formulation, which will have influence in the FTIR results, as it will be shown later.

Table 6.3: Measurements of T_g, ΔC_p and moisture content obtained by MTDSC and TGA, respectively, for the milled and non-milled HME and SD samples.

System	Non-milled			Milled		
	DSC		TGA	DSC		TGA
	$T_g \pm$ s.d. (^{o}C)	$\Delta C_p \pm$ s.d. (J/g ^{o}C)	Water loss $\pm$ s.d. (%)	$T_g \pm$ s.d. (^{o}C)	$\Delta C_p \pm$ s.d. (J/g ^{o}C)	Water loss $\pm$ s.d. (%)
50% HME Form I:PVPVA	74.6 ± 1.4	0.18 ± 0.03	1.52 ± 0.40	95.9 ± 0.3	0.36 ± 0.05	2.50 ± 0.16
50% HME Form II:PVPVA	61.0 ± 4.9	0.25 ± 0.03	1.47 ± 0.19	93.3 ± 0.6	0.38 ± 0.04	2.57 ± 0.27
50% SD Form I:PVPVA	97.2 ± 0.2	0.34 ± 0.06	2.62 ± 0.20	n.a.	n.a.	n.a.
50% SD Form II:PVPVA	95.9 ± 0.8	0.34 ± 0.02	4.29 ± 0.32	n.a.	n.a.	n.a.

n.a. – not applicable

6.3.4.2   Structural Characterisation of the Solid Dispersion Systems

The DSC findings outlined above were supported by XRPD studies which revealed that all the formulations prepared via HME and SD were amorphous with a characteristic halo pattern (data not shown).

ATR-FTIR was used to study intermolecular interactions between APIs and PVPVA. The spectra of crystalline drug substances, polymer and drug-polymer PMs were compared with the spectra of the hot melt extrudates and spray dried products, as shown in Figure 6.9 and Figure 6.10, respectively.

Paroxetine HCl Forms I and II are easily distinguished by a double or two single bands at high wavenumber, respectively. These bands are assigned to the stretching vibration of the O-H groups in different environments (Chapter 3).

The spectrum of PVPVA has two main bands corresponding to stretching of the carbonyl groups that are proton acceptors and are usually affected by hydrogen bonding: 1673 cm^{-1} (from the amide group) and at 1732 cm^{-1} (from the ester group). The N-H groups from the APIs, are proton donating groups and also participate in intermolecular interactions, although in this case its stretching vibration overlap in complex area of the spectra with the aromatic ring vibrations and hence are not considered here as a means of evaluating any drug-polymer interaction.
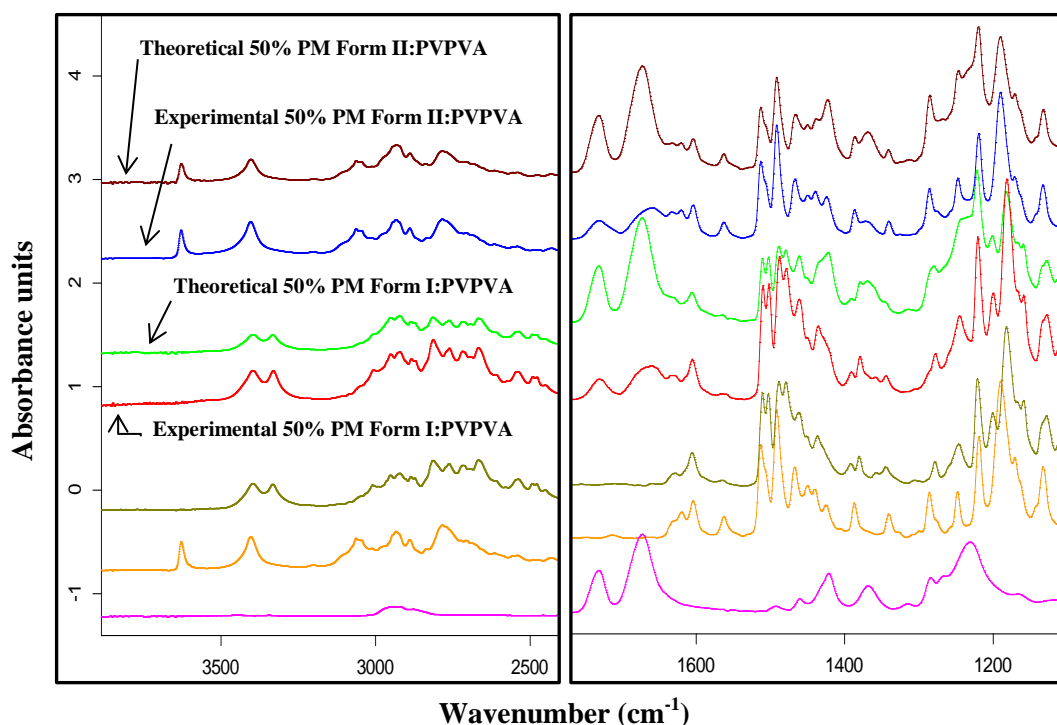
Figure 6.9: ATR-FTIR spectra of PVPVA, pure crystalline paroxetine HCl Form II and Form I (upwards) and respective PMs (theoretical and experimental).

In theory, a 50:50 w/w PM between each API and PVPVA would be expected to result in a combination of the FTIR spectrum of the individual components. However, by comparing the predicted spectra with the one obtained experimentally an evident difference in the main region of PVPVA was observed. The two main bands previously referred (1673 and 1732 cm^{-1}) became broader and significantly reduced in intensity, which was identical in both Form I and Form II systems. A reasonable explanation for this feature is probably related to the high water content of the individual raw materials. In fact, the interaction between water and hydrophilic polymers, such as PVP and PVPVA, was described to influence not only the position of the C=O but also its shape (Weuts et al., 2004).

In the case of the FTIR spectra for the freshly prepared solid dispersions (Figure 6.10) it is clear that the O-H stretching vibrations associated with the isolated APIs (located at a high wavenumber) disappeared and meanwhile a broad band at around 3400 cm^{-1} was identified in all the solid dispersions. This is an indication of the formation of an amorphous phase between the drug and polymer, which was also supported by the broadening of the peaks in the whole spectra. Additionally, the position of the C=O stretch vibration corresponding to the ester function of the polymer is practically unchanged, whereas the band corresponding to the C=O stretch of the amide function showed a shift towards lower wavenumbers. This is due to the different basic nature of the two groups, being the C=O of the pyrrolidone group a stronger proton acceptor as compared to the C=O of the vinyl-acetate (Shamblin et al., 1998).
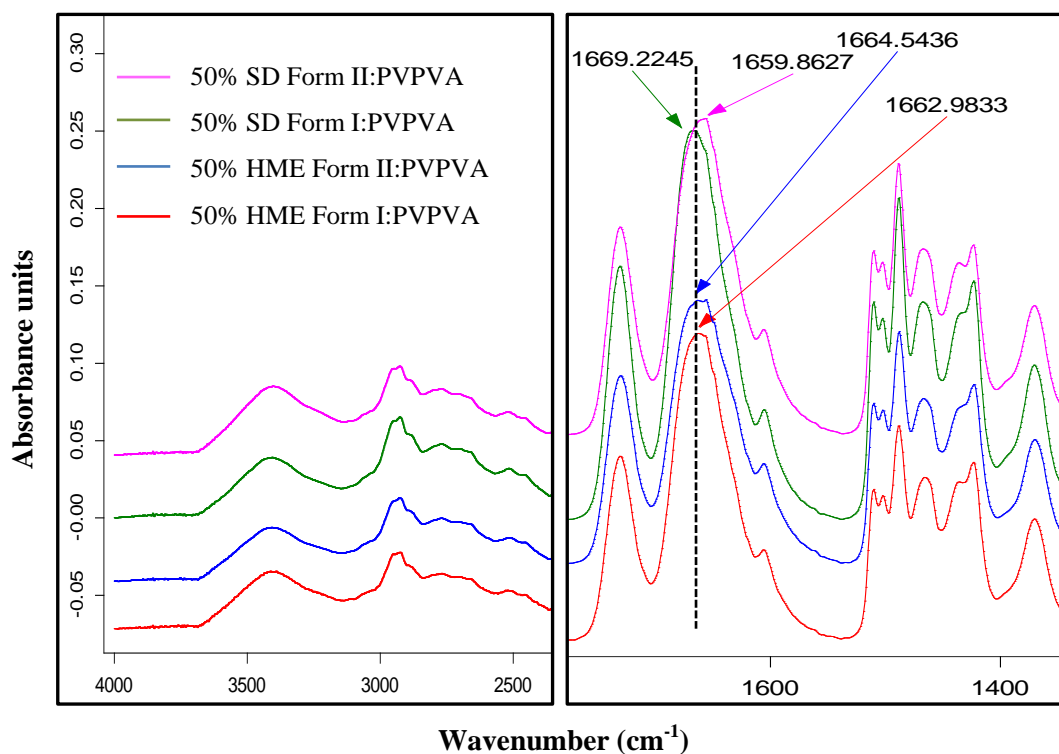
Figure 6.10: FTIR spectra of the freshly HME and SD solid dispersions of paroxetine HCl Form I and Form II with PVPVA.

In general for a group participating in a hydrogen bond, a shift to lower wavenumbers indicates a stronger bond while a shift to higher wavenumbers indicates the formation of a bond that is weaker than the original bond present in the pure phase (Trasi and Taylor, 2012). In this study, the downshift of the C=O peak from the amide group cannot be directly correlated to any significant hydrogen bonded interaction. Firstly, as it was already mentioned, the N-H band from either Forms I and II that could act as a proton donor is difficult to identify on the individual spectra and therefore changes cannot be tracked within the solid dispersed systems. Secondly, it is important to consider the influence of water. Matching the water content measured by TGA for each fresh solid dispersion formulation, presented in Table 6.3, the system 50% SD Form II:PVPVA showing the higher shift (from 1673 for pure PVPVA to 1659 cm^{-1}) has also higher moisture content (4.29 ± 0.32% w/w). In contrast, both HME systems (considering the water content measured in milled extrudates) and the spray dried Form I:PVPVA, have nearly half moisture content (≈ 2.6%) when compared to the spray dried Form II, which matches the smaller shifts observed in FTIR.

6.3.4.3   Moisture Uptake Studies

In the previous section, the effect of trapped water inside the extrudates was discussed and showed to have a great influence on the measured T_g when compared to the spray dried samples. Indeed, the presence of water lowers the T_g of amorphous systems and therefore increases the molecular mobility, which can also alter the chemical and physical stability of amorphous solid dispersions.

The moisture uptake capabilities of all systems were tested using DVS isohumic and isothermal tests (the DVS sample chamber was kept at a constant humidity and temperature during the tested period) at 98% RH/25 ^{o}C for a period of 16 h, when a constant weight for all the systems was achieved. This provides a rapid insight on the hygroscopic behaviour and water uptake rates of each system since an extremely high water vapour was used, which gives some insights prior the stability tests being performed. The results are presented in Figure 6.11 and as expected, the spray dried products absorbed water at higher rate when compared to the HME ones, which were tested in its rod-shape, as milling could increase molecular mobility and give misleading results when submitted to high RH environments. After nearly 3 h of testing both SD samples and HME Form II:PVPVA showed a similar increase in weight nearly 40% w/w whereas HME Form I:PVPVA showed a slightly lower absorption of nearly 32% w/w. However, in the end of the experiments (after 16 h) all systems showed a similar water uptake ($\approx$ 45% w/w).
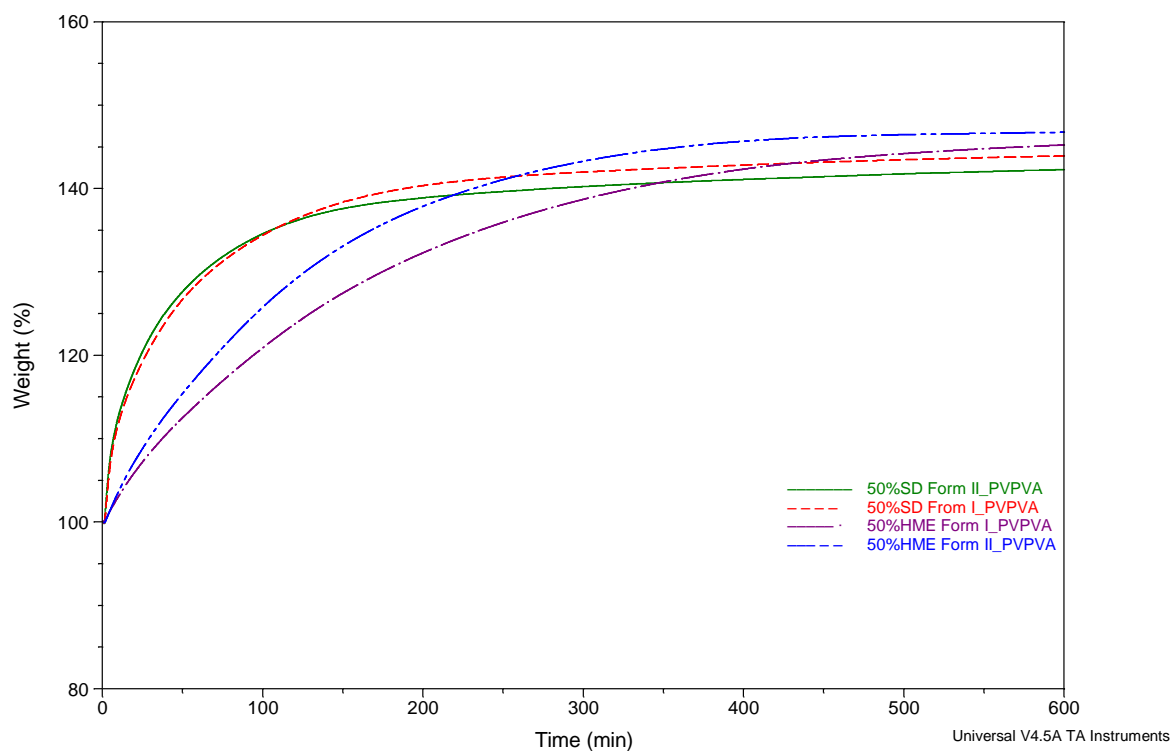
**Figure 6.11: DVS results of the freshly prepared HME and SD systems
kept under 98% RH/25 °C for a period of 16 h.**

Another important information that can be exploit from DVS experiments is related to the crystallisation of amorphous materials when exposed to changes in humidity. Amorphous samples are described to absorb large amounts of water and as they crystallise the water is expelled and a weight loss is observed (Grisedale et al.). In this study none of the products showed a decrease in weight during the experimental time in DVS suggesting a great stability of these systems, which will be further studied during the storage stability.

6.3.4.4   Dissolution Studies

The drug content was determined spectrophotometrically, as described in the Methods section, and was within the range 98.4–101.6% for all the systems prepared.

It is well-known that the dissolution behaviour of pharmaceutical drugs is a complex process and depends on several factors such as particle size, surface area, degree of

crystallinity and solvation state of the drug. Also, some examples can be scattered from the literature showing the influence of the preparative techniques on the dissolution process of amorphous solids (Patterson et al., 2007; Dong et al., 2008; Mura et al., 1999c; Mura et al., 1999a; Karmwar et al., 2012).

In this section the dissolution profiles of each solid dispersion system prepared via HME and SD were investigated and compared with the pure crystalline drugs and binary mixtures with PVPVA. Sink conditions were used and the particle size was controlled for all the experiments (63-106 μm).
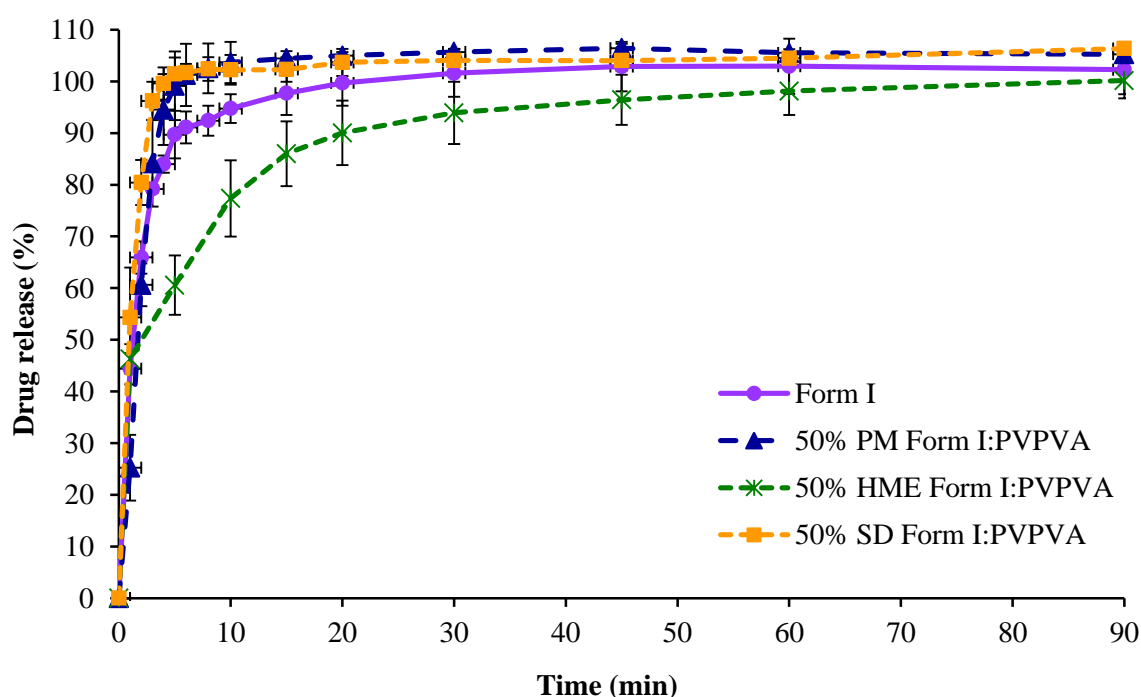
Figure 6.12: Dissolution profiles of pure paroxetine HCl Form I, binary mixture with PVPVA and respective solid dispersions prepared by SD and HME.

Form I has a dissolution rate similar to the PMs and SD samples, as shown in Figure 6.12. This is not completely surprising since paroxetine HCl is described to be a slightly water soluble drug (Kasim et al., 2004). However, a lower dissolution rate was observed for the HME product. These differences in the release rates were quantitatively compared by using the magnitude of similarity factor f_2, as described in the Methods section. The SD and HME systems of Form I have a similarity factor f_2 of 29.10 suggesting

that the release profile of Form I from the SD and HME formulations were different ($f_2 < 50$). Although, SD and HME solid dispersions were prepared as fully amorphous forms, which was confirmed by DSC and XRPD, other parameters seemed to influence the dissolution of these solid dispersions systems.

A similar visual behaviour of the solid dispersions during dissolution testing was observed, with all the samples dispersing well in the media without any evidence of material floating or forming a solid plug at the bottom of the dissolution vessel. However, the diffusion coefficient of the dissolution medium into the micrometer spray dried and hot melt extrudated particles is expected to be different with a slower rate for the latter one. This fact could explain the initial slower release of the HME system in comparison with the PM and SD samples. Additionally, the slower wetting properties of the compact HME particles could contribute for these observations.
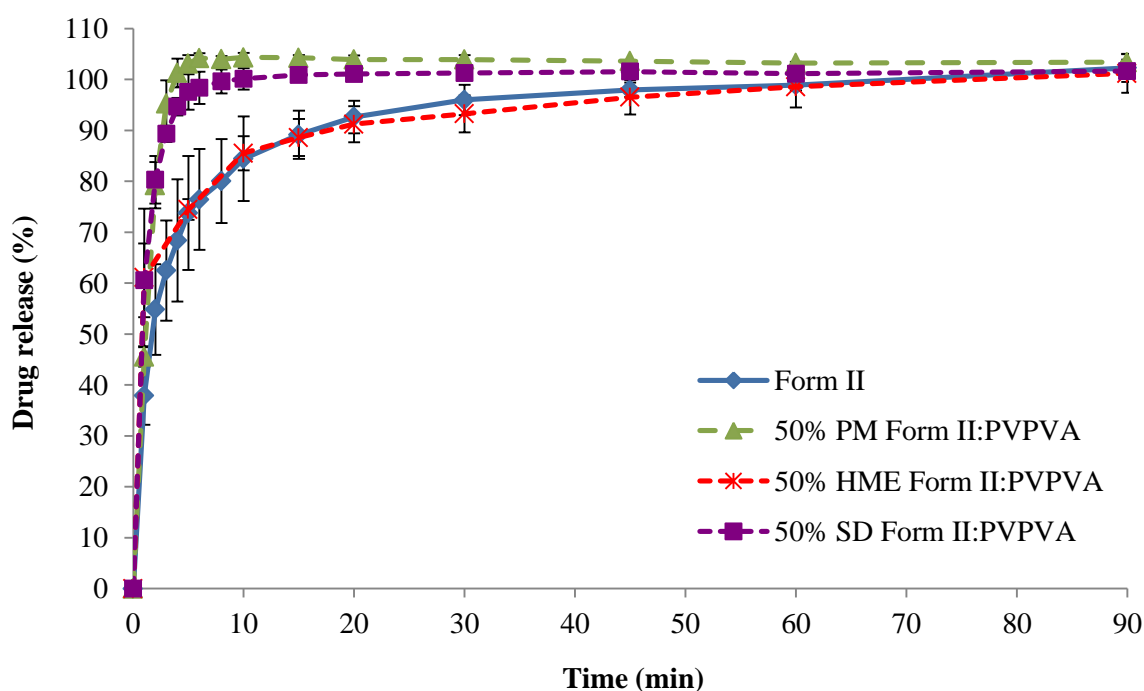
Figure 6.13: Dissolution profiles of pure paroxetine HCl Form II, binary mixture with PVPVA and respective solid dispersions prepared by SD and HME.

The SD and PMs with Form II had a similar dissolution profiles to the ones observed for Form I, though the pure crystalline Form II showed a dissolution behaviour close to the

HME sample. This might be due to the higher water content of Form II. Also the f_2 factor had a value equals to 38.09, as an indication of the different release profiles between SD and HME systems of Form II perhaps for similar reasons as exposed above.

6.3.5   Physical Stability of Solid Dispersions over Storage

In this section, the physical stability of all solid dispersion systems here being studied was evaluated. In addition, the existence of a possible relationship between the two different preparation techniques, SD and HME, used in this work and its influence on the stability of amorphous solid dispersions was also assessed. Stability studies were carried out under two different RH levels (53 and 75% RH) at room temperature ($\approx 25\ ^{\text{o}}$C), as it is well-known that humidity plays an important role in the stability of amorphous formulations. It has been extensively reported that the presence of moisture contributes not only to increase molecular mobility, which can lead to crystallisation, but at the same time promotes the tendency for phase separation to happen.

Due to the high water vapour pressure at 75% RH and high hygroscopic behaviour of amorphous formulations, all the extrudates and spray dried products stored under this environment, formed coalesced masses making certain physical analysis problematic, in particular XRPD measurements.

6.3.5.1   DSC Studies

DSC studies were performed considering two important aspects: firstly, dehydration of Form I happening during heating and therefore hermetic pans were used during stability testing; secondly, to avoid recrystallisation or dissolution of the API into the polymer during heating, a fast heating rate of 10 $^{\text{o}}$C/min was chosen.

Figure 6.14 presents the typical DSC traces for all the systems after 30 days of storage under 75% RH/25 $^{\text{o}}$C. From the plot, all the formulations showed a single thermal event

that corresponds to the melting of Form I, after confirmation by using ATR-FTIR. An important point to account is related to the initial miscibility studies, which showed that Form I was miscible with PVPVA and Form II completely immiscible. However, the analyses of the freshly prepared solid dispersions showed that both pseudopolymorphs formed a single amorphous phase with the polymer and this might be reflected in their physical stability. For the aged samples, the onset melting event detected for all the samples ranged from 95-100 ^{o}C, which is clearly lower than the melting observed when Form I was just physically mixed with PVPVA ($\approx$ 130 ^{o}C) in the same drug loading (50:50 w/w). This could be an indication that processing contributes to further increase the miscibility between the drug and the polymer, which is detected by a higher melting point depression. Nevertheless, it is also important to bear in mind that the API is a slightly water soluble drug stored at high humidity and analysed in hermetic pans, thus the combination of these factors could accelerate the dissolution of the drug in the polymer even with a heating rate of 10 ^{o}C/min.
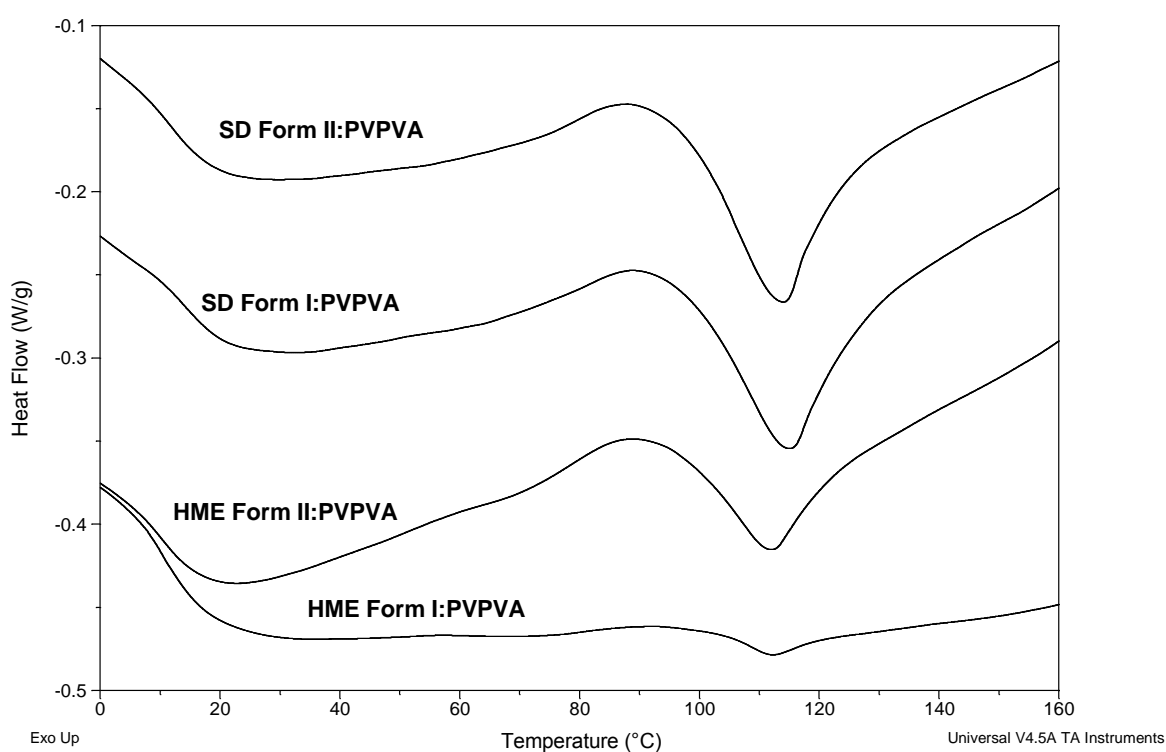
Figure 6.14: DSC curves for HME and SD systems after 30 days storage under 75% RH/25 ^{o}C and analysed in hermetic pans at 10 ^{o}C/min.

All the samples stored at 53% RH/25 $^{\circ}$C remained fully amorphous during the whole experimental time (four months), with a single T_g ranging from 29-32 $^{\circ}$C being observed.

The percentage of crystallised drug in each formulation was estimated by using the ratio between the enthalpy of fusion of the pure API (ΔH_m (0)) and enthalpy of fusion measured in the DSC for the aged systems (ΔH_m (*t*)) multiplied by the drug loading (50% w/w for all the formulations in this case) (Shah et al., 2006), as shown in Equation 6.11,

$$Recrystallisation\ (\%) = \left(\frac{\Delta H_m(t)}{\Delta H_m(0)}\right) * 0.5$$

Equation 6.11

Figure 6.15 shows the recrystallisation profiles of all formulations calculated from DSC data using Equation 6.11 during four months of storage under 75% RH/25 $^{\circ}$C. Significant differences were observed in the stability behaviour of the different systems, especially regarding the initial time point when recrystallisation was firstly detected by DSC, but also the overall profile of recrystallisation. Both spray dried products of Form I and II showed a high recrystallisation tendency, reaching its maximum amount of crystals detected after 30 days, which remained nearly constant during the remain experimental period. The sample HME Form II:PVPVA showed a continuous increase in its crystal content over time, achieving its maximum after 90-120 days.
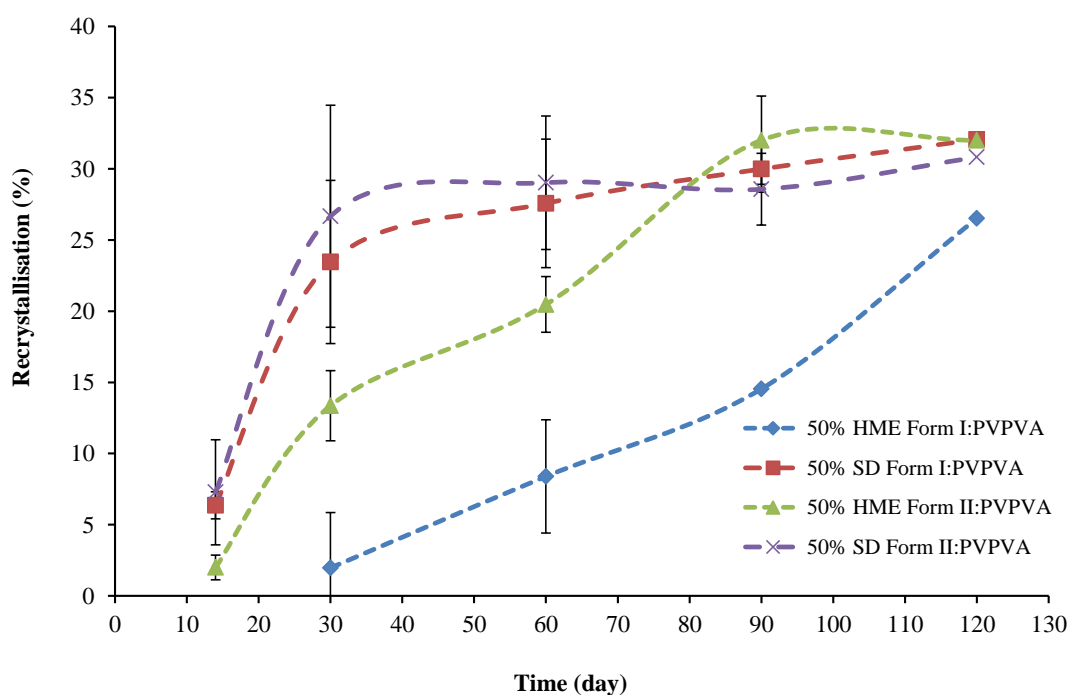
Figure 6.15: Recrystallisation profiles of the HME and SD systems stored at 75% RH/25 $^{\circ}$C.

The HME Form I:PVPVA sample showed the lower tendency for recrystallisation. Firstly, the presence of crystals started to be noticed in DSC after 30 days of storage, whereas all the other solid dispersion systems started to recrystallise after two weeks; secondly this system had a lower crystal content at each sampling point when compared to the others solid dispersions, though presenting a similar percentage of crystals by the end of the study. This fact could be correlated with the glass forming ability of the pure APIs showed in the beginning of this study. The glass material obtained from Form I was classified as a strong glass and therefore lower tendency to recrystallise compared to the obtained glass prepared from Form II that was identified as fragile glass. The fact that all the spray dried samples had a similar profile, it could be related to the higher surface area exposed to the environmental, promoting the recrystallisation to be more uniform and difficult to isolate any difference in the behaviours of Forms I and II.

6.3.5.2   TGA

The water content of each system during the experimental time was measured by using TGA. The results obtained for the samples stored under 75% RH/25 $^\circ$C are presented in Figure 6.16. All the systems showed to have a very similar water behaviour uptake when stored at these conditions, being observed a slight decrease over time, probably as an indication of API recrystallisation and therefore less hygroscopicity when compared with the amorphous state.
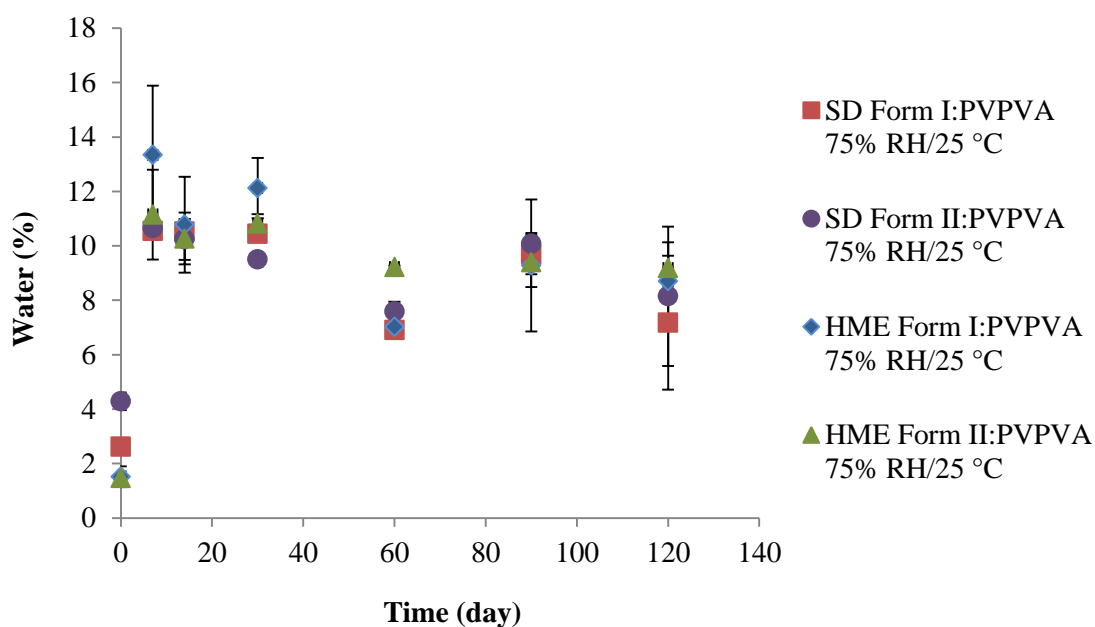
Figure 6.16: Water content of each solid dispersion system overtime stored at 75% RH/25 $^\circ$C.

All the samples stored under 53% RH/25 $^\circ$C showed a slight increase in their moisture content, varying from 6-8% for the HME samples and from 4-7% for the spray dried samples. However, these differences did not significantly influence the measured T_g of these systems when run in DSC.

6.3.5.3   ATR-FTIR

Using FTIR analysis, all the solid dispersion systems stored at a high RH were found to recrystallise to Form I. Due to the complexity of the FTIR spectra of this type of systems, the second derivative was found helpful to reveal characteristic unresolved peaks, essential to distinguish between Forms I and II. Figure 6.17 below shows the changes highlighted with arrows in the spectra of HME Form II:PVPVA system over time.
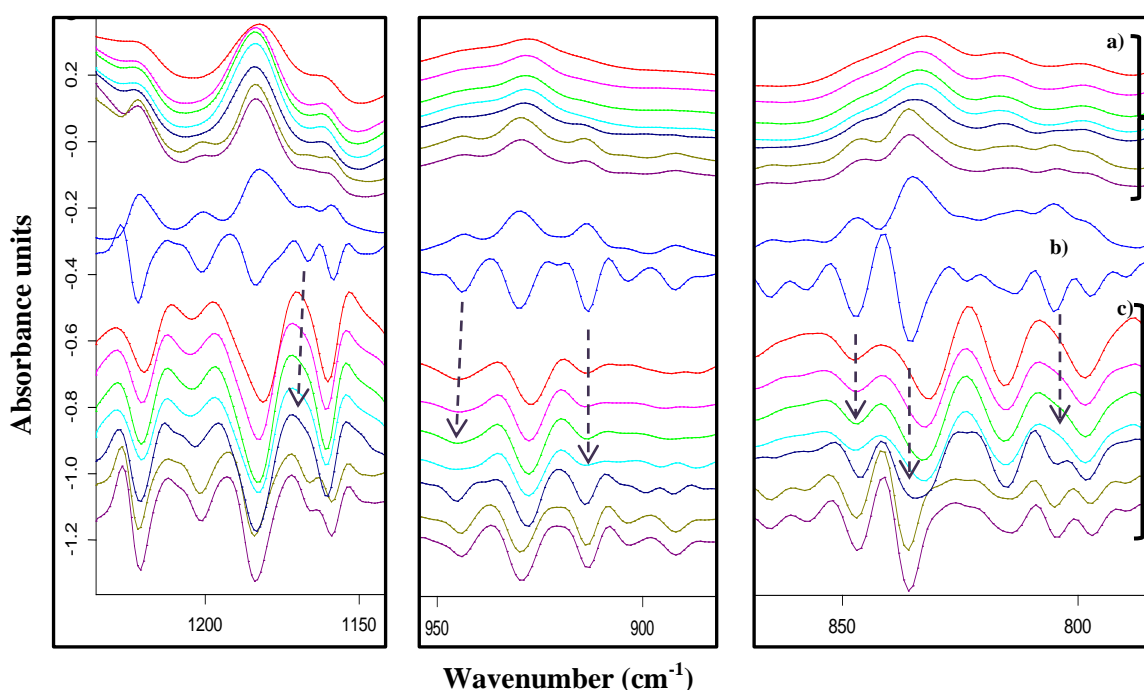
Figure 6.17: ATR-FTIR spectra of HME Form II:PVPVA (a), pure Form I and its 2nd derivative (b) and second derivative of the same system (c). Please note that each spectrum was collected at each sampling point (0, 7, 14, 30, 60, 90 and 120 days) downwards.

Spray dried samples and HME Form II:PVPVA started to show differences in their FTIR patterns after 60 days, while HME Form I:PVPVA only after 90 days. These observations do not completely agree with the DSC results, but confirmed the differences in their recrystallisation rates.

6.3.5.4   XRPD

All the samples stored under 53% RH/25 ^{o}C confirmed to be X-ray amorphous during the whole experimental time (data not shown). For the samples stored at 75% RH/25 ^{o}C, their physical state made XRPD analysis difficult, as the requirements of forming a flat lightly compressed sample surface was hard to obtain. This could also explain the delay in observing any peaks from the recrystallised API earlier. Figure 6.18 presents the diffractograms for the Forms I and II systems prepared by SD and HME after four months of storage under 75% RH/25 ^{o}C. All the X-ray traces show a poor ratio signal to noise without well-defined and sharp diffraction peaks. In addition, the presence of a halo pattern on the background of each plot indicates the presence of a reasonable amorphous content.
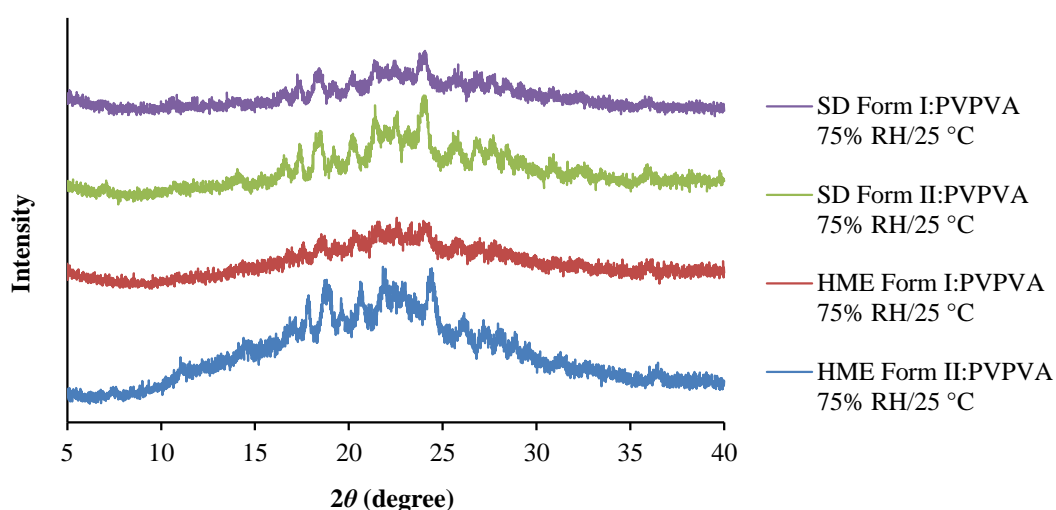
Figure 6.18: XRPD traces of SD and HME samples of Form I and Form II with PVPVA (50:50 w/w) aged at 75% RH/25 ^{o}C for four months.

The HME samples, in particular the Form I:PVPVA system, seemed to have a lower crystalline content compared to the rest of the formulations, though matching with the DSC results all the systems had a similar crystal content by the end of the study. Therefore, these observations might just be due to the sample preparation, since no difference in their physical aspect was observed between the samples stored under these conditions. By

comparing the peak lists collected for each system with the corresponding peak lists for Form I and II, all the samples recrystallised into Form I, which was also suggested by FTIR analysis and it is not surprising since Form I is the most stable form.

6.4   Conclusions

Currently, the development of solid dispersions in the industry remains largely a trial and error procedure, with the final performance and physical stability the key features to be achieved.

Several theoretical predictions have been developed over the past few years to aid the successful preparation of such systems. In this study, MPD was selected to predict the miscibility and interaction between two pseudopolymorphs, Form I and Form II, of paroxetine HCl and PVPVA. Accordingly to these predictions only paroxetine HCl Form I was miscible with the polymer. The MPD approaches for Form II, did not give any conclusive results. However experimentally, both forms were able to be molecularly dispersed within the polymer matrix, thus forming one-phase system. These results supported the limitations of the melting point depression applications and reliability on predicting the drug-polymer miscibility.

The work presented here also demonstrated that the use of different preparation techniques, HME and SD, resulted in products with different physical properties. SD produced porous particulate samples while HME yielded to denser (as a result of high intensity of mixing and pressure during extrusion) products with lower porosity. These differences can therefore influence not only the dissolution profile of the prepared system but also its physical stability under storage. Moreover, special awareness must be taken when characterising hot melt extruded systems due to the effect of trapped water that can lead to misinterpretations, namely with respect to the measured T_g. This can be particularly important when comparing with dispersions obtained in a powder form, such as spray dried systems. In this case, a gentle milling of the extrudates is recommended in order to establish more reasonable comparisons.

In terms of the dissolution performance, the HME systems showed, in both cases of Forms I and II, lower dissolution rate when compared to SD samples. This behaviour was ascribed to the compact state of the HME microparticules and therefore slower diffusion rate in the dissolution media. However, considering pure Form I and Form II individually, the dissolution profile of Form I was similar to the PMs and SD samples whereas pure

Form II, in contrast, had a dissolution rate similar to the HME sample. This fact might be related to the higher water content of Form II compared to Form I.

Finally, in terms of the physical stability of the formulated systems HME systems showed, overall, higher stability than the SD samples. More specifically, HME Form I:PVPVA was found to be the most stable system with the lowest recrystallisation rate. This could be attributed with the higher glass forming ability of Form I compared to Form II.

7 OLANZAPINE SOLID DISPERSIONS PREPARED VIA HME: IMPACT OF THE DRUG PHYSICAL STATE AND DIFFERENT POLYMERS ON THE DISSOLUTION ENHANCEMENT AND STORAGE STABILITY

Abstract

In this chapter, particular attention was paid to the physicochemical properties of different polymeric carriers and their influence on the manufacturing process and capability of inhibiting crystal growth over storage. In addition, the relationship between the physical structure of the prepared systems and the dissolution behaviour was also assessed critically, with a view to examine whether full amorphicity is necessary to achieve a favourable dissolution profile. Solid dispersions of olanzapine (OLZ) were prepared via hot melt extrusion (HME) in three polymers (PVP, PVPVA and Soluplus$^{®}$ (SLP)). The influence of the drug loading and extrusion temperature on the processability by HME was also investigated. Drug-polymer miscibility was estimated using melting point depression (MPD) and Hansen solubility parameters (δ). Solid dispersions were characterised using differential scanning calorimetry (DSC), thermogravimetric analysis (TGA), Fourier transform infrared (FTIR), X-ray powder diffraction (XRPD) and scanning electron microscopy (SEM).

All the polymers were found to be miscible with OLZ (interaction parameter, $\chi < 0$ and $\Delta\delta < 7$ MPa$^{1/2}$), in a decreasing order of PVP > PVPVA > SLP. At a lower extrusion temperature (160 ^{o}C), PVP generated fully amorphous dispersions with OLZ, while the formulations with PVPVA and SLP contained 14-16% crystalline OLZ. Increasing the extrusion temperature to 180 ^{o}C allowed the preparation of fully amorphous systems with PVPVA and SLP. Despite these differences, the dissolution rates of these preparations were comparable, with PVP showing a lower release rate despite being fully amorphous. These findings suggested that, at least in the particular case of OLZ, the absence of crystalline material may not be critical to the dissolution performance. Regarding the storage stability under 75% RH/40 ^{o}C, the extrudates prepared with SLP and extruded at 180 ^{o}C were found to have the greatest stability. Properties such as low hygroscopicity and high viscosity (high molecular weight) of SLP might have a strong effect in decreasing molecular mobility and thus impairing crystallisation. These two properties seemed to control the stability of amorphous OLZ, rather than the stabilisation via hydrogen bonding between OLZ and the different polymers.

7.1   Introduction

The oral bioavailability enhancement of poorly soluble active pharmaceutical ingredients (APIs) continues to represent a significant issue in drug development. One strategy to overcome this obstacle is the development of amorphous solid dispersion systems using hydrophilic polymers. The term 'solid dispersion' was described by Chiou and Riegelman as *"the dispersion of one or more active ingredients in an inert carrier matrix at solid-state prepared by melting (fusion), solvent or melting-solvent method"* (Chiou and Riegelman, 1971). This definition is still applicable despite the field having developed considerably to include a wider range of manufacturing techniques (e.g. hot melt extrusion (HME)) and new concepts in structural characteristics, particularly involving the recognition of complexities of molecular dispersion of drugs in polymers.

The mechanisms underpinning the dissolution increase of these formulations are still not yet clearly understood. Currently, there is a belief that the fundamental critical factor is the molecular dispersion of the drug in the polymer, thereby representing the ultimate in particle size reduction and lattice energy negation. A number of papers have addressed these and associated issues such as wetting and reduction in agglomeration (Janssens and Van den Mooter, 2009; Vasconcelos et al., 2007). In addition, earlier work in the pre-HME solid dispersion field suggested that the drug dissolution may be controlled by the behaviour of the carrier (so-called 'carrier controlled dissolution'), by implication suggesting that the physical state of the drug may not be important in such systems (Corrigan, 1985; Craig, 2002). The specific issue of whether full amorphisation (in terms of either molecular dispersion or amorphous phase generation) is actually necessary to achieve fast and complete dissolution has been addressed by previous authors. For example, Verheyen et al. observed that the dissolution rate of diazepam and temazepam could be enhanced when prepared into solid dispersions with polyethylene glycol (PEG) 6000, although both drugs remained in a highly crystalline state (Verheyen et al., 2002). The reason for this behaviour was attributed to the existence of a micro-environment created by the polymer at the surface of the drug particles leading to a better wetting and solubilisation properties.

Another point of concern when dealing with amorphous solid dispersions is their physical stability over storage. It is generally accepted that the recrystallisation of these systems is dependent on the molecular mobility and the degree of supersaturation of the solute in the matrix (Weuts et al., 2005). As the molecular mobility increases, the risk of crystallisation also increases. In general, the addition of polymers exerts a protective effect, which can be a result of two main factors: an antiplasticising effect of the polymer or interactions between the drug and the polymer, or a combination of both. An antiplasticising effect of the polymer may contribute significantly by increasing the temperature at which the molecular mobility become significant (Van den Mooter et al., 2000). However, several studies have shown that crystallisation occurs well below the T_g and hydrogen bonding between the drug and the polymer is not always a prerequisite in the stabilisation of amorphous compounds (Van den Mooter et al., 2000; Zhu et al., 2010). Based on the preceding discussion, it is clear that the physiochemical properties of polymers and their role during dissolution and as inhibitors of crystallisation from the amorphous state are not yet fully understood.

In this study, olanzapine (OLZ) was selected as the model drug and formulated with three hydrophilic polymers, polyvinylpyrrolidone K30 (PVP), polyvinylpyrrolidone vinyl-acetate 6:4 (PVPVA) and polyvinyl-caprolactam polyvinyl-acetate polyethylene glycol graft copolymer (Soluplus®, SLP) via hot melt extrusion (HME). HME is a widely used technology in which API and carrier are converted into a product of uniform shape and density by the effect of heat and mechanical stress (Crowley et al., 2007; Repka et al., 2007). HME represents a continuous solvent-free manufacturing method and is relatively easy to scale-up, hence presenting a commercially viable approach to dosage form development.

OLZ is an atypical antipsychotic agent used to treat both negative and positive symptoms of schizophrenia, acute mania with bipolar disorder, agitation, and psychotic symptoms in dementia (Burns, 2001). According to Biopharmaceutical Classification System (BCS), OLZ is classified as a Class II drug (low solubility, high permeability) with water solubility around 43 mg/L (Thakuria and Nangia, 2011). OLZ has been suggested to crystallise in more than 50 different crystalline forms, including anhydrates, hydrates and solvates (Reutzel-Edens et al., 2003a; Bhardwaj et al., 2013). In this study, anhydrous OLZ Form I, the most stable form and currently used in pharmaceutical formulations, was

chosen as the model form. Regarding the polymers used in this work, numerous studies have been conducted on the solubility enhancement of water insoluble compounds, in particular using PVP and its derivatives as carriers (Moneghini et al., 1998; Hülsmann et al., 2000; Tantishaiyakul et al., 1996, 1999). High solubilisation effect and the ability of establishing hydrogen bonding with APIs are well recognised properties of PVP based polymers (Konno and Taylor, 2006; Trasi and Taylor, 2012). PVP K30 has a higher glass transition temperature (T_g) and a relatively low degradation temperature (T_{deg}) when compared with PVPVA 6:4 what can represent an issue during processing via HME. Moreover, PVP is classified as an extremely hygroscopic substance, which is attributed to the electronegative groups (C=O) in the pyrrolidone structure being able to establish hydrogen bonding with water (Callahan et al., 1982). The co-polymer PVPVA 6:4 has a 40% replacement with lipophilic vinyl-acetate functional groups and therefore it is less hygroscopic than the homopolymer system (Bu☐hler, 2005). SLP on the other hand is a synthetic polymer that combines both hydrophilic and hydrophobic components in its structure which facilitates increased solubilisation of drugs and thus the preparation of fully amorphous solid dispersions. Moreover, its low T_g (≈ 70 ^{o}C) compared to the PVP based polymers permits easier processing of thermolabile APIs, while its low hygroscopicity can have an important stabilising effect during storage. Lately, polymer blends have also gained considerable attention as they can offer several physicochemical attributes to the dosage form as opposed to the use of a single polymer (Six et al., 2004; Sakurai et al., 2012; Bley et al., 2010; Yang et al., 2013).

In this study, the effect of different polymers on the manufacturing process and stabilisation over storage was critically assessed. Moreover, attention was paid to the physical state of the prepared extrudates and its influence during the dissolution performance. At first, the optimal extrusion temperatures for the OLZ-polymer systems based on the properties of each material (i.e. T_g, T_m and T_{deg}) was evaluated. In addition, the thermodynamic solubility/miscibility and interaction of OLZ in each polymer were assessed using melting point depression (Marsac et al., 2009; Marsac et al., 2006) and solubility parameter approaches (Kontogeorgis, 2007; Hansen, 2007; Krevelen and Nijenhuis, 2009). The physicochemical properties and the morphology of the fresh and aged extrudates were evaluated using differential scanning calorimetry (DSC), Fourier

transform infrared (FTIR), X-ray powder diffraction (XRPD) and scanning electron microscopy (SEM). Dissolution experiments and stability studies were as well carried out.

7.2   Materials and Methods

7.2.1   Materials

Olanzapine (OLZ, molecular weight (MW) = 312.43 g/mol, density (ρ) = 1.30 g/cm^3) was purchased from Myjoy Ltd. (India), PVP K30 (MW $\approx$ 41 550 g/mol, ρ = 1.16 g/cm^3), PVPVA 6:4 (MW = 57 500 g/mol, ρ = 1.17 g/cm^3) and Soluplus$^®$ (SLP, MW = 118 000 g/mol, ρ = 1.20 g/cm^3) were kindly donated by BASF Chemicals (Germany). Methanol (analytical grade) was obtained from Sigma Aldrich (UK). Phosphate buffer, pH = 6.8 (BP), used for the dissolution studies was prepared with potassium dihydrogen orthophosphate (Fischer Scientific, UK) and sodium phosphate dibasic (Sigma Aldrich, UK). Storage environment with 75% RH was prepared using a salt solution of sodium chloride (Fischer Scientific, UK).

7.2.2   Methods

7.2.2.1   Preparation of Hot Melt Extrudates

Hot melt extrudates were prepared using a co-rotating twin screw extruder Thermo Scientific HAAKE MiniLab II (Thermo Scientific). Extrudates of OLZ with PVPVA and SLP were prepared with ratios of 20:80 and 50:50 (w/w) and extruded at 160 and 180 $^{\circ}$C; OLZ:PVP extrudates were only successfully prepared at 50:50 (w/w) and extruded at 160 $^{\circ}$C. Each system was prepared using a total weight of 5 g at a speed of 100 rpm and mixed inside the barrel for 10 min.

7.2.2.2   Drug-Polymer Miscibility Prediction

(a) Melting Point Depression (MPD)

OLZ and polymers were passed through a combination of sieves and a fraction between 63-106 μm was used in all melting point depression experiments. Polymers were dried over P_2O_5 for 48 h prior to usage. Physical mixtures (PMs) with a drug ratio of 70, 75, 80, 85, 90 and 100% w/w were prepared at least in triplicate. The melting temperature of OLZ both in the absence and presence of polymers was measured using DSC at a scanning rate of 10 ^{o}C/min in standard crimped pans.

(b) Hansen Solubility Parameter

The Hansen solubility parameters, δ, of the drug and the polymers were calculated from their chemical structures using the van Krevelen and Hoftyzer method according to the Equation 7.1 and Equation 7.2 (Krevelen and Nijenhuis, 2009). The total solubility parameter (δ_t) was determined from the interactions between dispersion forces (δ_d), polar interactions (δ_p) and hydrogen bonding (δ_h) of the functional groups in the parent molecule divide by the molar volume, V. The units of the solubility parameters are $MPa^{1/2}$.

$$\delta^2 = \delta_d^2 + \delta_p^2 + \delta_h^2$$

Equation 7.1

$$\delta = \sqrt{\left(\frac{\sum F_{di}}{V}\right)^2 + \left(\frac{\sqrt{\sum F_{pi}^2}}{V}\right)^2 + \left(\sqrt{\frac{\sum E_{hi}}{V}}\right)^2}$$

Equation 7.2

where, F_{di}, F_{pi} and E_{hi} are the group contributions for different components (dispersion forces, polar interactions and hydrogen bonding, respectively) of structural groups which are reported in the literature at 25 ^{o}C (Krevelen and Nijenhuis, 2009).

The drug-polymer interaction parameter, χ, using the solubility parameters difference between the drug and the polymer, can be estimated as follow (Krevelen and Nijenhuis, 2009),

$$\chi = \frac{V_0}{RT} \left(\delta_{drug} - \delta_{polymer}\right)^2$$

Equation 7.3

where, V_0 is the volume of the lattice site, R is the gas constant and T is the absolute temperature.

7.2.2.3 Crystallinity Quantification

The amount of crystalline OLZ present in the fresh extrudates was estimated by constructing a calibration curve using the enthalpy of melting of OLZ in the presence of the polymer versus the ratio of the drug in the mixture. This was performed in order to account for changes in the melting behaviour and enthalpy caused by the presence of the polymer. Physical mixtures (PMs) were prepared by mixing OLZ and each polymer with a mortar and pestle in ratios of 10:90, 20:80, 30:70, 50:50, 70:30 and 90:10 w/w and analysed in DSC. All the PMs were used with a 63−106 μm particle size range. Measurements were made at least in triplicate.

7.2.2.4 Thermal Analysis

Standard differential scanning calorimetry (DSC, Q2000 TA Instruments) analysis was performed at a heating rate of 10 ^{o}C/min. Modulated temperature DSC (MTDSC, Q2000 TA Instruments) analysis was conducted using a heating rate of 2 ^{o}C/min, amplitude $\pm$ 0.318 ^{o}C and a period of 60 seconds. Scans were carried out within the temperature range 0 °C to 220 °C and standard crimped pans were used in all experiments.

Thermogravimetric analysis (TGA, Q5000 TA Instruments) was used to measure the degradation temperature (T_{deg}) of the raw materials and the water content of the fresh extrudates. Studies were conducted at 10 ^{o}C/min from room temperature to 300 ^{o}C. Aluminium open pans were used.

7.2.2.5   Attenuated Total Reflection-Fourier Transform Infrared (ATR-FTIR)

FTIR (IFS 66/S, Bruker Optics Ltd.) equipped with a Golden Gate attenuated total reflection (ATR) accessory was used. Sixty-four scans, from 4000 cm^{-1} to 550 cm^{-1}, were acquired for each sample with a resolution of 2 cm^{-1}. Extrudates were scanned in powder form after gentle grinding with a mortar and pestle.

7.2.2.6   Dynamic Vapour Sorption (DVS)

DVS (Q5000 SA, TA Instruments) was used to study the water uptake behaviour of all solid dispersions systems immediately after preparation and without any pre-treatment of the samples. Isothermal (25 ^{o}C) and isohumic (98% RH) conditions were used for a period of 16 h.

7.2.2.7   X-Ray Powder Diffraction (XRPD)

XRPD (Thermo-ARL Xtra, Thermo Scientific) spectra were collected from scans within the range 5.0^o to 40.0^o at 2θ. Extrudates were pre-milled by mortar and pestle before the tests.

7.2.2.8   Scanning Electron Microscopy (SEM)

SEM (JSM 4900 LV, JOEL) was used to acquire microphotographs on the surface and cross-section of the freshly prepared extrudates. To improve conductivity prior examination, samples were coated with gold using a Polaron SC7640 sputter gold coater (Quorum Technologies).

7.2.2.9   Dissolution Studies

The drug content of each system was determined by UV detection (Lambda XLS UV/VIS, Perkin Elmer) at 253 nm. Samples were dissolved in methanol and diluted with the same solvent as appropriate.

Dissolution studies were carried out on a Copley CIS 8000 dissolution bath (Copley Scientific). The BP paddle method with a rotation speed of 50 rpm was employed and 900 mL of phosphate buffer pH = 6.8 (BP) at the temperature of 37.0 ± 0.5 ^{o}C was used. Samples (pure OLZ, PMs and HME) equivalent to 12 mg of OLZ (based on the drug loading of each formulation) were used with a 63-106 μm sieve fraction. At predetermined intervals, 10 mL of solution was withdrawn and filtered through a 0.45 μm filter. Subsequently, the filtrate was analysed spectrophotometrically at 253 nm. All the dissolution experiments were performed under sink conditions.

To compare the dissolution performances between the different systems, a similarity factor (f_2) was used (see Chapter 6 for the theoretical background).

7.2.2.10   Physical Stability

The stability of the extrudates was assessed using accelerated conditions according to ICH Topic Q 1 A (R2) Stability Testing of new Drug Substances and Products (EMA, 2003). The samples were stored in desiccators at $75\% \pm 5\%$ RH/40 ± 2 °C for three months. The humidity environment was obtained by using saturated salt solution of sodium chloride (75% RH). Sampling at different time points and respective characterisation was done for each system using DSC, XRPD and SEM.

7.3   Results and Discussion

7.3.1   Estimation of Drug-Polymer Miscibility

The thermodynamic miscibility between OLZ and each polymer was investigated by using two different approaches (described earlier in the Methods section): melting point depression (MPD) and Hansen solubility parameter. The former method describes the drug-polymer miscibility based on the Flory-Huggins theory (Flory, 1942), which

delineates entropy and enthalpy components at a given temperature (Qian et al., 2010). Considering the lattice-based models, the entropy of mixing is predicted to be relatively constant (and favourable to mixing), being the balance between adhesive and cohesive interactions that determines miscibility (see Chapter 6). As a result, the mixing can be exothermic (Flory-Huggins interaction parameter, $\chi < 0$), endothermic ($\chi > 0$) or athermal ($\chi = 0$), which leads to different reduction magnitudes in the melting point of the drug (Marsac et al., 2009; Marsac et al., 2006).

The MPD results obtained for OLZ and each polymer system are shown in Figure 7.1. In this case, all the interaction parameters, χ, were found to be negative indicating that all the three polymers were miscible with OLZ and can be presented as follow: -3.34 ($R^2 = 0.984$) for OLZ:PVP, -3.26 ($R^2 = 0.998$) for OLZ:PVPVA and finally -2.54 ($R^2 = 0.995$) for the OLZ:SLP system. Based on this results, the degree of miscibility and interaction between OLZ and each polymer was suggested to follow the decreasing rank order PVP > PVPVA > SLP.
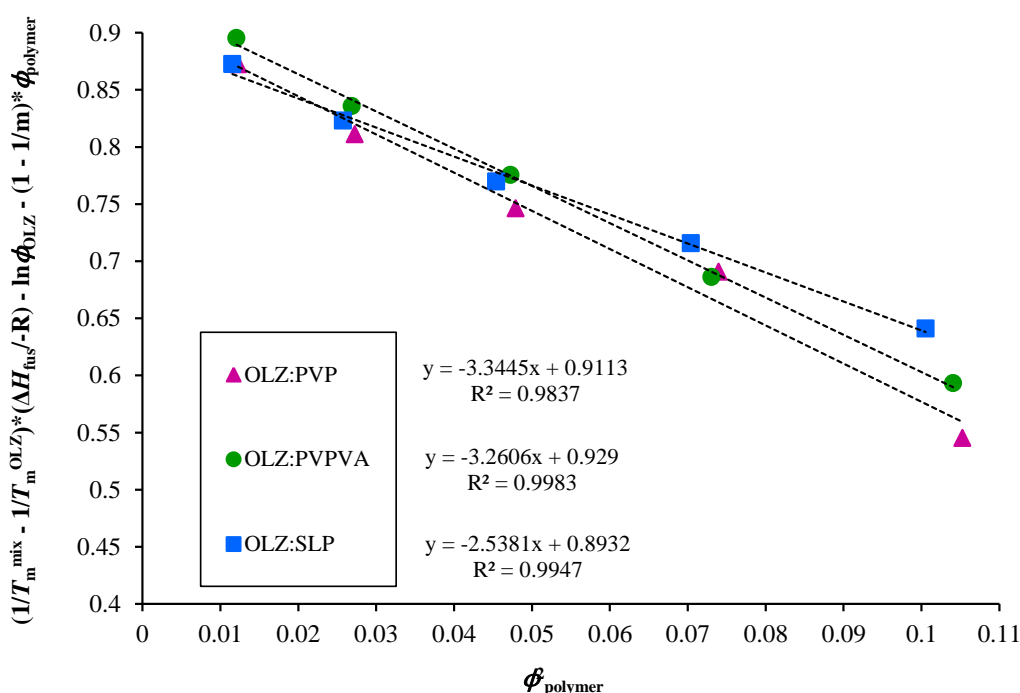
Figure 7.1: Melting point depression results obtained for each olanzapine (OLZ):polymer system (PVP, PVPVA and Soluplus® (SLP)). Slope of each curve included for subsequent calculation of the Flory-Huggins interaction parameter (χ).

Figure 7.2 shows the changes in the Gibbs free energy (see Chapter 6 for the background theory) for the three systems. For small values of the interaction parameter, the free energy of mixing is negative and shows a concave dependence on composition indicating miscibility. As expected and according to Equation 6.6 in Chapter 6, the ΔG_{mix} is negative for all the OLZ:polymer systems, though presenting lower values for the OLZ:PVP and OLZ:PVPVA systems when compared to the OLZ:SLP and therefore indicating greater miscibility for these systems.
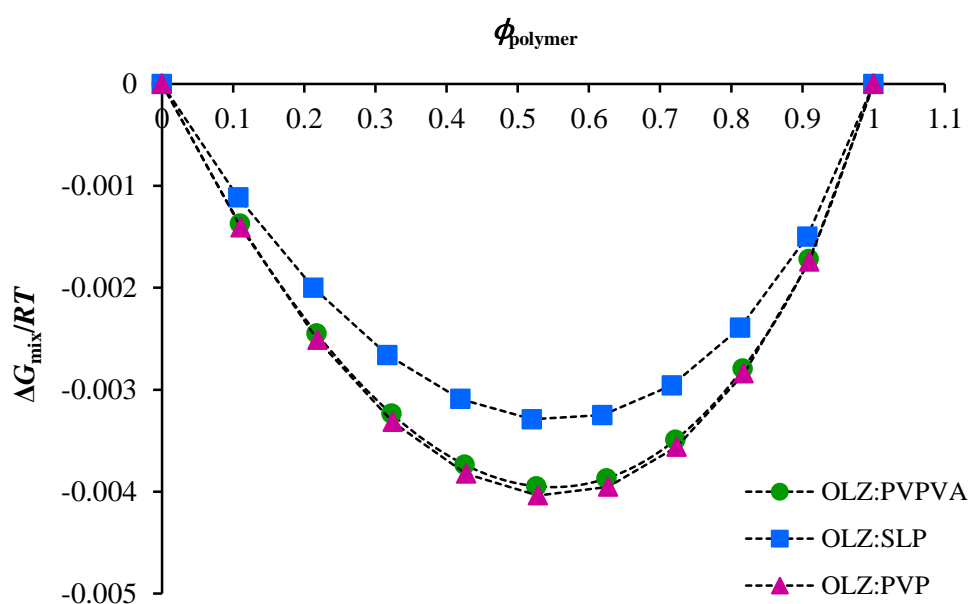
Figure 7.2: Free energy-composition phase diagrams of olanzapine (OLZ) and each polymer system (PVP, PVPVA and Soluplus® (SLP)).

The second approach in analysing OLZ:polymer system miscibility was by using Hansen solubility parameters (δ), which were calculated based on van Krevelen and Hoftyzer group contribution (Equation 7.2). Figure 7.3 shows the chemical structure of OLZ. As an example, the calculations of the Hansen solubility parameter carried out for OLZ are given in Table 7.1. The van Krevelen and Hoftyzer group contribution method used to calculate the total interaction forces for OLZ and each polymer was based on literature values (Krevelen and Nijenhuis, 2009).
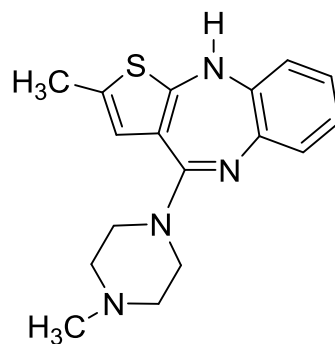
Figure 7.3: Chemical structure of olanzapine.

Table 7.1: Solubility parameter component group contribution using van Krevelen-Hoftyzer method.

Structural Groups	F_{di} $((MJ/m^3)^{1/2} mol^{-1})$	F_{pi}^2 $((MJ/m^3)^{1/2} mol^{-2})$	E_{hi} (J/mol)	V (cm^3/mol)
(2) –CH$_3$	840	0	0	67
(4) –CH$_2$	1 080	0	0	64.4
(1) =CH	200	0	0	13.5
(4) =C	280	0	0	-22
(1) –Phenyl	1 270	12 100	0	52.4
(1) –S–	440	0	0	12
(1) –NH–	160	44 100	3 100	4.5
(2) –N	40	2 560 000	10 000	-18
(1) –N=	20	640 000	15 000	5.0
(3) – Ring (> 5 atoms)	570	0	0	48
$\sum$	4 900	5 816 200	18 100	226.8

The δ for each component, difference between drug and each polymer ($\Delta\delta$), and interaction parameter (χ) are provided in Table 7.2. It is reported that compounds with similar values of solubility parameter, nominally $\Delta\delta < 7.0$ MPa$^{1/2}$, are more likely to be miscible, whereas if $\Delta\delta > 10.0$ MPa$^{1/2}$ the compounds are most probably immiscible (Greenhalgh et al., 1999). From the presented results, OLZ had a solubility parameter (25.68 MPa$^{1/2}$) closer to PVP (26.28 MPa$^{1/2}$), while PVPVA and SLP had a slightly lower solubility parameter values, 24.37 and 23.07 MPa$^{1/2}$, respectively. In the present case, the difference between the solubility parameter of OLZ and each polymer was lower than 7.0 MPa$^{1/2}$ indicating good miscibility for all systems.

Table 7.2: Calculated solubility parameters and interaction parameters using Hansen group contribution theory for OLZ and each polymer.

Compound	δ (MPa)$^{1/2}$	$\Delta\delta$ (MPa)$^{1/2}$	χ
OLZ	25.68	n.a.	n.a.
PVP	26.28	0.60	0.03
PVPVA	24.37	1.31	0.16
SLP	23.07	2.61	0.62

n.a. – not applicable

The value of χ, calculated based on Equation 7.3, refers to the square of the difference in solubility parameters that were calculated from the values of group contributions at 25 $^{\circ}$C. A closer value of χ to zero suggests greater interaction between the drug and the polymer (Krevelen and Nijenhuis, 2009). According to the results in Table 7.2 miscibility between OLZ and each polymer is likely to follow the same order as observed with MPD experiments (PVP > PVPVA > SLP).

These two methods used here to predict drug-polymer miscibility have concomitant strengths and limitations, as has been discussed extensively in the literature. In brief, the MPD approach is temperature and composition dependent whereas the calculation of solubility parameters allows the estimation of the degree of miscibility based on the chemical structure of the drug and polymer at room temperature (Forster et al., 2001b; Hancock et al., 1997). Moreover, MPD methods may not be performed properly if the drug degrades at the melting temperature, while the group contribution method for the calculation of Hansen solubility is not applicable for drug-polymer systems presenting strong intermolecular interactions (Zhao et al., 2011). In this work, the two approaches used to predict the miscibility between OLZ and each polymer were in good agreement, with PVP being identified by both as the polymer presenting the greatest degree of miscibility with OLZ, followed by PVPVA and finally SLP. The agreement between the two approaches lends weight to the applicability of the theoretical approaches used, although clearly experimental measurements, as performed below, are ultimately the most reliable means of testing miscibility.

7.3.2   Properties of the Raw Materials

In general, for HME processing the temperature should be higher than the glass transition temperature (T_g) of the carrier in order to decrease its viscosity and promote an adequate mixing with the drug and an ideal flow through the extruder. The optimal extrusion temperature has to be carefully determined based on the melting temperature (T_m) of the drug, the T_g of the amorphous carrier and the thermoplastic properties of the carrier (Srinarong et al., 2011). Therefore, it is imperative that the thermal properties of drug substances and excipients are well understood prior to extrusion.

Table 7.3 shows the main thermal properties of OLZ and each polymer. PVP has the highest T_g and the lowest degradation temperature ($T_{deg,}$ measured by using TGA as the onset temperature) when compared to PVPVA and SLP. According to the presented results, neither OLZ nor the polymers appeared to degrade at the extrusion temperatures used in this study (160 ^{o}C for all the three systems and 180 ^{o}C for PVPVA and SLP as PVP

degraded at this temperature). Particular attention was paid to PVP due to the smaller temperature interval between its T_g, T_{deg} and the processing temperature. However, holding PVP isothermally in the TGA at 160 ^{o}C for 30 min resulted in a $0.81 \pm 0.10\%$ loss of mass, suggesting that 160 ^{o}C might be a suitable temperature for the extrusion of the OLZ:PVP formulation.

Table 7.3: Experimental thermal properties of OLZ and polymers.

Material	$T_{m\ onset} \pm$ s.d. (^{o}C)	$T_g \pm$ s.d. (^{o}C)	$T_{deg} \pm$ s.d. (^{o}C)	Water content $\pm$ s.d. (%)
OLZ	193.6 ± 0.3	$71.4 \pm 0.4^*$	265.3 ± 4.0	0.36 ± 0.06
PVP	n.a	161.6 ± 0.2	179.8 ± 1.6	5.53 ± 0.94
PVPVA	n.a.	105.6 ± 1.4	282.3 ± 1.0	3.48 ± 1.15
SLP	n.a.	72.9 ± 0.3	309.1 ± 1.3	2.36 ± 0.14

n.a. – not applicable
*T_g value obtained from heat-cool-heat cycle inside the DSC at 2 ^{o}C/min in crimped pans

7.3.3 Physical Characterisation of HME Systems

Attempts to extrude PVP with a low drug loading of 20% were unsuccessful. It is well known that the use of PVP in HME formulations is limited due to its high T_g ($\approx$ 160 ^{o}C) and low T_{deg} which is below 180 °C. Therefore, the incorporation of small molecules of API allow the polymer segments to have greater mobility due to plasticisation effects and hence be extruded at lower temperatures (Lakshman et al., 2008). Studies with ibuprofen and ethyl cellulose showed that higher drug loadings of ibuprofen not only eased the extrusion behaviour of ethyl cellulose by decreasing its T_g but also improved the physical properties of the prepared films (De Brabander et al., 2003; De Brabander et al., 2002). In

the present work, the low drug loading of 20% w/w did not elicit a suitable plasticisation effect for PVP and thus did not allow extrusion. However, when the drug loading was increased to 50% w/w, the extrusion process was difficult, but possible. As a result, the extrudates were prepared in block-like shape with a rough appearance instead of thin spaghetti-like strands as usually obtained in a smooth extrusion process. Despite the difficulties associated with the extrusion process, this formulation (50% OLZ:PVP) appeared to be completely amorphous with a single T_g value and no evidence of recrystallisation or melting of OLZ was seen when analysed in DSC, as shown in Figure 7.4.
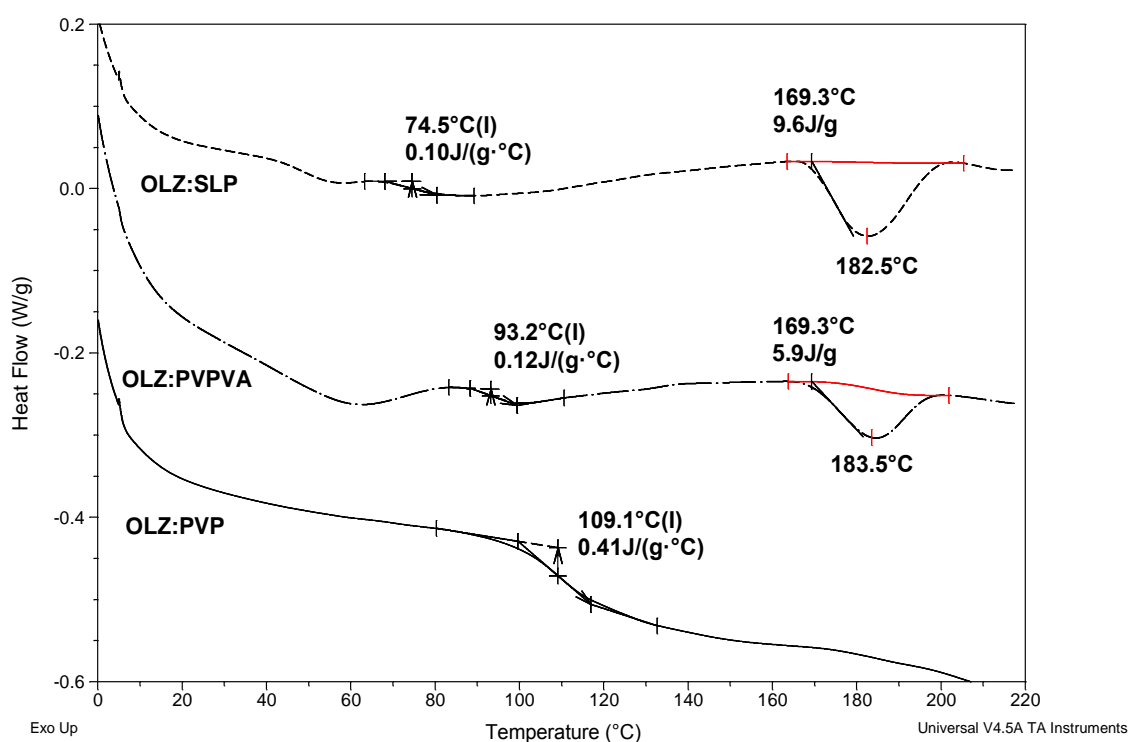
Figure 7.4: DSC curves of 50% drug-loaded systems with Soluplus® (SLP), PVPVA and PVP (downwards) extruded at 160 °C and run at 10 °C/min in standard crimped pans.

The data in Figure 7.4 shows an initial water loss peak reflecting the approximately 1-2% water content of these systems, as measured by TGA, followed by a glass transition and, in some cases, melting of the crystalline drug. Extrudates of PVPVA and SLP with 20% drug loading were easily extruded even at 160 °C since the T_g of these polymers is much lower

($T_{g\,(PVPVA)} \approx 105\ ^oC$; $T_{g\,(SLP)} \approx 70\ ^oC$). Therefore their liquid-like state at that temperature allowed an appropriate mixing with OLZ and a consistent flow of the material through the barrel. However, in contrast to the 50% OLZ:PVP system, the 50% drug-loaded PVPVA and SLP systems extruded at 160 ^oC were not fully but only partially amorphous, which was confirmed by the melting of OLZ at $\approx$ 170 ^oC.

The quantification of crystalline OLZ in those extrudates was calculated using calibration curves of the melting enthalpy of OLZ when physically mixed with PVPVA or SLP in different ratios, as shown in Figure 7.5. The percentage of drug crystallinity was calculated to be 14.5 $\pm$ 1.6% and 16.5 $\pm$ 0.1% for the OLZ:PVPVA and OLZ:SLP systems, respectively. These findings are nevertheless evidence of the high solubilisation effect of PVP previously predicted by the MPD and Hansen methods when compared to the other polymers.
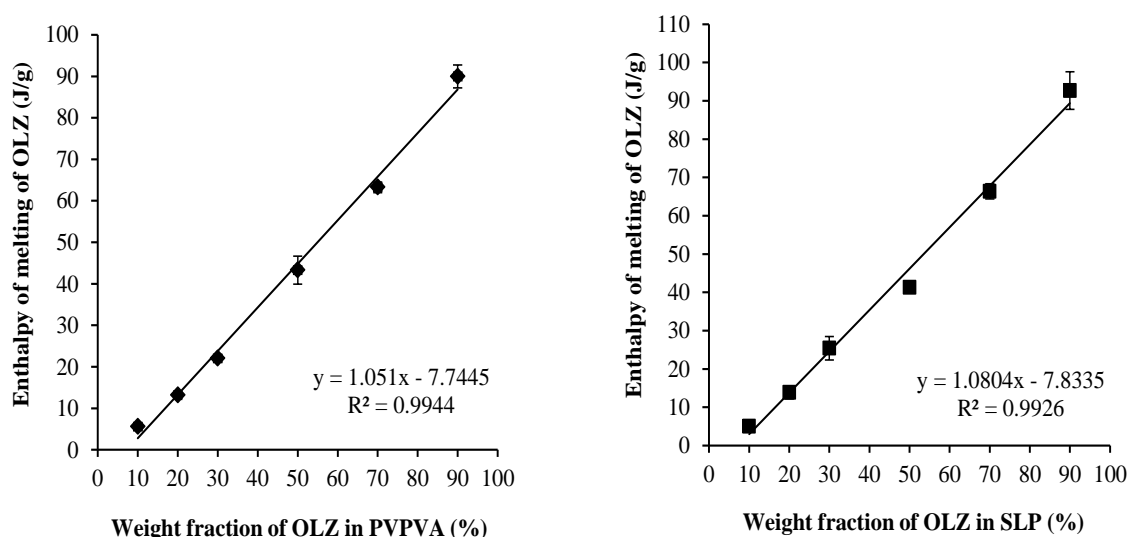
Figure 7.5: Calibration curves of the enthalpy of melting of olanzapine (OLZ) in the presence of PVPVA (left) or SLP (right) versus the ratio of crystalline OLZ in the physical mixtures. Measurements were carried out at 10 ^oC/min in crimped pans.

In terms of the PVPVA and SLP systems with a 50% drug loading, when the temperature was increased to 180 ^oC, fully amorphous solid dispersion systems were prepared without any evidence of crystalline OLZ observed in DSC. Figure 7.6 shows the measured T_g for all the formulated systems. The difference in the processing conditions (extrusion temperature) and consequently the existence of crystalline OLZ in the final extrudates did

not have a great influence on the measured T_g of the PVPVA and SLP systems. As expected, 50% OLZ:PVP showed the highest T_g ($\approx$ 108 ^{o}C), followed by the formulations with PVPVA ($\approx$ 90 ^{o}C) and finally SLP ($\approx$ 74 ^{o}C).
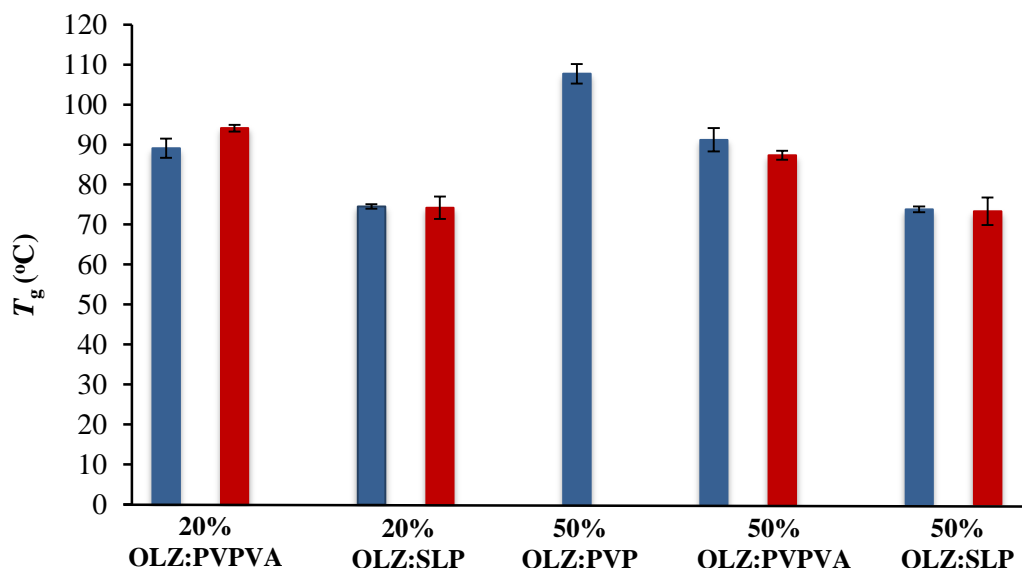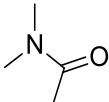
Figure 7.6: Measured T_g values for all the freshly prepared formulations using DSC (total heat flow) at 10 ^{o}C/min in crimped pans. Blue and red bars represent systems extruded at 160 ^{o}C and 180 ^{o}C, respectively.

FTIR spectroscopy was employed to study the interactions in solid dispersions between OLZ and the three polymers. The FTIR spectra of all PMs were only the summation of the OLZ and each polymer isolated spectrum, giving no evidence of any interaction between the drug and polymers in PMs (data not shown). OLZ has a single hydrogen bond donor (N-H) and all the polymers have in common at least one proton acceptor (C=O) able to participate in hydrogen bonding. In the case of PVPVA and SLP, a second group (C=O) from the vinyl-acetate component is present, however it is stereo chemically hindered and it does not participate in hydrogen bonding. Typically, the formation of hydrogen bonds within a given system may be readily identified through either, a downshift in the absorption band, band broadening, and/or peak intensification (Konno and Taylor, 2006).

As shown in Table 7.4 a greater level of interaction between OLZ:PVP and OLZ:PVPVA systems was observed with downshifts higher than 4 cm^{-1}. In contrast, no interaction between OLZ and SLP seemed to take place as no shifts to lower wavenumber were

detected. The N-H stretching vibration of OLZ was not detected in all the three systems as an indication of the conversion to an amorphous phase.

Table 7.4: Shifts on the carbonyl groups for each polymer and respective HME system (cm^{-1}).

Polymers and HME systems	O (acetyl C=O)	N-C=O (amide)
PVP		1667
50% OLZ:PVP (160 ^{o}C)		1655
PVPVA	1731	1673
20% OLZ:PVPVA (160 ^{o}C)	1731	1664
20% OLZ:PVPVA (180 ^{o}C)	1732	1666
50% OLZ:PVPVA (160 ^{o}C)	1733	1664
50% OLZ:PVPVA (180 ^{o}C)	1733	1663
SLP	1731	1632
20% OLZ:SLP (160 ^{o}C)	1732	1632
20% OLZ:SLP (180 ^{o}C)	1732	1632
50% OLZ:SLP (160 ^{o}C)	1734	1633
50% OLZ:SLP (180 ^{o}C)	1734	1634

The DSC findings outlined above were supported by the XRPD studies which showed a considerable presence of crystalline OLZ (Figure 7.7a) for the 50% drug-loaded PVPVA and SLP extruded at 160 ^{o}C (Figure 7.7b).
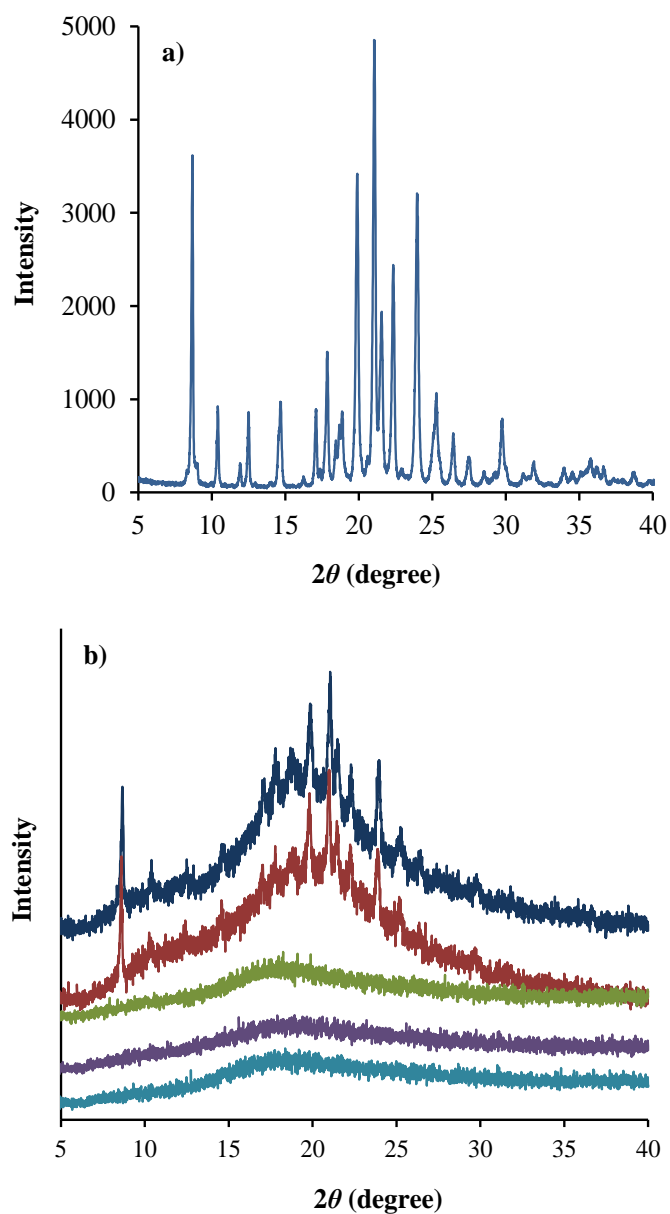
Figure 7.7: XRPD spectra of (a) pure OLZ and (b) 50% drug-loaded formulations from top to bottom: SLP, PVPVA and PVP extruded at 160 ^{o}C and SLP and PVPVA extruded at 180 ^{o}C.

Although the XRPD peaks in those systems were relatively broad and with significant background noise associated it is still possible to confirm that the diffraction peaks did

correspond to OLZ Form I. It was noted that the diffraction peaks were broader than for the pure drug, possibly indicating a reduction in crystal size. In contrast, no distinct intensity peaks were observed in the diffractograms of the PVP 50% and in all 20% extruded systems, confirming the formation of fully amorphous solid dispersions.

In terms of their optical appearance, all the systems had a characteristic reddish coloration, as shown in Figure 7.8 for the 50% drug-loaded extrudates. The first assumption to explain this feature would be degradation of OLZ, since the colour tonality is similar in all formulations and thus degradation of the carrier could be excluded. However, when OLZ melts, the yellow bright crystals turn into a red liquid. Additionally, TGA showed that the degradation of OLZ has an onset point at around 265 ^{o}C. Moreover, the drug content was determined spectrophotometrically in methanol and ranged between 95.6-104.0% in all systems excluding the possibility of drug degradation. This transformation in colour needs further investigation, as a chemical reaction not yet reported might be taking place. A similar behaviour was observed with crystalline piroxicam that transforms from colourless to a yellow bright colour when melted, dissolved in water or transformed to an amorphous state. The reason for this observation was found to be associated with the ionic character of the charged piroxicam molecules formed by intermolecular proton transfer (Sheth et al., 2005).
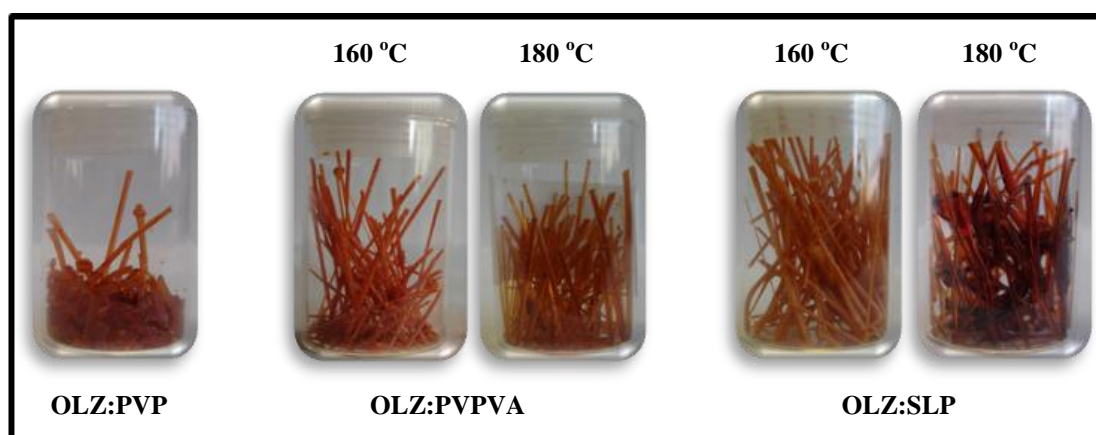
Figure 7.8: Photographs of 50% drug-loaded extrudates.

It was also noticed that the extrudates prepared with PVPVA and SLP at 160 ^{o}C are not transparent contrarily to those extruded at 180 ^{o}C, as a result of the incomplete melting of

OLZ. Also the OLZ:PVP extrudates did not have the typical rod-shape appearance due to its difficult extrusion. All the 20% drug-loaded extrudates had a transparent appearance and a lighter colour as less amount of OLZ was present.

Overall, following the physical characterisation of the different solid dispersion systems prepared with OLZ, they can be mainly divided into two major groups:

(a) Fully amorphous solid dispersions: 50% OLZ:PVP extruded at 160 °C, 50% OLZ with PVPVA and SLP extruded at 180 ^{o}C and all the 20% drug-loaded formulations prepared with PVPVA and SLP;

(b) Partially amorphous solid dispersions: 50% OLZ with PVPVA and SLP extruded at 160 ^{o}C.

It was noted that the greater miscibility of OLZ with PVP, suggested by the MPD and solubility parameter calculations, was supported by these findings. The question then arises as to whether the variability in the degree of crystallinity will have an influence on the associated drug release behaviour.

7.3.4   Dissolution Studies

The drug content of all formulations was at 95.6–104.0% of the theoretical values. Figure 7.9 and Figure 7.10 show the dissolution curves of pure OLZ and freshly prepared HME systems at 50% and 20% drug loading, respectively. A significant enhancement in the dissolution rate was observed for all solid dispersion systems prepared by HME compared to the pure crystalline OLZ. More specifically, in the case of the 50% drug-loaded extrudates, the T_{50} values were circa 3 min for the dispersions with PVPVA and SLP (either extruded at 160 or 180 ^{o}C) compared to 10 min for the OLZ:PVP and finally 30 min for the drug alone. The systems containing 20% OLZ extruded with PVPVA and SLP showed an even faster dissolution rate with T_{50} values between 1 and 2 min at both processing temperatures. It was interesting to observe in Figure 7.9 that with a constant drug loading (50%) and processing temperature (160 °C), the decreasing order of drug release rate from different polymer based systems was PVPVA (partially amorphous) >

SLP (partially amorphous) > PVP (fully amorphous). This was an indication that drug release may not always be faster from a fully amorphous state than a partially amorphous structure with crystal domains.

In addition, PVPVA and SLP systems extruded at the two different temperatures produced very similar dissolution profiles. More specifically, the similarity factor, f_2, for the 50% OLZ:PVPVA systems was calculated to be 65.6, whereas for the case of OLZ:SLP f_2 had a borderline value of 50.5. Nevertheless, in both cases f_2 was greater than 50 indicating that the release profile of the drug from the partially (extrusion at 160 ^{o}C) and fully (extrusion at 180 ^{o}C) amorphous solid dispersions was comparable in this specific case.
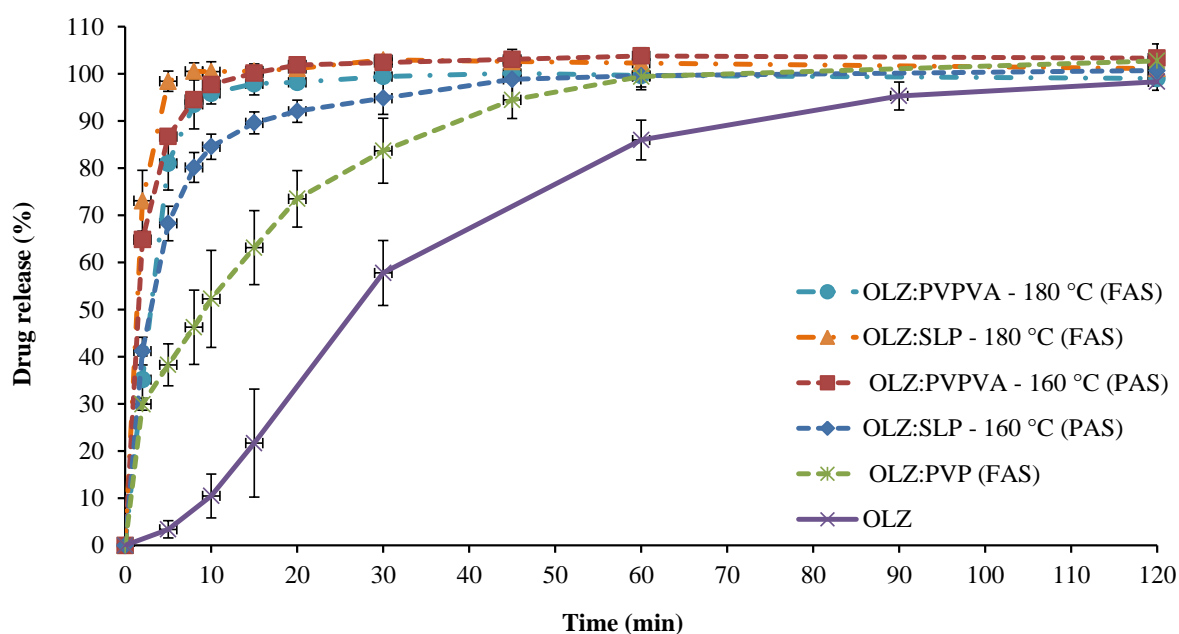
Figure 7.9: Dissolution profiles of pure OLZ and HME systems with PVP, PVPVA and Soluplus®(SLP) with 50% drug loading extruded at 160 and 180 ^{o}C (FAS – fully amorphous systems and PAS – partially amorphous systems). The legend on the right hand side follows the same order as the curves in the plot (downwards).

The dissolution curves of the 20% drug-loaded systems extruded at the different temperatures were found to be superimposable for each polymer system (Figure 7.10). Furthermore, the release profile was controlled by the type of polymer with the formulations prepared with SLP showing a slower release rate when compared to PVPVA.

However, at this drug loading fully amorphous solid solutions were obtained with both processing temperatures and therefore these results are not surprising.
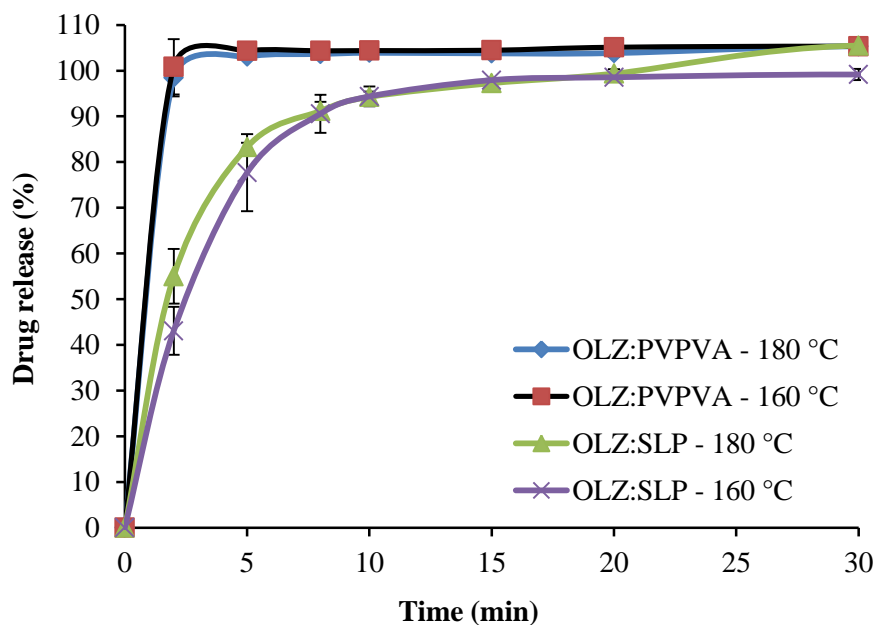
Figure 7.10: Dissolution profiles of 20% drug-loaded HME extrudates with PVPVA and SLP extruded at 160 and 180 °C (all systems were characterised as fully amorphous systems). The legend on the right hand side follows the same order as the curves in the plot (downwards).

From the above results, clearly, the nature of the polymer is an important determinant of dissolution as well as the degree of crystallinity. However what is particularly interesting is that the two 50% dispersions in PVPVA and SLP at 160 °C and 180 °C also showed no differences, despite these being the same polymers but with differing degrees of drug crystallinity. Earlier work in the solid dispersion literature (Corrigan, 1985; Craig, 2002) has suggested that dissolution rate of some or many binary systems may be determined by the dissolution of the carrier polymer and not the drug at all. More specifically it has been suggested that the polymer may form a concentrated layer adjacent to the solid surface into which the drug may dissolve rapidly, hence it is the dissolution of the polymer-rich layer that determines drug release and not the actual dissolution of the drug itself. The results presented here are consistent with this approach, suggesting that it is the polymer and not the drug that determines the dissolution profile. Therefore, it may in fact be the

characteristics of the polymer that are changing and the drug structure may, in some cases at least, be incidental and irrelevant to performance.

In contrast, the release rate of the drug from the physical mixtures as shown in Figure 7.11 is slightly reduced for the PVP and PVPVA systems in comparison to the drug alone and this effect is much more obvious for the PM of OLZ:SLP resulting in only less than 60% drug release at the last sampling point of 120 min with visible particles remaining in the medium. The reason for this feature it is not yet clearly understood, but apparently the incomplete dissolution of the polymer at this pH influenced somehow the dissolution behaviour of the drug. This was more evident when the polymer ratio increased in the 20% OLZ formulations with a drug release of about $\approx$ 36% in the end of the test (data not shown).
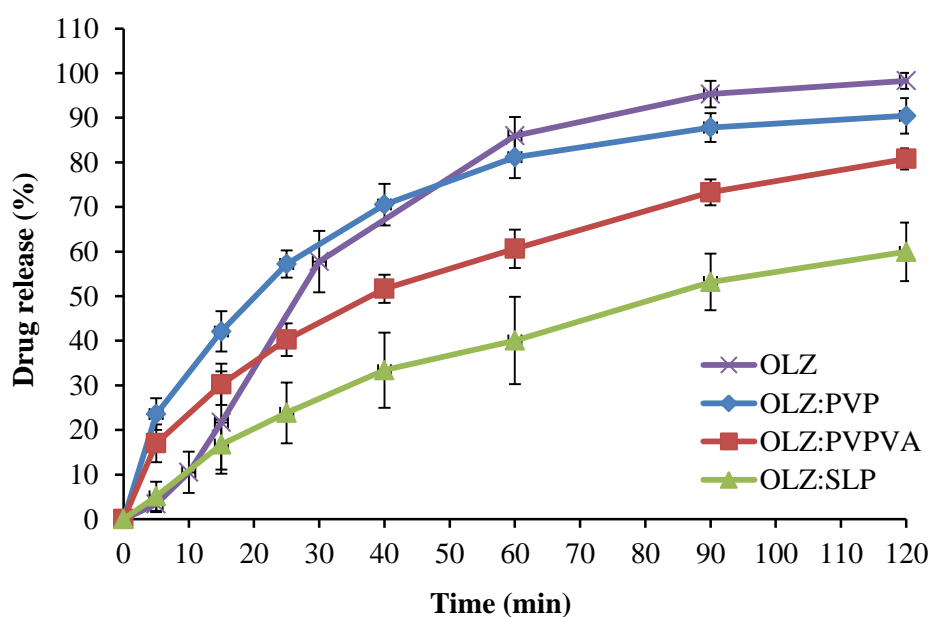
Figure 7.11: Dissolution profiles of OLZ and PM with PVP, PVPVA and SLP in 1:1 drug-polymer ratio.

These particles were collected from the dissolution vessel and examined under SEM, as shown in Figure 7.12. Considering that SLP showed in FTIR no degree of interaction with OLZ when compared to the other polymers, the assumption that the formation of strong hydrogen bonds between OLZ and SLP was the reason for the incomplete dissolution profile may not be correct. One explanation could be entrapment of the drug on the porous

structure of SLP leading to kind of 'insoluble complex' and therefore incomplete release of the drug.

Figure 7.12 shows also microphotographs of pure OLZ with an irregular shape; PVP and PVPVA as round microspheres due to the fact that these two polymers are industrially prepared via spray drying and finally SLP appearing as irregular particulates. The cylindrical shape of PVP and PVPVA is probably favourable for the dissolution of OLZ from the PMs in comparison to SLP.
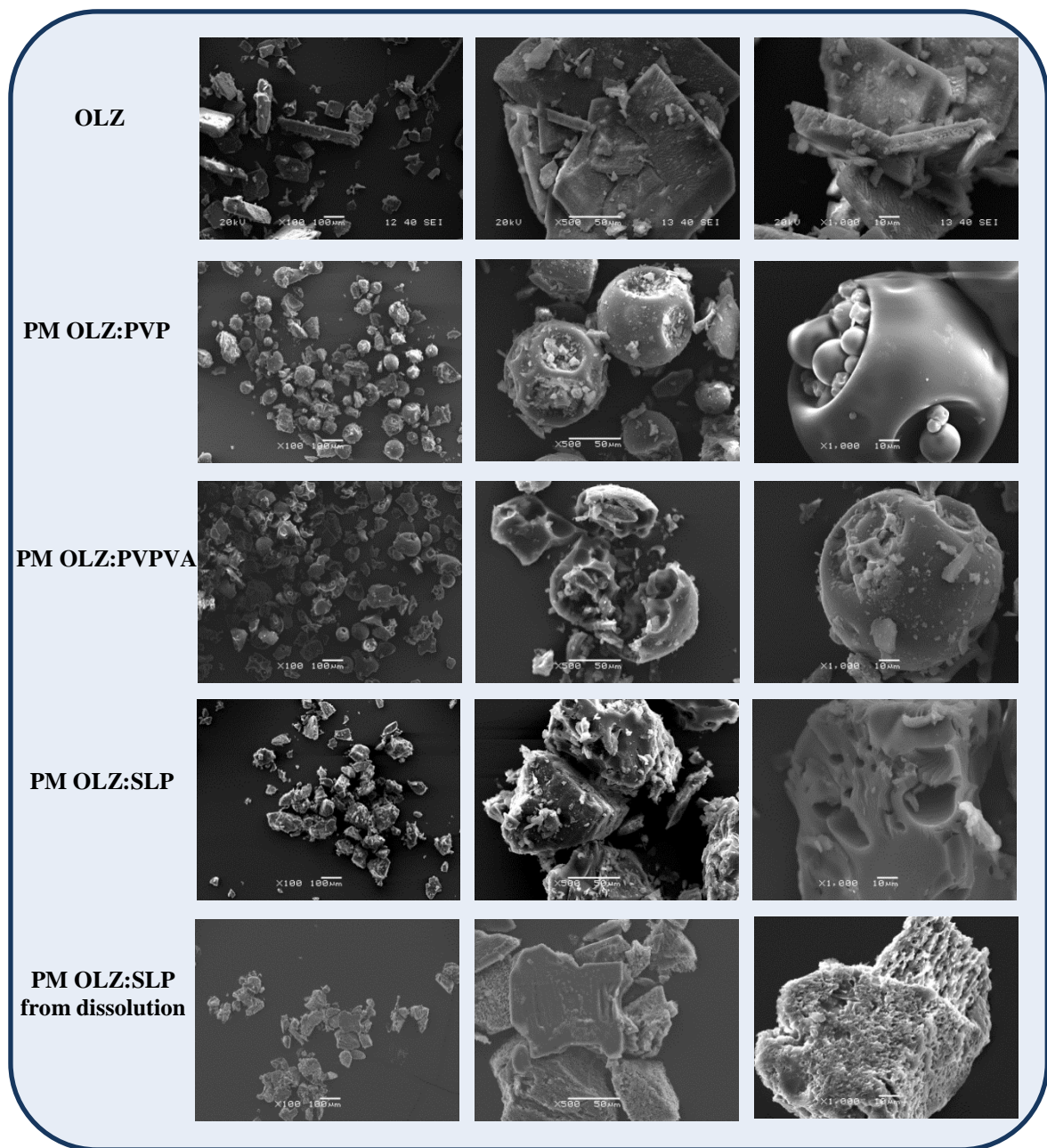
Figure 7.12: SEM microphotographs of pure OLZ, PMs of OLZ with each polymer and finally the particles collected from the dissolution vessel of 50% PM OLZ:SLP after 120 min of testing.

7.3.5 Polymer Effect on the Inhibition of OLZ Crystallisation in HME Solid Dispersions

In this study, the physical stability of all prepared solid dispersion systems was investigated under storage at accelerated conditions, testing at the same time the influence of high humidity (75% RH) and temperature (40 $^{\circ}$C) on the recrystallisation of OLZ.

The stability of OLZ-polymer systems as a function of time was found to depend greatly on the polymer physicochemical properties. Overall, OLZ:SLP system extruded at 180 $^{\circ}$C showed the greatest stability of all solid dispersion systems studied with only the first signs of drug recrystallisation observed in DSC and under SEM after the three months of storage, although no crystals were detected in XRPD.

During the stability studies, the 50% drug-loading systems with PVPVA and SLP extruded at 160 $^{\circ}$C, even though not fully amorphous after its preparation, did not show an increase in their crystal content during storage. This was confirmed by the enthalpy of melting of OLZ Form I that remained nearly constant during the entire period of study and by the OLZ crystallinity in XRPD. The sample 50% OLZ:PVP was prepared fully amorphous at the same extrusion temperature, and it was proved amorphous until two months of storage, when the first evidence of recrystallised OLZ started to be noticed. The 50% OLZ:PVPVA prepared at 180 $^{\circ}$C showed a similar stability profile to the 50% OLZ:SLP extruded at the same temperature, although some evidence of crystalline OLZ was possible to be detected in XRPD after the three months of storage, contrarily to the SLP system. Figure 7.13 shows the XRPD data for all the 50% systems after being stored for three months under 75% RH/40 $^{\circ}$C. All the 20% drug-loaded extrudates with PVPVA and SLP remained amorphous during the whole study according to the DSC analysis, however due to the high percentage of polymer they formed a coalescence masses which complicates XRPD and SEM analysis.

Generally, greater stability of solid dispersion systems is often linked to the high T_g of the polymer. In the present case however, the polymer T_g does not appear to be the key factor influencing and predicting the recrystallisation tendency of OLZ. In fact, in this study SLP has the lowest T_g compared to PVP and PVPVA but showed the greatest stability. Also the formation of specific interactions, such as hydrogen bonding, between the drug and the

polymer have been extensively correlated with greater stability of solid dispersions and better inhibitors on the crystal growth of APIs (Matsumoto and Zografi, 1999; Khougaz and Clas, 2000; Kestur and Taylor, 2010). Although, some controversies were found related to this matter and further investigations should aim at quantifying the degree of these bonds between drug and polymer to improve predictions on physical stability of melt extrudates (Forster et al., 2001a). As shown earlier, the extrudates prepared with SLP did not give any evidence of hydrogen bonding using FTIR spectroscopy as compared to the extrudates prepared with the other polymers. As a result, the existence of intermolecular interactions might not be a relevant factor in the stabilisation mechanism between OLZ and each polymer system although this should not be completely discarded.
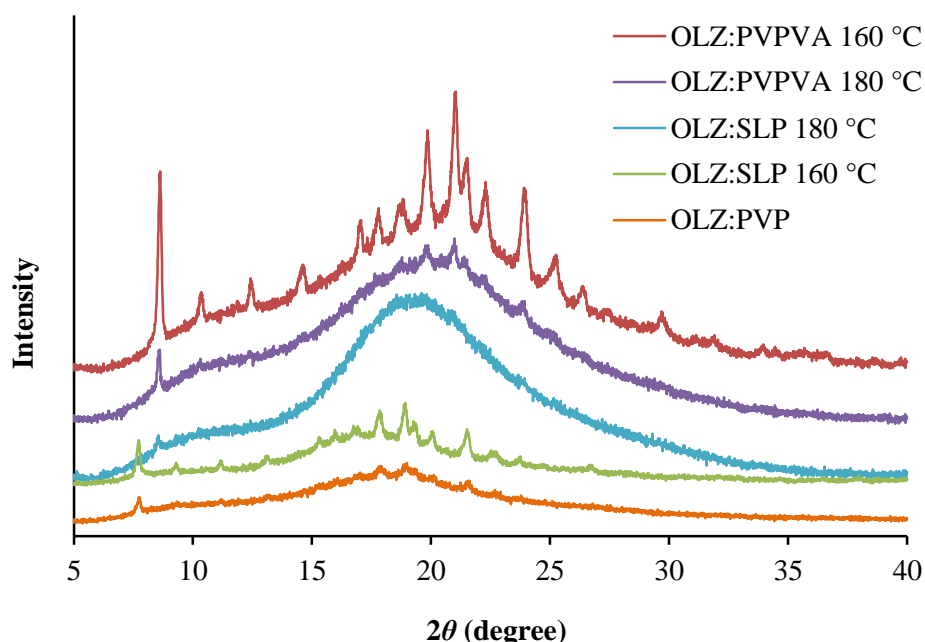
Figure 7.13: XRPD data collected for the 50% formulations (both extrusion temperatures) after three months of storage at 75% RH/40 °C. For simplicity, the legend on the plot follows the same order as the presented curves.

Following the preceding discussions, two other factors need to be considered, the molecular weight (MW) and the hygroscopic nature of the polymer. The MW of a polymer is expected to influence viscosity and therefore reduce crystal growth. In addition, hygroscopicity is always linked to instability, as it increases molecular mobility and therefore tendency for nucleation to happen. In order to evaluate the hygroscopic tendency

of each fully amorphous system, DVS studies were conducted. The results obtained showed that after 16 h at 98% RH/25 ^{o}C, PVP solid dispersion had a water uptake of around 58%, followed by PVPVA system with 44% and finally SLP samples with only an increase in weight of 20%. Therefore, it seems likely that the stabilisation of OLZ solid dispersions during storage is highly dependent on the high MW and lower hygroscopic nature of SLP, when compared with the other polymers.

Absorption of high amounts of water can lead to the formation of drug-rich and polymer-rich amorphous phase as a result of moisture-induced drug-polymer immiscibility (Rumondor et al., 2009; Konno and Taylor, 2008; Van Eerdenbrugh and Taylor, 2010). In this study, the use of standard DSC with a heating rate of 10 ^{o}C/min in order to avoid dissolution of OLZ in the polymer matrix upon heating, did not allow the identification of any phase separation in the PVP and PVPVA systems, which can be considered in further studies.

Figure 7.14 depicts the scanning electron micrographs of the surface and internal (cross-section surface) appearance of the 50% drug-loaded extrudates, fresh and after three months of storage. The fresh extrudates prepared with PVPVA and SLP at 160 ^{o}C showed a distribution of OLZ crystals, either on the surface and cross-section, confirming the incomplete melting of the drug during extrusion. In contrast, the formulations extruded at 180 ^{o}C showed a complete smooth surface without any evidence of crystalline OLZ. For the system prepared with PVP, although no crystals were identified, the surface of these extrudates was not completely smooth as a consequence of the difficult extrusion process of this system. For all the 20% drug-loaded extrudates no signal of crystallinity was observed (data not shown). After three months of storage, the PVP systems showed evidence of recrystallised OLZ either on the surface and cross-section of the extrudates. Similar observations to the fresh samples were obtained for the PVPVA and SLP systems extruded at 160 ^{o}C. The samples extruded at 180 ^{o}C showed clearly recrystallisation of OLZ on the surface of the extrudates, but no sign on the internal cross-section.

	Fresh samples	Aged samples after being stored for three months at 75% RH/40 ^{o}C
OLZ:PVP		
OLZ:PVPVA 160 ^{o}C		
OLZ:SLP 160 ^{o}C		
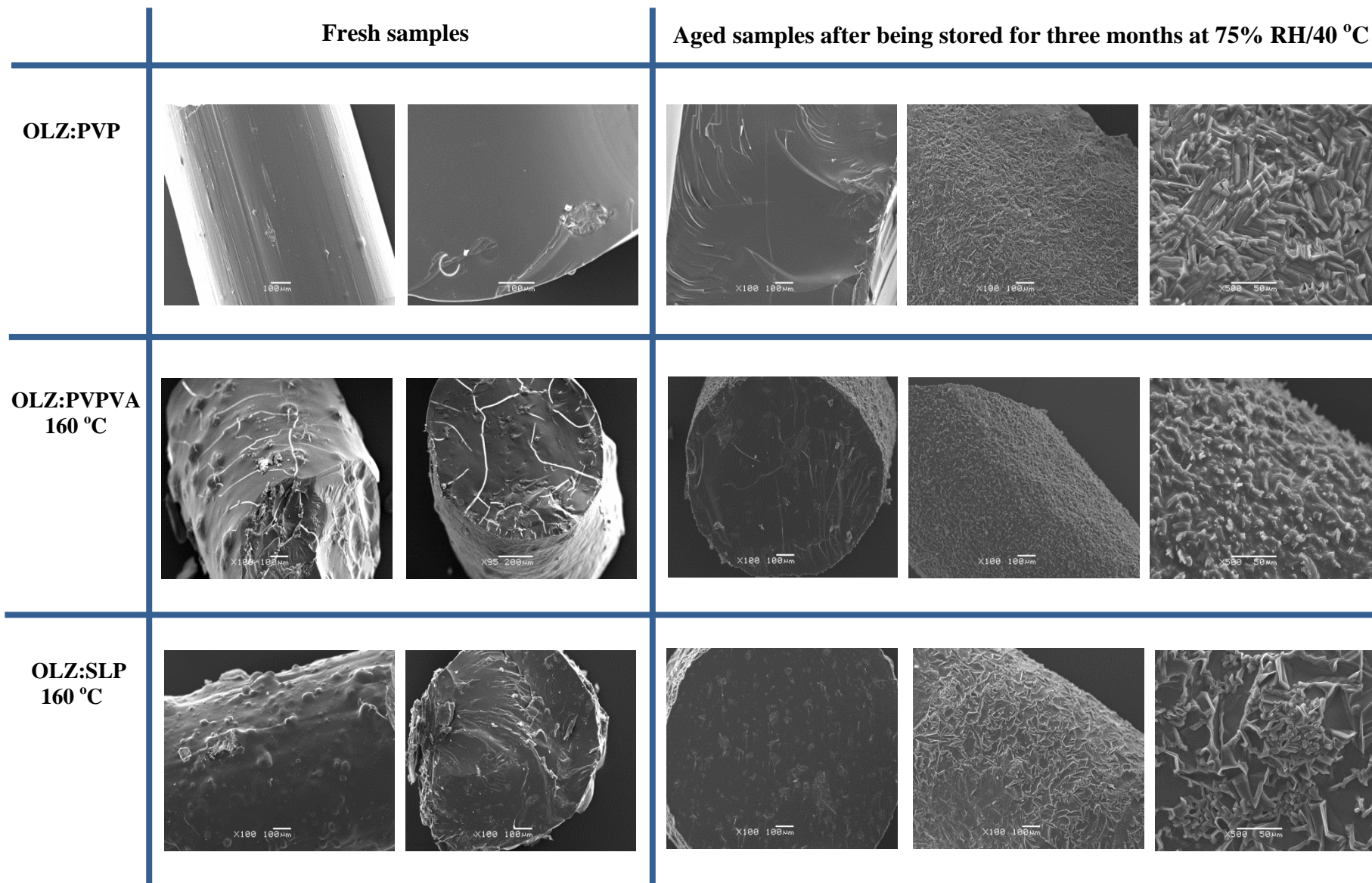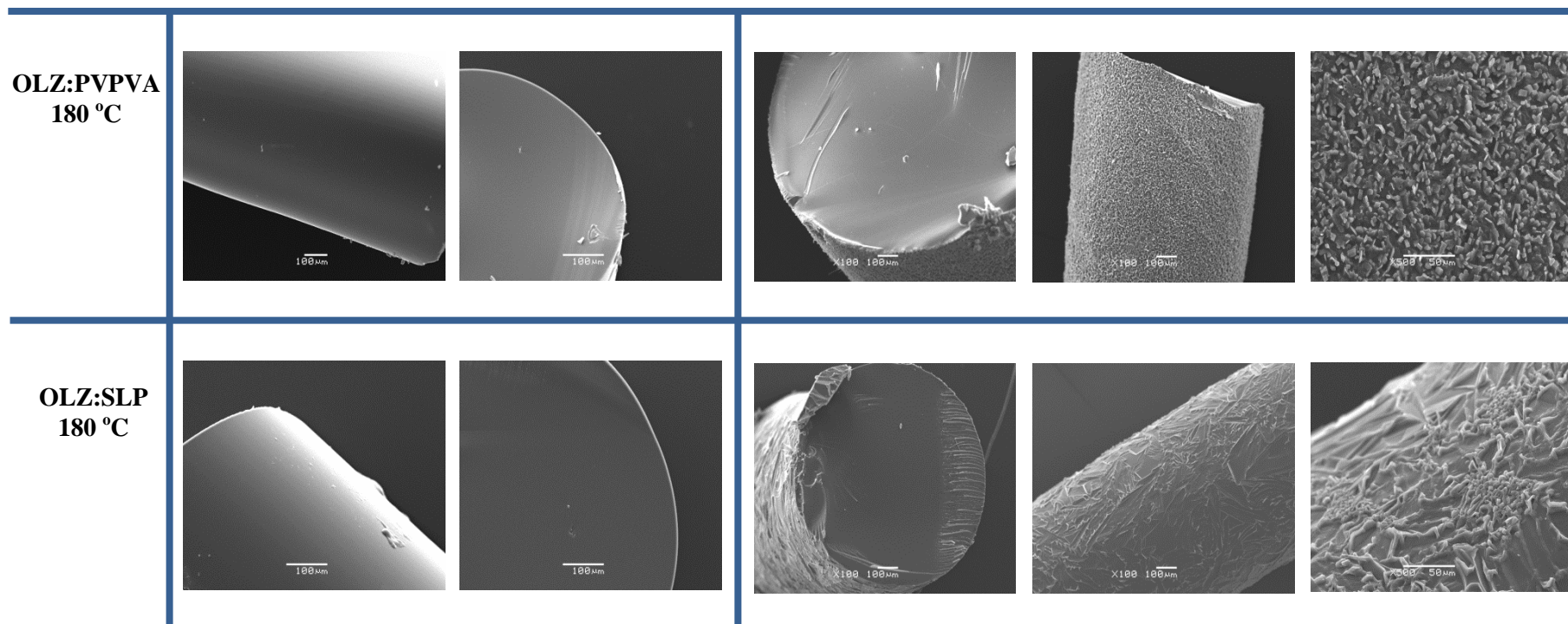
Figure 7.14: SEM microphotographs of 1:1 fresh solid dispersion systems (surface and cross-section) and after storage at 75% RH/40 °C for three months (cross-section and surface). The extrusion temperature for the PVPVA and SLP systems is also stated.

7.4   Conclusions

Overall, the predicted miscibility and interaction between OLZ and each polymer calculated based on MPD and Hansen solubility parameters agreed with the experimental results in that at the same extrusion temperature (160 ^{o}C) and drug loading (50%), PVP was found to have the greatest miscibility with OLZ leading to the molecular dispersion of OLZ. In contrast, the extrudates prepared with PVPVA and SLP, under the same conditions, crystalline OLZ was detected via DSC, XRPD and SEM observations. At a higher extrusion temperature, both systems with PVPVA and SLP were characterised as one-phase systems with a single T_g value observed in DSC. This therefore demonstrates the complex interplay between miscibility and processing but also demonstrates that there is a role for solubility parameter and MPD predictions in anticipating experimental findings.

In terms of the dissolution performance, the general assumption that a higher dissolution rate is obtained when the drug is completely converted to an amorphous form is not consistent with the findings presented in this chapter. In this specific case, it was noted that at 50% loading and 160 ^{o}C processing, PVP showed the slowest release despite being the only fully amorphous system. It was interesting to note that no clear relationship was found between dissolution and drug crystallinity or indeed with processing temperature, with the release rates being much more dependent on the choice of polymer. Therefore, in this case at least, it may be the behaviour of the polymer that determines dissolution performance rather than the physical state of the drug.

The chemistry of the polymer was also found to determine the stability of the OLZ solid dispersion systems. The extrudates prepared with SLP were found to have the greatest stability, despite the lower T_g of this polymer and the inexistence of any specific interactions detectable by FTIR between OLZ and SLP. Properties such as the high MW and low hygroscopicity of this polymer might be responsible for the greatest stability observed.

Another interesting finding is related to the SEM observations of the aged HME samples. The 50% drug loaded formulations showed that the recrystallised crystals of OLZ differed on their shape and arrangement on the surface of the extrudates. This observation is system dependent as expected due to the different polymer chemistry. Local thermal analysis

(LTA) might be a helpful technique to be used in further studies, enabling, if present, the identification of different polymorphic forms of OLZ. This might be significantly important in the case of SLP which showed a limited crystal growth after three months of storage.

8   CONCLUSIONS AND FUTURE WORK

Learn from yesterday, live for today, hope for tomorrow.
The important thing is not to stop questioning.
Curiosity has its own reason for existing.

Albert Einstein

8.1   Summary and Concluding Remarks

Polymorphism and pseudopolymorphism are nowadays recognised as an important phenomenon during the early research screening and throughout development. This has been a result of successful scientific improvements, strong regulatory and economic demand. Although methods for polymorph control and characterisation are still imperfect, more sophisticated and sensitive characterisation techniques are now available to control this important and challenging problem. The work presented in this thesis has reiterated the importance of having integrated characterisation strategies, as a way to achieve an in-depth understanding of the structure-property relationship in organic solids. This scientific approach was applied throughout this thesis for the solid state characterisation of olanzapine and paroxetine HCl, and the respective prepared systems.

Paroxetine HCl has been in the market for more than two decades and it has been extensively used for the treatment of depression, general anxiety and social phobia. Despite its widespread use, the physicochemical properties of the two crystalline forms of this drug, Form I and Form II, have not been fully investigated. Paroxetine HCl Form II was assigned in previous works to be an unstable anhydrate form with a very hygroscopic behaviour and paroxetine HCl Form I is a stoichiometric hemihydrate and the most stable form (Buxton et al., 1988; Barnes et al., 1988).

In Chapter 3, a broad range of physical characterisation techniques were used in order to obtain a detailed view of the effect and interaction of water with the structure of Form II. High water content ($\approx 3.83\%$, 0.80 mol of water/mol of paroxetine HCl) and an unusual thermal behaviour, presented the first doubt on the designation of Form II as an anhydrous form. It was then crucial to clarify the relationship between water and Form II. VH-XRPD was the key technique in this study since it provided enough evidence of hydrate formation as only changes in lattice spacings were observed accompanying the uptake of water. This fact indicated that Form II exists as a non-stoichiometric hydrate and its designation as an anhydrous form is no longer valid.

Overall, this work has highlighted the importance of distinguishing between water adsorption, as a consequence of a hygroscopic nature, and hydrate formation. Also

important to emphasise that Form II was a non-stoichiometric hydrate with characteristics and behaviour similar to channel hydrates, although these channels were not found in the structure at a molecular level. Furthermore, these results reiterate the importance of using a combination of several techniques and taking advantage of the available computational tools in the characterisation of pharmaceutical materials, particular with non-stoichiometric hydrates as they often produce a further level of complexity.

Continuing within the solid state characterisation of paroxetine HCl, the conditions that led to the dehydration of Form I were investigated and a new anhydrous form, structurally different than the dehydrated Form II, was identified as a consequence of this process (Chapter 4). The dehydration process of Form I was far more complex than initially expected and the dehydrated product was found to be very unstable and quickly rehydrated to the initial hydrate Form I. With these challenges, structural investigation of the dehydrated Form I was performed using VT-XRPD which allowed the dehydration process to be carried out *in situ*. These results showed that the patterns obtained at high temperatures were different than those of the dehydrated Form II, indicating that the two forms were structurally different. In addition, the pattern of the dehydrated Form I was highly similar to the hydrate Form I, with the unit cell parameters remaining the same, just smaller in volume as a consequence of dehydration.

From the work presented in this chapter, a new anhydrous form of paroxetine HCl has been identified. This new form is, however, extremely unstable and difficult to handle under normal environment conditions. The structure solution of the new anhydrate from powder diffraction data was not possible. In addition, the use of single crystal X-ray technique was unsuccessful as the crystal broke during heating. Nevertheless, important insights and understanding on the dehydration of pharmaceutical compounds can be further applied in the particular case of stoichiometric hydrates with a peculiar behaviour of dehydration.

After the fundamental characterisation studies, paroxetine HCl Form II was converted into an amorphous state via a melt quench method. From a pharmaceutical perspective, amorphous materials can improve solubility and therefore bioavailability of APIs. However, any potential benefits of amorphous systems are counterbalanced by their metastable nature and intrinsic tendency to recrystallise when submitted to stress conditions. In this work thermodynamic and kinetic parameters were investigated and

applied to the characterisation of the prepared amorphous form. Although theoretical approaches have been extensively used on the prediction of amorphous compounds as glass formers, limited work has been carried out in order to correlate those approaches with the experimental physical stability. Parameters such as Kauzmann temperature (T_K), fragility (*m*) and relaxation time (τ) classified the amorphous paroxetine HCl prepared from Form II as a fragile glass. The predicted fragility of this form was in agreement with the experimental results obtained during physical stability studies and also after prolonged exposure to water during the solubility experiments. In addition, the storage conditions, more specifically the water vapour pressure, was found to influence the pathway of recrystallisation from the amorphous state. This might be of practical importance during the stability studies of APIs converted into an amorphous state.

Later in this thesis (Chapters 6 and 7), attention was paid to the parameters involved in the formulation of drug products into solid dispersions. As referred, single amorphous phase compounds are usually tempered by a number of potential drawbacks, mainly physical and chemical instability. The preparation of amorphous solid dispersions represents, nowadays, the ultimate strategy to stabilise those systems. Numerous parameters must be accounted when intending to prepare amorphous solid dispersions.

A thorough investigation on the preparation, performance and stability of solid dispersion systems prepared with paroxetine HCl Form I and II was carried out. PVPVA was selected as the carrier and the influence of preparation techniques (spray drying (SD) and hot melt extrusion (HME)) was also evaluated. Melting point depression approach was used to predict the miscibility between each pseudopolymorphic form of paroxetine HCl and PVPVA. Interestingly, Form I was found to be miscible with PVPVA whereas Form II did not show any depression on the onset melting in the presence of the polymer. Regardless the theoretical predictions, the experimental results showed that both forms were able to be molecularly dispersed within the polymer carrier, with a single T_g value observed in DSC and a halo pattern in XRPD. This was an interesting finding and shed some light on the validity of the use of melting point depression method in the prediction of miscibility and interaction in drug-polymer blends. The influence of the preparation method was observed on the thermal behaviour of the fresh samples and on the propensity for recrystallisation during the stability studies. Differences concerning the dissolution performance and stability of the SD and HME systems were also encountered. Higher dissolution rates were

observed for the spray dried samples, either containing Form I or Form II, relative to the HME samples. However, the situation was reversed in terms of stability.

The work on the formulation into solid dispersions was endeavoured to further study the impact of different polymers on the processing, dissolution behaviour and physical stability of a BCS Class II drug (olanzapine, OLZ) using HME. Chapter 7 addressed the different parameters that should be taken into consideration when preparing solid dispersions in particular using HME. Miscibility between the drug (OLZ) and each polymer system (PVP, PVPVA and Soluplus® (SLP)), drug loading, extrusion temperatures and the chemical structure of the polymer were found to be of great importance in determining the solid state of the prepared systems (fully or partially amorphous systems). Interestingly in the particular case of OLZ, the physical solid state of the final products did not have any significant influence on their dissolution performance. These findings suggested that it was the nature of the polymer rather than the physical state of the drug in the dispersed system that determined the dissolution profiles. Despite the plethora of reports suggesting that high dissolution rates can be achieved when the drug is dispersed in the polymer carrier at a molecular lever, further investigation in this field with more care is required. Furthermore, the physicochemical properties of the selected polymers also play an important role in the stabilisation of these kinds of systems. In particular, parameters such as high T_g and the ability to establish hydrogen bonding with the drug are not always strictly necessary, at least in this case, to achieve great stabilisation. Indeed, the systems prepared with SLP were found to be more stable than those prepared with PVP or PVPVA, despite its lower T_g and its inability of establishing hydrogen bonding with OLZ. Therefore, more attention should be paid to properties such as molecular weight and lower hygroscopic nature when developing solid dispersion systems.

Overall this work provided important insights into formulating poorly soluble APIs into solid dispersions. The mechanisms behind the dissolution enhancement are complex and formulation dependent. The selection of a suitable polymer in order to maximise the potential advantages associated to solid dispersions should be done carefully. In addition, the formulation of solid dispersions containing the API in a highly crystalline state might be a promising strategy, at least in certain cases, to improve both dissolution and stability of solid dispersions.

8.2   Recommendations for Future Work

Whilst carrying out this Project, a number of possible areas were identified and can be further investigated. However, due to the limited time available or because they were outside the scope of this research, they were not considered in this thesis.

The first two chapters of this thesis focused on the solid state characterisation of two pseudopolymorphic forms of paroxetine HCl. The knowledge acquired here could benefit the characterisation and/or identification of non-stoichiometric hydrates as misinterpretations are likely to happen with this particular class of compounds.

In terms of the dehydration studies carried out with paroxetine HCl Form I, although the new anhydrate form was found to be highly unstable, the determination of its crystal structure could perhaps give important insights in correlating the determined crystalline arrangement with its extremely high hygroscopic behaviour and thereby instability. Since the use of single crystal X-ray could not be used due to the breakdown of the crystal of Form I during the heating up process, the use of synchrotron radiation (high resolution XRPD) might be a feasible possibility.

Concerning the formulation studies carried out in this thesis, a few aspects could be further investigated. Starting with the solid dispersions systems prepared with paroxetine HCl. The understanding, at a molecular level, of the interactions between PVPVA and paroxetine HCl, could help to improve molecular modeling dynamics techniques that allow to predict, in a more reliable manner, drug-polymer miscibility.

Finally, with the studies carried out in the last chapter, two possible areas can be taken further. The first one would include the use nano-thermal analysis (nano-TA) to analyse in more detail the spatial distribution of crystalline/amorphous material on the surface of the extrudates. In addition, this technique would provide important information in distinguishing between the different crystalline forms of OLZ, in case more than one form was present, since this was not possible by using bulk characterisation techniques (e.g. DSC). Secondly, the development of solid dispersion systems containing more than one carrier (concept of polymer blend), in particular combining Soluplus® (low hygroscopicity) with PVP based system polymers (higher solubilisation properties) could be a way to

improve both dissolution and stability. In addition, the generation of crystalline nano-suspensions of OLZ within that polymer matrix might be a fruitful strategy to formulate this drug.

9 APPENDICES

9.1 Appendix A – Chapter 3

Table A1 lists the unit cell dimensions of paroxetine HCl Form II as a function of relative humidity (RH). Representative Pawley-fits are shown in Figure A1.

Table A1: Unit cell dimensions of paroxetine HCl Form II determined from XRPD measurements at various relative humidity levels. *Rwp* indicates the quality of the Pawley-fit.

	Relative humidity (%)	a (Å³)	b (Å)	c (Å)	β (°)	Volume (Å³)	*Rwp*
Sorption	10	11.374(2)	5.9380(11)	13.828(2)	100.876(13)	917.1(3)	3.70
	30	11.416(3)	5.9757(13)	13.880(3)	100.499(15)	931.0(4)	3.84
	40	11.419(3)	5.9839(13)	13.895(3)	100.485(14)	933.6(4)	3.79
	50	11.424(3)	5.9869(13)	13.902(3)	100.472(14)	935.0(4)	3.80
	60	11.425(4)	5.9889(13)	13.907(3)	100.462(14)	935.7(4)	3.78
	70	11.430(4)	5.9914(13)	13.916(2)	100.471(13)	937.1(4)	3.72
	80	11.431(3)	5.9945(13)	13.921(2)	100.473(13)	938.0(4)	3.76
	90	11.435(3)	5.9974(12)	13.925(2)	100.479(12)	939.0(4)	3.65
Desorption	25	11.418(3)	5.9712(11)	13.880(2)	100.585(12)	930.2(3)	3.68
	15	11.403(3)	5.9576(11)	13.866(2)	100.721(12)	925.5(3)	3.75
	5	11.354(2)	5.9295(10)	13.811(2)	100.987(11)	912.8(3)	3.53
	1	11.325(2)	5.9140(9)	13.788(2)	101.207(12)	905.8(3)	3.65
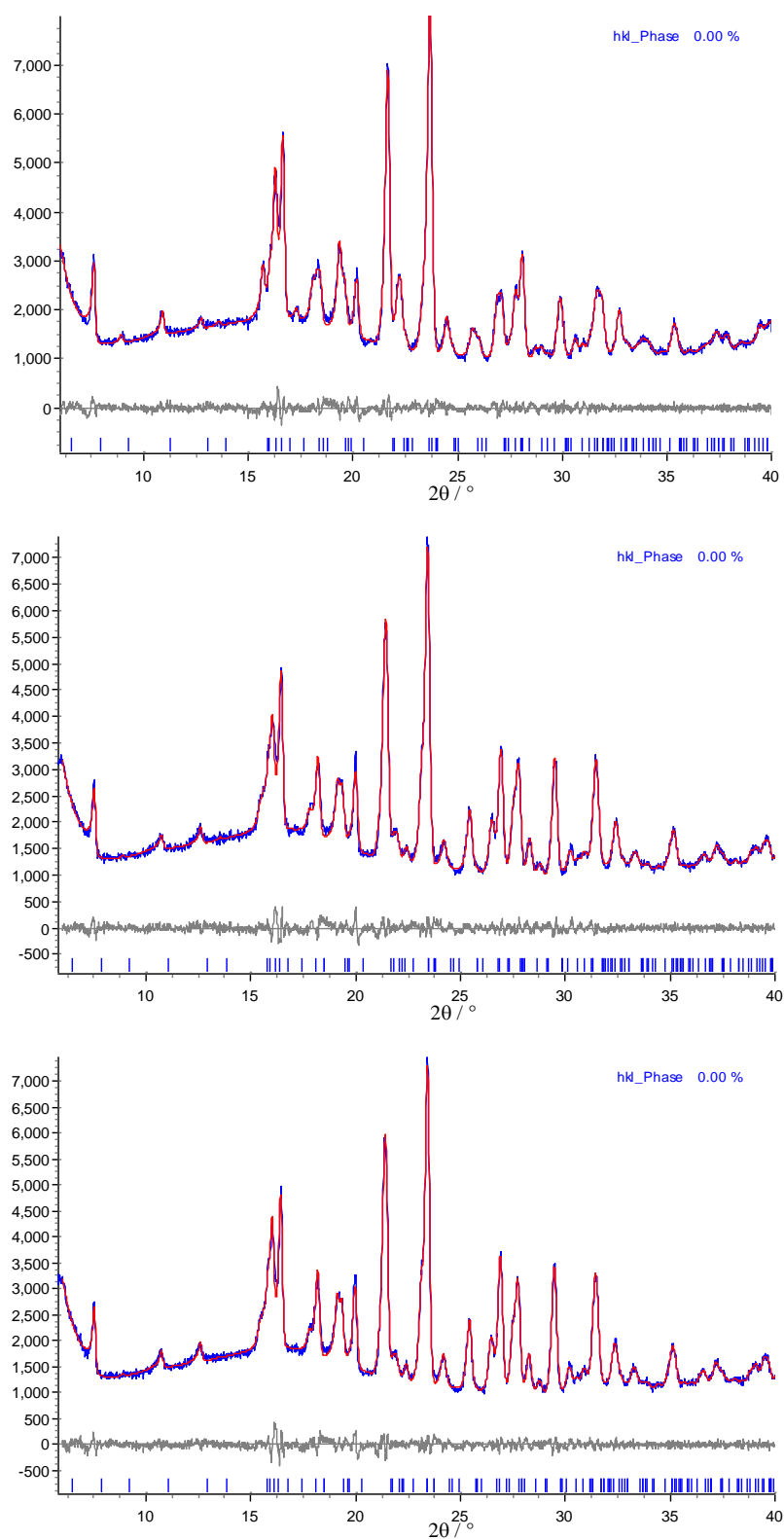
Figure A1: Experimental XRPD pattern (blue), fitted curve (red) and difference (grey) obtained in the Pawley fit for data measured at 1% RH (top), 50% RH (middle) and 90% RH (bottom).

9.2   Appendix B – Chapter 4

Analysis of Diffraction Patterns

Pawley refinement (Coelho, 2007) was performed at each temperature either using the unit cell parameters of the hemihydrate Form I or the new parameters obtained for the anhydrous form. The results of the fitting are presented below in Figure B1. The unit cell parameters obtained are presented in Table B1.

a) Heating 25 $^{\mathrm{o}}$C/1 h – Unit cell parameters of the hydrate Form I
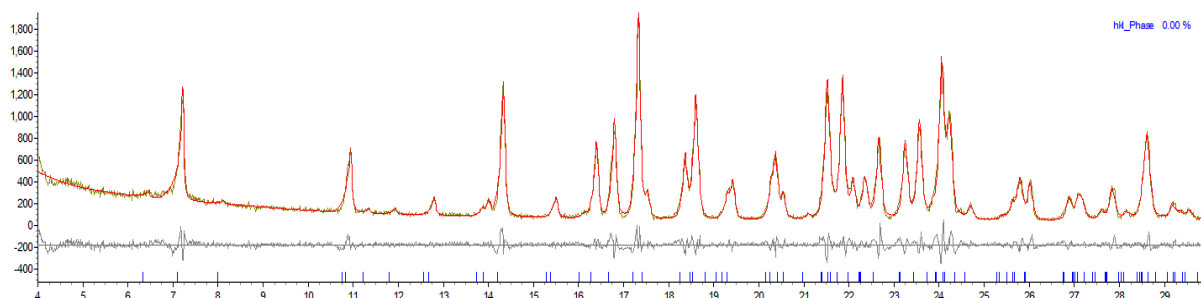
b) Heating 50 $^{\mathrm{o}}$C/1 h – Unit cell parameters of the hydrate Form I
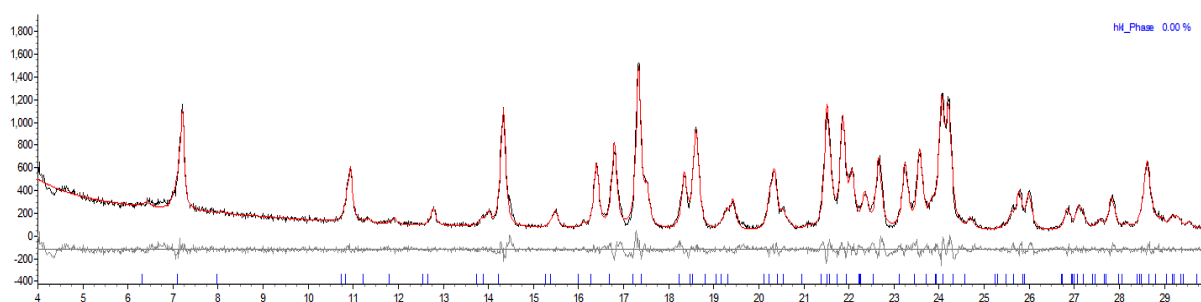
c) Heating 75 ^{o}C/1 h – Unit cell parameters of the hydrate Form I
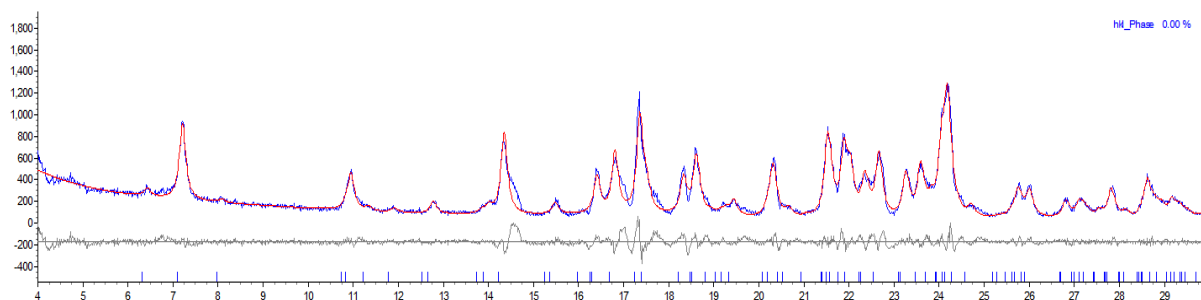
d) Heating 100 ^{o}C/5 h – Unit cell parameters of the hydrate Form I
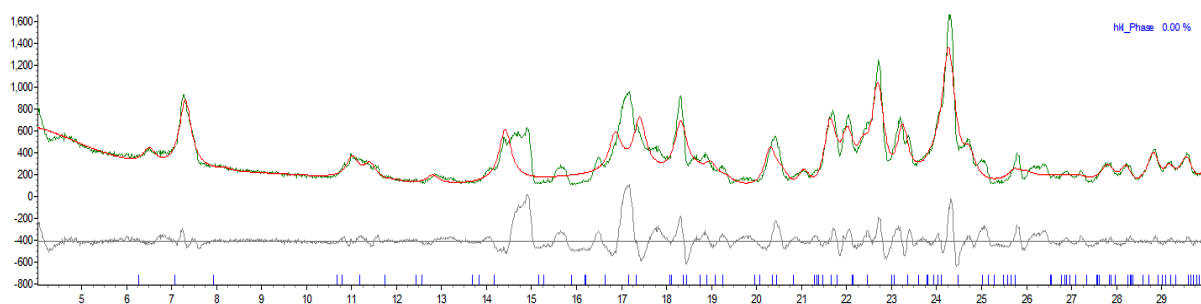
e) Cooling 100 ^{o}C/1 h – Unit cell parameters of the new anhydrous form
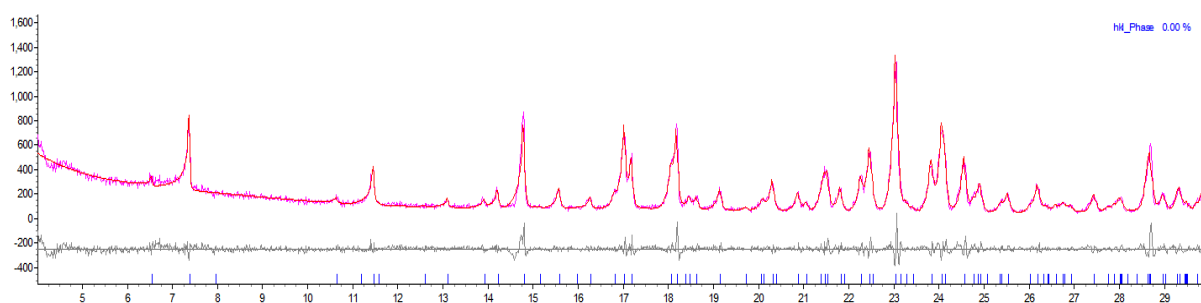
f) Cooling 75 ^{o}C/1 h – Unit cell parameters of the new anhydrous form
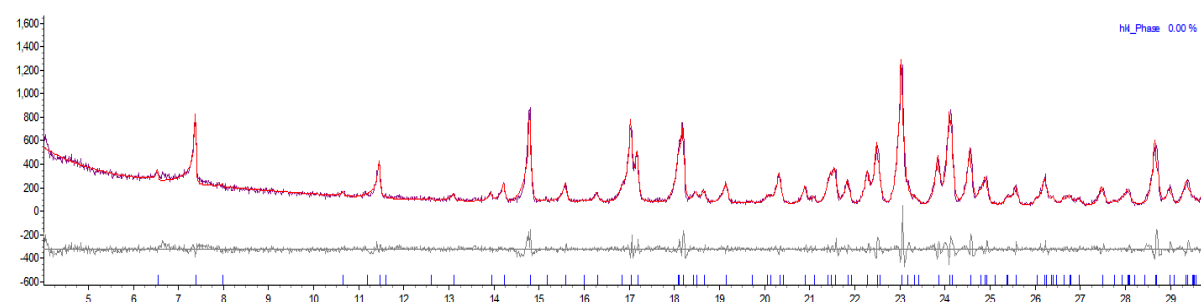
g) Cooling 50 ^{o}C/1 h – Unit cell parameters of the new anhydrous form
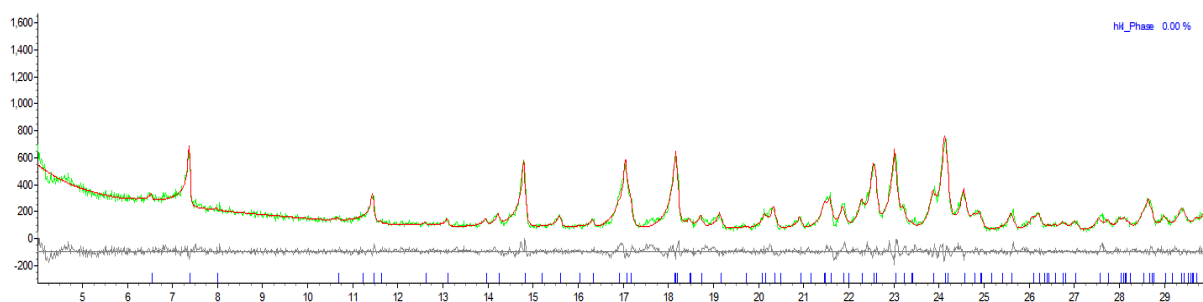
h) Cooling 25 ^{o}C/1 h – Unit cell parameters of the new anhydrous form

i) Cooling 25 ^{o}C/6 h – Unit cell parameters of the new anhydrous form
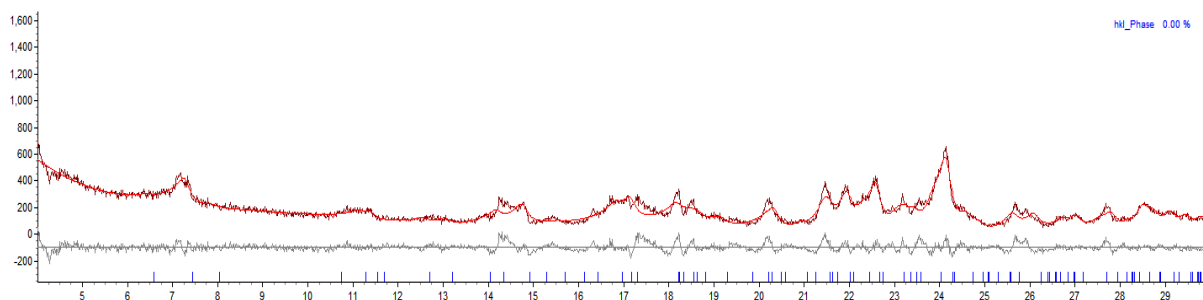
j) Cooling 25 °C/6 h – Unit cell parameters of the hydrate Form I
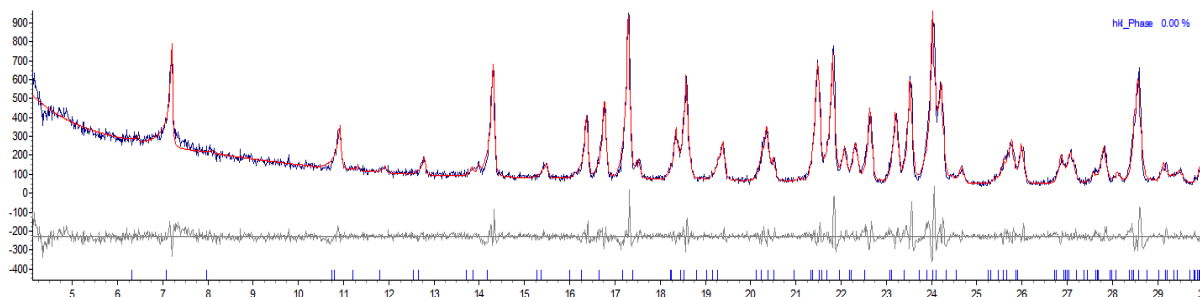
Figure B1: Experimental XRPD pattern, fitted curve (red) and difference (grey) obtained in the Pawley fit.

Table B1 presents the unit cell parameters obtained at each temperature. The rows in red are less reliable due to the poor fit. During heating the unit cell parameters of the hydrate Form I (hyd) were used and during cooling the unit cell parameters of the new anhydrous form (anh), except for the last measurement at 25 °C/6 h, where the parameters of the hydrate cell were used.

	Temperature (°C)	*a* (Å)	*b* (Å)	*c* (Å)	*β* (°)	V (Å³)
Heating	25 °C/1 h (hyd)	14.615(2)	10.1819(11)	13.0419(17)	107.194(5)	1854.0(4)
	50 °C/1 h (hyd)	14.632(2)	10.1864(14)	13.044(2)	107.273(7)	1856.5(5)
	75 °C/1 h (hyd)	14.655(5)	10.191(3)	13.039(5)	107.411(13)	1858.2(12)
	100 °C/5 h (hyd)	14.75(3)	10.227(18)	13.09(3)	107.44(9)	1884(7)
Cooling	100 °C/1 h (anh)	14.400(2)	10.5362(15)	12.7706(13)	110.490(5)	1814.9(4)
	75 °C/1 h (anh)	14.392(2)	10.5184(14)	12.7572(13)	110.396(5)	1810.1(4)
	50 °C/1 h (anh)	14.385(2)	10.473(2)	12.738(2)	110.297(7)	1799.8(6)
	25 °C/1 h (anh)	14.291(16)	10.439(12)	12.662(13)	110.37(7)	1771(4)
	25 °C/6 h (anh)	14.427(5)	10.464(3)	12.711(5)	110.866(14)	1793.1(11)
	25 °C/6 h (hyd)	14.6253(16)	10.1862(13)	13.0620(16)	107.150(5)	1859.4(4)

Dehydration Kinetics

Table B2 and Figure B2 represent an example of the E_a calculation for a single value of conversion fraction, (α) by using OFW method with non-isothermal data. The procedure is repeated for the all the conversion values.

Table B2: Calculations using OFW method for an individual value of α.

β (K/min)	1	2	3	4	5
Temperature (K)	344	352	354	357	361
log (β)	0	0.69	1.10	1.39	1.61
1000/T (K^{-1})	2.91	2.84	2.82	2.80	2.77
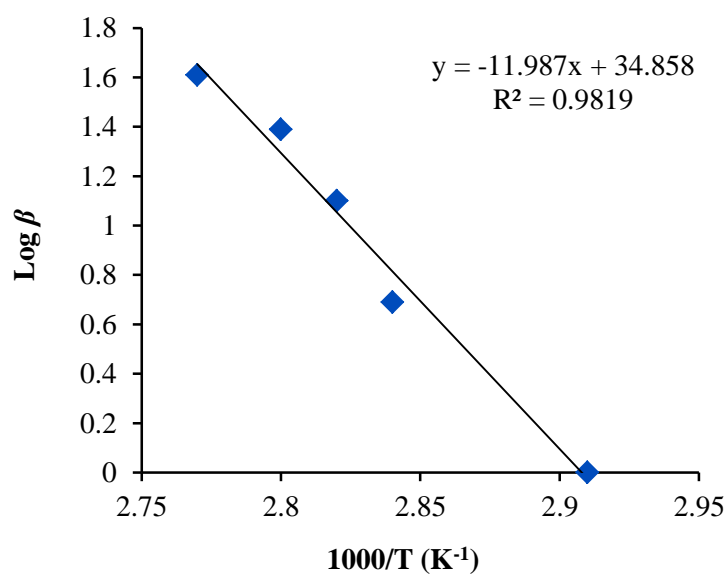
Figure B2: Plot of the OFW method, for a single value of conversion at the different heating rates 1, 2, 3, 4 and 5 K/min.

Table B3 lists the reaction models considered in this work, to which the isothermal data was fitted.

Table B3: Reaction models used in solid-state reaction kinetics.

Model	Reaction Model	Symbol	Differential Form f(α)	Integral Form g(α)
Nucleation	Power law	P1	$4\alpha^{\frac{3}{4}}$	$\alpha^{\frac{1}{4}}$
	Power law	P2	$3\alpha^{\frac{2}{3}}$	$\alpha^{\frac{1}{3}}$
	Power law	P3	$2\alpha^{\frac{1}{2}}$	$\alpha^{\frac{1}{2}}$
	Power law	P4	$\left(\frac{2}{3}\right)\alpha^{-\frac{1}{2}}$	$\alpha^{\frac{3}{2}}$
	Avrami-Eroféev (n=1.5)	A3/2	$\left(\frac{3}{2}\right)(1-\alpha)[-\ln(1-\alpha)]^{\frac{1}{3}}$	$[-\ln(1-\alpha)]^{\frac{2}{3}}$
	Avrami-Eroféev (n=2)	A2	$2(1-\alpha)[-\ln(1-\alpha)]^{\frac{1}{2}}$	$[-\ln(1-\alpha)]^{\frac{1}{2}}$
	Avrami-Eroféev (n=3)	A3	$3(1-\alpha)[-\ln(1-\alpha)]^{\frac{2}{3}}$	$[-\ln(1-\alpha)]^{\frac{1}{3}}$
	Avrami-Eroféev (n=4)	A4	$4(1-\alpha)[-\ln(1-\alpha)]^{\frac{3}{4}}$	$[-\ln(1-\alpha)]^{\frac{1}{4}}$
Geometrical Contraction	Zero-order (Polany-Winger Eq.)	R1	1	α
	Phase-Boundary controlled reaction - contracting area	R2	$2(1-\alpha)^{\frac{1}{2}}$	$[1-(1-\alpha)^{\frac{1}{2}}]$
	Phase-Boundary controlled reaction - contracting area	R3	$3(1-\alpha)^{\frac{2}{3}}$	$[1-(1-\alpha)^{\frac{1}{3}}]$
Reaction-order	First-order (Mampel)	F1	$(1-\alpha)$	$-\ln(1-\alpha)$
	Three-halves order	F3/2	$(1-\alpha)^{\frac{3}{2}}$	$2[(1-\alpha)^{-\frac{1}{2}}-1]$
	Second-order	F2	$(1-\alpha)^2$	$(1-\alpha)^{-1}-1$

	Third-order	F3	$(1-\alpha)^3$	$(\frac{1}{2})[(1-\alpha)^{-2}-1]$
Diffusion	One-dimensional diffusion	D1	$\left(\dfrac{1}{2}\right)\alpha$	α^2
	Two-dimensional diffusion (Valensi Eq.)	D2	$1/[-\ln(1-\alpha)]$	$(1-\alpha)\ln(1-\alpha)+\alpha$
	Three-dimensional diffusion (Jander Eq.)	D3	$3(1-\alpha)^{\frac{1}{3}}/2[(1-\alpha)^{\frac{-1}{3}}-1]$	$[1-(1-\alpha)^{1/3}]^2$
	Three-dimensional diffusion (Ginstling-Brousnshtein Eq.)	D4	$\left(\dfrac{3}{2}\right)[(1-\alpha)^{\frac{-1}{3}}-1]$	$(1-2\dfrac{\alpha}{3})-(1-\alpha)^{\frac{2}{3}}$

10 REFERENCES

AHLNECK, C. and ZOGRAFI, G. 1990. The molecular basis of moisture effects on the physical and chemical stability of drugs in the solid state. *International Journal of Pharmaceutics,* 62**,** 87-95.

AHLQVIST, M. U. A. and TAYLOR, L. S. 2002. Water dynamics in channel hydrates investigated using H/D exchange. *International Journal of Pharmaceutics,* 241**,** 253-261.

ALLEN, F. 2002. The Cambridge Structural Database: a quarter of a million crystal structures and rising. *Acta Crystallographica Section B,* 58**,** 380-388.

AMBIKE, A. A., MAHADIK, K. R. and PARADKAR, A. 2004. Stability study of amorphous valdecoxib. *International Journal of Pharmaceutics,* 282**,** 151-162.

ANDRONIS, V. and ZOGRAFI, G. 1998. The Molecular Mobility of Supercooled Amorphous Indomethacin as a Function of Temperature and Relative Humidity. *Pharmaceutical Research,* 15**,** 835-842.

ANGELL, C. A. 1988. Perspective on the glass transition. *Journal of Physics and Chemistry of Solids,* 49**,** 863-871.

ANGELL, C. A. 1991. Relaxation in liquids, polymers and plastic crystals - strong/fragile patterns and problems. *Journal of Non-Crystalline Solids,* 131-133**,** 13-31.

BAIRD, J. A. and TAYLOR, L. S. 2012. Evaluation of amorphous solid dispersion properties using thermal analysis techniques. *Advanced Drug Delivery Reviews,* 64**,** 396-421.

BAIRD, J. A., VAN EERDENBRUGH, B. and TAYLOR, L. S. 2010. A classification system to assess the crystallization tendency of organic molecules from undercooled melts. *Journal of Pharmaceutical Sciences,* 99**,** 3787-3806.

BARNES, R. D., WOOD-KACZMAR, M. W., CURZONS, A. D., LYNCH, I. R., RICHARDSON, J. E. and BUXTON, P. C. 1988. *Anti-depressant crystalline paroxetine hydrochloride hemihydrate*. US4,721,723.

BERNSTEIN, J. 2002. *Polymorphism in Molecular Crystals,* Oxford [England]; New York, Clarendon Press; Oxford University Press.

BHANA, N., FOSTER, R. H., OLNEY, R. and PLOSKER, G. L. 2001. Olanzapine: An Updated Review of its Use in the Management of Schizophrenia. *Drugs,* 61**,** 111-161.

BHANA, N. and PERRY, C. M. 2001. Olanzapine: A Review of its Use in the Treatment of Bipolar I Disorder. *CNS Drugs,* 15**,** 871-904.

BHARDWAJ, R. M., PRICE, L. S., PRICE, S. L., REUTZEL-EDENS, S. M., MILLER, G. J., OSWALD, I. D. H., JOHNSTON, B. F. and FLORENCE, A. J. 2013. Exploring the Experimental and Computed Crystal Energy Landscape of Olanzapine. *Crystal Growth & Design,* 13**,** 1602-1617.

BHATTACHARYA, S. and SURYANARAYANAN, R. 2009. Local mobility in amorphous pharmaceuticals—characterization and implications on stability. *Journal of Pharmaceutical Sciences,* 98**,** 2935-2953.

BIKIARIS, D. N. 2011. Solid dispersions, Part II: New strategies in manufacturing methods for dissolution rate enhancement of poorly water-soluble drugs. *Expert Opinion on Drug Delivery,* 8**,** 1663-1680.

BLEY, H., FUSSNEGGER, B. and BODMEIER, R. 2010. Characterization and stability of solid dispersions based on PEG/polymer blends. *International Journal of Pharmaceutics,* 390**,** 165-173.

BOURIN, M., CHUE, P. and GUILLON, Y. 2001. Paroxetine: A Review. *CNS Drug Reviews,* 7**,** 25-47.

BREITENBACH, J. 2002. Melt extrusion: from process to drug delivery technology. *European Journal of Pharmaceutics and Biopharmaceutics,* 54**,** 107-117.

BRITTAIN, H. G. 2009. *Polymorphism in Pharmaceutical Solids,* New Jersey, Informa Healthcare.

BROUWERS, J., BREWSTER, M. E. and AUGUSTIJNS, P. 2009. Supersaturating drug delivery systems: The answer to solubility-limited oral bioavailability? *Journal of Pharmaceutical Sciences,* 98**,** 2549-2572.

BRUNO, C. H. and GEORGE, Z. 1997. Characteristics and significance of the amorphous state in pharmaceutical systems. *Journal of Pharmaceutical Sciences,* 86**,** 1-12.

BU☐CHI 2003. Bu☐chi Mini Spray Dryer B-290 Instructions.

BUCKTON, G. and DARCY, P. 1995. The use of gravimetric studies to assess the degree of crystallinity of predominantly crystalline powders. *International Journal of Pharmaceutics,* 123**,** 265-271.

BÜHLER, V. 2005. Polyvinylpyrrolidone excipients for pharmaceuticals povidone, crospovidone, and copovidone. New York: Springer.

BU☐HLER, V. 2005. *Polyvinylpyrrolidone Excipients for Pharmaceuticals: Povidone, Crospovidone, and Copovidone,* Berlin, Springer.

BUNNELL, C. A., HENDRIKSEN, B. A. and LARSEN, S. D. 1996. *Crystal forms of a thieno(2,3-B)(1,5) benzodiazepine derivative and process for their preparation*.

BUNNELL, C. A., HENDRIKSEN, B. A. and LARSEN, S. D. 1998. *Olanzapine Polymorph Crystal Form*. U.S. patent application.

BUNNELL, C. A., LARSEN, S. D., NICHOLS, J. R., REUTZEL, S. M. and STEPHENSON, G. A. 2001. *Intermediates and process for preparing olanzapine*.

BUNNELL, C. A., LARSEN, S. D. and TUPPER, D. E. 1997. *Process and solvate of 2-methyl-thieno-benzodiazepine*. U.S. patent application.

BURGER, A. and RAMBERGER, R. 1979a. On the polymorphism of pharmaceuticals and other molecular crystals. I. Theory of thermodynamic rules. *Mikrochimica Acta,* II**,** 259-271.

BURGER, A. and RAMBERGER, R. 1979b. On the polymorphism of pharmaceuticals and other molecular crystals. II. Applicability of thermodynamic rules. *Mikrochimica Acta,* II**,** 273-316.

BURNS, M. J. 2001. The pharmacology and toxicology of atypical antipsychotic agents. *Journal of Toxicology - Clinical Toxicology,* 39**,** 1-14.

BUXTON, P. C., LYNCH, I. R. and ROE, J. M. 1988. Solid-state forms of paroxetine hydrochloride. *International Journal of Pharmaceutics,* 42**,** 135-143.

BYRN, S. R., PFEIFFER, R. R., STEPHENSON, G., GRANT, D. J. W. and GLEASON, W. B. 1994. Solid-state pharmaceutical chemistry. *Chemistry of Materials,* 6**,** 1148-1158.

CAL, K. and SOLLOHUB, K. 2010. Spray drying technique. I: Hardware and process parameters. *Journal of Pharmaceutical Sciences,* 99**,** 575-586.

CALLAHAN, J. C., CLEARY, G. W., ELEFANT, M., KAPLAN, G., KENSLER, T. and NASH, R. A. 1982. EQUILIBRIUM MOISTURE-CONTENT OF PHARMACEUTICAL EXCIPIENTS. *Drug Development and Industrial Pharmacy,* 8**,** 355-369.

CAPUANO, B., CROSBY, I. T., FALLON, G. D., LLOYD, E. J., YURIEV, E. and EGAN, S. J. 2003. 2-methyl-4-(4-methylpiperazin-1-yl)-10H-thieno 2,3-b 1,5 benzodiazepine methanol solvate monohydrate. *Acta Crystallographica Section E-Structure Reports Online,* 59**,** O1367-O1369.

CHAKRAVARTY, P., BERENDT, R. T., MUNSON, E. J., YOUNG, V. G., GOVINDARAJAN, R. and SURYANARAYANAN, R. 2009a. Insights into the Dehydration Behavior of Thiamine Hydrochloride (Vitamin B(1)) Hydrates: Part I. *Journal of Pharmaceutical Sciences,* 99**,** 816-827.

CHAKRAVARTY, P., BERENDT, R. T., MUNSON, E. J., YOUNG, V. G., GOVINDARAJAN, R. and SURYANARAYANAN, R. 2009b. Insights Into the Dehydration Behavior of Thiamine Hydrochloride (vitamin B(1)) Hydrates: Part II. *Journal of Pharmaceutical Sciences,* 99**,** 1882-1895.

CHAN, H. K. and DOELKER, E. 1985. Polymorphic transformation of some drugs under compression. *Drug Development and Industrial Pharmacy,* 11**,** 315-332.

CHEMBURKAR, S. R., BAUER, J., DEMING, K., SPIWEK, H., PATEL, K., MORRIS, J., HENRY, R., SPANTON, S., DZIKI, W., PORTER, W., QUICK, J., BAUER, P., DONAUBAUER, J., NARAYANAN, B. A., SOLDANI, M., RILEY, D. and MCFARLAND, K. 2000. Dealing with the Impact of Ritonavir Polymorphs on the Late Stages of Bulk Drug Process Development. *Organic Process Research & Development,* 4**,** 413-417.

CHEN, L. R., YOUNG JR, V. G., LECHUGA-BALLESTEROS, D. and GRANT, D. J. W. 1999. Solid-state behavior of cromolyn sodium hydrates. *Journal of Pharmaceutical Sciences,* 88**,** 1191-1200.

CHIENG, N., ZUJOVIC, Z., BOWMAKER, G., RADES, T. and SAVILLE, D. 2006. Effect of milling conditions on the solid-state conversion of ranitidine hydrochloride form 1. *International Journal of Pharmaceutics,* 327**,** 36-44.

CHIOU, W. L. and RIEGELMAN, S. 1971. Pharmaceutical applications of solid dispersion systems. *Journal of Pharmaceutical Sciences,* 60**,** 1281-1302.

CHOKSHI, R. J., SANDHU, H. K., IYER, R. M., SHAH, N. H., MALICK, A. W. and ZIA, H. 2005. Characterization of physico-mechanical properties of indomethacin and polymers to assess their suitability for hot-melt extrusion processs as a means to manufacture solid dispersion/solution. *Journal of Pharmaceutical Sciences,* 94**,** 2463-2474.

CHOW, K., TONG, H. H., LUM, S. and CHOW, A. H. 2008. Engineering of pharmaceutical materials: An industrial perspective. *Journal of Pharmaceutical Sciences,* 97**,** 2855-2877.

COELHO, A. 2007. *TOPAS Academic User Manual. Version 4.1,* Australia.

COLEMAN, N. J. and CRAIG, D. Q. M. 1996. Modulated temperature differential scanning calorimetry: A novel approach to pharmaceutical thermal analysis. *International Journal of Pharmaceutics,* 135**,** 13-29.

CORRIGAN, O. I. 1985. Mechanisms of Dissolution of Fast Release Solid Dispersions. *Drug Development and Industrial Pharmacy,* 11**,** 697-724.

CORRIGAN, O. I. 1995. Thermal analysis of spray dried products. *Thermochimica Acta,* 248**,** 245-258.

COUCHMAN, P. R. and KARASZ, F. E. 1978. A classical thermodynamic discussion of the effect of composition on glass-transition temperatures. *Macromolecules,* 11**,** 117-119.

COX, J. S. G., WOODARD, G. D. and MCCRONE, W. C. 1971. Solid-state chemistry of cromolyn sodium (disodium cromoglycate). *Journal of Pharmaceutical Sciences,* 60**,** 1458-1465.

CRAIG, D. Q. M. 2002. The mechanisms of drug release from solid dispersions in water-soluble polymers. *International Journal of Pharmaceutics,* 231**,** 131-144.

CRAIG, D. Q. M. and JOHNSON, F. A. 1995. Pharmaceutical applications of dynamic mechanical thermal analysis. *Thermochimica Acta,* 248**,** 97-115.

CRAIG, D. Q. M. and READING, M. 2007. *Thermal Analysis of Pharmaceuticals,* London, CRC Press.

CRAIG, D. Q. M., ROYALL, P. G., KETT, V. L. and HOPTON, M. L. 1999. The relevance of the amorphous state to pharmaceutical dosage forms: glassy drugs and freeze dried systems. *International Journal of Pharmaceutics,* 179**,** 179-207.

CROWLEY, K. J. and ZOGRAFI, G. 2001. The use of thermal methods for predicting glass-former fragility. *Thermochimica Acta,* 380**,** 79-93.

CROWLEY, M. M., ZHANG, F., REPKA, M. A., THUMMA, S., UPADHYE, S. B., BATTU, S. K., MCGINITY, J. W. and MARTIN, C. 2007. Pharmaceutical applications of hot-melt extrusion: Part I. *Drug Development and Industrial Pharmacy,* 33**,** 909-926.

CUI, Y. and YAO, E. 2008. Evaluation of hydrate-screening methods. *Journal of Pharmaceutical Sciences,* 97**,** 2730-2744.

CULLITY, B. D. 1956. *Elements of X-ray Diffraction,* Reading, Mass., Addison-Wesley Pub. Co.

DAVID, W. I. F., SHANKLAND, K. and SHANKLAND, N. 1998. Routine determination of molecular crystal structures from powder diffraction data. *Chemical Communications*, 931-932.

DE BRABANDER, C., VAN DEN MOOTER, G., VERVAET, C. and REMON, J. P. 2002. Characterization of ibuprofen as a nontraditional plasticizer of ethyl cellulose. *Journal of Pharmaceutical Sciences,* 91, 1678-1685.

DE BRABANDER, C., VERVAET, C. and REMON, J. P. 2003. Development and evaluation of sustained release mini-matrices prepared via hot melt extrusion. *Journal of Controlled Release,* 89, 235-247.

DEBNATH, S. and SURYANARAYANAN, R. 2004. Influence of processing-induced phase transformations on the dissolution of theophylline tablets. *AAPS PharmSciTech,* 5.

DESAI, J., ALEXANDER, K. and RIGA, A. 2006. Characterization of polymeric dispersions of dimenhydrinate in ethyl cellulose for controlled release. *International Journal of Pharmaceutics,* 308, 115-123.

DESIRAJU, G. R. 2004. Counterpoint: What's in a Name? *Crystal Growth & Design,* 4, 1089-1090.

DJURIS, J., NIKOLAKAKIS, I., IBRIC, S., DJURIC, Z. and KACHRIMANIS, K. 2013. Preparation of carbamazepine–Soluplus® solid dispersions by hot-melt extrusion, and prediction of drug–polymer miscibility by thermodynamic model fitting. *European Journal of Pharmaceutics and Biopharmaceutics,* 84, 228-237.

DONG, Z., CHATTERJI, A., SANDHU, H., CHOI, D. S., CHOKSHI, H. and SHAH, N. 2008. Evaluation of solid state properties of solid dispersions prepared by hot-melt extrusion and solvent co-precipitation. *International Journal of Pharmaceutics,* 355, 141-149.

EMA 2003. ICH Topic Q1A (R2) - Stability Testing of new Drug Substances and Products. UK.

FARJAS, J., BUTCHOSA, N. and ROURA, P. 2010. A simple kinetic method for the determination of the reaction model from non-isothermal experiments. *Journal of Thermal Analysis and Calorimetry,* 102, 615-625.

FDA 1997. Dissolution Testing of Immediate Release Solid Oral Dosage Forms.

FENG, J., XU, L., GAO, R., LUO, Y. and TANG, X. 2012. Evaluation of polymer carriers with regard to the bioavailability enhancement of bifendate solid dispersions prepared by hot-melt extrusion. *Drug Development and Industrial Pharmacy,* 38**,** 735-743.

FLORENCE, A. T. and ATTWOOD, D. 2006. *Physicochemical principles of pharmacy,* London, Chicago : Pharmaceutical Press.

FLORY, P. J. 1942. Thermodynamics of High Polymer Solutions. *The Journal of Chemical Physics,* 10**,** 51-61.

FLYNN, J. H. and WALL, L. A. 1966. A quick direct method for determination of activation energy from thermogravimetric data. *Journal of Polymer Science Part B-Polymer Letters,* 4**.**

FORSTER, A., HEMPENSTALL, J. and RADES, T. 2001a. Characterization of glass solutions of poorly water-soluble drugs produced by melt extrusion with hydrophilic amorphous polymers. *Journal of Pharmacy and Pharmacology,* 53**,** 303-315.

FORSTER, A., HEMPENSTALL, J., TUCKER, I. and RADES, T. 2001b. Selection of excipients for melt extrusion with two poorly water-soluble drugs by solubility parameter calculation and thermal analysis. *International Journal of Pharmaceutics,* 226**,** 147-161.

FUKUOKA, E., MAKITA, M. and YAMAMURA, S. 1989. Glassy state of pharmaceuticals. III. Thermal properties and stability of glassy pharmaceuticals and their binary glass systems. *Chemical and Pharmaceutical Bulletin,* 37**,** 1047-1050.

GALE, J. D. 2005. GULP: Capabilities and prospects. *Zeitschrift fur Kristallographie,* 220**,** 552-554.

GALWEY, A. K. 2000. Structure and order in thermal dehydrations of crystalline solids. *Thermochimica Acta,* 355**,** 181-238.

GHEBREMESKEL, A. N., VEMAVARAPU, C. and LODAYA, M. 2007. Use of surfactants as plasticizers in preparing solid dispersions of poorly soluble API: Selection of polymer–surfactant combinations using solubility parameters and testing the processability. *International Journal of Pharmaceutics,* 328**,** 119-129.

GILL, P. S., SAUERBRUNN, S. R. and READING, M. 1993. Modulated differential scanning calorimetry. *Journal of Thermal Analysis,* 40**,** 931-939.

GILMORE, C. J. 2011. X-Ray Diffraction. *In:* STOREY, R. A. and YMÉN, I. (eds.) *Solid State Characterization of Pharmaceuticals.* Chichester, UK: John Wiley & Sons

GIRON, D. 1995. Thermal analysis and calorimetric methods in the characterisation of polymorphs and solvates. *Thermochimica Acta,* 248**,** 1-59.

GIRON, D., GOLDBRONN, C., MUTZ, M., PFEFFER, S., PIECHON, P. and SCHWAB, P. 2002. Solid State Characterizations of Pharmaceutical Hydrates. *Journal of Thermal Analysis and Calorimetry,* 68**,** 453-465.

GOLDBERG, A. H., GIBALDI, M. and KANIG, J. L. 1965. Increasing dissolution rates and gastrointestinal absorption of drugs via solid solutions and eutectic mixtures I. Theoretical considerations and discussion of the literature. *Journal of Pharmaceutical Sciences,* 54**,** 1145-1148.

GOLDBERG, A. H., GIBALDI, M., KANIG, J. L. and MAYERSOHN, M. 1966. Increasing dissolution rates and gastrointestinal absorption of drugs via solid solutions and eutectic mixtures IV: Chloramphenicol—urea system. *Journal of Pharmaceutical Sciences,* 55**,** 581-583.

GORDON, M. and TAYLOR, J. S. 1952. Ideal copolymers and the second-order transitions of synthetic rubbers. i. non-crystalline copolymers. *Journal of Applied Chemistry,* 2**,** 493-500.

GRAESER, K. A., PATTERSON, J. E. and RADES, T. 2009a. Applying Thermodynamic and Kinetic Parameters to Predict the Physical Stability of Two Differently Prepared Amorphous Forms of Simvastatin. *Current Drug Delivery,* 6**,** 374-382.

GRAESER, K. A., PATTERSON, J. E., ZEITLER, J. A., GORDON, K. C. and RADES, T. 2009b. Correlating thermodynamic and kinetic parameters with amorphous stability. *European Journal of Pharmaceutical Sciences,* 37**,** 492-498.

GRAESER, K. A., STRACHAN, C. J., PATTERSON, J. E., GORDON, K. C. and RADES, T. 2008. Physicochemical Properties and Stability of Two Differently Prepared Amorphous Forms of Simvastatin. *Crystal Growth and Design,* 8**,** 128-135.

GRANT, D. J. W. and BRITTAIN, H. G. 1995. Solubility of Pharmaceutical Solids. *In:* BRITTAIN, H. G. (ed.) *Physical Characterization of Pharmaceutical Solids.* New Jersey: Marcel Dekker. 321-386

GREENHALGH, D. J., WILLIAMS, A. C., TIMMINS, P. and YORK, P. 1999. Solubility parameters as predictors of miscibility in solid dispersions. *Journal of Pharmaceutical Sciences,* 88**,** 1182-1190.

GREINER, A. and WENDORFF, J. H. 2007. Electrospinning: A Fascinating Method for the Preparation of Ultrathin Fibers. *Angewandte Chemie International Edition,* 46**,** 5670-5703.

GRIESSER, U. J. 2006. The Importance of Solvates. *Polymorphism in the Pharmaceutical Industry.* Germany: WILEY-VCH.211-230.

GRIESSER, U. J. and BURGER, A. 1995. The effect of water vapor pressure on desolvation kinetics of caffeine 4/5-hydrate. *International Journal of Pharmaceutics,* 120**,** 83-93.

GRIESSER, U. J., JETTI, R. K. R., HADDOW, M. F., BREHMER, T., APPERLEY, D. C., KING, A. and HARRIS, R. K. 2008. Conformational Polymorphism in Oxybuprocaine Hydrochloride. *Crystal Growth & Design,* 8**,** 44-56.

GRISEDALE, L. C., JAMIESON, M. J., BELTON, P. S., BARKER, S. A. and M. CRAIG, D. Q. Characterization and quantification of amorphous material in milled and spray-dried salbutamol sulfate: A comparison of thermal, spectroscopic, and water vapor sorption approaches. *Journal of Pharmaceutical Sciences,* 100**,** 3114-3129.

GUGUTA, C., MEEKES, H. and DE GELDER, R. 2006. Crystal Structure of Aspartame Anhydrate from Powder Diffraction Data. Structural Aspects of the Dehydration Process of Aspartame. *Crystal Growth and Design,* 6**,** 2686-2692.

GUPTA, J., NUNES, C., VYAS, S. and JONNALAGADDA, S. 2011. Prediction of Solubility Parameters and Miscibility of Pharmaceutical Compounds by Molecular Dynamics Simulations. *The Journal of Physical Chemistry B,* 115**,** 2014-2023.

HAIKALA, R., EEROLA, R., TANNINEN, V. P. and YLIRUUSI, J. 1997. Polymorphic changes of mannitol during freeze-drying: Effect of surface- active agents. *PDA Journal of Pharmaceutical Science and Technology,* 51**,** 96-101.

HALEBLIAN, J. and MCCRONE, W. 1969. Pharmaceutical Applications of Polymorphism. *Journal of Pharmaceutical Sciences,* 58**,** 911-929.

HALLBRUCKER, A., MAYER, E. and JOHARI, G. P. 1989. Glass-liquid transition and the enthalpy of devitrification of annealed vapor-deposited amorphous solid water: a comparison with hyperquenched glassy water. *The Journal of Physical Chemistry,* 93**,** 4986-4990.

HAMIED, Y. K., KANKAN, R. N. and RAO, D. R. 2002. *Polymorphic Forms of Olanzapine*. U.S. patent application 6348458B1.

HANCOCK, B. C. and SHAMBLIN, S. L. 2001. Molecular mobility of amorphous pharmaceuticals determined using differential scanning calorimetry. *Thermochimica Acta,* 380**,** 95-107.

HANCOCK, B. C., SHAMBLIN, S. L. and ZOGRAFI, G. 1995. Molecular Mobility of Amorphous Pharmaceutical Solids Below Their Glass Transition Temperatures. *Pharmaceutical Research,* 12**,** 799-806.

HANCOCK, B. C., YORK, P. and ROWE, R. C. 1997. The use of solubility parameters in pharmaceutical dosage form design. *International Journal of Pharmaceutics,* 148**,** 1-21.

HANCOCK, B. C. and ZOGRAFI, G. 1994. The Relationship Between the Glass Transition Temperature and the Water Content of Amorphous Pharmaceutical Solids. *Pharmaceutical Research,* 11**,** 471-477.

HANSEN, C. M. 2007. Solubility Parameters - An Introduction *In:* HANSEN, C. M. (ed.) *Hansen Solubility Parameters, A User's Handbook.* 2nd ed. London: CRC Press.1-24

HEACOCK, R. A. and MARION, L. O. 1956. THE INFRARED SPECTRA OF SECONDARY AMINES AND THEIR SALTS. *Canadian Journal of Chemistry,* 34**,** 1782-1795.

HENWOOD, S. Q., LIEBENBERG, W., TIEDT, L. R., LOTTER, A. P. and DE VILLIERS, M. M. 2001. Characterization of the Solubility and Dissolution Properties of Several New Rifampicin Polymorphs, Solvates, and Hydrates. *Drug Development and Industrial Pharmacy,* 27**,** 1017-1030.

HERBSTEIN, F. H. 2004. Diversity Amidst Similarity: A Multidisciplinary Approach to Phase Relationships, Solvates, and Polymorphs. *Crystal Growth & Design,* 4**,** 1419-1429.

HERMAN, J., VISAVARUNGROJ, N. and REMON, J. P. 1989. Instability of drug release from anhydrous theophylline-microcrystalline cellulose formulations. *International Journal of Pharmaceutics,* 55**,** 143-146.

HILDEN, L. R. and MORRIS, K. R. 2004. Physics of amorphous solids. *Journal of Pharmaceutical Sciences,* 93**,** 3-12.

HILFIKER, R. 2006. *Polymorphism in the Pharmaceutical Industry,* Weinheim, Wiley-VCH.

HIRAYAMA, F., HONJO, M., ARIMA, H., OKIMOTO, K. and UEKAMA, K. 2000. X-ray crystallographic characterization of nilvadipine monohydrate and its phase transition behavior. *European Journal of Pharmaceutical Sciences,* 11**,** 81-88.

HODGE, I. M. 1996. Strong and fragile liquids - A brief critique. *Journal of Non-Crystalline Solids,* 202**,** 164-172.

HÖRTER, D. and DRESSMAN, J. B. 2001. Influence of physicochemical properties on dissolution of drugs in the gastrointestinal tract. *Advanced Drug Delivery Reviews,* 46**,** 75-87.

HOSOKAWA, T., DATTA, S., SHETH, A. R., BROOKS, N. R., YOUNG, V. G. and GRANT, D. J. W. 2004. Isostructurality among Five Solvates of Phenylbutazone. *Crystal Growth & Design,* 4**,** 1195-1201.

HOWARD, J. A. K., PATTISON, P. and CHETINA, O. 2003. Private communication to the Cambridge Crystallographic Data Centre.

HUANG, J., WIGENT, R. J., BENTZLEY, C. M. and SCHWARTZ, J. B. 2006. Nifedipine solid dispersion in microparticles of ammonio methacrylate copolymer and ethylcellulose binary blend for controlled drug delivery. Effect of drug loading on release kinetics. *International Journal of Pharmaceutics,* 319**,** 44-54.

HUGGINS, M. L. 1942. THERMODYNAMIC PROPERTIES OF SOLUTIONS OF LONG-CHAIN COMPOUNDS. *Annals of the New York Academy of Sciences,* 43**,** 1-32.

HÜLSMANN, S., BACKENSFELD, T., KEITEL, S. and BODMEIER, R. 2000. Melt extrusion - An alternative method for enhancing the dissolution rate of 17β-estradiol hemihydrate. *European Journal of Pharmaceutics and Biopharmaceutics,* 49**,** 237-242.

IBERS, J. A. 1999. Paroxetine hydrochloride hemihydrate. *Acta Crystallographica Section C: Crystal Structure Communications,* 55**,** 432-434.

IGNATIOUS, F., SUN, L., LEE, C.-P. and BALDONI, J. 2010. Electrospun Nanofibers in Oral Drug Delivery. *Pharmaceutical Research,* 27**,** 576-588.

JAKALIAN, A., JACK, D. B. and BAYLY, C. I. 2002. Fast, efficient generation of high-quality atomic charges. AM1-BCC model: II. Parameterization and validation. *Journal of Computational Chemistry,* 23**,** 1623-1641.

JANSSENS, S., DE ZEURE, A., PAUDEL, A., VAN HUMBEECK, J., ROMBAUT, P. and VAN DEN MOOTER, G. 2010. Influence of preparation methods on solid state supersaturation of amorphous solid dispersions: A case study with itraconazole and eudragit E100. *Pharmaceutical Research,* 27**,** 775-785.

JANSSENS, S. and VAN DEN MOOTER, G. 2009. Review: physical chemistry of solid dispersions. *Journal of Pharmacy and Pharmacology,* 61**,** 1571-1586.

JO, W. H. and KWON, I. H. 1991. Equation of state theory for melting point depression in miscible polymer blends. *Macromolecules,* 24**,** 3368-3372.

JOHNSON, A. M. 1992. Paroxetine: a pharmacological review. *International Clinical Psychopharmacology,* 6 Suppl 4**,** 15-24.

KANIG, J. L. 1964. Properties of fused mannitol in compressed tablets. *Journal of Pharmaceutical Sciences,* 53**,** 188-192.

KARMWAR, P., GRAESER, K., GORDON, K. C., STRACHAN, C. J. and RADES, T. 2011. Investigation of properties and recrystallisation behaviour of amorphous indomethacin samples prepared by different methods. *International Journal of Pharmaceutics,* 417**,** 94-100.

KARMWAR, P., GRAESER, K., GORDON, K. C., STRACHAN, C. J. and RADES, T. 2012. Effect of different preparation methods on the dissolution behaviour of amorphous indomethacin. *European Journal of Pharmaceutics and Biopharmaceutics,* 80**,** 459-464.

KASIM, N. A., WHITEHOUSE, M., RAMACHANDRAN, C., BERMEJO, M., LENNERNÄS, H., HUSSAIN, A. S., JUNGINGER, H. E., STAVCHANSKY, S. A., MIDHA, K. K., SHAH, V. P. and AMIDON, G. L. 2004. Molecular properties of WHO essential drugs and provisional biopharmaceutical classification. *Mol Pharm,* 1**,** 85-96.

KAUSHAL, A. M. and BANSAL, A. K. 2008. Thermodynamic behavior of glassy state of structurally related compounds. *European Journal of Pharmaceutics and Biopharmaceutics,* 69**,** 1067-1076.

KAUZMANN, W. 1948. The nature of the glassy state and the behavior of liquids at low temperatures. *Chemical Reviews,* 43**,** 219-256.

KAVITHA, C., LAKSHMI, S., BASAPPA, MANTELINGU, K., SRIDHAR, M., PRASAD, J. and RANGAPPA, K. 2005. Synthesis and molecular structure analysis of venlafaxine intermediate and its analog. *Journal of Chemical Crystallography,* 35**,** 957-963.

KAWAKAMI, K. and PIKAL, M. J. 2005. Calorimetric investigation of the structural relaxation of amorphous materials: Evaluating validity of the methodologies. *Journal of Pharmaceutical Sciences,* 94**,** 948-965.

KE, P., HASEGAWA, S., AL-OBAIDI, H. and BUCKTON, G. 2012. Investigation of preparation methods on surface/bulk structural relaxation and glass fragility of amorphous solid dispersions. *International Journal of Pharmaceutics,* 422**,** 170-178.

KESTUR, U. S. and TAYLOR, L. S. 2010. Role of polymer chemistry in influencing crystal growth rates from amorphous felodipine. *CrystEngComm,* 12**,** 2390-2397.

KHANKARI, R. K. and GRANT, D. J. W. 1995. Pharmaceutical hydrates. *Thermochimica Acta,* 248**,** 61-79.

KHAWAM, A. and FLANAGAN, D. R. 2006a. Basics and applications of solid-state kinetics: A pharmaceutical perspective. *Journal of Pharmaceutical Sciences,* 95**,** 472-498.

KHAWAM, A. and FLANAGAN, D. R. 2006b. Solid-state kinetic models: Basics and mathematical fundamentals. *Journal of Physical Chemistry B,* 110**,** 17315-17328.

KHOUGAZ, K. and CLAS, S.-D. 2000. Crystallization inhibition in solid dispersions of MK-0591 and poly(vinylpyrrolidone) polymers. *Journal of Pharmaceutical Sciences,* 89**,** 1325-1334.

KITAMURA, S., KODA, S., MIYAMAE, A., YASUDA, T. and MORIMOTO, Y. 1990. Dehydration effect on the stability of cefixime trihydrate. *International Journal of Pharmaceutics,* 59**,** 217-224.

KOBAYASHI, K., KIMURA, S., TOGAWA, E., WADA, M. and KUGA, S. 2009. Crystal transition of paramylon with dehydration and hydration. *Carbohydrate Polymers,* 80**,** 492-498.

KONNO, H. and TAYLOR, L. S. 2006. Influence of different polymers on the crystallization tendency of molecularly dispersed amorphous felodipine. *Journal of Pharmaceutical Sciences,* 95**,** 2692-2705.

KONNO, H. and TAYLOR, L. S. 2008. Ability of different polymers to inhibit the crystallization of amorphous felodipine in the presence of moisture. *Pharmaceutical Research,* 25**,** 969-978.

KONTOGEORGIS, G. M. 2007. The Hansen Solubility Parameters (HSP) in Thermodynamic Models for Polymer Solutions. *In:* HANSEN, C. M. (ed.) *Hansen Solubility Parameters, A User's Handbook.* 2nd ed. London: CRC Press.75-93

KORADIA, V., FONTELONGA DE LEMOS, A. F., ALLESØ, M., LOPEZ DE DIEGO, H., RINGKJØBING-ELEMA, M., MÜLLERTZ, A. and RANTANEN, J. 2011. Phase transformations of amlodipine besylate solid forms. *Journal of Pharmaceutical Sciences,* 100**,** 2896-2910.

KOTAR-JORDAN, B., LENARSIC, R., GREMAN, M., SMRKOLJ, M., MEDEN, A., SIMONIC, I., ZUPET, R., GNIDOVEC, J. and BENKIC, P. 2011. *Isopropanol water solvate of olanzapine*.

KREVELEN, D. W. V. and NIJENHUIS, K. T. 2009. *Properties of Polymers,* Oxford, Elsevier.

KUMAR, L. and BANSAL, A. K. 2011. Effect of humidity on the hydration behaviour of prazosin hydrochloride polyhydrate: Thermal, sorption and crystallographic study. *Thermochimica Acta,* 525**,** 206-210.

LAKSHMAN, J. P., CAO, Y., KOWALSKI, J. and SERAJUDDIN, A. T. M. 2008. Application of melt extrusion in the development of a physically and chemically stable high-energy amorphous solid dispersion of a poorly water-soluble drug. *Molecular Pharmaceutics,* 5**,** 994-1002.

LARSEN, S. D. 1997. *Solvate of Olanzapine*. US Patent 5637584.

LEE, A. Y., ERDEMIR, D. and MYERSON, A. S. 2011. Crystal polymorphism in chemical process development. *Annual Review of Chemical and Biomolecular Engineering,* 2**,** 259-280.

LEE, S., RAW, A. and YU, L. 2008. Dissolution Testing. *In:* KRISHNA, R. and YU, L. (eds.) *Biopharmaceutics Applications in Drug Development.* Springer US.47-74

LEUNG, S. S., PADDEN, B. E., MUNSON, E. J. and GRANT, D. J. W. 1998. Hydration and dehydration behavior of aspartame hemihydrate. *Journal of Pharmaceutical Sciences,* 87**,** 508-513.

LIU, J., RIGSBEE, D. R., STOTZ, C. and PIKAL, M. J. 2002. Dynamics of pharmaceutical amorphous solids: The study of enthalpy relaxation by isothermal microcalorimetry. *Journal of Pharmaceutical Sciences,* 91**,** 1853-1862.

LLOYD, G. R., CRAIG, D. Q. M. and SMITH, A. 1997. An investigation into the melting behavior of binary mixes and solid dispersions of paracetamol and PEG 4000. *Journal of Pharmaceutical Sciences,* 86**,** 991-996.

LU, Q. and ZOGRAFI, G. 1998. Phase behavior of binary and ternary amorphous mixtures containing indomethacin, citric acid, and PVP. *Pharmaceutical Research,* 15**,** 1202-1206.

MACEDO, P. B. and LITOVITZ, T. A. 1965. On the Relative Roles of Free Volume and Activation Energy in the Viscosity of Liquids. *The Journal of Chemical Physics,* 42**,** 245-256.

MACKIN, L., ZANON, R., PARK, J. M., FOSTER, K., OPALENIK, H. and DEMONTE, M. 2002. Quantification of low levels (<10%) of amorphous content in micronised active batches using dynamic vapour sorption and isothermal microcalorimetry. *International Journal of Pharmaceutics,* 231**,** 227-236.

MAJERIK, V., CHARBIT, G., BADENS, E., HORVÁTH, G., SZOKONYA, L., BOSC, N. and TEILLAUD, E. 2007. Bioavailability enhancement of an active substance by supercritical antisolvent precipitation. *Journal of Supercritical Fluids,* 40**,** 101-110.

MAO, C., CHAMARTHY, S. and PINAL, R. 2006. Time-Dependence of Molecular Mobility during Structural Relaxation and its Impact on Organic Amorphous Solids: An Investigation Based on a Calorimetric Approach. *Pharmaceutical Research,* 23**,** 1906-1917.

MARSAC, P., LI, T. and TAYLOR, L. 2009. Estimation of Drug–Polymer Miscibility and Solubility in Amorphous Solid Dispersions Using Experimentally Determined Interaction Parameters. *Pharmaceutical Research,* 26**,** 139-151.

MARSAC, P., SHAMBLIN, S. and TAYLOR, L. 2006. Theoretical and Practical Approaches for Prediction of Drug-Polymer Miscibility and Solubility. *Pharmaceutical Research,* 23**,** 2417-2426.

MATSUMOTO, T. and ZOGRAFI, G. 1999. Physical properties of solid molecular dispersions of indomethacin with poly(vinylpyrrolidone) and poly(vinylpyrrolidone-co-vinyl-acetate) in relation to indomethacin crystallization. *Pharmaceutical Research,* 16**,** 1722-1728.

MAYO, S. L., OLAFSON, B. D. and GODDARD III, W. A. 1990. DREIDING: A generic force field for molecular simulations. *Journal of Physical Chemistry,* 94**,** 8897-8909.

MCGARVEY, O. S., KETT, V. L. and CRAIG, D. Q. M. 2003. An investigation into the crystallization of alpha,alpha-trehalose from the amorphous state. *Journal of Physical Chemistry B,* 107**,** 6614-6620.

MCNAMARA, D. P., CHILDS, S. L., GIORDANO, J., IARRICCIO, A., CASSIDY, J., SHET, M. S., MANNION, R., O'DONNELL, E. and PARK, A. 2006. Use of a glutaric acid cocrystal to improve oral bioavailability of a low solubility API. *Pharmaceutical Research,* 23**,** 1888-1897.

MEAURIO, E., ZUZA, E. and SARASUA, J. R. 2005. Miscibility and specific interactions in blends of poly(L-lactide) with poly(vinylphenol). *Macromolecules,* 38**,** 1207-1215.

MILLER, D. A., MCCONVILLE, J. T., YANG, W., WILLIAMS III, R. O. and MCGINITY, J. W. 2007. Hot-melt extrusion for enhanced delivery of drug particles. *Journal of Pharmaceutical Sciences,* 96**,** 361-376.

MONEGHINI, M., CARCANO, A., ZINGONE, G. and PERISSUTTI, B. 1998. Studies in dissolution enhancement of atenolol. Part I. *International Journal of Pharmaceutics,* 175**,** 177-183.

MORRIS, K. R., GRIESSER, U. J., ECKHARDT, C. J. and STOWELL, J. G. 2001. Theoretical approaches to physical transformations of active pharmaceutical ingredients during manufacturing processes. *Advanced Drug Delivery Reviews,* 48**,** 91-114.

MURA, P., FAUCCI, M. T., MANDERIOLI, A. and BRAMANTI, G. 1999a. Influence of the preparation method on the physicochemical properties of binary systems of econazole with cyclodextrins. *International Journal of Pharmaceutics,* 193**,** 85-95.

MURA, P., FAUCCI, M. T., PARRINI, P. L., FURLANETTO, S. and PINZAUTI, S. 1999b. Influence of the preparation method on the physicochemical properties of ketoprofen-cyclodextrin binary systems. *International Journal of Pharmaceutics,* 179**,** 117-128.

MURA, P., FAUCCI, M. T., PARRINI, P. L., FURLANETTO, S. and PINZAUTI, S. 1999c. Influence of the preparation method on the physicochemical properties of ketoprofen–cyclodextrin binary systems. *International Journal of Pharmaceutics,* 179**,** 117-128.

MURDANDE, S. B., PIKAL, M. J., SHANKER, R. M. and BOGNER, R. H. 2011. Aqueous solubility of crystalline and amorphous drugs: Challenges in measurement. *Pharmaceutical Development and Technology,* 16**,** 187-200.

NAKAMOTO, K., MARGOSHES, M. and RUNDLE, R. E. 1955. STRETCHING FREQUENCIES AS A FUNCTION OF DISTANCES IN HYDROGEN BONDS. *Journal of the American Chemical Society,* 77**,** 6480-6486.

NANGIA, A. 2005. Pseudopolymorph: Retain This Widely Accepted Term. *Crystal Growth & Design,* 6**,** 2-4.

NISHI, T. and WANG, T. T. 1975. Melting point depression and kinetic effects of cooling on crystallization in poly(vinylidene fluoride)-poly(methyl methacrylate) mixtures. *Macromolecules,* 8**,** 909-915.

O'NEIL, A. and EDWARDS, H. 2011. Spectroscopic Characterization. *In:* STOREY, R. A. and YMÉN, I. (eds.) *Solid State Characterization of Pharmaceuticals.* UK: Wiley

OBERHOLTZER, E. R. and BRENNER, G. S. 1979. Cefoxitin sodium: solution and solid-state chemical stability studies. *Journal of Pharmaceutical Sciences,* 68**,** 863-866.

OSSI, P. M. 2010. *Disordered Materials*, Springer Berlin Heidelberg.

OTSUKA, M., HASEGAWA, H. and MATSUDA, Y. 1997. Effect of polymorphic transformation during the extrusion-granulation process on the pharmaceutical properties of carbamazepine granules. *Chemical and Pharmaceutical Bulletin,* 45**,** 894-898.

OTSUKA, M., OFUSA, T. and MATSUDA, Y. 1999. Effect of environmental humidity on the transformation pathway of carbamazepine polymorphic modifications during grinding. *Colloids and Surfaces B: Biointerfaces,* 13**,** 263-273.

OZAWA, T. 1965. A NEW METHOD OF ANALYZING THERMOGRAVIMETRIC DATA. *Bulletin of the Chemical Society of Japan,* 38**,** 1881-1886.

PATTERSON, J. E., JAMES, M. B., FORSTER, A. H., LANCASTER, R. W., BUTLER, J. M. and RADES, T. 2007. Preparation of glass solutions of three poorly water soluble drugs by spray drying, melt extrusion and ball milling. *International Journal of Pharmaceutics,* 336**,** 22-34.

PAUDEL, A., VAN HUMBEECK, J. and VAN DEN MOOTER, G. 2010. Theoretical and experimental investigation on the solid solubility and miscibility of naproxen in poly(vinylpyrrolidone). *Molecular Pharmaceutics,* 7**,** 1133-1148.

PAUDEL, A., WORKU, Z. A., MEEUS, J., GUNS, S. and VAN DEN MOOTER, G. 2012. Manufacturing of solid dispersions of poorly water soluble drugs by spray drying: Formulation and process considerations. *International Journal of Pharmaceutics*.

PERCY, S. R. 1872. Improvement in drying and concentrating liquid substances by atomizing. *Letters Patent* n. 125,406.

PETIT, S. and COQUEREL, G. 1996. Mechanism of several solid-solid transformations between dihydrated and anhydrous copper(II) 8-hydroxyquinolinates. Proposition for a unified model for the dehydration of molecular crystals. *Chemistry of Materials,* 8**,** 2247-2258.

PFEIFFER, R. R., YANG, K. S. and TUCKER, M. A. 1970. Crystal pseudopolymorphism of cephaloglycin and cephalexin. *Journal of Pharmaceutical Sciences,* 59**,** 1809-1814.

PIRTTIMAKI, J., LAINE, E., KETOLAINEN, J. and PARONEN, P. 1993. EFFECTS OF GRINDING AND COMPRESSION ON CRYSTAL-STRUCTURE OF ANHYDROUS CAFFEINE. *International Journal of Pharmaceutics,* 95**,** 93-99.

POKHARKAR, V. B., MANDPE, L. P., PADAMWAR, M. N., AMBIKE, A. A., MAHADIK, K. R. and PARADKAR, A. 2006. Development, characterization and stabilization of amorphous form of a low Tg drug. *Powder Technology,* 167**,** 20-25.

POLLA, G. I., VEGA, D. R., LANZA, H., TOMBARI, D. G., BAGGIO, R., AYALA, A. P., FILHO, J. M., FERNÁNDEZ, D., LEYVA, G. and DARTAYET, G. 2005. Thermal behaviour and stability in Olanzapine. *International Journal of Pharmaceutics,* 301**,** 33-40.

POOLE, J. W., OWEN, G., SILVERIO, J., FREYHOF, J. N. and ROSENMAN, S. B. 1968. Physiochemical factors influencing the absorption of the anhydrous and trihydrate forms of ampicillin. *Current Therapeutic Research - Clinical and Experimental,* 10**,** 292-303.

POUTON, C. W. 2000. Lipid formulations for oral administration of drugs: Non-emulsifying, self-emulsifying and 'self-microemulsifying' drug delivery systems. *European Journal of Pharmaceutical Sciences,* 11**,** S93-S98.

PRICE, C. P., GRZESIAK, A. L., LANG, M. and MATZGER, A. J. 2002. Polymorphism of Nabumetone. *Crystal Growth & Design,* 2**,** 501-503.

PUDIPEDDI, M. and SERAJUDDIN, A. T. M. 2005. Trends in solubility of polymorphs. *Journal of Pharmaceutical Sciences,* 94**,** 929-939.

QI, S., AVALLE, P., SAKLATVALA, R. and CRAIG, D. Q. M. 2008. An investigation into the effects of thermal history on the crystallisation behaviour of amorphous paracetamol. *European Journal of Pharmaceutics and Biopharmaceutics,* 69**,** 364-371.

QIAN, F., HUANG, J. and HUSSAIN, M. A. 2010. Drug–polymer solubility and miscibility: Stability consideration and practical challenges in amorphous solid dispersion development. *Journal of Pharmaceutical Sciences,* 99**,** 2941-2947.

RASTOGI, S., ZAKRZEWSKI, M. and SURYANARAYANAN, R. 2001. Investigation of solid-state reactions using variable temperature X-ray powder diffractometry. I. Aspartame hemihydrate. *Pharmaceutical Research,* 18**,** 267-273.

RASTOGI, S., ZAMANSKY, I., ROY, S., TYLE, P. and SURYANARAYANAN, R. 1999. Solid-state phase transitions of AG337, an antitumor agent. *Pharmaceutical Development and Technology,* 4**,** 623-632.

RÉ, M. I. 2006. Formulating drug delivery systems by spray drying. *Drying Technology,* 24**,** 433-446.

REDMAN-FUREY, N., DICKS, M., BIGALOW-KERN, A., CAMBRON, R. T., LUBEY, G., LESTER, C. and VAUGHN, D. 2005. Structural and analytical characterization of three hydrates and an anhydrate form of risedronate. *Journal of Pharmaceutical Sciences,* 94**,** 893-911.

REINTJES, T. (ed.) 2011. *Solubility Enhancement with BASF Pharma Polymers* Germany.

REPKA, M. A., BATTU, S. K., UPADHYE, S. B., THUMMA, S., CROWLEY, M. M., ZHANG, F., MARTIN, C. and MCGINITY, J. W. 2007. Pharmaceutical applications of hot-melt extrusion: Part II. *Drug Development and Industrial Pharmacy,* 33**,** 1043-1057.

REPKA, M. A., GERDING, T. G., REPKA, S. L. and MCGINITY, J. W. 1999. Influence of plasticizers and drugs on the physical-mechanical properties of hydroxypropylcellulose films prepared by hot melt extrusion. *Drug Development and Industrial Pharmacy,* 25**,** 625-633.

REUTZEL-EDENS, S. M., BUSH, J. K., MAGEE, P. A., STEPHENSON, G. A. and BYRN, S. R. 2003a. Anhydrates and Hydrates of Olanzapine: Crystallization, Solid-State Characterization, and Structural Relationships. *Crystal Growth & Design,* 3**,** 897-907.

REUTZEL-EDENS, S. M., KLEEMANN, R. L., LEWELLEN, P. L., BORGHESE, A. L. and ANTOINE, L. J. 2003b. Crystal forms of LY334370 HCl: Isolation, solid-state characterization, and physicochemical properties. *Journal of Pharmaceutical Sciences,* 92**,** 1196-1205.

REUTZEL, S. M. 1998. Origins of the unusual hygroscopicity observed in LY297802 tartrate. *Journal of Pharmaceutical Sciences,* 87**,** 1568-1571.

RODRÍGUEZ-SPONG, B., PRICE, C. P., JAYASANKAR, A., MATZGER, A. J. and RODRÍGUEZ-HORNEDO, N. 2004. General principles of pharmaceutical solid polymorphism: A supramolecular perspective. *Advanced Drug Delivery Reviews,* 56**,** 241-274.

ROY, S., GOUD, N. R., BABU, N. J., IQBAL, J., KRUTHIVENTI, A. K. and NANGIA, A. 2008. Crystal Structures of Norfloxacin Hydrates. *Crystal Growth & Design,* 8**,** 4343-4346.

RUMONDOR, A. C. F., STANFORD, L. A. and TAYLOR, L. S. 2009. Effects of polymer type and storage relative humidity on the kinetics of felodipine crystallization from amorphous solid dispersions. *Pharmaceutical Research,* 26**,** 2599-2606.

SAKURAI, A., SAKAI, T., SAKO, K. and MAITANI, Y. 2012. Polymer combination increased both physical stability and oral absorption of solid dispersions containing a low glass transition temperature drug: Physicochemical characterization and in vivo study. *Chemical and Pharmaceutical Bulletin,* 60**,** 459-464.

SANPHUI, P., SARMA, B. and NANGIA, A. 2011. Phase transformation in conformational polymorphs of nimesulide. *Journal of Pharmaceutical Sciences,* 100**,** 2287-2299.

SCHNEIDER, H. A. and DI MARZIO, E. A. 1992. The glass temperature of polymer blends: comparison of both the free volume and the entropy predictions with data. *Polymer,* 33**,** 3453-3461.

SEDDON, K. R. 2004. Pseudopolymorph: A Polemic. *Crystal Growth & Design,* 4**,** 1087-1087.

SEKIGUCHI, K. and OBI, N. 1961. Studies on Absorption of Eutectic Mixture. I. A Comparison of the Behavior of Eutectic Mixture of Sulfathiazole and that of Ordinary Sulfathiazole in Man. *Chemical & pharmaceutical bulletin,* 9**,** 866-872.

SHAH, B., KAKUMANU, V. K. and BANSAL, A. K. 2006. Analytical techniques for quantification of amorphous/crystalline phases in pharmaceutical solids. *Journal of Pharmaceutical Sciences,* 95**,** 1641-1665.

SHAH, S., MADDINENI, S., LU, J. and REPKA, M. A. 2012. Melt extrusion with poorly soluble drugs. *International Journal of Pharmaceutics*, 1, 233-252.

SHALAEV, E. Y. and ZOGRAFI, G. 1996. How does residual water affect the solid-state degradation of drugs in the amorphous state? *Journal of Pharmaceutical Sciences,* 85**,** 1137-1141.

SHAMBLIN, S. L., HANCOCK, B. C., DUPUIS, Y. and PIKAL, M. J. 2000. Interpretation of relaxation time constants for amorphous pharmaceutical systems. *Journal of Pharmaceutical Sciences,* 89**,** 417-427.

SHAMBLIN, S. L., TANG, X., CHANG, L., HANCOCK, B. C. and PIKAL, M. J. 1999. Characterization of the time scales of molecular motion in pharmaceutically important glasses. *Journal of Physical Chemistry B,* 103**,** 4113-4121.

SHAMBLIN, S. L., TAYLOR, L. S. and ZOGRAFI, G. 1998. Mixing behavior of colyophilized binary systems. *Journal of Pharmaceutical Sciences,* 87**,** 694-701.

SHAMMA, R. N. and BASHA, M. 2013. Solupluse (R): A novel polymeric solubilizer for optimization of Carvedilol solid dispersions: Formulation design and effect of method of preparation. *Powder Technology,* 237**,** 406-414.

SHAN, N. and ZAWOROTKO, M. J. 2008. The role of cocrystals in pharmaceutical science. *Drug Discovery Today,* 13**,** 440-446.

SHENG, J., VENKATESH, G. M., DUDDU, S. P. and GRANT, D. J. W. 1999. Dehydration behavior of eprosartan mesylate dihydrate. *Journal of Pharmaceutical Sciences,* 88**,** 1021-1029.

SHETH, A. R., LUBACH, J. W., MUNSON, E. J., MULLER, F. X. and GRANT, D. J. W. 2005. Mechanochromism of piroxicam accompanied by intermolecular proton transfer probed by spectroscopic methods and solid-phase changes. *Journal of the American Chemical Society,* 127**,** 6641-6651.

SHIMANOVICH, R., COOKE, M. and PETERSON, M. L. 2012. A rapid approach to the preliminary assessment of the physical stability of pharmaceutical hydrates. *Journal of Pharmaceutical Sciences,* 101**,** 4013-4017.

SIMHA, R. and BOYER, R. F. 1962. On a general relation involving the glass temperature and coefficients of expansion of polymers. *The Journal of Chemical Physics,* 37**,** 1003-1007.

SIMONELLI, A. P., MEHTA, S. C. and HIGUCHI, W. I. 1969. Dissolution rates of high energy polyvinylpyrrolidone (PVP)-sulfathiazole coprecipitates. *Journal of Pharmaceutical Sciences,* 58**,** 538-549.

SIX, K., VERRECK, G., PEETERS, J., BREWSTER, M. and VAN DEN MOOTER, G. 2004. Increased Physical Stability and Improved Dissolution Properties of Itraconazole, a Class II Drug, by Solid Dispersions that Combine Fast- and Slow-Dissolving Polymers. *Journal of Pharmaceutical Sciences,* 93**,** 124-131.

SOLLOHUB, K. and CAL, K. 2010. Spray drying technique: II. Current applications in pharmaceutical technology. *Journal of Pharmaceutical Sciences,* 99**,** 587-597.

SRINARONG, P., DE WAARD, H., FRIJLINK, H. W. and HINRICHS, W. L. J. 2011. Improved dissolution behavior of lipophilic drugs by solid dispersions: The production process as starting point for formulation considerations. *Expert Opinion on Drug Delivery,* 8**,** 1121-1140.

STEPHENSON, G. A. 2000. Structure determination from conventional powder diffraction data: Application to hydrates, hydrochloride salts, and metastable polymorphs. *Journal of Pharmaceutical Sciences,* 89**,** 958-966.

STEPHENSON, G. A. and DISEROAD, B. A. 2000. Structural relationship and desolvation behavior of cromolyn, cefazolin and fenoprofen sodium hydrates. *International Journal of Pharmaceutics,* 198**,** 167-177.

STEPHENSON, G. A., GROLEAU, E. G., KLEEMANN, R. L., XU, W. and RIGSBEE, D. R. 1998. Formation of isomorphic desolvates: Creating a molecular vacuum. *Journal of Pharmaceutical Sciences,* 87**,** 536-542.

STICKEL, F., FISCHER, E. W. and RICHERT, R. 1995. Dynamics of glass-forming liquids. I. Temperature-derivative analysis of dielectric relaxation data. *The Journal of Chemical Physics,* 102**,** 6251-6257.

SUGANO, K., OKAZAKI, A., SUGIMOTO, S., TAVORNVIPAS, S., OMURA, A. and MANO, T. 2007. Solubility and dissolution profile assessment in drug discovery. *Drug Metabolism and Pharmacokinetics,* 22**,** 225-254.

SUN, C. C. 2007. Thermal expansion of organic crystals and precision of calculated crystal density: A survey of Cambridge Crystal Database. *Journal of Pharmaceutical Sciences,* 96**,** 1043-1052.

SURANA, R., PYNE, A. and SURYANARAYANAN, R. 2004. Effect of Aging on the Physical Properties of Amorphous Trehalose. *Pharmaceutical Research,* 21**,** 867-874.

SUZUKI, T., ARAKI, T., KITAOKA, H. and TERADA, K. 2012. Characterization of non-stoichiometric hydration and the dehydration behavior of sitafloxacin hydrate. *Chemical and Pharmaceutical Bulletin,* 60**,** 45-55.

TACHIBANA, T. and NAKAMURA, A. 1965. A methode for preparing an aqueous colloidal dispersion of organic materials by using water-soluble polymers: Dispersion ofB-carotene by polyvinylpyrrolidone. *Kolloid-Zeitschrift und Zeitschrift für Polymere,* 203**,** 130-133.

TANG, X. and PIKAL, M. J. 2004. Design of Freeze-Drying Processes for Pharmaceuticals: Practical Advice. *Pharmaceutical Research,* 21**,** 191-200.

TANG, X. C., PIKAL, M. J. and TAYLOR, L. S. 2002. A spectroscopic investigation of hydrogen bond patterns in crystalline and amorphous phases in dihydropyridine calcium channel blockers. *Pharmaceutical Research,* 19**,** 477-483.

TANTISHAIYAKUL, V., KAEWNOPPARAT, N. and INGKATAWORNWONG, S. 1996. Properties of solid dispersions of piroxicam in polyvinylpyrrolidone K-30. *International Journal of Pharmaceutics,* 143**,** 59-66.

TANTISHAIYAKUL, V., KAEWNOPPARAT, N. and INGKATAWORNWONG, S. 1999. Properties of solid dispersions of piroxicam in polyvinylpyrrolidone. *International Journal of Pharmaceutics,* 181**,** 143-151.

TAYLOR, L. S. and SHAMBLIN, S. L. 1999. Amorphous Solids. *In:* BRITTAIN, H. G. (ed.) *Polymorphism in Pharmaceutic Solids.* 2nd ed. New York: Informa Healthcare.

TE, R. L., GRIESSER, U. J., MORRIS, K. R., BYRN, S. R. and STOWELL, J. G. 2003. X-ray diffraction and solid-state NMR investigation of the single-crystal to single-crystal dehydration of thiamine hydrochloride monohydrate. *Crystal Growth and Design,* 3**,** 997-1004.

THAKURIA, R. and NANGIA, A. 2011. Polymorphic form IV of olanzapine. *Acta Crystallographica Section C,* 67**,** 461-463.

THO, I., LIEPOLD, B., ROSENBERG, J., MAEGERLEIN, M., BRANDL, M. and FRICKER, G. 2010. Formation of nano/micro-dispersions with improved dissolution properties upon dispersion of ritonavir melt extrudate in aqueous media. *European Journal of Pharmaceutical Sciences,* 40**,** 25-32.

TRASI, N. S. and TAYLOR, L. S. 2012. Effect of polymers on nucleation and crystal growth of amorphous acetaminophen. *CrystEngComm,* 14**,** 5188-5197.

TRASK, A. V., MOTHERWELL, W. D. S. and JONES, W. 2006. Physical stability enhancement of theophylline via cocrystallization. *International Journal of Pharmaceutics,* 320**,** 114-123.

TRUONG, V., BHANDARI, B. R., HOWES, T. and ADHIKARI, B. 2002. Analytical model for the prediction of glass transition temperature of food systems. *In:* LEVINE, H. (ed.) *Amorphous Food and Pharmaceutical Systems.* The Royal Society of Chemistry.31-47

URBANETZ, N. A. 2006. Stabilization of solid dispersions of nimodipine and polyethylene glycol 2000. *European Journal of Pharmaceutical Sciences,* 28**,** 67-76.

VAN DEN MOOTER, G., WUYTS, M., BLATON, N., BUSSON, R., GROBET, P., AUGUSTIJNS, P. and KINGET, R. 2000. Physical stabilisation of amorphous ketoconazole in solid dispersions with polyvinylpyrrolidone K25. *European Journal of Pharmaceutical Sciences,* 12**,** 261-269.

VAN DROOGE, D. J., HINRICHS, W. L. J., VISSER, M. R. and FRIJLINK, H. W. 2006. Characterization of the molecular distribution of drugs in glassy solid dispersions at the nano-meter scale, using differential scanning calorimetry and gravimetric water vapour sorption techniques. *International Journal of Pharmaceutics,* 310**,** 220-229.

VAN EERDENBRUGH, B. and TAYLOR, L. S. 2010. Small scale screening to determine the ability of different polymers to inhibit drug crystallization upon rapid solvent evaporation. *Molecular Pharmaceutics,* 7**,** 1328-1337.

VASCONCELOS, T., SARMENTO, B. and COSTA, P. 2007. Solid dispersions as strategy to improve oral bioavailability of poor water soluble drugs. *Drug Discovery Today,* 12**,** 1068-1075.

VEHRING, R., FOSS, W. R. and LECHUGA-BALLESTEROS, D. 2007. Particle formation in spray drying. *Journal of Aerosol Science,* 38**,** 728-746.

VERHEYEN, S., BLATON, N., KINGET, R. and VAN DEN MOOTER, G. 2002. Mechanism of increased dissolution of diazepam and temazepam from polyethylene glycol 6000 solid dispersions. *International Journal of Pharmaceutics,* 249**,** 45-58.

VIDGREN, M. T., VIDGREN, P. A. and PARONEN, T. P. 1987. Comparison of physical and inhalation properties of spray-dried and mechanically micronized disodium cromoglycate. *International Journal of Pharmaceutics,* 35**,** 139-144.

VIPPAGUNTA, S. R., BRITTAIN, H. G. and GRANT, D. J. W. 2001. Crystalline solids. *Advanced Drug Delivery Reviews,* 48**,** 3-26.

VITEZ, I. M., NEWMAN, A. W., DAVIDOVICH, M. and KIESNOWSKI, C. 1998. The evolution of hot-stage microscopy to aid solid-state characterizations of pharmaceutical solids. *Thermochimica Acta,* 324**,** 187-196.

VOGT, F. G., DELL'ORCO, P. C., DIEDERICH, A. M., SU, Q., WOOD, J. L., ZUBER, G. E., KATRINCIC, L. M., MUELLER, R. L., BUSBY, D. J. and DEBROSSE, C. W. 2006. A study of variable hydration states in topotecan hydrochloride. *Journal of Pharmaceutical and Biomedical Analysis,* 40**,** 1080-1088.

VYAZOVKIN, S., BURNHAM, A. K., CRIADO, J. M., PÉREZ-MAQUEDA, L. A., POPESCU, C. and SBIRRAZZUOLI, N. 2011. ICTAC Kinetics Committee recommendations for performing kinetic computations on thermal analysis data. *Thermochimica Acta,* 520**,** 1-19.

WAFIK GOUDA, H., MOUSTAFA, M. A. and AL SHORA, H. I. 1984. Effect of storage on nitrofurantoin solid dosage forms. *International Journal of Pharmaceutics,* 18**,** 213-215.

WANG, L. M., VELIKOV, V. and ANGELL, C. A. 2002. Direct determination of kinetic fragility indices of glassforming liquids by differential scanning calorimetry: Kinetic versus thermodynamic fragilities. *Journal of Chemical Physics,* 117**,** 10184-10192.

WARD, N. and JACEWICZ, V. W. 2000. *Paroxetine Hydrochloride form A or C*. United Kingdom patent application 6133289.

WAWRZYCKA-GORCZYCA, I., BOROWSKI, P., OSYPIUK-TOMASIK, J., MAZUR, L. and KOZIOL, A. E. 2007. Crystal structure of olanzapine and its solvates. Part 3. Two and three-component solvates with water, ethanol, butan-2-ol and dichloromethane. *Journal of Molecular Structure,* 830**,** 188-197.

WAWRZYCKA-GORCZYCA, I., KOZIOL, A. E., GLICE, M. and CYBULSKI, J. 2004a. Polymorphic form II of 2-methyl-4-(4-methyl-1-piperazinyl)-10H-thieno- 2,3-b 1,5 benzodiazepin e. *Acta Crystallographica Section E-Structure Reports Online,* 60**,** 66-68.

WAWRZYCKA-GORCZYCA, I., MAZUR, L. and KOZIOL, A. E. 2004b. 2-methyl-4-(4-methyl-1-piperazinyl)-10H-thieno 2,3-b 1,5 benzodiazepine methanol solvate. *Acta Crystallographica Section E-Structure Reports Online,* 60**,** 69-71.

WEUTS, I., KEMPEN, D., DECORTE, A., VERRECK, G., PEETERS, J., BREWSTER, M. and VAN DEN MOOTER, G. 2004. Phase behaviour analysis of solid dispersions of loperamide and two structurally related compounds with the polymers PVP-K30 and PVP-VA64. *European Journal of Pharmaceutical Sciences,* 22**,** 375-385.

WEUTS, I., KEMPEN, D., DECORTE, A., VERRECK, G., PEETERS, J., BREWSTER, M. and VAN DEN MOOTER, G. 2005. Physical stability of the amorphous state of loperamide and two fragment molecules in solid dispersions with the polymers PVP-K30 and PVP-VA64. *European Journal of Pharmaceutical Sciences,* 25**,** 313-320.

WILLART, J. F., DE GUSSEME, A., HEMON, S., DESCAMPS, M., LEVEILLER, F. and RAMEAU, A. 2002. Vitrification and Polymorphism of Trehalose Induced by Dehydration of Trehalose Dihydrate. *The Journal of Physical Chemistry B,* 106**,** 3365-3370.

WOSTHEINRICH, K. and SCHMIDT, P. C. 2001. Polymorphic changes of thiamine hydrochloride during granulation and tableting. *Drug Development and Industrial Pharmacy,* 27**,** 481-489.

YANG, Z., NOLLENBERGER, K., ALBERS, J., CRAIG, D. and QI, S. 2013. Microstructure of an Immiscible Polymer Blend and Its Stabilization Effect on Amorphous Solid Dispersions. *Molecular Pharmaceutics,* 10**,** 2767-2780.

YOKOTA, M., UEKUSA, H. and OHASHI, Y. 1999. Structure Analyses of Two Crystal Forms of Paroxetine Hydrochloride. *Bulletin of the Chemical Society of Japan,* 72**,** 1731-1736.

YOUNG, W. W. L. and SURYANARAYANAN, R. 1991. Kinetics of transition of anhydrous carbamazepine to carbamazepine dihydrate in aqueous suspensions. *Journal of Pharmaceutical Sciences,* 80**,** 496-500.

YU, D. G., GAO, L. D., WHITE, K., BRANFORD-WHITE, C., LU, W. Y. and ZHU, L. M. 2010. Multicomponent amorphous nanofibers electrospun from hot aqueous solutions of a poorly soluble drug. *Pharmaceutical Research,* 27**,** 2466-2477.

YU, L. 2001. Amorphous pharmaceutical solids: preparation, characterization and stabilization. *Advanced Drug Delivery Reviews,* 48**,** 27-42.

YU, L., MILTON, N., GROLEAU, E. G., MISHRA, D. S. and VANSICKLE, R. E. 1999. Existence of a mannitol hydrate during freeze-drying and practical implications. *Journal of Pharmaceutical Sciences,* 88**,** 196-198.

YU, L., REUTZEL-EDENS, S. M. and MITCHELL, C. A. 2000. Crystallization and Polymorphism of Conformationally Flexible Molecules: Problems, Patterns, and Strategies. *Organic Process Research & Development,* 4**,** 396-402.

YÜKSEL, N., KARATAŞ, A., ÖZKAN, Y., SAVAŞER, A., ÖZKAN, S. A. and BAYKARA, T. 2003. Enhanced bioavailability of piroxicam using Gelucire 44/14 and Labrasol: In vitro and in vivo evaluation. *European Journal of Pharmaceutics and Biopharmaceutics,* 56**,** 453-459.

ZHANG, F., AALTONEN, J., TIAN, F., SAVILLE, D. J. and RADES, T. 2009. Influence of particle size and preparation methods on the physical and chemical stability of amorphous simvastatin. *European Journal of Pharmaceutics and Biopharmaceutics,* 71**,** 64-70.

ZHANG, G. G. Z., LAW, D., SCHMITT, E. A. and QIU, Y. H. 2004. Phase transformation considerations during process development and manufacture of solid oral dosage forms. *Advanced Drug Delivery Reviews,* 56**,** 371-390.

ZHAO, Y., INBAR, P., CHOKSHI, H. P., MALICK, A. W. and CHOI, D. S. 2011. Prediction of the thermal phase diagram of amorphous solid dispersions by flory–huggins theory. *Journal of Pharmaceutical Sciences,* 100**,** 3196-3207.

ZHOU, D., ZHANG, G. G. Z., LAW, D., GRANT, D. J. W. and SCHMITT, E. A. 2002. Physical stability of amorphous pharmaceuticals: Importance of configurational thermodynamic quantities and molecular mobility. *Journal of Pharmaceutical Sciences,* 91**,** 1863-1872.

ZHU, H. 2006. Dehydration behavior and structural characterization of the GW275919X monohydrate. *International Journal of Pharmaceutics,* 315**,** 18-23.

ZHU, H. and GRANT, D. J. W. 2001. Dehydration behavior of nedocromil magnesium pentahydrate. *International Journal of Pharmaceutics,* 215**,** 251-262.

ZHU, L., JONA, J., NAGAPUDI, K. and WU, T. A. 2010. Fast Surface Crystallization of Amorphous Griseofulvin Below T (g). *Pharmaceutical Research,* 27**,** 1558-1567.

I stand at the seashore, alone, and start to
think. . .
There are the rushing
waves mountains of molecules
each stupidly minding its own business
trillions apart
yet forming white surf in unison.

Ages on ages before
any eyes could see
year after year
thunderously pounding the shore as now.
For whom, for what?
On a dead planet
with no life to entertain.

Never at rest
tortured by energy
wasted prodigiously by the sun
poured into space.
A mite makes the sea roar.

Deep in the sea
all molecules repeat
the pattern of one another
till complex new ones are formed.
They make others like themselves
and a new dance starts.

Growing in size and complexity
living things
masses of atoms
DNA, protein
dancing a pattern ever more intricate.

Out of the cradle
onto dry land
here it is
standing:
atoms with consciousness;
matter with curiosity.

Stands at the sea,
wonders at wondering:
I a universe of atoms,
an atom in the universe.

Richard P. Feynman